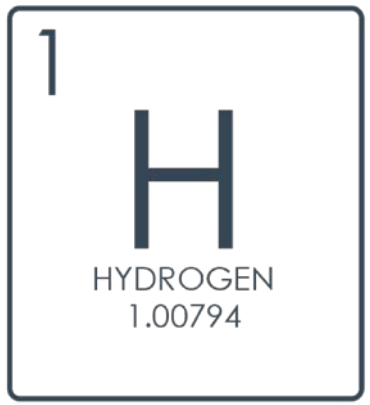

Universidad Rey Juan Carlos

Hydrogen production through steam reforming of model bio-oil aqueous fraction using metal-supported mesoporous catalysts

Pedro J. Megía Hervás

2020

Universidad Rey Juan Carlos

TESIS DOCTORAL

Hydrogen production through steam reforming of model bio-oil aqueous fraction using metal-supported mesoporous catalysts

Autor:

Pedro J. Megía Hervás

Directores:

Alicia Carrero Fernández

José A. Calles Martín

Programa de Doctorado en Tecnologías Industriales: Química, Ambiental, Energética, Electrónica, Mecánica y de los Materiales

Escuela Internacional de Doctorado

2020

Universidad Rey Juan Carlos

TESIS DOCTORAL

Hydrogen production through steam reforming of model bio-oil aqueous fraction using metal-supported mesoporous catalysts

Autor:

Pedro J. Megía Hervás

Directores:

Alicia Carrero Fernández

José A. Calles Martín

Programa de Doctorado en Tecnologías Industriales: Química, Ambiental, Energética, Electrónica, Mecánica y de los Materiales

Escuela Internacional de Doctorado

Madrid, 2020

“A subtle thought that is in error may yet give rise to fruitful inquiry that can establish truths of great value”

Isaac Asimov

Agradecimientos

En primer lugar, quiero expresar mi más sincero agradecimiento a mis directores de tesis Alicia Carrero y José A. Calles, quienes me han transmitido gran parte de los conocimientos que tengo a día de hoy y me han guiado durante mi formación como investigador. Gracias por todo el tiempo y dedicación durante estos años. No puedo continuar con los agradecimientos sin hacer una mención especial a Arturo J. Vizcaíno, quien me ha llevado de la mano durante este proceso de aprendizaje, con quien he compartido día a día todos los avances de la investigación y que, sin duda alguna, sin su ayuda no estaría en el punto en el que hoy me encuentro.

A María, con quien tuve la suerte de compartir dos años de trabajo en el laboratorio. Gracias a ella, salieron muchos resultados cuando no tenía tiempo para nada más, y siempre lo hizo con la mejor de sus sonrisas.

A todos y cada uno de los miembros el Grupo de Ingeniería Química y Ambiental de la Universidad Rey Juan Carlos, compañeros y técnicos de laboratorio, de quienes he recibido ayuda siempre que lo he necesitado. Entre ellos, se encuentra Clara, que, a pesar de conocernos desde hace muchos años, no habíamos compartido apenas tiempo, y, ha sido un grato descubrimiento. No me quiero olvidar de mis compañeros de despacho Alberto y Miguel, quienes me han hecho más amenas las largas horas de trabajo.

Además, quería hacer una mención especial a Gema y a Alba, a quienes me une un vínculo muy especial que me hace sentir que, más que amigas, son parte de mi familia. A Ana, mi eterna compañera de despacho, con quien, además de compartir muchos buenos momentos, fue con quien empezó todo y no lo cambiaría por nada en el mundo. Creo que habéis sido mi mayor golpe de suerte.

Me gustaría también mostrar mi agradecimiento al Prof. Vincenzo Palma por darme la oportunidad de hacer la estancia predoctoral en su laboratorio. A todas las personas que trabajan con él, que, desde el primer momento me trataron como uno más. De mi estancia en Salerno, además, me llevo grandes recuerdos y amigos. No hubiese sido lo

mismo sin “mi familia italiana”: Marta, Simona, Luigi y Paola, que, me hicieron sentir como en casa a pesar de estar lejos de mi familia.

A mis amigos, que por suerte son muchos. Todos de una manera u otra habéis aportado vuestro granito de arena. Con vosotros he compartido momentos inolvidables, he aprendido de cada aventura y sé que, aunque no nos veamos a menudo, puedo contar con vosotros siempre.

A mi familia, en especial a mis padres y mi hermana. Siempre habéis confiado en mí y me habéis apoyado incondicionalmente en todas las decisiones que he tomado durante estos años. Gracias de corazón.

Por último, y no por ello menos importante, a mi compañero de viaje. Apareciste en mi vida para ponerla patas arriba y te has convertido en una persona imprescindible. Gracias por estar siempre ahí.

A todos, GRACIAS.

Scientific publications included in the Doctoral Thesis

- **Pedro J. Megía,** Alicia Carrero, José A. Calles, Arturo J. Vizcaíno, "Hydrogen production from steam reforming of acetic acid as a model compound of the aqueous fraction of microalgae HTL using Co-M/SBA-15 (M: Cu, Ag, Ce, Cr) catalysts". Catalysts 9 (2019) 1013.

- José A. Calles, Alicia Carrero, Arturo J. Vizcaíno, **Pedro J. Megía**, "Agglomerated Co-Cr/SBA-15 catalysts for hydrogen production through acetic acid steam reforming". International Journal of Hydrogen Energy. 45 (2020) 15941-15950.

- **Pedro J. Megía**, Arturo J. Vizcaíno, María Ruiz-Abad, José A. Calles, Alicia Carrero, "Coke evolution in simulated bio-oil aqueous fraction steam reforming using Co/SBA 15 catalyst". Catalysis Today (2020). Accepted manuscript (In press). https://doi.org/10.1016/j.cattod.2020.04.069.

- **Pedro J. Megía**, José A. Calles, Alicia Carrero, Arturo J. Vizcaíno, "Effect of the incorporation of reducibility promoters (Cu, Ce, Ag) in Co/CaSBA-15 catalysts for acetic acid steam reforming". International Journal of Energy Research (2020). Accepted manuscript (In press). https://doi.org/10.1002/er.5832.

Other related scientific publications

- José A. Calles, Alicia Carrero, Arturo J. Vizcaíno, Lourdes García-Moreno, **Pedro J. Megía**, "Steam Reforming of Model Bio-Oil Aqueous Fraction Using Ni-(Cu, Co, Cr)/SBA-15 Catalysts". International Journal of Molecular Sciences 20 (2019) 512.

Contribution to Conferences

- Arturo J. Vizcaíno, Lourdes García-Moreno, **Pedro J. Megía**, José A. Calles, Alicia Carrero, "Valorization of bio-oil aqueous fraction: Hydrogen production by steam reforming using Ni-M/SBA-15 (M: Co, Cu, Cr) catalysts". Workshop RESTOENE-2, June 2016, Móstoles (Spain). Poster presentation.

- **Pedro J. Megía**, Arturo J. Vizcaíno, Alicia Carrero, José A. Calles, "Hydrogen production through acetic acid steam reforming using Ni and Co catalysts supported on Ca-SBA-15". Workshop RESTOENE-2, June 2017, Miraflores de la Sierra (Spain). Oral presentation.

- Alicia Carrero, José A. Calles, Arturo J. Vizcaíno, **Pedro J. Megía**, "Reformado con vapor de ácido acético con catalizadores basados en Ni y Co soportados sobre SBA-15". SECAT'17, June 2017, Oviedo (Spain). Poster presentation.

- **Pedro J. Megía,** Alicia Carrero, José A. Calles, Arturo J. Vizcaíno, "Influence of promoters addition to Co-based catalysts on acetic acid steam reforming". European Hydrogen Energy Conference 2018, March 2018, Malaga (Spain). Oral presentation.

- José A. Calles, Alicia Carrero, Arturo J. Vizcaíno, **Pedro J. Megía**, "Agglomerated Co-Cr/SBA-15 catalysts for hydrogen production through acetic acid steam reforming". 16th International Conference on Clean Energy, May 2018, Famagusta (North Cyprus). Oral presentation.

- Arturo J. Vizcaíno, **Pedro J. Megía**, José A. Calles, Alicia Carrero, "Reformado con vapor de ácido acético usando catalizadores tipo Co/Ca-SBA-15: Efecto de la incorporación de promotores de la reducción". XXVI Congresso Ibero-Americano de Catálise. September 2018, Coimbra (Portugal). Oral presentation.

- **Pedro J. Megía**, "Reformado con vapor de ácido acético utilizando catalizadores aglomerados tipo Co-Cr/SBA-15". I Congreso EID 2018, November 2018, Móstoles (Spain). Oral presentation.

- **Pedro J. Megía**, Arturo J. Vizcaíno, María Ruiz-Abad, José A. Calles, Alicia Carrero, "Coke evolution in bio-oil aqueous fraction steam reforming using Co/SBA 15 catalyst". CatBior V, September 2019, Turku (Finland). Oral presentation.

- Marta Cortese, **Pedro J. Megía**, Concetta Ruocco, Vincenzo Palma, Alicia Carrero, José A. Calles, "Experimental study of supported catalysts for the steam reforming of acetic acid". IV International Conference on Catalysis and Chemical Engineering, February 2020, Los Angeles (United States). Oral presentation.

Index

Resumen

El trabajo recogido en la presente Tesis Doctoral forma parte la línea de producción y almacenamiento de hidrógeno y, ha sido desarrollado en los laboratorios del Grupo de Ingeniería Química y Ambiental de la Universidad Rey Juan Carlos. Concretamente, se ha centrado en la producción de hidrógeno renovable mediante reformado con vapor de compuestos modelo presentes en las fracciones acuosas procedentes de tratamientos termoquímicos de biomasa y residuos. Para ello, se han desarrollado catalizadores de cobalto soportados con el objeto de maximizar la producción de hidrógeno, minimizando la formación de productos secundarios tales como coque, que disminuyen la actividad del catalizador.

Antecedentes

La demanda mundial de energía primaria aumenta un 1.3 % cada año como consecuencia del crecimiento económico, el aumento de la población y los avances tecnológicos. Actualmente, más del 90% de la demanda mundial de energía se abastece con combustibles de origen fósil, emitiendo a la atmósfera aproximadamente 32 mil millones de toneladas de CO_2 cada año. Además de los fuertes impactos ambientales, los combustibles fósiles son recursos limitados, y los precios del petróleo fluctúan enormemente afectando a la industria y a la capacidad de los consumidores para comprar bienes y servicios. Por ello, el número de países con políticas energéticas basadas en tecnologías de hidrógeno está aumentando [1].

El uso de hidrógeno para la producción de energía no genera emisiones contaminantes, ya que, en su combustión, solo se produce calor y vapor de agua. Asimismo, la aplicación del hidrógeno en pilas de combustible permite obtener energía eléctrica de forma sostenible y con elevados rendimientos. Por ello, el hidrógeno tiene el potencial de disminuir significativamente las emisiones de CO_2, contribuyendo a mitigar el cambio climático. A pesar de todas estas ventajas, el hidrógeno no se encuentra disponible en forma libre en la naturaleza, es por eso que, hoy en día, el hidrógeno se produce principalmente a partir del reformado con vapor de gas natural. En consecuencia, la aplicación energética del hidrógeno como vector del futuro, requiere el desarrollo de nuevas tecnologías que permitan producirlo a partir de fuentes renovables. Entre los distintos procesos de producción de hidrógeno renovable, resulta interesante el reformado con vapor de la fracción acuosa del bioaceite obtenido mediante procesos termoquímicos de conversión de biomasa y residuos.

En general, el reformado con vapor de los compuestos oxigenados contenidos en la fracción acuosa del bioaceite, es un proceso complejo en el cual intervienen un gran número de reacciones. Por ello, el rendimiento a hidrógeno se ve afectado por la presencia de reacciones secundarias como la de metanación y la de formación de coque, además de la limitación termodinámica de la reacción de reformado con vapor y de la reacción water-gas shift. De este modo, la viabilidad del proceso está muy relacionada con el desarrollo de catalizadores activos y estables, con alta selectividad hacia el producto de interés, el hidrógeno.

Objetivos

El principal objetivo del presente trabajo de investigación es el desarrollo de catalizadores de cobalto soportados sobre el material mesoestructurado SBA-15, que, permite una mejor dispersión de la fase activa. A día de hoy, los catalizadores de Co han sido menos estudiados que los de Ni, aunque presentan una elevada actividad a temperaturas moderadas y mejores rendimientos a hidrógeno. Además, en esta tesis,

se ha modificado el catalizador base Co/SBA-15 con varios promotores para mejorar su comportamiento en el reformado con vapor.

Metodología

El soporte utilizado para la preparación de catalizadores de cobalto fue el material silíceo mesoestructurado SBA-15, sintetizado por el método hidrotérmico descrito en la literatura. Con el objetivo de mejorar las propiedades catalíticas, el catalizador fue modificado incorporando promotores tales como Ca, Cu, Ce, Ag, Cr por impregnación a humedad incipiente utilizando disoluciones acuosas de los correspondientes nitratos.

Las reacciones de reformado con vapor se llevaron a cabo en un reactor de lecho fijo situado en el interior de una unidad Microactivity-Pro (PID Eng&Tech) a 600ºC y presión atmosférica. Con el objetivo de tener Co en estado metálico (fase activa), antes de cada la reacción, los catalizadores se redujeron in situ haciendo pasar una corriente de H_2 por el reactor. En los capítulos 1-3 se llevó a cabo el reformado con vapor de ácido acético como compuesto modelo, mientras que en el capítulo 4 se utilizó como alimento una mezcla formada por ácido acético, hidroxiacetona y fenol cuya composición se aproxima mayoritariamente a la de la fracción acuosa del bioaceite.

Los catalizadores, tanto calcinados como reducidos y usados, se caracterizaron usando distintas técnicas: fisisorción de N_2, ICP-AES, DRX, H_2-TPR, TEM, TGA y CHN entre otras.

Resultados y conclusiones

Esta Tesis Doctoral se ha dividido en cuatro capítulos, cuyos resultados y conclusiones más relevantes se resumen a continuación:

I. Efecto de la incorporación de promotores de reducibilidad sobre Co/CaSBA-15.

En la primera parte de este capítulo, se estudia el efecto de la modificación del soporte SBA-15 con Ca antes de la impregnación del cobalto, ya que, de acuerdo con la

bibliografía, el calcio aumenta la interacción metal-soporte y aporta basicidad al catalizador. Los resultados de caracterización permitieron comprobar cómo la incorporación de Ca mejoró la dispersión de la fase activa a expensas de disminuir la reducibilidad, tal y como se pudo comprobar mediante las técnicas H_2-TPR y XPS. La menor reducibilidad de la muestra Co/CaSBA-15, dio lugar a una conversión y rendimiento de hidrógeno inferiores a los alcanzados con el catalizador sin modificar. Para abordar este efecto adverso, en la segunda parte del capítulo, se propuso la adición de promotores de reducibilidad como el Cu, Ag y Ce que mejoraron el comportamiento catalítico aumentando la conversión de ácido acético. Sin embargo, la presencia de Cu no mejoró el rendimiento de hidrógeno, debido a su papel predominante en la reacción de descarboxilación del ácido acético en lugar de la reacción de reformado. Como consecuencia de la alta dispersión y una buena reducibilidad (comparable a la obtenida para Co/SBA-15), la muestra Co-Ce/CaSBA-15 dio lugar al mejor comportamiento catalítico en el reformado con vapor de ácido acético aumentando la conversión y el rendimiento de hidrógeno hasta 99% y 71,8% respectivamente. Es decir, un aumento del 20% para la conversión y del 62% para el rendimiento a hidrógeno, en comparación con el catalizador Co/CaSBA-15.

II. Reformado de ácido acético empleando catalizadores bimetálicos Co-M/SBA-15 (M: Cu, Ag, Cr, Ce).

Dado que la incorporación de calcio en el soporte SBA-15 implica una etapa adicional en la preparación del catalizador y que los resultados del capitulo anterior no mejoraban los alcanzados con el catalizador Co/SBA-15, se decidió continuar utilizando únicamente como soporte el material mesoestructurado SBA-15. En este capitulo se prepararon catalizadores bimetalicos añadiendo Cu, Ag, Ce y Cr para analizar su influencia sobre las propiedades fisicoquímicas del catalizador Co/SBA-15 y, sobre la actividad catalítica en el reformado con vapor de ácido acético. Los resultados mostraron como la adición de Cu y Ag condujo a una disminución de la temperatura de reducción del Co. En el caso del catalizador con Cu, se mantuvo el tamaño de cristal en comparación con el catalizador Co/SBA-15, mientras que, en el

caso del catalizador con Ag, el tamaño de cristal de Co aumentó. La adición de Ce, no produjo cambios significativos en la capacidad de reducción de los óxidos de Co ni en el tamaño de los cristales. Por su parte, al incorporar Cr disminuyó considerablemente el tamaño de cristal de Co, dando lugar a una mayor dispersión de la fase activa sobre el soporte. Los resultados catalíticos mostraron como las muestras Co-Cu/SBA-15, Co-Ag/SBA-15 y Co-Ce/SBA-15 redujeron el rendimiento hacia hidrógeno en comparación con el catalizador Co/SBA-15. Sin embargo, la adición de Cr, dio lugar a una mejora del comportamiento catalítico alcanzando el rendimiento a hidrógeno más alto de los catalizadores preparados, con valores por encima del 70% que se encuentran muy cercanos al equilibrio termodinámico. Además, con el catalizador Co-Cr/SBA-15 se observó una menor deposición de coque con mayor presencia de nanofilamentos de carbón defectuosos.

III. Preparación de catalizadores Co-Cr/SBA-15 aglomerados para la obtención de hidrogeno por reformado con vapor de acido acético.

Este capítulo está centrado en la optimización del proceso de aglomeración del catalizador Co-Cr/SBA-15. Se prepararon una serie de catalizadores extruidos variando el contenido de bentonita, utilizado como aglomerante, y el tamaño de partícula para obtener partículas de catalizador adecuadas para su uso en procesos de reformado con vapor a escala industrial. Los resultados de la caracterización no mostraron cambios reseñables en las propiedades fisicoquímicas del mismo tras el proceso de extrusión de la muestra en polvo, mientras que, la resistencia mecánica aumentaba con el contenido de aglomerante. Las pruebas de difusión externas e internas permitieron la selección del caudal y el tamaño de partícula del catalizador adecuados para evitar gradientes de concentración internos y/o externos. En estas condiciones experimentales, los catalizadores extruidos de Co-Cr/SBA-15 con un 30% en peso de bentonita y un tamaño de partícula con un diámetro efectivo de 1,5 mm, mostraron un buen comportamiento catalítico en el reformado de ácido acético, alcanzando un valor de rendimiento a hidrógeno cercano al 60% y, valores de conversión similares que los obtenidos con catalizador en polvo.

IV. Estudio de la formación de coque en el reformado con vapor de fracciones acuosas de bioaceite.

Con el objetivo de estudiar las causas de la desactivación en las reacciones de reformado utilizando Co/SBA-15 como catalizador, este capítulo analiza la evolución del catalizador usado a diferentes tiempos en la reacción de reformado de una mezcla de compuestos modelo que representan mayoritariamente la fracción acuosa obtenida a partir de biomasa. La desactivación del catalizador Co/SBA-15 es consecuencia de la formación de coque, su composición y la sinterización de las partículas de Co. La oxidación de Co no se tuvo en cuenta como causa de desactivación ya que, en los difractogramas de rayos X no se detectaron óxidos de cobalto. Los resultados evidenciaron que el catalizador se desactiva siguiendo un proceso con dos etapas consecutivas. La primera, que tiene lugar a tiempos de reacción cortos, se atribuye a la formación de nanofibras de carbono defectuosas sobre la superficie del catalizador, así como dentro de los poros de SBA-15, lo que da lugar a la presencia de partículas de Co aisladas. Durante esta etapa, también se observaron algunas partículas de Co encapsuladas dentro de nanofibras de coque, lo cual, dificulta el papel catalítico de estos centros activos. Durante la segunda etapa, los nanofilamentos de carbono resultaron ser más ordenados que en la etapa anterior y, siguieron creciendo hacia afuera del soporte sin taponar nuevos poros, motivo por el cual, los valores de superficie BET permanecen prácticamente constantes. En ambas etapas, el tamaño de los cristales de cobalto tras la reacción de reformado indicaba cierta sinterización con poca influencia en la desactivación del catalizador Co/SBA-15. Estos resultados, junto con un análisis estadístico t de Student, permitieron concluir que el crecimiento progresivo de las nanofibras de carbono y su naturaleza tienen más influencia en la caída de la conversión que el resto de las variables estudiadas.

Summary

The work presented in this Doctoral Thesis is part of the hydrogen production and storage line and has been developed in the Rey Juan Carlos University, specifically, in the Chemical and Environmental Engineering Group laboratories. In particular, it has been focused on the production of renewable hydrogen from model compounds present in the aqueous fractions obtained from thermochemical treatments of biomass and residual waste. For this purpose, cobalt supported catalysts have been developed in order to maximize the production of hydrogen, minimizing the formation of secondary products such as coke, which decrease the catalyst activity.

World demand for primary energy rises by 1.3% each year as a consequence of global economic growth, the increase in population and advances in technology. Currently, more than 90% of the world's energy demand is supplied by fossil fuels, emitting approximately 32 billion tons of CO_2 into the atmosphere each year. In addition to the strong environmental impacts, fossil fuels are ever-dwindling supplies, and oil prices wildly fluctuate, affecting the industry and the ability of consumers to buy goods and services. Therefore, the number of countries with energy policies based on hydrogen technologies is increasing [1].

The use of hydrogen for energy production does not generate polluting emissions, since only heat and water vapor are produced. Likewise, the application of hydrogen in fuel cells allows the production of sustainable electricity with high yields. Therefore, it has the potential to significantly reduce CO_2 emissions, contributing to limiting

global climate change. Despite all these advantages, hydrogen is not available in free form in nature, reason why, currently hydrogen is produced mainly from the steam reforming of natural gas. Consequently, the application of hydrogen as the energy vector of the future, requires the development of new technologies that allow its production from renewable sources. Among the different processes for the production of renewable hydrogen, the steam reforming of the bio-oil aqueous fraction obtained from thermochemical treatments of biomass and wastes becomes interesting.

In general, the steam reforming of the oxygenated compounds contained in the bio-oil aqueous fractions is a complex process that involves a large number of reactions. Hence, the hydrogen yield is affected by the development of secondary reactions such as methanation and coke formation reactions, in addition to the thermodynamic limitation of the reforming reaction and the water-gas shift reaction. Thus, the viability of this process is related to the development of stable and active catalysts, with high selectivity towards hydrogen as the product of interest.

Therefore, the main objective of this research work is the development of cobalt-based catalysts supported on the mesoporous SBA-15 material, which allows a better dispersion of the active phase. To date, Co catalysts have been less studied than Ni catalysts despite they provide high activity at moderate temperatures and increase the hydrogen yield. In addition, in this Thesis, Co/SBA-15 has been modified using several promoters, to improve their catalytic performance in the steam reforming of both: acetic acid, as a model compound of the aqueous phase obtained from thermal treatments of biomass (chapters 1-3), and, a mixture of model compounds (acetic acid, hydroxyacetone and phenol), that represent an approximation to a real aqueous fraction in the last chapter.

This Doctoral Thesis has been divided into four different chapters, the most relevant results of which are summarized below:

I. Effect of the incorporation of reducibility promoters on Co/CaSBA-15.

In the first part of this chapter, the effect of SBA-15 modification with Ca before the Co impregnation is studied since according to the literature, calcium increases the metal-support interaction and provides basicity to the catalyst. The characterization results showed how Ca incorporation improved the metal dispersion at the expense of the reducibility as demonstrated by H_2-TPR and XPS. The lower reducibility of Co/CaSBA-15 led to lower conversion and hydrogen yield compared to the unpromoted sample. To address this detrimental effect, in the second part of this chapter, the addition of reducibility promoters such as Cu, Ag and Ce was perform leading to an enhancement of the catalytic performance increasing the acetic acid conversion and the hydrogen yield. However, the presence of Cu did not improve the hydrogen yield, attributed to its predominant role in the decarboxylation reaction of acetic acid rather than in the reforming reaction. As a consequence of the high dispersion and good reducibility (comparable to that obtained for Co/SBA-15), Co-Ce/CaSBA-15 sample reached the best catalytic behavior in the acetic acid steam reforming increasing the conversion and the hydrogen yield up to 99% and 71.8% respectively. That means, a 20% increase for the conversion and 62% for the hydrogen yield, compared to Co/CaSBA-15 catalyst.

II. Acetic acid steam reforming using bimetallic Co-M/SBA-15 (M: Cu, Ag, Cr, Ce).

Since the incorporation of calcium in the SBA-15 support implies an additional stage in the catalyst preparation and based on previous chapter where catalytic results did't improve Co/SBA-15, we decided to continue using bare SBA-15 as support. In this chapter, the influence of promoters (Cu, Ag, Ce and Cr) addition on the physicochemical properties of Co/SBA-15 catalyst and, on the catalytic activity of acetic acid steam reforming is studied. The results showed how Cu and Ag addition led to a decrease in the Co reduction temperature. In the case of the Cu-doped catalyst,

the Co crystal size was maintained when compared to the Co/SBA-15 catalyst, while, in the case of the Ag-containing catalyst, the Co crystal size was increased. The addition of Ce does not affect significantly neither Co-oxides reducibility nor Co crystallites size. For its part, the addition of Cr considerably reduced the Co crystallite size, giving rise to higher dispersion of the active phase over the support. Catalytic results showed how Co-Cu/SBA-15, Co-Ag/SBA-15 and Co-Ce/SBA-15 reduced the hydrogen selectivity. However, the addition of Cr gave rise to an improvement in the catalytic behavior, leading to the highest hydrogen selectivity of the prepared catalysts with values above 70% that are very close to the thermodynamic equilibrium (above 70%). In addition, a lower coke deposition was observed in this catalyst with a greater presence of defective carbon nanofilaments.

III. Preparation of agglomerated Co-Cr/SBA-15 catalysts for hydrogen production through acetic acid steam reforming.

This chapter is devoted to the optimization of the agglomeration process of Co-Cr/SBA-15. A series of Co-Cr/SBA-15 extrudates were prepared by varying the bentonite content, used as binder, and particle size in order to get catalyst particles suitable to be used in a steam reformer at industrial scale. The characterization results did not show remarkable changes in the physicochemical properties after the extruding process of the powdered sample, while the mechanical strength increases with the binder content. The external and internal diffusion tests allowed the selection of the suitable flow rate and catalysts particle size to avoid any concentration gradients. Under these experimental conditions, Co-Cr/SBA-15 extrudates with a 30 wt.% of bentonite and a particle size with an effective diameter of 1.5 mm, showed a good catalytic performance in the acetic acid steam reforming, reaching a hydrogen yield around 58% and similar results in terms of conversion when compared to the powder form.

IV. Study of coke formation in the steam reforming of bio-oil aqueous fractions.

With the aim of studying the causes of deactivation in the reforming reactions using Co/SBA-15, this chapter studies the evolution of the used catalyst at different times in the steam reforming of a mixture of model compounds that mostly represent the aqueous fraction obtained from biomass. Deactivation of Co/SBA-15 is a consequence of coke formation, its composition and Co sintering. The oxidation of Co was discarded as a cause of deactivation since no cobalt oxides were found by XRD in the used catalysts. Results evidenced that Co/SBA-15 is deactivated following a process with two consecutive stages. The first one, at short reaction times, ascribed to the formation of defective carbon nanofibers over the catalyst surface as well as inside the SBA-15 pores leading to isolated metallic Co particles. During this step, some Co particles were also encapsulated within coke nanofibers, hindering the catalytic role of these active centers. During the second stage, coke nanofilaments became more ordered growing out of the support without covering new pores, as inferred from almost constant BET surface values. In both stages, Co crystallites size indicated a slight sintering with minor influence on Co/SBA-15 deactivation. These results, along with a t-Student analysis, have led to the conclusion that the progressive growth of carbon nanofibers and its nature (C/H ratio) have more influence on the conversion drop than the rest of the studied variables.

1. Introduction

1.1. Current energy situation

Global demand for primary energy rises by 1.3% each year to 2040, with increasing demand for energy services [2] as a consequence of global economic growth, the increase in population and advances in technology. In this sense, fossil fuels (petroleum, natural gas and coal) have been widely used for energy production and are projected to remain the dominant energy source until at least 2050 [3, 4] (see Figure 1. 1). The use of fossil fuels for energy production and/or chemicals result in the emission of greenhouse gases such as carbon dioxide, nitrogen oxides and other volatile compound as well as solid particles into the atmosphere contributing to global climate change [5].

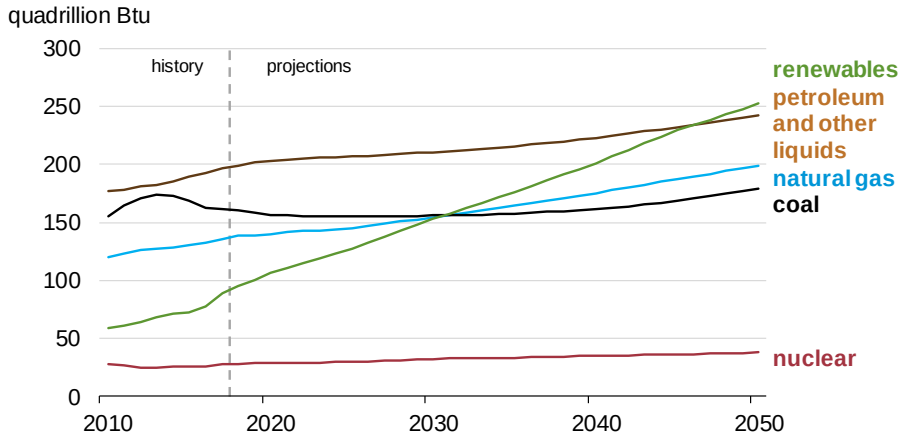

Figure 1. 1. World primary energy consumption by energy source [4]

Currently, carbon-based fuels supply 85% of the total world's energy demand. To meet the energy demand, approximately 36 billion tons of CO_2 are emitted into the atmosphere every year of which over 90% comes from fossil fuels [6] and it is expected to further increase in coming years, as shown in Figure 1. 2. Besides the strong environmental impacts, the fossil fuels are ever-dwindling supplies, and oil prices wildly fluctuate, impacting profits for industries that produce and use oil and consumers' ability to purchase goods and services [7]. Energy consumption and carbon emissions represent two crucial elements of the European Union energy strategy [8]. To ensure a reduction of both energy consumption and carbon emissions, different targets have been set up. In this sense, the next European Union binding agreement for energy efficiency target (primary energy consumption) is focused on the 30% of reduction in 2030 compared to the 1990 level [9]. Based upon the foregoing, multiple studies have been focused in the development of new technologies towards renewable energy sources as alternative to fossil fuels [10-15].

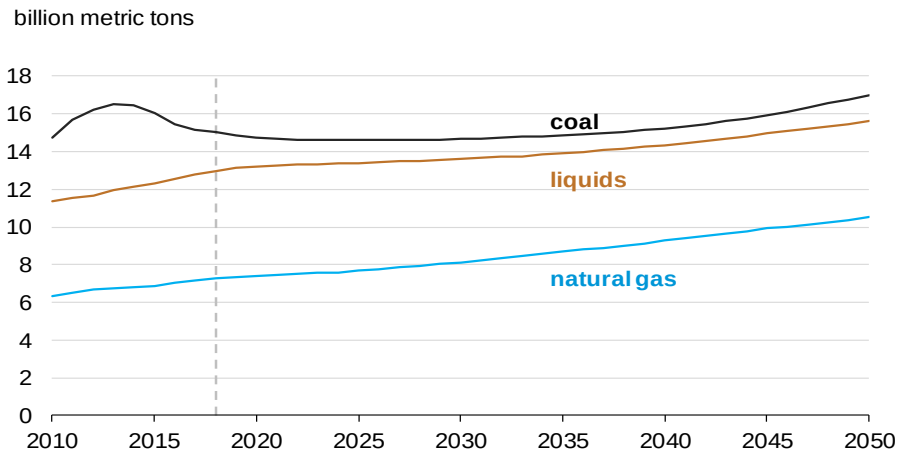

Figure 1. 2. Energy-related carbon dioxide emissions [4]

Against the use of fossil fuel technologies, the number of countries with policies that directly support investment in hydrogen technologies is increasing [1]. Hydrogen is the most abundant gas in the universe and has the maximum energy content per unit of weight when compared to any other known fuel [16, 17]. Using hydrogen for energy

production does not result in pollutant emissions since only heat and water vapor are produced [18-20], reducing the emission of greenhouse gases. Besides energy applications, hydrogen is widely used in chemical and petroleum industries [16, 17, 21]. Despite the abundance of hydrogen, it is not available in free form in nature [22]. Nowadays, hydrogen is mainly produce trough thermochemical processes using fossil fuels: hydrocarbon reforming, coal gasification, hydrocarbon pyrolysis and plasma reforming [16]. As a consequence, significant CO_2 emissions are produced (around 830 million tonnes per year) [1]. Thus, hydrogen production from renewable sources can face this problem by lowering the carbon footprint, leading to a sustainable energy system in the near future as shown in Figure 1. 3.

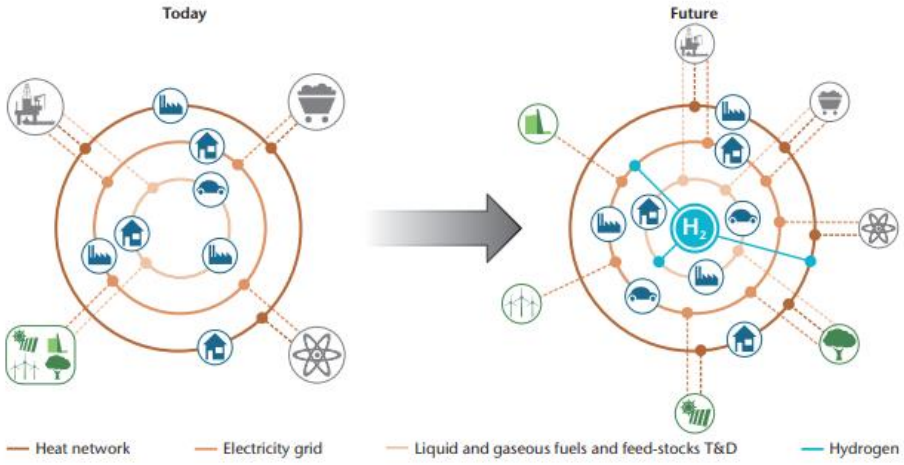

Figure 1. 3. Schematic representation of energy system today and in the future [23].

1.2. Technologies for hydrogen production

Hydrogen in molecular form can be obtained from many different sources such as fossil fuels, biomass and water [1]. Fossil fuels keep their dominant role in the global hydrogen supply since production costs are strongly correlated with fuel prices, which are still maintained at acceptable levels. Currently, there are several technologies to produce hydrogen from fossil fuels, being hydrocarbon reforming and pyrolysis the most used. These techniques almost allow the production of the entire hydrogen

demand [22]. More specifically, hydrogen is being produced 48% from natural gas, 30% from petroleum, and 18% from coal [23].

Despite most hydrogen is nowadays produced from hydrocarbons, carbon-free sources have attracted the attention to produce renewable hydrogen [24]. Hydrogen with a low-carbon footprint has the potential to facilitate significant reductions in energy-related CO_2 emissions and to contribute to limiting global temperature rise to 2°C [23]. Besides water, biomass is a renewable source of primary energy derived from plants and animal materials [22] such as forest residues, crops, municipal solid waste, microalgae or animal by-products [25, 26]. This renewable feedstock is considered a potential source of fuels and chemicals. Hydrogen production from biomass and residual wastes is technically and economically feasible given the current state of technology and economic conditions in many developed countries [27]. It has been stated that biomass will cover the energy demand by more than 25% by 2050 [24]. On the contrary to fossil fuels, biomass-to-energy processes reduce the CO_2 emission and absorbs CO_2 from natural environment [28], leading to a neutral carbon emission scenario.

1.2.1. Steam reforming

Steam reforming, is the reaction of a mixture of steam and hydrocarbons at high temperature to produce hydrogen and carbon oxides. Steam reforming is used to extract hydrogen from natural gas and much less frequently from liquefied petroleum gas and naphtha [1]. The most widely used hydrocarbon reformation process is methane steam reforming from natural gas or light hydrocarbons. In this process, carbon monoxide is first produced together with hydrogen giving rise to synthesis gas ($CH_4 + H_2O \rightarrow CO + 3\ H_2$), and then through water-gas shift reaction carbon monoxide is converted into carbon dioxide and additional hydrogen ($CO + H_2O \rightarrow CO_2 + H_2$) [29]. The overall methane steam reforming reaction can be represented as follows:

$$CH_4 + 2\ H_2O \rightarrow CO_2 + 4\ H_2$$

The reforming reaction is highly endothermic and a large amount of heat is required. For that reason, these reactions are typically carried out at a temperatures between 800-1000 °C [30]. The methane steam reforming produces a hydrogen-rich gas, along with less amounts of mainly carbon dioxide, carbon monoxide and methane. Since hydrogen is mixed with other compounds, a separation step is required for purification. In modern hydrogen plants, the purification is accomplished via Pressure Swing Adsorption system, which can produce up to 99.999% pure hydrogen with a recovery ranging from 70-95% [31].

1.2.2. Partial oxidation

Partial oxidation is an exothermic process, used to convert hydrocarbon fuels into a mixture of hydrogen, carbon monoxide, and other partially oxidized species [32]. The product distribution of partial oxidation reactions depends on C/O ratio and are constrained by high reaction temperatures (> 1000 °C). Thus, partial oxidation reactions are usually carried out using heterogeneous catalysts at lower temperatures [33]. Overall, the partial oxidation reaction could be described as follows:

$$C_nH_m + ½\ n\ O_2 \rightarrow n\ CO + ½\ m\ H_2$$

Thermodynamically, in this process H_2 and CO are the most abundant products above 550ºC [34], being CO a coke precursor. It can be removed by its oxidation towards CO_2 or by the water-gas shift reaction increasing the H_2 production. Despite the partial oxidation could be performed at moderate temperatures, the high exothermicity of the reaction could lead to hot-spots and, consequently, leading to catalyst deactivation [35].

1.2.3. Auto-thermal reforming

The auto-thermal reforming includes the exothermic partial oxidation with O_2, which provides the energy needed for the endothermic steam reforming reactions to increase the produced hydrogen [36]. In essence, both steam and oxygen are introduced into the reformer leading to the reforming and oxidation reactions occurring simultaneously

to get a thermodynamically neutral reaction [37]. This process has higher yield than the partial oxidation but lower than the steam reforming process.

1.2.4. Electrolysis

Electrolysis is one of the simplest ways to produce hydrogen from water. It can be summarized as conversion of electric power to chemical energy in the form of hydrogen and oxygen as a by-product with two reactions in each electrode; anode and cathode [38, 39]:

$$\text{Anode: } H_2O \rightarrow \tfrac{1}{2}\, O_2 + 2\, H^+ + 2\, e^-$$

$$\text{Cathode: } 2\, H^+ + 2\, e^- \rightarrow H_2$$

$$\text{Overall process: } H_2O \rightarrow H_2 + \tfrac{1}{2}\, O_2$$

Water electrolysis powered by renewable energy sources, is expected to enable the scale-up of hydrogen production (high purity, 99.9%), and zero CO_2 emissions are produced in water electrolysis processes [40]. However, the cost of H_2 produced by electrolysis is still significantly higher than that produced by fossil fuels [41].

1.2.5. Thermolysis

Thermolysis is a thermochemical water splitting process based on water decomposition to hydrogen and oxygen by heating at high temperatures. Despite this process implies an easy procedure, the water decomposition requires temperatures above 2500 °C [42, 43]. Thermolysis process is reversible, one of the main challenges in the application is the separation of the produced hydrogen and oxygen, since the recombination of both gaseous products may cause the formation of an explosive mixture [44]. The other challenge is the availability of materials, which can withstand the desired temperatures.

Against thermolysis, thermochemical water-splitting cycles proceed at lower maximum operating temperatures and produce both H_2 and O_2 in separate steps,

thereby avoiding their recombination and bypassing the need for high-temperature and costly downstream gas separation [43].

1.2.6. Photo-electrolysis

The process of water splitting by photo-electrolysis is similar to electrolysis but with the integration of this process with solar energy adsorption in a single unit. Water photo-electrolysis can be achieved by absorption of photons with energies greater than band gaps of semiconducting photo-electrodes, producing holes and electrons in photo-electrochemical cells [45]. The semiconductor uses the photons with energy greater than the semiconductor band gap to generate electron-hole pairs that are split by the electric field, which traverses the electrolyte [17].

1.2.7. Biological processes

Due to increased attention to sustainable development and waste minimization, hydrogen obtained from biological processes research has increased substantially in the recent years. The main biological processes used for hydrogen production include: photolytic hydrogen produced from water (bio-photolysis), dark-fermentative hydrogen production and photo-fermentative processes [42].

Bio-photolysis and photo-fermentation are photonic-driven biochemical hydrogen production processes from water [17]. In direct bio-photolysis, a water molecule split into oxygen and hydrogen ion via photosynthesis by microorganisms such as green microalgae [16, 46]. One advantage of this process is that hydrogen can be produced from water in an aqueous environment at ambient conditions. It could be considered as an environmentally sustainable and economically feasible method from both, water and CO_2 utilization perspectives [16, 22]. Currently, this technology requires a significant surface area to collect enough sunlight [42], due to the low hydrogen yield.

For fermentative processes, anaerobic bacteria are used on carbohydrate-rich substrates, deprived of light and under anoxic conditions [16, 47]. As light is not required, it can produce hydrogen at any time. Bio-hydrogen production through the

dark fermentation process occurs through a series of bio-chemical reactions [47]. On the contrary, in photo-fermentation, under anaerobic conditions, photosynthetic bacteria use sunlight as a source of energy and assimilate small organic molecules present in the biomass obtaining H_2 and CO_2 as the byproducts [48]. The hydrogen yield is typically lower in dark conditions when compared to the yield under sunlight [16].

1.2.8. Thermochemical processes

The thermochemical processes are one of the effective methods for producing hydrogen-rich gases from biomass [49, 50]. This technology mainly involve pyrolysis, gasification and hydrothermal liquefaction [22, 24, 25]. Both, gasification and pyrolysis technologies produce CO and CH_4 which can be processed in order to increase the hydrogen production trough steam reforming and water-gas shift reaction [16]. Pyrolysis is considered to be the starting point of all thermochemical conversion technologies because it involves all chemical reactions to form solid, liquid, and gas as the main products with low concentration of oxygen [51]. In the recent years, advanced research on using biomass for liquid fuels has been performed, ranging from studies of pyrolysis and hydrothermal liquefaction of lignocellulose material, gasification and biomass-to-liquid technologies to the upgrading processes [26].

Pyrolysis is a thermal decomposition process, occurring in the absence of oxygen [52]. It is normally performed at temperatures between 300-1000 ºC [53, 54]. When biomass is used as feedstock, the pyrolytic products after thermal decomposition include bio-char, bio-oil, and non-condensable gases including hydrogen, methane, carbon oxides and other gaseous hydrocarbons. Products yields depend on the operational conditions: when temperature is below 450 ºC bio-char formation is favored whereas bio-oil is the main product at temperatures between 450-800 ºC [25]. With the respect of operating conditions, pyrolysis is divided into fast pyrolysis and conventional pyrolysis. For hydrogen production, fast pyrolysis, which implies high temperatures and very short

residence times, is preferred since the major product for conventional pyrolysis is charcoal [24].

Biomass gasification is the conversion of biomass into a combustible gas mixture at high temperatures (800-900 ºC) in order to increase the hydrogen yield [16]. It is a variation of pyrolysis and, thus, is based upon partial oxidation [42]. At the end of the gasification, biomass is mainly converted into CO and H_2 along with some water, CO_2 and CH_4. Gasification requires oxidation agents such as air, oxygen or steam [25]. Following this technology, it is possible to obtain a fuel much cleaner and versatile than the original biomass [50].

Hydrothermal liquefaction of biomass is normally operated at moderate temperature of 250-370 ºC and high pressure (4-22 MPa) to break down the polymer structure of biomass [25]. The main product throughout this process is a liquid bio-crude along with a gaseous stream, an aqueous phase and a solid residue as byproducts [55]. The aqueous phase can be recirculated to the hydrothermal unit to enhance the bio-oil yield. Furthermore, it also could be used to produce hydrogen rich syngas from steam reforming. When compared with pyrolysis, the main advantages of hydrothermal liquefaction are higher energy efficiency, lower operating temperature and tar yield [26].

The bio-oil produced from hydrothermal liquefaction or pyrolysis processes is a liquid product which has larger energy density than biomass being composed of different kind of oxygenated such as acids, ketones, aldehydes and phenols among others [25, 26, 56]. This complex composition depends on the composition of the original biomass [57] and it is responsible for many adverse properties of bio-oil: low heating value, corrosivity or immiscibility with others fuels that make it considered as a low-quality fuel [58, 59]. The bio-oil can be segregated into two different fractions: one organic and other aqueous [60]. Whereas the organic fraction is composed of non-polar compounds and it can be upgraded by hydro-treating to obtain fuels, the aqueous phase has low value and it contains mainly water but also several oxygenated organic

compounds such as acetic acid, phenol and hydroxyacetone [11]. The worthless aqueous phase, can be revalorized by producing hydrogen through a catalytic reforming process [10]. The viability of this process is related to the development of active and stable catalysts, with high selectivity towards hydrogen production.

1.3. Catalytic steam reforming

Nowadays, catalytic steam reforming of gas, hydrocarbons and oxygenated hydrocarbons is a promising technology to produce hydrogen [61]. Bio-oil aqueous fraction is a complex mixture of different compounds where carboxylic acids, ketones, phenols, aldehydes [62-64] can be easily found along with a high water content. The concentration of each compound depends on the biomass feedstock used for its production. Due to the oxygenated nature of the bio-oil aqueous fraction and its high water content, it has the potential to be revalorized by catalytic steam reforming with hydrogen production. Although bio-oil aqueous fraction steam reforming has a complex reaction network, it can be described by the following reaction stoichiometry:

$$C_nH_mO_k + (n - k)\ H_2 \rightarrow n\ CO + (n + m/2 - k)\ H_2$$

The steam reforming reaction is followed by the water-gas shift reaction:

$$CO + H_2O \leftrightarrow CO_2 + H_2$$

Thus, assuming full conversion, the overall process can be represented as:

$$C_nH_mO_k + (2\ n - k)\ H_2 \rightarrow n\ CO_2 + (2\ n + m/2 - k)\ H_2$$

Steam reforming is an endothermic process and therefore is favored at high temperatures [65, 66]. Furthermore, pressure plays a key role in the reforming process. According to Le-Chatelier's principle, it has a negative equilibrium effect on hydrogen yield due to the non-zero stoichiometric molar balance between the gas products and reactants [67]. The hydrogen yield is also affected by the thermodynamic limitation of the water-gas shift reaction and other reactions such as methanation ($CO + 3\ H_2 \rightarrow CH_4 + H_2O$; $CO_2 + 4\ H_2 \rightarrow CH_4 + 2\ H_2O$), and coking [68].

Additionally, the methane from the methanation reactions can be steam reformed to produce more hydrogen:

$$CH_4 + 2\ H_2O \rightarrow CO_2 + 4\ H_2$$

A side effect of these reactions is the carbonaceous deposits on the catalyst surface. Coke deposition has been described as the main cause of catalyst deactivation in the steam reforming processes of hydrocarbons and oxygenated compounds [69-71]. Coke is mainly formed due to the Boudouard reaction ($2CO\ (g) \leftrightarrow CO_2\ (g) + C$), methane decomposition ($CH_4 \leftrightarrow C + 2H_2$), reverse carbon gasification ($CO + H_2 \rightarrow H_2O + C$) or polymerization of oxygenates/hydrocarbons ($C_nH_mO_k \rightarrow$ polymers $\rightarrow$ coke) [71-73]. The attenuation of these reactions depends on the composition and physicochemical properties of the catalysts as well as the reaction conditions [74]. Thus, the design of suitable catalysts must be undertaken. Those catalysts should present high activity and hydrogen selectivity and high resistance to deactivation.

As mentioned above, the bio-oil aqueous fraction has a complex composition, reason why many studies have focused the attention in the use of bio-oil model compounds such as acetic acid, phenol, furfural and hydroxyacetone among others [61, 75-77].

1.3.1. Steam reforming catalysts

Steam reforming catalysts are nowadays a critical point of study where activity, hydrogen selectivity and deactivation are the main aspects on which the related researches are focused. The reforming catalyst commonly undertakes the responsibility for cracking not only C-C and C-H bonds but also O-H bonds [78].

1.3.1.1. Active phases

Noble metal-based catalysts have been described as active and stable catalysts but their prices is extremely high [18, 78-80]. However, transition metals have lower cost when compared to noble metals. Since they have demonstrated suitable activity in steam reforming, researchers are paying much more attention to them in recent years [68, 80-82].

1.3.1.1.1. Noble metals

Supported noble metals catalysts such as Rh, Ru, Pt, Pd and Ir have been widely reported in oxygenated hydrocarbons steam reforming [78, 83-86]. The use of noble metals-based catalysts increase the hydrogen selectivity while carbon deposition is decreased increasing the catalytic stability [87, 88]. To reduce the catalyst cost, thus improving the reforming economics, low loadings (< 1 wt.%) are usually used [88, 89]. Even so, they are still expensive when compared to non-noble metal-based catalysts being the utilization limited at large scale [78].

Rioche et al. [83], studied the steam reforming of model compounds, similar to those found in bio-oil (acetic acid, ethanol, acetone and phenol) over noble metal-based catalyst supported on $CeZrO_2$ and Al_2O_3. They found that Rh supported over $CeZrO_2$ exhibited the highest hydrogen yield when compared to Pt and Pd, being this support much more efficient than the alumina. Tomishige et al. [84] found that Rh supported on CeO_2/SiO_2 for the steam reforming of tar was significantly more active when compared to other noble metals, with a hydrogen selectivity order of Rh > Pt > Pd > Ru. Basagiannis et al. [85] observed other trend in the ethanol steam reforming in the temperature range of 300–450 °C using noble metals and Al_2O_3 as support. They found that the catalytic performance varies according to Pt > Pd > Rh > Ru. More recently, Senseni et al. [86] reported the catalytic behavior of noble metal catalysts supported on $MgAl_2O_4$ trough glycerol steam reforming. Their results led to the conclusion that Rh-based catalyst was the optimum, showing high catalytic performance under different feed ratios and feed flow rates. Specifically, they observed the following trends for conversion: Rh > Pt > Ru > Ir, and hydrogen selectivity: Rh > Ir > Ru > Pt.

In general, Rh was found to be the most active catalyst in steam reforming processes [80] with also, the highest resistance to coke formation. This behavior is attributed to the Rh capacity towards C–C bond dissociation, which is greater than other noble metals. This fact results in better catalytic performance in terms of activity, selectivity, and stability [90].

1.3.1.1.2. Transition metals

Because of their suitable performance in steam reforming processes and their lower cost when compared to noble metals, transition metals have raised considerable attention in the past decades including Ni, Co, Cu and Fe [68, 91-93]; being Ni, the most studied one.

Hu et al. [91] studied the performance of different transition metals (Ni, Co, Fe and Cu) supported over Al_2O_3 in acetic acid steam reforming. Their study led to the conclusion that Ni and Co were more active than Fe and Cu. They attributed this behavior to the ability for cracking the chemical bonds of acetic acid. Ni and Co were not only active in cracking C-C bonds, but also C-H bonds, while Cu was only active for the cracking of C-H bond and Fe species were only active for cracking C-C bonds. Konsolakis et al. [92] evaluate the influence of Ni, Co, Cu and Fe supported on Co/CeO_2 in the ethanol steam reforming in the temperature range of 400-800 °C. Stability experiments showed excellent stability of the catalysts, but some differences were observed particularly at low temperatures, following the order Co > Ni > Cu > Fe. Another work conducted by Chen et al. [93] was performed using attapulgite-supported transition metals in glycerol steam reforming. They observed how Ni and Co improved the ability to convert glycerol into hydrogen when compared with Cu and Fe catalysts, ascribed to its superior ability for cracking C-C and C-H bonds and the improvement of the water-gas shift reaction.

Generally, it is reported that Ni and Co-based catalyst achieved similar catalytic performances when compared to those described in literature for noble metals. Co-based catalysts have been less reported although they also provide high activity at moderate temperatures and increases hydrogen yield [94, 95]. Ni is more active for methanation reactions and acetic acid decomposition towards CH_4, while Co is more active for the reverse water-gas shift reaction and the decomposition of acetic acid to CO [91]. Both, Ni and Co, suffer from deactivation. Co-based catalyst are commonly deactivated from the oxidation and sintering of the metallic phase [96]. Conversely,

the greatest challenge for Ni-based catalyst is the rapid deactivation due to high coke deposition as well as Ni particles sintering [90]. To overcome the coke formation and catalyst deactivation, there are some strategies to follow during the catalyst design such as promoter addition and/or support selection.

1.3.1.2. Promoters

Combining the advantages of different active species in the same carrier has been describe as an effective way to improve the catalyst performance [97]. Promoters can be classified in two main groups: textural and chemical promoters. Textural promoters generally facilitate the preparation of well-dispersed catalytic phases, to prevent and delay the sintering of active species by enhancing the textural properties of the catalysts. However, most promoters in industrial reforming are chemical promoters, which can be alkali and alkaline earth metals or metal oxides, that enhance the activity of reactions and moderate the carbon formation [98, 99].

There is a wide variety of research in literature, in which the beneficial effects of promoters' addition to steam reforming catalysts is studied. In this sense, different works can be found using alkaline (Na, K) [100-103], alkaline earth (Mg, Ca, Ba, Sr) [104-109] and rare-earth promoters (Ce, La, Yb) [110-115].

The addition of alkali elements (alkaline and alkaline earth metals) to supported catalysts results in a decrease in coke formation. This is explained by an increase in surface basicity of the materials, promoting water adsorption and OH surface mobility, thus, decreasing the rate of coke deposition on catalyst surface. They also improve the dispersion of the active phase, preventing metal sintering and strengthening the metal-support interaction.

Similarly, the presence of rare-earth metals in supported steam reforming catalysts was found to significantly enhance catalytic activity and stability, resulting in higher hydrogen yield and better carbon formation resistance by decreasing the selectivity towards ethylene, which is a coke precursor. This behavior is ascribed to the fact that lanthanides inhibit the growth of large crystals and prevent the re-oxidation of the

active phase during the steam reforming reaction. More specifically, both Ce and La, also promote carbon gasification ascribed to the higher amount of mobile lattice oxygen induced by the CeO_2 and the formation of lanthanum oxycarbonate from La_2O_3, respectively [115].

Furthermore, considerable research work has also been undertaken adding other transition or noble metals such as Cr, Mn, Fe, Co, Ni, Cu, Zn, Zr, Ru, Rh, Pd, Ag, Pt and Au [10, 80, 87, 116-119]. The combination of different active metals together giving rise to bimetallic M-M catalysts is an effective way to improve the catalytic performance by decreasing the reduction temperature, inhibiting carbon formation and/or improving the active phase dispersion.

1.3.1.3. Supports

It has been widely reported in literature that the catalytic performance is not only related to the active phase and/or promoters, but also to the support, which plays a key role in the catalyst activity and stability [120]. Support provides textural and physicochemical properties essential for keeping the catalyst well dispersed and resistant to coke formation. An adequate support should tap into the textural and chemical properties, such as surface area, porosity, thermal stability, redox properties, oxygen storage capacity and surface basicity. These characteristics, will improve the metal-support interaction, increase the dispersion of active metal particles and enable the reduction of the catalyst, in addition to avoid the formation of carbon species [121]. According to pore size, supports are categorized into three groups according to the International Union of Pure and Applied Chemistry (IUPAC): microporous (3-20 Å), mesoporous (20-500 Å) and macroporous materials (> 500 Å).

Regarding the supports used for reforming catalysts, a wide variety of oxides have been used such as Al_2O_3, Ce_2O_3, La_2O_3, SiO_2, MgO, TiO_2, ZrO_2, Nb_2O_5, Y_2O_3 [121-123]. Among them, Al_2O_3 is the most studied support given that it afford high specific surface area allowing high dispersion and its chemical strength provides stability to the catalyst [68, 90]. Nevertheless, the acidic properties of this support under reaction

conditions promote dehydration process leading to coke precursors, thus resulting in fast deactivation [71, 90, 124]. In contrast, mesoporous silica materials have received considerable attention given that their structural versatility for applications including catalysis, separation, and nanomedicine [125]. Specifically, mesoporous SBA-15 and MCM-41 have been widely researched for the catalytic steam reforming technology [126]. Both materials are two-dimensional hexagonal pore arrangements of uniform cylindrical mesopores [127], however, SBA-15 exhibit larger pore size and thick walls leading to high thermal stability when compared to MCM-41 [128].

Indeed, several studies have come to the conclusion that SBA-15 support lead to the best catalytic results ascribed to smaller particle size and high dispersion, strengthened metal-support interaction, sintering resistance and less carbon deposition derived from smaller particles size [127, 129-131].

Synthesis of SBA-15 material was described for first time in 1998 by Zhao et al. [132], prepared in acid media at low temperature and under hydrothermal conditions. The synthesis procedure requires a non-ionic block copolymer comprised of hydrophilic (polyethylene oxide) and hydrophobic (polypropylene oxide) units as a structure directing agent (surfactant) and a silica precursor (tetraethyl orthosilicate or tetramethyl orthosilicate). Synthesis of SBA-15 involves the surfactant dissolution in acidic media followed by addition of silica source. The development of micellar structures from the surfactant allow the interaction of ethylene oxide units with cationic silica species from the silica source leading to highly ordered hexagonal phases with mesoporous channels after the surfactant removal by its calcination as schematically represented in Figure 1. 4.

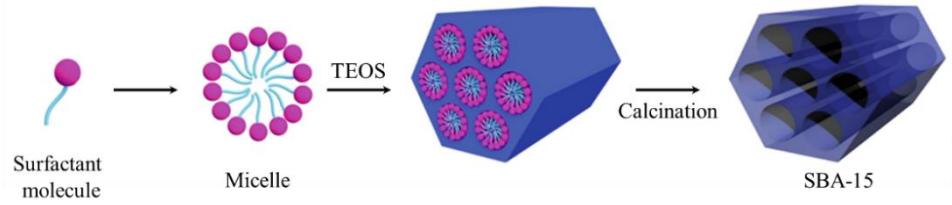

Figure 1. 4. Schematic representation of different stages during the SBA-15 synthesis (Adapted from [133]).

The synthesis conditions such as pH, block copolymer and hydrothermal temperature can be modified in a wide range, leading to different textural properties: mesopores size from 50 to 300 Å and pore wall thickness between 31- 64 Å [132]. Furthermore, as shown in Figure 1. 5, micropores are generated perpendicular to hexagonal channel, which penetrate the silica wall during synthesis. Micropososity is created from the more hydrophilic ethylene oxide chains of the surfactant, which make a way into the silica wall during synthesis and leave microporosity after calcination [134, 135].

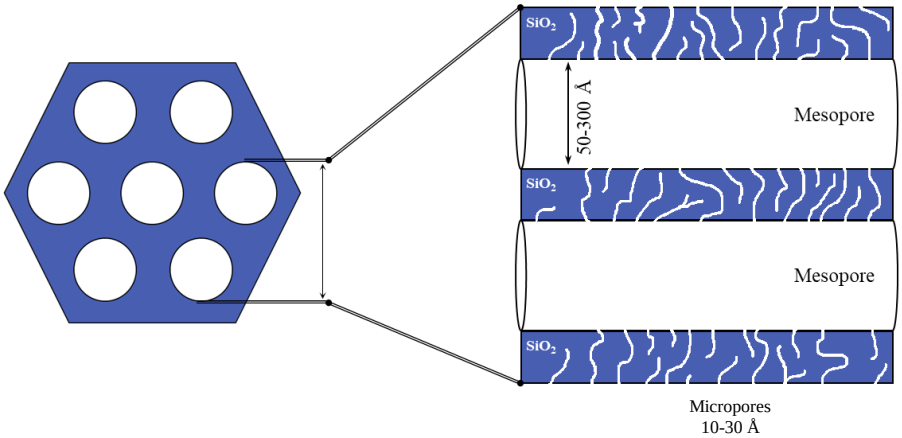

Figure 1. 5. Microporous and mesoporous structures of SBA-15 material.

1.3.2. Catalyst deactivation

The development of stable catalysts is a key point in the steam reforming reactions since they undergo severe deactivation. Regardless of the metal used as active phase and the support selected, stability is still one of the main challenges for steam

reforming catalysts design [90]. The mechanisms of catalyst deactivation can be divided into coke formation, metal sintering and metallic phase oxidation.

1.3.2.1. Coke formation

Coke formation during steam reforming might be considered one of the main cause catalyst deactivation [69-71]. Carbon deposition is typically derived from undesirable secondary reactions of the intermediates and products, whose formation is not only related with the nature of the catalyst but also to the reaction temperature [78, 90]. Coke formation leads to activity loss since active sites and/or pores are blocked [136]. Different reactions are proposed in literature to account for the coke formation: the Boudouard reaction ($2CO \leftrightarrow CO_2 + C$), methane decomposition ($CH_4 \leftrightarrow C + 2H_2$), reverse carbon gasification ($CO + H_2 \rightarrow H_2O + C$) or polymerization of oxygenates/hydrocarbons ($C_nH_mO_k \rightarrow$ polymers $\rightarrow$ coke) [71-73]. As mentioned above, the extent of these reactions is closely related to the reaction temperature. Whereas at lower temperatures (below 400 ºC) coke deposition by Boudouard reaction and reverse carbon gasification is favored, at higher temperatures (above 600 ºC) the promoted reaction is the methane decomposition [78, 90]. Different kind of carbon deposits can be formed depending on the active phase used and the reaction conditions. Sehested [137] reported the formation of different kinds of carbon deposits, amorphous or filamentous, with disparate roles in catalyst deactivation. Coke with amorphous structure has a greater impact on deactivation due to the encapsulation of the active metal sites [71, 138, 139]. When filamentous coke is formed, it covers the catalyst but the access of reactants to metal active sites may not be hindered. Accordingly, the deactivating effect of filamentous coke only becomes important when it blocks the access of reactants within the catalyst pores [71, 140, 141].

1.3.2.2. Metal sintering

Sintering is another deactivation mechanism that must be taken into account in the steam reforming reactions. Sintering is a thermally activated physical phenomenon wherein the active metallic nanoparticles agglomerate leading to a decrease in the

number of the surface active sites, thus lowering the activity [142-145]. The principal mechanisms of sintering on supported catalysts, represented in Figure 1. 6. A and B, are the atomic migration of smaller metal particles to larges particles, known as Ostwald ripening, and the small particle migration and coalescence to larger particles, respectively [136, 137, 145, 146]. Both mechanisms involve the formation of larger particles and, therefore, the decrease in the number of smaller particles.

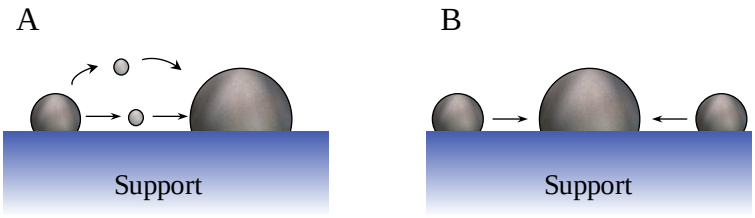

Figure 1. 6. Main mechanisms of metal sintering: (A) Ostwald ripening and (B) particle migration and coalescence (Adapted from [147]).

Several factors have been found to have influence on active metal sintering in steam reforming reactions such as high temperatures and high pressures of steam [137, 148]. The changes produced during sintering processes have been considered irreversible, being the original activity of the catalyst, nearly impossible to be restored [90, 149].

1.3.2.3. Metallic phase oxidation

Since metallic phase is the active one in steam reforming processes, its oxidation towards an inactive metal oxide is another phenomenon, which lead to a decrease in the catalytic activity. The presence of oxygen in partial oxidation or oxidative steam reforming, CO_2 in dry reforming [150, 151] and, to a lesser extent, steam in steam reforming, might result in the oxidation of the metallic species. Owing to the reduction capacity of hydrogen, present in the reaction medium, and since currently almost all reactions are carried out in an inert N_2-atmosphere, deactivation effect ascribe to the oxidation of the active phase is limited in the reforming reactions not being as serious as the deposition of coke and sintering [78].

2. Objectives and scope

As discussed in the Introduction section, besides the strong environmental effects, the fossil fuels are ever-dwindling supplies, thus, the development of new technologies towards renewable energy sources is crucial. Different technologies for hydrogen production from renewable and non-renewable sources have been described emphasizing in sustainable hydrogen production trough catalytic steam reforming of bio-oil aqueous fraction. Since this fraction usually present different and complex compositions depending on the feedstock used for its production, many authors work on steam reforming of model compounds. For this purpose, the development of suitable catalysts to achieve high hydrogen yields by minimizing its deactivation is required.

In this context, the present Doctoral Thesis, carried out in the Chemical and Environmental Engineering Group of Rey Juan Carlos University, is focused on the steam reforming of model bio-oil aqueous fractions using metal-supported mesostructured catalysts. Steam reforming is a complex process in which simultaneous reactions take place, therefore, the formation of undesirable secondary products such as coke is frequently, which can lead to the catalyst deactivation. Cobalt and nickel based catalysts have demonstrated good performance in steam reforming processes achieving similar results when compared to noble metal based catalysts. Co-based catalysts have been less reported although they also provide high activity at moderate temperatures and increases hydrogen yield. Thereby, the main scope of this work, is

the design of new Co-based catalysts supported over SBA-15, using promoters to improve the catalytic performance towards hydrogen and minimize their deactivation.

In order to achieve the main goal of this Thesis, the following specific objectives, which correspond with the different appendix included next, have been proposed:

I. **Effect of the incorporation of reducibility promoters on Co/CaSBA-15.** SBA-15 modification with Ca improves the metal dispersion but increases the reduction temperature of Co, therefore, this objective evaluates the incorporation of reducibility promoters giving rise to Co-M/CaSBA-15 (M: Cu, Ag and Ce) to improve the catalytic performance of Co/CaSBA-15 in the acetic acid steam reforming.

II. **Acetic acid steam reforming using bimetallic Co-M/SBA-15 (M: Cu, Ag, Cr, Ce).** This specific target studies the modification of Co/SBA-15 catalyst with the incorporation of a second metal leading to Co-M/SBA-15 (M: Cu, Ag, Ce and Cr) in order to improve the catalytic performance. For this purpose, acetic acid will be used as a model compound of the bio-oil aqueous fraction obtained from biomass.

III. **Preparation of agglomerated Co-Cr/SBA-15 catalysts for hydrogen production through acetic acid steam reforming.** The main goal of this objective is the preparation of Co-Cr/SBA-15 extrudates to be used in the acetic acid steam reforming as bio-oil aqueous fraction model compound. The bentonite content (binder) and particle size will be evaluated in order to achieve a suitable catalyst for it use in a steam reformer at industrial scale.

IV. **Study of coke formation in the steam reforming of bio-oil aqueous fractions.** The main purpose of this target is the establishment of the relationship between Co/SBA-15 catalysts deactivation during the steam reforming of model bio-oil aqueous fraction from biomass, by studying the evolution of coke deposition and Co sintering.

3. Experimental procedure

3.1. Materials

3.1.1. Chemicals

Chemical used during this scientific research, both solid and liquid, are summarized in Table 3. 1.

Table 3. 1. List of chemical used.

Chemical	Formula	Purity/ concentration	Provided by	Application
Clorhydric acid	HCl	35 wt.%	Scharlab	SBA-15 synthesis
Tetraethyl orthosilicate	$C_8H_{20}O_4Si$	98%	Aldrich	SBA-15 synthesis
Pluronic 123	triblock copolymer	-	Aldrich	SBA-15 synthesis
Calcium nitrate tetrahydrate	$Ca(NO_3)_2 \cdot 4\ H_2O$	99%	Aldrich	Catalysts preparation
Cobalt nitrate hexahydrate	$Co(NO_3)_2 \cdot 6H_2O$	99%	Aldrich	Catalysts preparation
Copper nitrate trihydrate	$Cu(NO_3)_2 \cdot 3H_2O$	99%	Aldrich	Catalysts preparation
Silver nitrate	$AgNO_3$	99%	Aldrich	Catalysts preparation
Cerium nitrate hexahydrate	$Ce(NO_3)_3 \cdot 6H_2O$	99%	Aldrich	Catalysts preparation
Chromium nitrate nonahydrate	$Cr(NO_3)_3 \cdot 9H_2O$	99%	Aldrich	Catalysts preparation
Hydrofluoric acid	HF	48%	Scharlab	ICP analysis
Sulfuric acid	H_2SO_4	95-98%	Scharlab	ICP analysis
Acetic acid glacial	$C_2H_4O_2$	99%	Scharlab	Steam reforming reaction
Hydroxyacetone	$C_3H_6O_2$	95%	Alfa aesar	Steam reforming reaction
Phenol	C_6H_6O	99,5%	Aldrich	Steam reforming reaction
Acetone	C_3H_6O	99%	Aldrich	GC calibration
Ethanol	C_2H_6O	99,9%	Scharlab	GC calibration
Acetaldehyde	C_2H_4O	99,5%	Fluka	GC calibration
1,4 butanediol	$C_4H_{10}O_2$	99%	Aldrich	GC standard

3.1.2. Gases

Table 3. 2 displays a list of gases used, as well as their purity and specific application.

Table 3. 2. List of gases used.

Gas	Purity/ concentration	Provided by	Application
Ar	99,998%	Praxair	Carrier gas
He	99,996%	Praxair	Carrier gas
H_2	99,998%	Praxair	Catalyst reduction
N_2	99,999%	Air Liquide	Diluent
H_2-Ar	10.03% H_2 - 89.97% Ar	Air Liquide	TPR analysis
Mixture	20% C_2H_4, 10% C_2H_6, 20% CO, 30% CO_2,	Air Liquide	GC calibration
Air	100%	Praxair	TGA

3.2. Catalysts preparation

3.2.1. Synthesis of mesoporous SBA-15 material

SBA-15 used as the support was synthetized according the hydrothermal method described elsewhere [132] using Poly(ethylene glycol)-block-poly(propylene glycol)-block-poly(ethylene glycol), Pluronic 123, as non-ionic structure directing agent. A typical synthesis is schematized in Figure 3. 1.

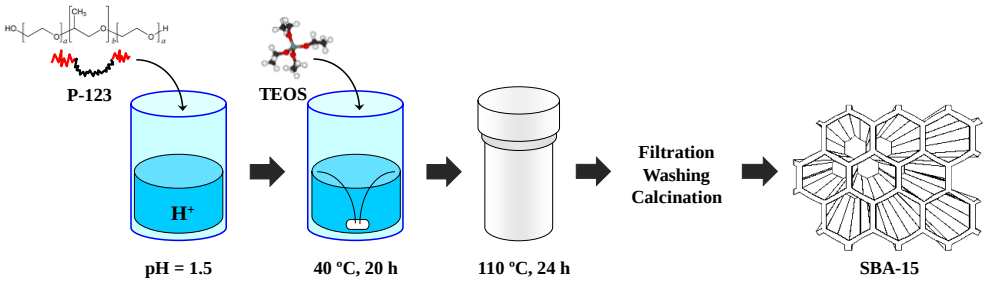

Figure 3. 1. Schematic synthesis of mesostructured SBA-15 material

4 g of Pluronic 123 are dissolved in 125 mL of HCL solution (1.9 M) under stirring at room temperature. Subsequently, 8.6 g of tetraethyl orthosilicate (TEOS) as silica

source is added at 40 ºC. Then, this aqueous solution of triblock copolymer and TEOS is kept under stirring conditions for 20 h for aging. In this period, the silica polymerization over the micelles formed by the surfactant takes place, leading to the ordered mesoporous structure typical for SBA-15. After that, the mixture is aged at 110 ºC for 24 h under autogenous pressure, thus, consolidating the mesoporous structure and providing greater thermal and mechanical resistance. Finally, the solid is recovered by filtration, washed with deionized water and dried first in air at room temperature overnight and then calcined in air to remove the templates at 550 ºC for 5 h with a heating ramp of 1.8 ºC/min. The latter step of the template removal is one of the crucial aspects in the synthesis of ordered mesoporous, because the procedure employed during calcination influenced the final textural properties of SBA-15 material [152].

3.2.2. Support modification with Ca

The incorporation of Ca as a doping agent in the SBA-15 material used as support, is carried out following the incipient wetness impregnation method, using calcium nitrate tetra-hydrate ($Ca(NO_3)_2 \cdot 4\ H_2O$) as precursor. Incipient wetness impregnation method is the simplest procedure for dispersing a catalytic species on a carrier by impregnating the support to incipient wetness with an aqueous or non-aqueous solution, which contain a salt precursor of the catalytic element/s.

Specifically, SBA-15 modification with calcium is performed by adding dropwise on the calcined support, which is previously outgassed for 30 min, the corresponding volume of the calcium nitrate aqueous solution equal to the catalysts pore volume, determined by N_2-physisorption as discussed in section 3.3.1. Subsequently, the solid is kept under vacuum for 4 h. In this way, the precise amount of catalytic species is assured to be present in the carrier. Finally, the Ca-modified support is calcined for 5 hours with a heating ramp of 1.8 ° C/min at 550 ºC, the appropriate temperature to assure the elimination of the nitrates groups from the precursor, according to the thermogravimetric analysis results.

3.2.3. Synthesis of the supported catalysts

Both, Co as the active phase and promoters (Cu, Ag, Ce or Cr) incorporation over SBA-15 or CaSBA-15 supports is accomplished by the incipient wetness impregnation method using mixed aqueous solutions of the corresponding nitrates: $Co(NO_3)_2 \cdot 6H_2O$ and $Cu(NO_3)_2 \cdot 3H_2O$, $AgNO_3$, $Ce(NO_3)_3 \cdot 6H_2O$, $Cr(NO_3)_3 \cdot 9H_2O$. The procedure is the same as that described above (section 3.2.2.).

3.3. Catalysts characterization

3.3.1. N_2 adsorption-desorption at 77 K

The textural properties of the catalysts were acquired by means of N_2 adsorption-desorption at 77 K on a Micromeritics Tristar 3000 sorptometer. Prior to the analysis samples were outgassed under vacuum at 200 °C for 4 h to clean de surface of the support (ambient components adsorbed).

In general, physisorption is a phenomenon that occurs whenever an adsorbable gas (the adsorptive) is brought into contact with the surface of a solid (the adsorbent). The shape of gas adsorption curve and hysteresis loop depend on the pore structures of the adsorbent and the gas-solid interaction. The adsorption isotherm is the relationship, between the amount of adsorbed with the upward equilibrium pressure (expressed as relative pressure P/P_0) of the adsorbable gas at isothermal conditions, whereas desorption isotherm is obtained at downward equilibrium pressure. When the adsorption and desorption curves do not coincide, a hysteresis loop arises generally associated with capillary condensation. Thus, physisorption can be divided into three different stages. (i) Monolayer adsorption, all the adsorbed molecules are in close contact with the surface of the adsorbent. (ii) Multilayer adsorption, not all the adsorbed molecules are in direct contact with the adsorbent surface, followed by capillary condensation in mesopores. (iii) Capillary condensation, phenomenon whereby a gas condenses to a liquid-like phase in a pore at pressure (P) less than the saturation pressure (P_0) of the liquid [153].

The specific surface area is estimated by means of Brunauer-Emmett-Teller (BET) method [154] applied to the nitrogen adsorption branch. Conversely, for the estimation of the pore size the Barret-Joyner-Halanda method (BJH) [155] is used, assuming a cylindrical pore geometry.

Figure 3. 2A shows the nitrogen adsorption-desorption isotherm of the SBA-15 material. This material presents a type IV isotherm, typical for mesoporous materials, with a H1-type hysteresis loop, stating a narrow range of uniform mesopores, according to the IUPAC classification. Meanwhile, Figure 3. 2B shows the pore size distribution according to the BJH method.

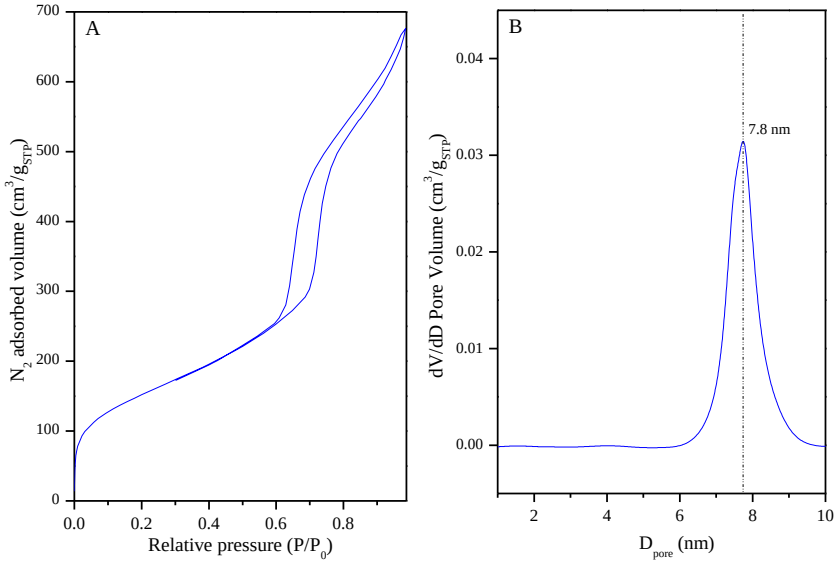

Figure 3. 2. (A) N_2 adsorption-desorption isotherm at 77 K; (B) pore size distribution of SBA-15 material.

3.3.2. Inductively coupled plasma atomic emission spectroscopy (ICP-AES)

For determining the chemical composition of the synthetized material, inductively coupled plasma atomic absorption spectroscopy analysis is used. This technique for the quantitative determination of elemental compositions [156], is used for the determination of the weight percent of each element present in the catalyst: Co, Ca,

Cu, Ag, Ce or Cr. The analyses were carried out by using a Varian a Vista-Pro AX CCD-Simultaneous ICP-AES spectrophotometer. Prior to the analysis, the sample is treated by acidic digestion with sulphuric and fluorhydric acids to dissolve the support and obtain metallic solutions. Afterwards, the solution is diluted in ultrapure Milli-Q water.

The basis of this technique is the excitation of metal atoms using an Ar plasma capable of reaching 10000 K ensuring the complete atomization of the liquid sample. When the excited atoms return to their fundamental energy state, radiation is emitted. The intensity of this radiation depends on the amount of metal atoms present in the liquid solution. For the metal quantification, calibration curves corresponding to each metal in the appropriate concentration range is required. For this purpose, a 1000-ppm standard solution in nitric acid of each metal is used.

3.3.3. X-ray diffraction (XRD)

XRD measurements can give information about the supports porous mesostructure, crystalline phase and crystallite size [157]. XRD patterns were acquired on a Phillips X'pert PRO diffractometer using Cu Kα radiation, a 2θ increment step of 0.02º and a collection time of 2 s. The identification of the crystalline phase is done by comparing the obtained diffractograms with those patterns of the Joint Committee on Powder Diffraction Standards (JCPDS) database.

X-rays is electromagnetic radiation with wavelengths in the range of 0.01 to 10 nanometers with energies in the range 100 eV to 100 keV. When the geometry of the incident X-ray beam that impact the sample satisfies the Bragg equation, constructive interference occurs and a peak is observed in the recorded scattered radiation according to:

$$n \cdot \lambda = 2 \cdot d_{hkl} \cdot \text{sen}\ \theta$$

where n is a natural number, λ is the wavelength of the incident wave, d_{hkl} the interplanar distance, characteristic of each diffraction plane with the corresponding

Miller index (h, k, l) and θ is the scattering angle of the X-ray beam. By using the Scherrer equation to the characteristic peaks, it is possible to determine the mean crystallite size (D_{hkl}) [158]. The equation is:

$$\beta = \frac{0.9 \cdot \lambda}{D_{hkl} \cdot \cos\theta}$$

where β is the full peak width at half of the maximum of intensity of the desired hkl plane, λ is the x-ray wavelength and θ is the angle of Bragg diffraction peak.

As an example, Figure 3. 3A displays the small angle XRD pattern of SBA-15 material, showing a the characteristic pattern of the hexagonal pore mesostructure of SBA-15, constituted by three well resolved diffraction peaks attributed to the planes indexed to (100), (110) and (200). While in Figure 3. 3B the represented XRD pattern is for Co-supported SBA-15, in which a wide peak between 20 and 30° attributed to the amorphous silica forming the walls of the support pores and peaks at 2θ = 31.4, 37.1 45.1, 59.7 and 65.3º corresponding to cubic Co_3O_4 (JCPDS 01-071-4921) can be distinguished.

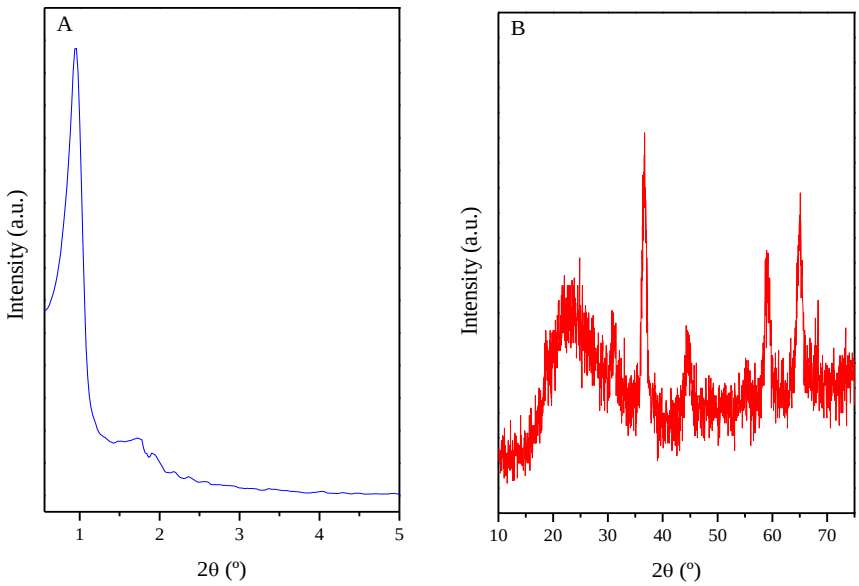

Figure 3. 3. (A) Small angle XRD pattern of mesoporous SBA-15 material; (B) XRD pattern of Co/SBA-15.

3.3.4. Temperature programmed reduction (H_2-TPR)

Temperature programmed reduction is an experimental technique for the characterization of heterogeneous catalysts, which gives information about their metal phase reducibility and information about the metal-support interactions. This technique allows the study of the reduction process of an oxidized sample, which is subjected to a programmed temperature ramp, while exposed to a reducing gas mixture (typically H_2 mixed with an inert gas). Thus, the reduction of a metal oxide by hydrogen to form metal and water vapor take place. This process can generally be described by the following reaction:

$$MO_x + xH_2 \rightarrow M^0 + xH_2O$$

To carry out the analysis, a Micromeritics AutoChem 2910 analyser was used. Experimentally, the sample is paced in a fixed-bed quartz tube under 10% H_2 in argon flow (35 mL/min) with a 5 ºC/min heating ramp from ambient temperature to 980 ºC. Effluent gas is forced to flow through a cold trap to remove water produced before reaching the thermal conductivity detector (TCD). Samples were previously degasified under dry argon flow (35 mL/min) at 110 ºC for 30 min with a heating rate of 15 ºC/min.

The reduction rate of the sample is online measured by monitoring the composition of the reducing gas mixture at the outlet of the quartz reactor. As the gas flow is constant during the experiment, the changes in hydrogen concentration lead to the emergence of reduction peaks. The interpretation of the TPR profile allows the identification of the maximum reduction temperatures, number of reduction peaks and hydrogen consumption from which the degree of reduction can be determined. In this sense, in Figure 3. 4 the reduction profile of Co/SBA-15 catalyst is represented.

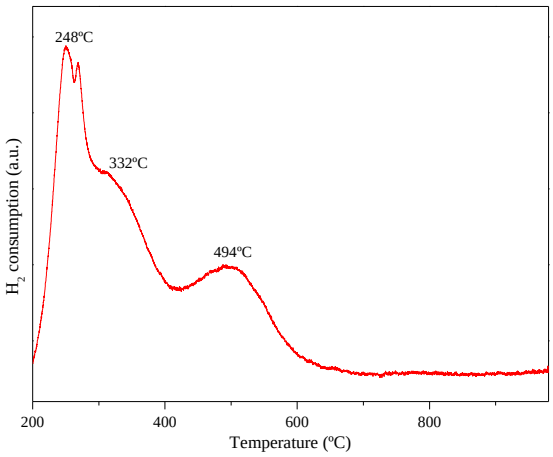

Figure 3. 4. Hydrogen temperature programmed reduction analysis of Co/SBA-15 catalyst.

As it can be observed, three main reduction stages can be stated according to three maxima at 248, 332 and 494 ºC. The maximum located at highest temperature, 494 ºC, is not only related to the maximum reduction temperature, but also those cobalt particles, which have greater interaction with the support.

3.3.5. Electron microscopy techniques

In heterogeneous catalysis, the surface structures of catalysts and supports are of particular interest. In this sense, electron microscopy techniques such as scanning electron microscopy (SEM) and transmission electron microscopy (TEM) provide information about the catalyst morphology, chemical composition and structure, by detecting characteristic X-ray produced in the interaction of the electrons with matter. While in TEM primary electron beam of high energy and high intensity (80-300 keV) are used, in SEM, these electrons are mainly secondary (or backscattered) with low energy (~50 eV) [159, 160]. Due to the low energy, these electrons can only escape from the surface of the sample and, therefore, provide information about the surface morphology. TEM uses transmitted electrons, which are passing through the sample to create an image (micrograph). In this way, information at nanoscale can be obtained.

Whereas SEM was performed on a Phillips XL30 Environmental Scanning Electron Microscope equipped with a tungsten filament and an accelerating voltage of 15 kV,

TEM micrographs were obtained using a 200 kV JEOL JEM 2100 microscope with a resolution of 0.25 nm at the National Centre for Electron Microscopy (CNME, Complutense University of Madrid, Madrid, Spain) or a 200 kV Philips TECNAI 20 microscope with a resolution of 0.28 nm at Technology Support Centre (CAT, Rey Juan Carlos University, Móstoles, Spain). Samples preparation involve their suspension in acetone and subsequently deposition on a carbon-coated copper grid (nickel grid for Cu-based samples). Both equipments are equipped with energy dispersive X-ray spectroscopy (EDS/EDX), which can help to analyse the local chemical composition of materials.

Figure 3. 5A shows a TEM micrograph of a calcined Co-Cr catalyst supported over SBA-15, in which metal particles as round dark particles and the distribution of well-ordered channels, typical for SBA-15 material, can be distinguished. Conversely, Figure 3. 5B shows a SEM image, in which the external surface of an agglomerated particle of Co-Cr/SBA-15 catalyst is displayed.

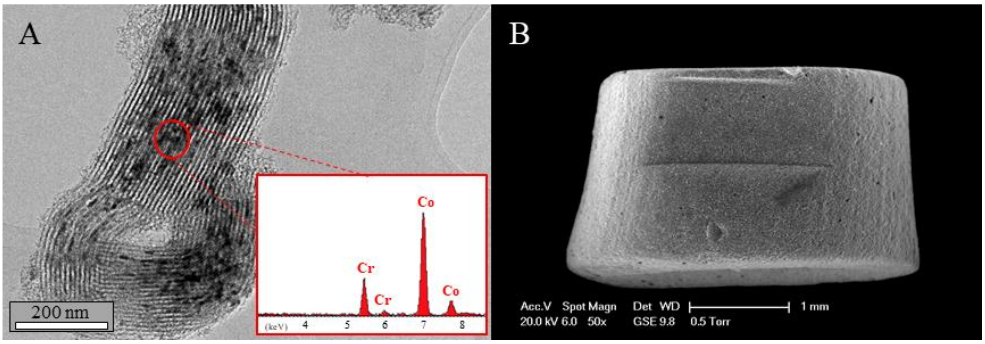

Figure 3. 5. (A) TEM micrograph of calcined Co-Cr/SBA-15; (B) SEM image of agglomerated Co-Cr/SBA-15

3.3.6. Thermogravimetric analysis (TGA)

Thermogravimetric analysis is used not only to determine the calcination temperature of the prepared supports/catalysts, but also to quantify the amount of coke deposited after the steam reforming reaction. This technique, measures weight changes of a sample when it is subjected to a controlled heating ramp under a controlled gas

atmosphere. Under these conditions, an analysis gas passes through the sample reacting with the solid leading to a weight variation. The reduction in sample weight is usually attributed to release of by-product produced in the reaction. Furthermore, using the derivative of the weight loss curve (DTG) a clear identification of different stages at different temperatures along the decomposition can be stated.

Measurements were performed in airflow with a heating rate of 5 °C/min up to 1000 °C using a TA Instruments SDT 2960 thermobalance. Figure 3. 6 displays the obtained results for a used Co/SBA-15 catalyst in the acetic acid steam reforming after 5 h time-on-steam

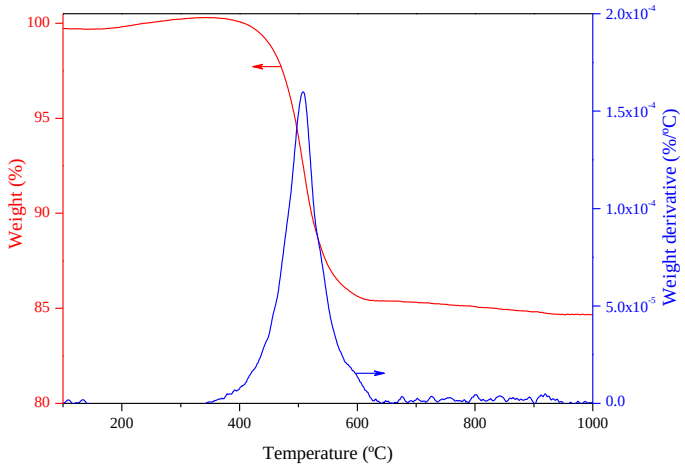

Figure 3. 6. Thermogravimetric analysis of Co/SBA-15 used in acetic acid steam reforming

3.3.7. Carbon-hydrogen-nitrogen-analysis (CHN)

CHN is a chemical standard method for quantification analysis C, N and H. The setup will combust and oxidize the sample into simple compounds (CO_2, H_2O, NO_x and CO_x), being subsequently detected with a thermal conductivity detector (TCD) which will generate a signal proportional to the concentration of the individual components. This technique is used to determine the nature of carbon deposits after the reforming reaction. Carbon-to-hydrogen ratio is an useful relationship that will indicate whether

the coke is more aromatic or more aliphatic, since higher carbon-to-hydrogen ratio is associated to more aromatic or condensed structures [74, 161].

The measurements were performed on an elemental analyser type Flash 2000 provided by Thermo Fisher Scientific equipped with a thermal conductivity detector (TCD) using sulphanilic acid as standard.

3.3.8. Raman spectroscopy

Raman spectroscopy is a technique that provides chemical and structural information about different materials. It relies on inelastic or Raman scattering of a monochromatic radiation beam (usually a laser beam) on interaction with the sample. The scattered laser beam gives information about the vibrational modes of the chemical bonds present in the sample [162]. Raman spectroscopy is used for the analysis of carbon deposits in the spent catalysts after the steam reforming reactions. Carbon-based samples usually have two main bands centred on ~1350 and ~1580 cm^{-1} associated with D-band and G-band, respectively. D-band is related to the carbon atoms vibration of disordered aromatic structures such as amorphous or defective filamentous carbon [115, 163], whereas G-band is ascribed to condensed graphitic aromatic structures such as graphite layer [164]. The intensity of the D band relative to the G band can be used as a qualitative measure of the formation of carbon with different degree of graphitization or disorder in the carbon structure [115, 162].

Raman spectra were recorded using a JASCO NRS-5000/7000 series Raman spectrometer. For illustration purposes, Figure *3. 7* displays a Raman spectrum of used Co/SBA-15 in acetic acid steam reforming.

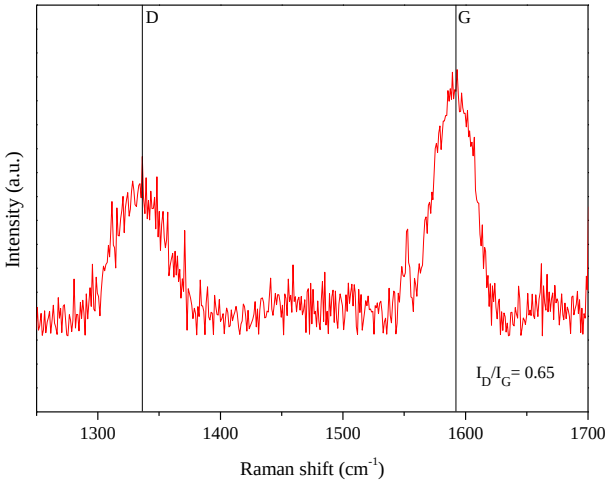

Figure 3. 7. Raman spectrum of used Co/SBA-15 in acetic acid steam reforming.

3.3.9. X-ray photoelectron spectroscopy (XPS)

X-ray photoelectron spectroscopy is a chemical characterization technique used for on the surface of solids. This technique is surface-sensitive quantitative spectroscopic that measures the electronic state of the elements present in the catalyst formulation. Is based in the photoelectric effect, in which electron spectra are recorder by irradiating a material with a beam of X-rays.

XPS spectra were recorded on an XPS Physical Electronics PHI 5700 spectrometer using non-monochromatic Al-Kα radiation (300 W, 15 kV and 1486.6 eV). Binding energy values were referenced to carbon C1s peak (284.8 eV). Figure 3. 8 shows the narrow scan spectra of the Co 2p region, in which two major binding energy features can be distinguished around 778-781 and 794 eV, assigned to Co $2p_{3/2}$ and Co $2p_{1/2}$, respectively. According to literature, peaks centred at 778 eV reveal the presence of Co^0, while peaks centred at 781 eV are characteristic of Co^{2+} [165, 166].

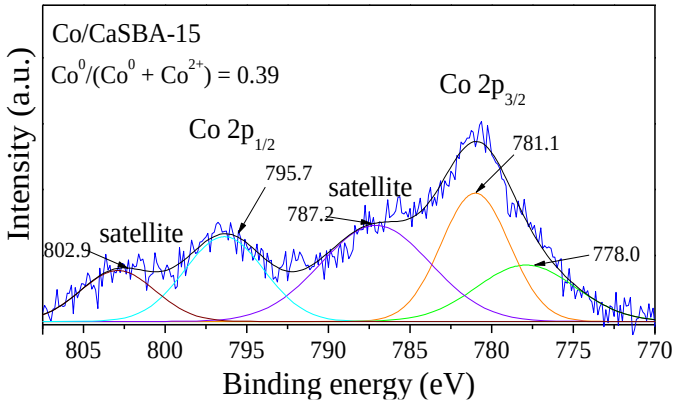

Figure 3. 8. Co 2p XPS of reduced of reduced Co/CaSBA-15 at 700ºC.

3.4. Catalytic tests

3.4.1. Experimental set-up

The experimental set-up for hydrogen production through catalytic steam reforming is shown in Figure 3. 9. The reaction system is a Microactivity-PRO unit (PID Eng&Tech. S.L.) controlled by means of Adkir software, and, connected with an online micro-GC for the analysis of the outlet gas stream.

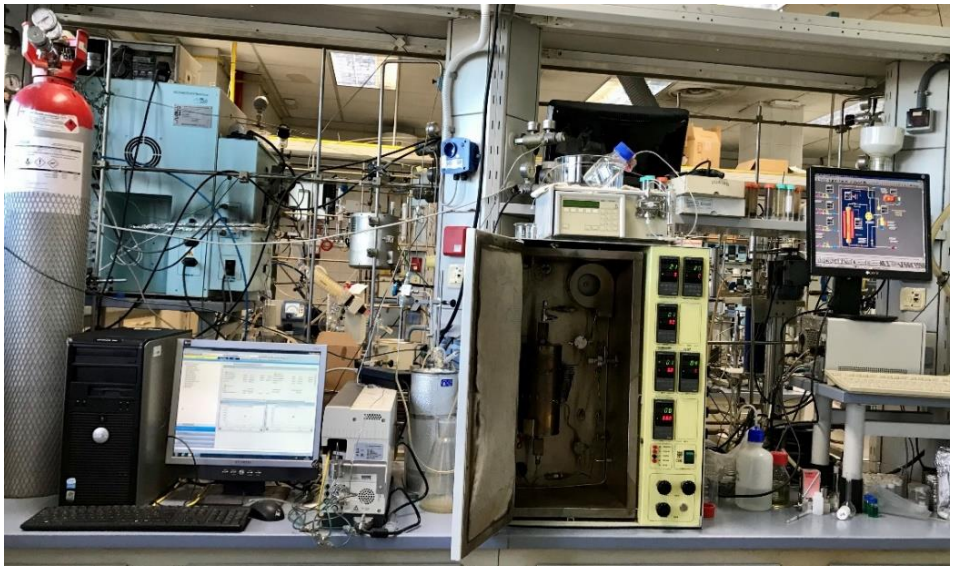

Figure 3. 9. Image of the experimental set-up.

The schematic diagram of the Microactivity-PRO unit is displayed in Figure 3. 10. The reaction system consists of a fixed-bed tubular reactor (1) in stainless steel 316 (i.d. = 9.2 mm, L = 300 mm), with the catalyst bed placed inside upon a porous plate. The reactor is located inside an electric oven (2), where temperature in the catalytic bed was measured by means of a K-thermocouple.

The gases are fed into the reactor by means of a system of Hi-Tec Bronkhorst mass flow controllers (3) that provide a known and controlled flow of gases. Conversely, liquids are dosed by means of a GILSON 307 HPLC alternative positive displacement pump (4). Liquid and gaseous flows are introduced into the hotbox system (5), which has one heater's forced flow (6) to maintain the temperature at 200 °C to prevent condensation in the pipes and to preheat the reactants. Once the gases have been preheated and liquids evaporated, these streams merge and flow to a 6-port valve (7) that allows two different positions: reaction or by-pass. The flow inside the reactor is up-down, whereby the reactant mixture is fed through the upper part of the reactor and the reaction products are obtained through the lower part. Products are conducted towards a liquid-gas separator (8), refrigerated by Peltier effect, that allows the condensation of liquids at low temperature separating them from the gas stream, which is reintroduced into the hot box and directed to the analysis system.

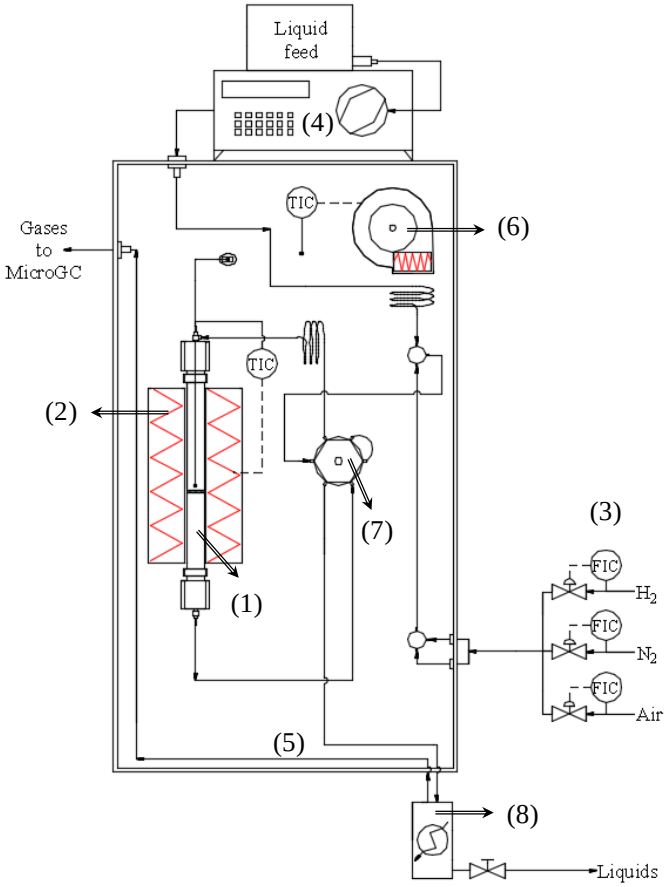

Figure 3. 10. Schematic diagram of the Microactivity-PRO unit adapted from [116].

3.4.2. Steam reforming reactions

Before the catalytic tests, the activation of the catalyst is performed to reduce the metal active phase to ground state. For this purpose, the required amount of catalyst is place upon the porous plate of the reactor. Afterwards, pure hydrogen (30 mL/min) is flowed up to 700 °C for 6.5 h with a heating rate of 2 °C/min. Then, the gas flow is changed to nitrogen in order to purge the reactor while the reaction temperature is reached. The reactions were carried out isothermally at 600 ºC and under atmospheric pressure in a fixed bed reactor as described in section 3.4.1, using N_2 as carrier gas and internal standard for the gas stream analysis. The steam-to-carbon molar ratio was fixed to

double the stoichiometric value in all cases with the exception of phenol due to its low solubility in water (S/C = 8).

During the tests, the analysis of the outlet steams at different times is performed. For example, in the case of reactions at 5 h time-on-stream, both gas and liquid streams are analysed at 15 min and every hour (1, 2, 3, 4 and 5 h). Before analysing the gas stream, its flow rate is measured in a manual bubble flow meter. After this, the condensable products are recovered from the liquid-gas separator and subsequently analysed in a gas chromatograph.

Finally, the amount of carbon deposited on the spent catalysts is evaluated by means of thermogravimetric analysis as described in section 3.3.6.

3.4.3. Products analysis

3.4.3.1. Gas products

Outlet gas stream composition is measured online using an Agilent 490 Micro-GC equipped with a PoraPlot U column (10 m) and a Molecular Sieve 5A column (20 m) using He and Ar as carrier gas, respectively. The injector has a built-in 10 µL sample loop that is filled with the gaseous sample. In the PoraPlot U column is possible to separate compounds such as CO_2, C_2H_4 and C_2H_6, while H_2, N_2, CH_4 and CO are separated in the other column. To avoid the presence of condensable vapors and solid particles in the capillary columns, a Genie filter is installed before them. For the gas detection, a thermal conductivity detector (TCD) is used at 120 ºC. To carry out the identification and quantification of each component from the gas phase, it is mandatory a pre-calibration. For this, a calibration bottle with known concentrations of the different gases was used (20% C_2H_4, 10% C_2H_6, 20% CO, 30% CO_2, and 20% CH_4).

This equipment allows immediate and continuous analytical analysis by means of the Open Lab CDS Chem Station software. In Figure 3. 11 there is an example of the chromatograms obtained for the gas stream.

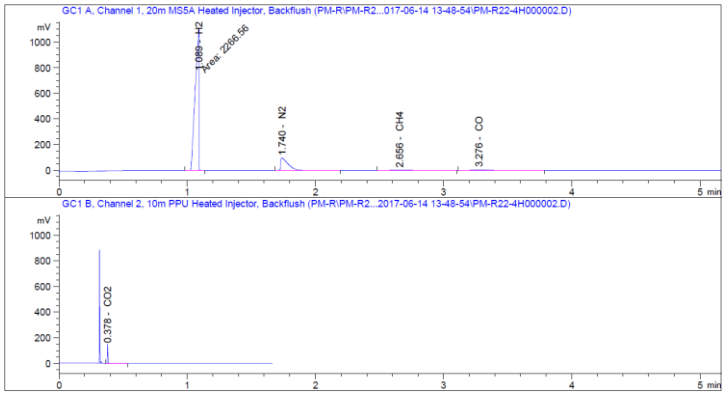

Figure 3. 11. Gas stream chromatogram using Open Lab CDS Chem Station software.

3.4.3.1. Liquid products

Condensable vapors are trapped in the liquid-gas separator and periodically recovered. For the analysis, the liquid samples are previously diluted in 1,4 butanediol, which also acts as internal standard. The preparation is done by weighing around 0.05 g of 1,4 butanediol and 0.3 g of liquid sample and subsequently analysed in a Varian CP-3900 chromatograph equipped with a CP-WAX 52CB column (30 m × 0.25 mm, DF = 0.25). For each analysis, 1 µL is injected by means of a 10 µL Agilent Syringe. For the detection of the different compounds present, a flame ionization detector (FID) is used. The main parameters and the heating ramp used in the chromatographic method are displayed in Figure 3. 12.

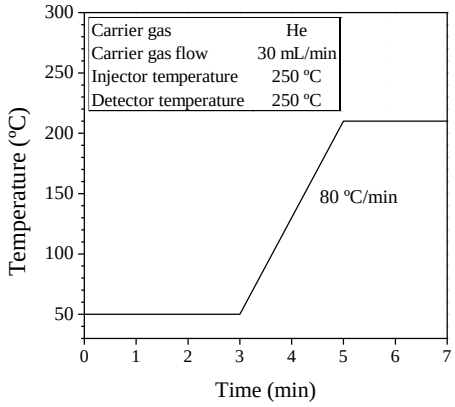

Figure 3. 12. Main parameters and heating ramp of the chromatographic method for the liquid sample analysis.

The recording of chromatograms and the measurement of the size of response peaks was done using the Star Chromatography Workstation 6.41 software. This software allows the identification and calculation of the different ratios between components based on retention times and the corresponding area of each peak. In Figure 3. 13, a chromatogram is shown in a representative way, recorded from a liquid sample analysis after acetic acid steam reforming. In order to quantify different compounds, present in the liquid sample after the steam reforming tests, a previous calibration is required, which will allow to calculate their concentration in the sample.

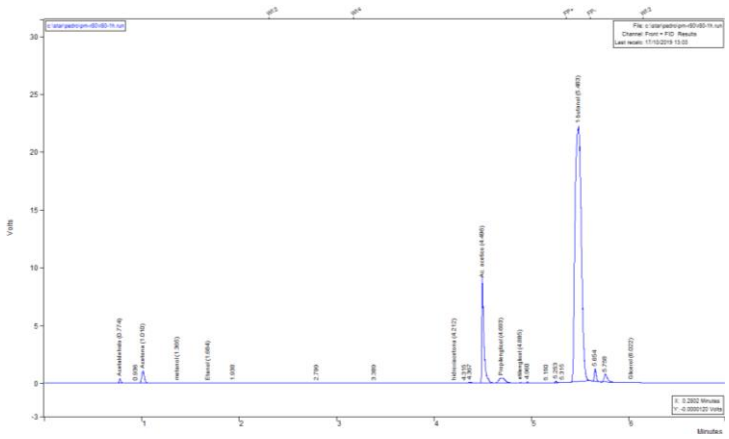

Figure 3. 13. Chromatogram obtained in the analysis of a liquid sample.

4. Results and Discussion

4.1. Effect of the incorporation of reducibility promoters on Co/CaSBA-15.

The results obtained in this chapter are discussed in detail in Article 1. The results provided in this work highlight the necessity of combining both dispersing additives and promoters of reducibility to improve the catalytic properties.

In this section, the effect of Ca addition to Co/SBA-15 in the acetic acid steam reforming is for first time studied. After the addition of calcium to the SBA-15 used as support, the overall ordered mesoporous structure of the initial material was maintained despite it decreased the BET surface area. This fact was verified from the N_2 adsorption-desorption isotherms which described a type IV isotherm with a H1-type hysteresis loop according to IUPAC classification, as well as from TEM micrographs, typical for SBA-15 material. When comparing the catalyst properties of Co/SBA-15 and Co/CaSBA-15, Ca addition led to a decrease in the crystallite size of Co species over the support at the expense of the reduction temperature, which was shifted towards higher temperatures due to higher interaction between the active phase and the support or to the development of new Ca-Co compound. This led to a decrease in the ratio of Co reduced species in the activated catalysts as demonstrated by XPS (Figure 4. 1).

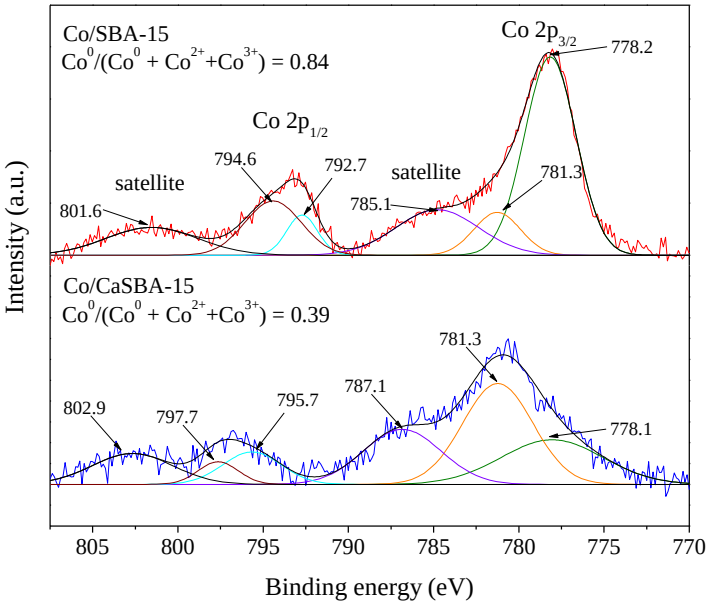

Figure 4. 1. Co 2p XPS of Co/SBA-15 and Co/CaSBA-15 samples reduced at 700 ºC.

This detrimental effect was traduced in lower conversion and hydrogen selectivity, and higher coke deposition when compared with Co/SBA-15 catalyst. The above results are the basis for the addition of reducibility promoters, such as Cu, Ag and Ce to Co/CaSBA-15 in order to keep its better metallic dispersion and metal-support interaction but increasing its reducibility to address the worse catalytic performance in the acetic acid steam reforming. As regard from Figure 4. 2, the addition of Cu, Ag and Ce as promoters, improved in terms of reduction temperature the reducibility of Co/CaSBA-15. This effect was more significant with the addition of Cu and Ce, which significantly shifted to lower reduction temperatures most of the area, being this effect more pronounced for Co-Ce/CaSBA-15 sample. On the basis of the reduction degree estimated by H_2-TPR analysis, XPS spectra of Co/CaSBA-15 and Co-Ce/CaSBA-15 were compared in Co 2p region. The $Co^0/(Co^0 + Co^{2+})$ ratio obtained for the activated Co-Ce/CaSBA-15 increases up to 0.76, reaching values close to those obtained with Co/SBA-15.

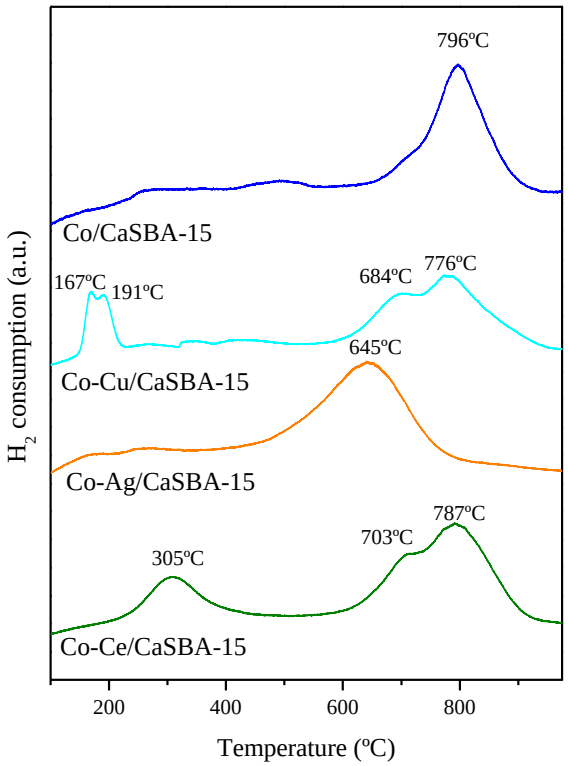

Figure 4. 2. H_2-TPR profiles for Co-(Cu, Ag or Ce)/CaSBA-15 samples.

The catalytic results, displayed in Figure 4. 3A show how the incorporation of reducibility promoters improved the acetic acid conversion, being for Co-Ce/CaSBA-15 the highest value. On the other hand, attending to hydrogen yield (Figure 4. 3B), Ag and Ce addition led to higher hydrogen yield, which is the main product of this reaction, while Cu-promoted sample reached slightly lower hydrogen yield than the unpromoted sample, ascribed to the participation of Cu in the decarboxylation reaction of acetic acid rather than the reforming reaction [167]. The most noticeable increase in H_2 yield was found by using Ce as promoter, achieving values very close to the thermodynamic one, estimated at the same reaction conditions. This effect is ascribed not only to the lowest Co particle size and the improvement in the reducibility, but also due to the fact that the presence of Ce creates more oxygen vacancies, facilitating the improvement of oxygen mobility [168] leading to the best catalytic performance.

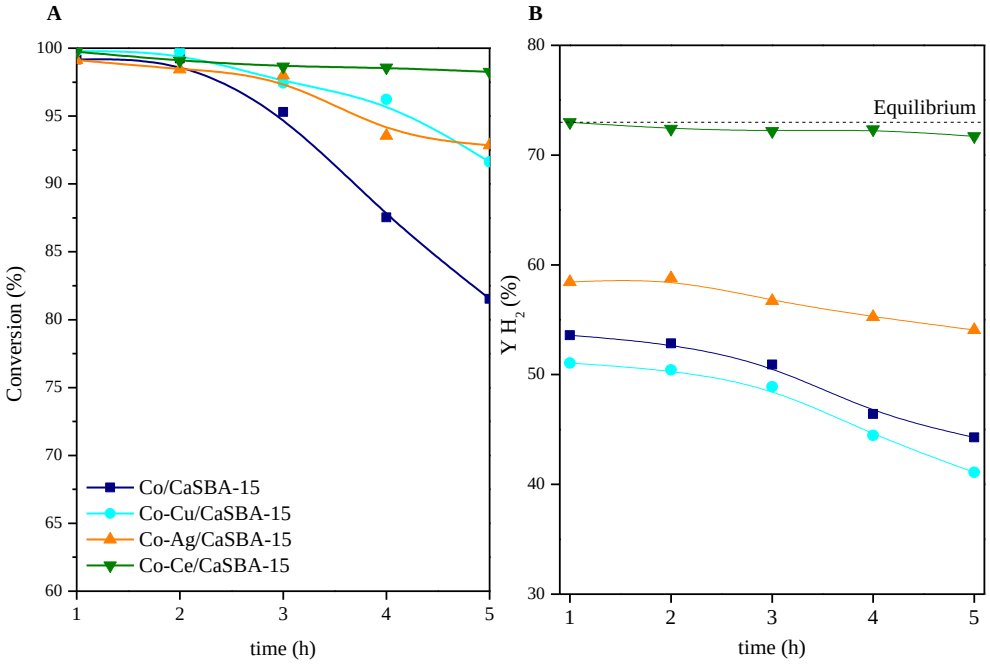

Figure 4. 3. Catalytic results for Co-M/CaSBA-15 (M: Cu, Ag or Ce) with TOS at 600ºC, WHSV=30.1h^{-1}.

4.2. Acetic acid steam reforming using bimetallic Co-M/SBA-15 (M: Cu, Ag, Cr, Ce).

The results obtained in this chapter are further discussed in Article 2. This manuscript, analyses the effect of promoter incorporation on Co/SBA-15 catalysis to be tested in acetic acid steam reforming. In this regard, Co/SBA-15 was modified with Cu, Ag, Ce and Cr, leading to Co-M/SBA-15 catalysts. All the prepared catalysts were characterized by different techniques. In Table 4. 1 the main physicochemical properties are summarized. As it can be observed from this table, depending on the promoter used, different physicochemical properties were obtained.

Table 4. 1. Physicochemical properties of Co-M/SBA-15 (M: Cu, Ag, Ce, Cr) catalysts.

Catalyst	Co[a] (wt.%)	M[a] (wt.%)	S_{BET} ($m^2 \cdot g^{-1}$)	D_{pore} [b] (nm)	V_{pore} [c] ($cm^3 \cdot g^{-1}$)	D_{Co^0} [d] (nm)	Dispersion (%) [e]
SBA-15	-	-	550	7.5	0.97	-	-
Co/SBA-15	6.4	-	503	7.2	0.83	9.5	7.5
Co-Cu/SBA-15	6.5	2.0	476	7.2	0.79	9.7	6.3
Co-Ag/SBA-15	6.4	1.6	419	6.9	0.71	12.3	3.9
Co-Ce/SBA-15	6.6	1.7	494	7.4	0.84	9.6	6.5
Co-Cr/SBA-15	6.8	1.8	469	7.1	0.81	7.2	9.9

[a] Determined by ICP-AES (M: Cu, Ag, Ce or Cr) in reduced samples, [b] BJH desorption average pore diameter, [c] Measured at $P/P_0 = 0.97$, [d] Determined from XRD of reduced catalysts by Scherrer equation from the (111) diffraction plane of Co^0,[e] Determined from H_2-TPD results using formula from Li et al. [169] assuming H/Co = 1.

Broadly, Cu and Ag addition led to a significant decrease in the reduction temperature according to H_2-TPR profiles (Figure 4. 4). Whereas Cu addition to Co/SBA-15 favors Co oxide reducibility, while maintaining almost unaltered Co^0 crystallites size; Co-Ag/SBA-15 showed also lower reduction temperatures but larger Co^0 crystallites than Co/SBA-15. However, Ce addition does not affect significantly neither reducibility nor Co^0 crystallite size. Finally, Cr addition to Co/SBA-15 shifted the CoO reduction feature towards higher temperatures due to the presence of Cr species [170] or to the

confinement of Co oxides into SBA-15 channels, because of their smaller size induced by the presence of chromium oxides.

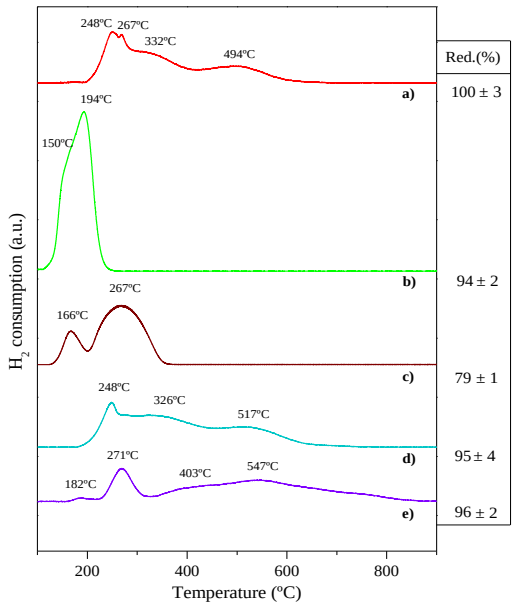

Figure 4. 4. H_2-TPR profiles for a) Co/SBA-15; b) Co-Cu/SBA-15; c) Co-Ag/SBA-15; d) Co-Ce/SBA 15; e) Co-Cr/SBA 15 samples. Red. (%) data displayed on the right correspond to reducibility.

The obtained catalytic results reveals almost complete conversion for all the catalysts tested while some differences in the hydrogen yields could be assessed. It must be highlighted that Co-Cr/SBA-15 achieved the highest H_2 yield (above 70 mol%) close to the thermodynamic value at the present reaction conditions. This behavior is related to the small Co crystallite size leading to higher active sites surface area [171, 172].

The amount of coke formed on Co-Cr/SBA-15 was much lower than the rest of the catalysts after 5 h of time on stream. Besides, Raman spectroscopy was used to determine the nature of coke deposited after the steam reforming reaction. The results showed how disordered aromatic structures such as amorphous or defective filamentous carbon were formed in a higher extent on Co-Cr/SBA-15 (I_D/I_G = 0.80) when compared to the other tested catalysts. Furthermore, it could be stated from the obtained results that H_2 yield and the I_D/I_G ratio are intimately related.

4.3. Preparation of agglomerated Co-Cr/SBA-15 catalysts for hydrogen production through acetic acid steam reforming.

Among all the prepared catalyst in the previous chapter, Co-Cr/SBA-15 was the catalysts with the best catalytic performance towards hydrogen production, reason why was selected for the agglomeration process in order to prepare suitable catalysts to be used in fixed bed reactor at industrial scale. When compared with other techniques such as coating or impregnation methods, extrusion easily produced agglomerated samples with high loading of active components since the use of solid core materials is avoided [173, 174]. In this line, Article 3 addresses the preparation of a series of Co-Cr/SBA-15 extrudates by varying the binder content and the particle size. Thus, the prepared samples were named as CoCrS-X-Y, where X corresponds to the amount of bentonite in terms of wt.%, while Y refers to the effective diameter in mm.

The characterization results summarized in Table 4. 2 showed that the agglomeration procedure has no remarkable influence over the textural properties, since the achieved results were close to those obtained for the powder sample.

Table 4. 2. Textural properties of powder Co-Cr/SBA-15 and extruded CoCr-X-Y catalysts.

Sample	S_{BET} (m^2/g)	V_p[a] (cm^3/g)	D_p[b] (nm)	$D_{Co_3O_4}$[c] (nm)
CoCrS	490	0.7	5.5	7.1
CoCrS-20-2.1	355	0.5	5.8	8.1
CoCrS-25-2.1	335	0.5	5.8	8.0
CoCrS-30-2.1	322	0.5	5.5	8.1

[a] Pore Volume measured at $P/P_0 = 0.97$; [b] BJH desorption average pore diameter;
[c] Determined from XRD of calcined catalysts by Scherrer equation from the (311) diffraction plane of Co_3O_4

The mechanical strength, on the other hand, becomes higher following a linear trend with the bentonite content. However, despite the mechanical strength increased, the conversion followed an opposite behavior under conditions in which external diffusion effects were absent. In order to evaluate the resistance to the mass transfer inside the

pores of the catalyst particles, several reactions were done using extruded catalysts with different sizes ranging from effective diameters between 1.3-2.1 mm (Figure 4.5).

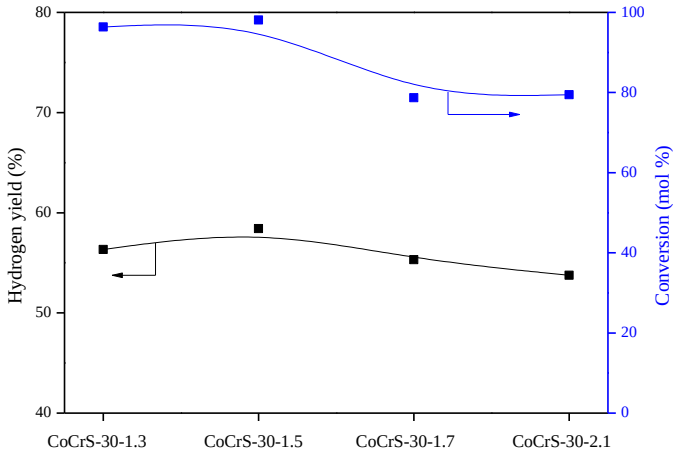

Figure 4.5. Catalytic results in terms of hydrogen yield and acetic acid conversion for extruded materials with different effective diameters.

By decreasing the particle size to an effective diameter of 1.5 mm, the acetic acid conversion increased up to 96 % from a conversion value near 80 % reached by the sample with the highest effective diameter. This effect can be explained since a decrease in effective particle diameter minimize the influence of internal mass transfer related to the resistance found by reactant molecules to reach active sites placed inside the catalyst particle pores [175]. Hydrogen yield, on the other side, did not exhibit remarkable changes.

From these results it can be concluded that a successful agglomeration process has been developed, opening a door towards the preparation of new catalysts for reforming purposes suitable for their use at industrial scale.

4.4. Study of coke formation in the steam reforming of bio-oil aqueous fractions.

With the aim of studying the causes of deactivation in the reforming reactions using Co/SBA-15, this chapter studies the evolution of the used catalyst at different times during the steam reforming of a mixture of model compounds representing the aqueous fraction from biomass HTL. The mixture was composed by 1.57, 8.25 and 17.5 mol% of phenol, hydroxyacetone and acetic acid, respectively, in water. In this regard, a brief summary of the major results of Article 4 is disclosed in this section.

The catalytic behavior with time-on-stream is represented in Figure 4. 6. As it can be observed, deactivation took place in two clearly differentiated stages. In the first one (TOS <20 h), the deactivation effect is more severe decreasing the conversion until 81 %. In this period, CO decreases while CO_2 increases suggesting that Boudouard reaction is favored. However, the fact that H_2 content in the gas stream remains almost constant suggests that water-gas-shift reaction can be also taking place. In the next stage (TOS >20 h), the conversion remains almost constant. This behavior indicates that the main deactivation is produced during the first 20 h of reaction.

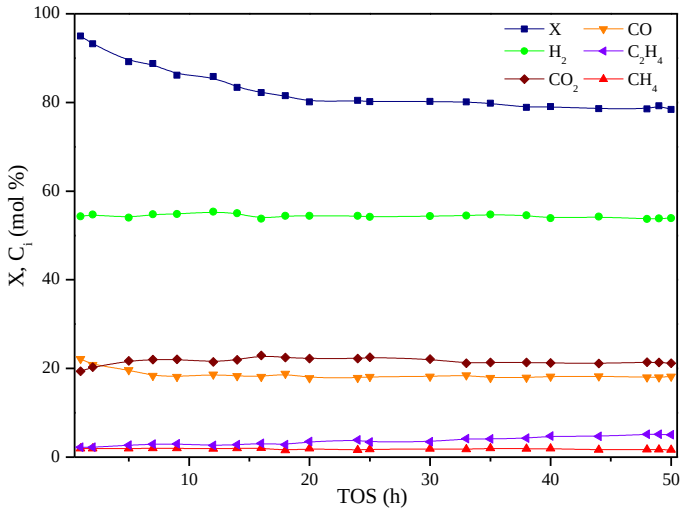

Figure 4. 6. Conversion (X) and reaction products distribution (C_i) with TOS (T=600 ºC, P=1 atm, WHSV=30.2 h^{-1}).

After the reaction, all the tested catalysts were characterized by means of TGA, XRD, elemental analysis, N_2 physisorption and TEM. During the first stage (TOS <20 h), deactivation is ascribed to the formation of defective carbon nanofibers over the catalyst surface as well as inside the SBA-15 pores. This fact led to a significant drop in conversion and BET surface area since coke was covering not only the pore mouths but it also was deposited inside them leading to isolated metallic Co particles. During this step, some Co particles were also encapsulated within coke nanofibers as could be appreciated by TEM, hindering the catalytic role of these active centers.

These facts are responsible of a conversion drop up to 81 mol % at 20 h time-on-stream. During the second stage of deactivation, between 20-50 h TOS, coke deposited became more ordered and aromatic as deduced by its higher C/H ratio. Coke deposits grow as filaments out of the support, as inferred from almost constant BET surface values and therefore not blocking the SBA-15 pores. In both stages, Co^0 crystallite size calculated form XRD of used samples indicated a slight sintering with minor influence on Co/SBA-15 deactivation. These outcomes are schematized in Figure 4. 7.

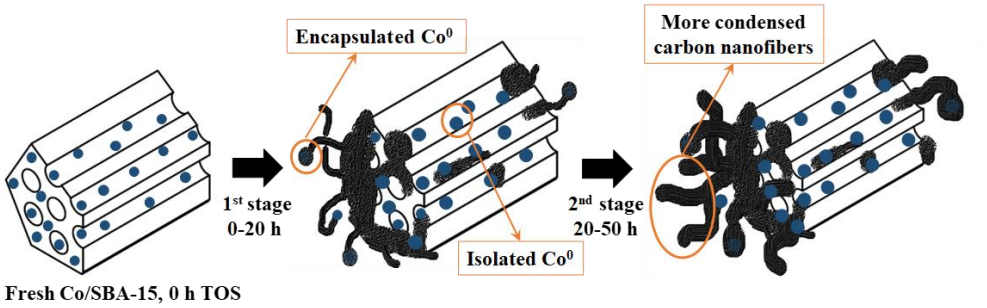

Figure 4. 7. Evolution of coke and Co^0 particles during the deactivation of Co/SBA-15 in the reforming of simulated bio-oil aqueous fraction.

In order to elucidate which parameter/s have more influence on the activity loss, their influence over total conversion was evaluated by means of a t-Student statistical analysis. The parameters studied were: mean diameter of Co particles, coke C/H ratio, coke mass (g coke / g cat), catalyst BET area and pore volume. The obtained results for used Co/SBA-15 led to the conclusion that the progressive growth of carbon

nanofibers and its nature (C/H ratio) have more influence than sintering on the conversion drop observed during the steam reforming of a mixture of acetic acid, hydroxyacetone and phenol as model compounds from the biomass HTL aqueous fraction.

5. Conclusions

The current Doctoral Thesis has been focused in the development of cobalt-based catalyst supported on SBA-15 for hydrogen production by means of steam reforming of model compound present in the bio-oil aqueous fraction. Hereafter, the most relevant conclusions are summarized.

- Ca addition to Co/SBA-15 resulted in the reduction of Co crystal size joined to a decrease in Co reducibility, as confirmed by H_2-TPR and XPS analysis, leading to worse catalytic results in the acetic acid steam reforming. The addition of reducibility promoters to Co/CaSBA-15, turned out an enhancement of the catalytic performance. As a consequence of the high dispersion and good reducibility (comparable to that obtained for Co/SBA-15), Co-Ce/CaSBA-15 sample reached the best catalytic performance achieving almost complete conversion (~ 99%) and high hydrogen yields (Y_{H_2} = 71.8%) in the acetic acid steam reforming.
- The incorporation of a second metal like Cu, Ag, Ce or Cr to Co/SBA-15 sample resulted in bimetallic catalysts with very different properties and catalytic behavior in acetic acid steam reforming. The results showed how Cr addition to Co/SBA-15 strongly decreased Co crystallites size, induced by the presence of chromium oxides, improving metal dispersion with a slight decrease in the reduction temperature. This fact gave rise to the best catalytic performance on

acetic acid steam reforming achieving hydrogen selectivities around 72 mol %, next to those predicted in the thermodynamic equilibrium.

- The performance of extruded Co-Cr/SBA-15 catalysts has been studied through acetic acid steam reforming. The characterization results showed that the agglomeration procedure had no remarkable influence over the textural properties or the reducibility of metallic active species, being these results close to those obtained for the powder sample. Besides, the external and internal diffusion tests allowed the selection of suitable flow rate and catalysts particle size in order to avoid concentration gradients. Under the selected conditions, CoCrS-30-1.5 (30 wt.% bentonite and 1.5 mm effective diameter) showed a good performance for hydrogen production, reaching a hydrogen yield around 58% and similar results in terms of conversion when compared to the powder form.
- The deactivation of Co/SBA-15 in the reforming of a mixture of acetic acid, hydroxyacetone and phenol as model compounds from the biomass HTL aqueous fraction was a consequence of coke formation, its composition (C/H ratio) and Co sintering. Oxidation of Co was not detected in the used catalysts and thus it was not considered in catalysts deactivation. Results evidenced two different stages to understand deactivation of Co/SBA-15. The first one, in which the conversion drop was more severe (up to 81 mol%), the deactivation is ascribed to the formation of defective carbon nanofibers over the catalyst surface as well as inside the SBA-15 pores leading to some isolated or encapsulated metallic Co particles. Conversely, during the second stage of deactivation, conversion remained almost constant and, the coke deposited became more ordered and aromatic, growing as filaments out of the support. From the statistical analysis t-Student, it was possible to conclude that the progressive growth of carbon nanofibers and its nature (C/H ratio) have more influence than sintering on the conversion drop.

Recommendations for future works

Taking into account the results and conclusions included in the present Doctoral Thesis, the next recommendations are enounced for future works:

- The development of a kinetic study for the acetic acid steam reforming reaction using Co-based catalysts.
- The use of different binders such as sepiolite, kaolin or attapulgite during the agglomeration process.
- The directly use the aqueous fraction of bio-oil obtained from thermochemical processes of biomass as feed to the reactor where the reforming tests are carried out.
- The addition of oxygen into the reaction medium, leading to oxidative steam reforming as an improvement to the conventional process to avoid/decrease the coke formation.

6. References

[1] I.E. Agency, The Future of Hydrogen, IEA Publications, Paris, France, **2019**.

[2] I.E. Agency, World Energy Outlook 2019, IEA Publications, Paris, France, **2019**.

[3] P.E. Brockway, A. Owen, L.I. Brand-Correa, L. Hardt, Estimation of global final-stage energy-return-on-investment for fossil fuels with comparison to renewable energy sources, Nature Energy, 4 (**2019**) 612-621.

[4] U.S.E.I. Administration, International Energy Outlook 2019, **2019**.

[5] D. Shindell, C.J. Smith, Climate and air-quality benefits of a realistic phase-out of fossil fuels, Nature, 573 (**2019**) 408-411.

[6] K. Uddin, Nuclear Energy, Environment and Public Safety: North-South Politics, Strategic Planning for Energy and the Environment, 38 (**2019**) 31-41.

[7] W. Thorbecke, How oil prices affect East and Southeast Asian economies: Evidence from financial markets and implications for energy security, Energy Policy, 128 (**2019**) 628-638.

[8] V. Bianco, F. Cascetta, A. Marino, S. Nardini, Understanding energy consumption and carbon emissions in Europe: A focus on inequality issues, Energy, 170 (**2019**) 120-130.

[9] G.I. Pereira, P.P. da Silva, Energy efficiency governance in the EU-28: analysis of institutional, human, financial, and political dimensions, Energy Efficiency, 10 (**2017**) 1279-1297.

[10] P.J. Megía, A. Carrero, J.A. Calles, A.J. Vizcaíno, Hydrogen Production from Steam Reforming of Acetic Acid as a Model Compound of the Aqueous Fraction of

Microalgae HTL Using Co-M/SBA-15 (M: Cu, Ag, Ce, Cr) Catalysts, Catalysts, 9 (**2019**) 1013.

[11] F.J. Gutiérrez Ortiz, A. Kruse, F. Ramos, P. Ollero, Integral energy valorization of municipal solid waste reject fraction to biofuels, Energy Conversion and Management, 180 (**2019**) 1167-1184.

[12] Y.E. García Vera, R. Dufo-López, J.L. Bernal-Agustín, Energy Management in Microgrids with Renewable Energy Sources: A Literature Review, Applied Sciences, 9 (**2019**) 3854.

[13] R.E. Guedes, A.S. Luna, A.R. Torres, Operating parameters for bio-oil production in biomass pyrolysis: A review, Journal of Analytical and Applied Pyrolysis, 129 (**2018**) 134-149.

[14] A.M. Abdalla, S. Hossain, O.B. Nisfindy, A.T. Azad, M. Dawood, A.K. Azad, Hydrogen production, storage, transportation and key challenges with applications: A review, Energy Conversion and Management, 165 (**2018**) 602-627.

[15] C. Acar, I. Dincer, Review and evaluation of hydrogen production options for better environment, Journal of Cleaner Production, 218 (**2019**) 835-849.

[16] Z. Abdin, A. Zafaranloo, A. Rafiee, W. Mérida, W. Lipiński, K.R. Khalilpour, Hydrogen as an energy vector, Renewable and Sustainable Energy Reviews, 120 (**2020**) 109620.

[17] I. Dincer, Green methods for hydrogen production, International Journal of Hydrogen Energy, 37 (**2012**) 1954-1971.

[18] A.J. Vizcaíno, A. Carrero, J.A. Calles, Hydrogen production from bioethanol, Nova Science Publishers, New York, **2012**, 247-294.

[19] I.E. Agency, Hydrogen Production and Storage: R&D Priorities and Gaps, IEA Publications, Paris, France, **2006**.

[20] C. Ruocco, V. Palma, A. Ricca, Kinetics of Oxidative Steam Reforming of Ethanol Over Bimetallic Catalysts Supported on CeO_2–SiO_2: A Comparative Study, Topics in Catalysis, 62 (**2019**) 467-478.

[21] Y. Wang, C. Wang, M. Chen, Z. Tang, Z. Yang, J. Hu, H. Zhang, Hydrogen production from steam reforming ethanol over Ni/attapulgite catalysts - Part I: Effect of nickel content, Fuel Processing Technology, 192 (**2019**) 227-238.

[22] P. Nikolaidis, A. Poullikkas, A comparative overview of hydrogen production processes, Renewable and Sustainable Energy Reviews, 67 (**2017**) 597-611.

[23] I.E. Agency, Technology Roadmap - Hydrogen and Fuel Cells, IEA Publications, Paris, France, **2015**.

[24] S.E. Hosseini, M.A. Wahid, Hydrogen production from renewable and sustainable energy resources: Promising green energy carrier for clean development, Renewable and Sustainable Energy Reviews, 57 (**2016**) 850-866.

[25] H.C. Ong, W.-H. Chen, A. Farooq, Y.Y. Gan, K.T. Lee, V. Ashokkumar, Catalytic thermochemical conversion of biomass for biofuel production: A comprehensive review, Renewable and Sustainable Energy Reviews, 113 (**2019**) 109266.

[26] A.R.K. Gollakota, N. Kishore, S. Gu, A review on hydrothermal liquefaction of biomass, Renewable and Sustainable Energy Reviews, 81 (**2018**) 1378-1392.

[27] M. Shahabuddin, B.B. Krishna, T. Bhaskar, G. Perkins, Advances in the thermo-chemical production of hydrogen from biomass and residual wastes: Summary of recent techno-economic analyses, Bioresource Technology, 299 (**2020**) 122557.

[28] M.N. Uddin, K. Techato, J. Taweekun, M.M. Rahman, M.G. Rasul, T.M.I. Mahlia, S.M. Ashrafur, An Overview of Recent Developments in Biomass Pyrolysis Technologies, Energies, 11 (**2018**) 3115.

[29] T.E. Lipman, Hydrogen Production Science and Technology, in: T.E. Lipman, A.Z. Weber (Eds.) Fuel Cells and Hydrogen Production: A Volume in the Encyclopedia of Sustainability Science and Technology, Springer New York, New York, **2019**, 783-798.

[30] L. Barelli, G. Bidini, F. Gallorini, S. Servili, Hydrogen production through sorption-enhanced steam methane reforming and membrane technology: A review, Energy, 33 (**2008**) 554-570.

[31] I.E. Agency, Techno-Economic Evaluation of SMR Based Standalone (Merchant) Hydrogen Plant with CCS, IEAGHG Technical Report 2017-02, Cheltenham, UK, **2017**.

[32] D. Hariharan, R. Yang, Y. Zhou, B. Gainey, S. Mamalis, R.E. Smith, M.A. Lugo-Pimentel, M.J. Castaldi, R. Gill, A. Davis, D. Modroukas, B. Lawler, Catalytic partial oxidation reformation of diesel, gasoline, and natural gas for use in low temperature combustion engines, Fuel, 246 (**2019**) 295-307.

[33] P. Arku, B. Regmi, A. Dutta, A review of catalytic partial oxidation of fossil fuels and biofuels: Recent advances in catalyst development and kinetic modelling, Chemical Engineering Research and Design, 136 (**2018**) 385-402.

[34] R. Batista da Silva, S.T. Brandão, A. Lucotti, M.S. Tommasini, C. Castiglioni, G. Groppi, A. Beretta, Chemical pathways in the partial oxidation and steam reforming of acetic acid over a Rh-Al_2O_3 catalyst, Catalysis Today, 289 (**2017**) 162-172.

[35] C. Pirez, W. Fang, M. Capron, S. Paul, H. Jobic, F. Dumeignil, L. Jalowiecki-Duhamel, Steam reforming, partial oxidation and oxidative steam reforming for hydrogen production from ethanol over cerium nickel based oxyhydride catalyst, Applied Catalysis A: General, 518 (**2016**) 78-86.

[36] M. Luneau, E. Gianotti, F.C. Meunier, C. Mirodatos, E. Puzenat, Y. Schuurman, N. Guilhaume, Deactivation mechanism of Ni supported on Mg-Al spinel during autothermal reforming of model biogas, Applied Catalysis B: Environmental, 203 (**2017**) 289-299.

[37] R. Baruah, M. Dixit, P. Basarkar, D. Parikh, A. Bhargav, Advances in ethanol autothermal reforming, Renewable and Sustainable Energy Reviews, 51 (**2015**) 1345-1353.

[38] O. Schmidt, A. Gambhir, I. Staffell, A. Hawkes, J. Nelson, S. Few, Future cost and performance of water electrolysis: An expert elicitation study, International Journal of Hydrogen Energy, 42 (**2017**) 30470-30492.

[39] F. Safari, I. Dincer, A review and comparative evaluation of thermochemical water splitting cycles for hydrogen production, Energy Conversion and Management, 205 (**2020**) 112182.

[40] J. Chi, H. Yu, Water electrolysis based on renewable energy for hydrogen production, Chinese Journal of Catalysis, 39 (**2018**) 390-394.

[41] J. Jia, L.C. Seitz, J.D. Benck, Y. Huo, Y. Chen, J.W.D. Ng, T. Bilir, J.S. Harris, T.F. Jaramillo, Solar water splitting by photovoltaic-electrolysis with a solar-to-hydrogen efficiency over 30%, Nature Communications, 7 (**2016**) 13237.

[42] J.D. Holladay, J. Hu, D.L. King, Y. Wang, An overview of hydrogen production technologies, Catalysis Today, 139 (**2009**) 244-260.

[43] S. Abanades, Metal Oxides Applied to Thermochemical Water-Splitting for Hydrogen Production Using Concentrated Solar Energy, ChemEngineering, 3 (**2019**) 63.

[44] C. Acar, Y. Bicer, M.E. Demir, I. Dincer, Transition to a new era with light-based hydrogen production for a carbon-free society: An overview, International Journal of Hydrogen Energy, 44 (**2019**) 25347-25364.

[45] Z. Chen, T.F. Jaramillo, T.G. Deutsch, A. Kleiman-Shwarsctein, A.J. Forman, N. Gaillard, R. Garland, K. Takanabe, C. Heske, M. Sunkara, E.W. McFarland, K. Domen, E.L. Miller, J.A. Turner, H.N. Dinh, Accelerating materials development for photoelectrochemical hydrogen production: Standards for methods, definitions, and reporting protocols, Journal of Materials Research, 25 (**2011**) 3-16.

[46] I. Dincer, C. Zamfirescu, Sustainable hydrogen production options and the role of IAHE, International Journal of Hydrogen Energy, 37 (**2012**) 16266-16286.

[47] Z.M.A. Bundhoo, Potential of bio-hydrogen production from dark fermentation of crop residues: A review, International Journal of Hydrogen Energy, 44 (**2019**) 17346-17362.

[48] E. Eroglu, A. Melis, Photobiological hydrogen production: Recent advances and state of the art, Bioresource Technology, 102 (**2011**) 8403-8413.

[49] M.A. Hossain, J. Jewaratnam, P. Ganesan, Prospect of hydrogen production from oil palm biomass by thermochemical process – A review, International Journal of Hydrogen Energy, 41 (**2016**) 16637-16655.

[50] Y. Kalinci, A. Hepbasli, I. Dincer, Biomass-based hydrogen production: A review and analysis, International Journal of Hydrogen Energy, 34 (**2009**) 8799-8817.

[51] M. Patel, X. Zhang, A. Kumar, Techno-economic and life cycle assessment on lignocellulosic biomass thermochemical conversion technologies: A review, Renewable and Sustainable Energy Reviews, 53 (**2016**) 1486-1499.

[52] S. Wang, G. Dai, H. Yang, Z. Luo, Lignocellulosic biomass pyrolysis mechanism: A state-of-the-art review, Progress in Energy and Combustion Science, 62 (**2017**) 33-86.

[53] S. Mutsengerere, C.H. Chihobo, D. Musademba, I. Nhapi, A review of operating parameters affecting bio-oil yield in microwave pyrolysis of lignocellulosic biomass, Renewable and Sustainable Energy Reviews, 104 (**2019**) 328-336.

[54] H. Zhang, Z. Gao, W. Ao, J. Li, G. Liu, J. Fu, C. Ran, X. Mao, Q. Kang, Y. Liu, J. Dai, Microwave-assisted pyrolysis of textile dyeing sludge using different additives, Journal of Analytical and Applied Pyrolysis, 127 (**2017**) 140-149.

[55] J.S. Rowbotham, P.W. Dyer, H.C. Greenwell, M.K. Theodorou, Thermochemical processing of macroalgae: a late bloomer in the development of third-generation biofuels?, Biofuels, 3 (**2012**) 441-461.

[56] K.G. Kalogiannis, S.D. Stefanidis, A.A. Lappas, Catalyst deactivation, ash accumulation and bio-oil deoxygenation during ex situ catalytic fast pyrolysis of biomass in a cascade thermal-catalytic reactor system, Fuel Processing Technology, 186 (**2019**) 99-109.

[57] G. Esteban-Díez, M.V. Gil, C. Pevida, D. Chen, F. Rubiera, Effect of operating conditions on the sorption enhanced steam reforming of blends of acetic acid and acetone as bio-oil model compounds, Applied Energy, 177 (**2016**) 579-590.

[58] A.V. Bridgwater, Review of fast pyrolysis of biomass and product upgrading, Biomass Bioenergy, 38 (**2012**) 68-94.

[59] S. Xiu, A. Shahbazi, Bio-oil production and upgrading research: A review, Renewable and Sustainable Energy Reviews, 16 (**2012**) 4406-4414.

[60] R.V.S. Silva, V.B. Pereira, K.T. Stelzer, T.A. Almeida, G.A. Romeiro, D.A. Azevedo, Comprehensive study of the liquid products from slow pyrolysis of crambe seeds: Bio-oil and organic compounds of the aqueous phase, Biomass Bioenergy, 123 (**2019**) 78-88.

[61] W. Nabgan, T.A. Tuan Abdullah, R. Mat, B. Nabgan, Y. Gambo, M. Ibrahim, A. Ahmad, A.A. Jalil, S. Triwahyono, I. Saeh, Renewable hydrogen production from bio-oil derivative via catalytic steam reforming: An overview, Renewable and Sustainable Energy Reviews, 79 (**2017**) 347-357.

[62] Y. Guo, T. Yeh, W. Song, D. Xu, S. Wang, A review of bio-oil production from hydrothermal liquefaction of algae, Renewable and Sustainable Energy Reviews, 48 (**2015**) 776-790.

[63] J. Alvarez, G. Lopez, M. Amutio, J. Bilbao, M. Olazar, Bio-oil production from rice husk fast pyrolysis in a conical spouted bed reactor, Fuel, 128 (**2014**) 162-169.

[64] A.G. Adeniyi, K.S. Otoikhian, J.O. Ighalo, Steam Reforming of Biomass Pyrolysis Oil: A Review, 17 (**2019**) 20180328.

[65] A. Bahadori, T. Kashiwao, Modeling and analysis of hydrogen production in steam methane reforming (SMR) process, Petroleum Science and Technology, 37 (**2019**) 1425-1435.

[66] B. Wang, Y. Xiong, Y. Han, J. Hong, Y. Zhang, J. Li, F. Jing, W. Chu, Preparation of stable and highly active Ni/CeO_2 catalysts by glow discharge plasma technique for glycerol steam reforming, Applied Catalysis B: Environmental, 249 (**2019**) 257-265.

[67] S.Z. Abbas, V. Dupont, T. Mahmud, Modelling of H_2 production via sorption enhanced steam methane reforming at reduced pressures for small scale applications, International Journal of Hydrogen Energy, 44 (**2019**) 1505-1513.

[68] J. Chen, J. Sun, Y. Wang, Catalysts for Steam Reforming of Bio-oil: A Review, Industrial & Engineering Chemistry Research, 56 (**2017**) 4627-4637.

[69] B. Valle, B. Aramburu, M. Olazar, J. Bilbao, A.G. Gayubo, Steam reforming of raw bio-oil over Ni/La_2O_3-αAl_2O_3: Influence of temperature on product yields and catalyst deactivation, Fuel, 216 (**2018**) 463-474.

[70] A. Carrero, J.A. Calles, A.J. Vizcaíno, Effect of Mg and Ca addition on coke deposition over Cu–Ni/SiO_2 catalysts for ethanol steam reforming, Chemical Engineering Journal, 163 (**2010**) 395-402.

[71] C. Montero, A. Ochoa, P. Castaño, J. Bilbao, A.G. Gayubo, Monitoring Ni0 and coke evolution during the deactivation of a Ni/La_2O_3–αAl_2O_3 catalyst in ethanol steam reforming in a fluidized bed, Journal of Catalysis, 331 (**2015**) 181-192.

[72] D.L. Trimm, Coke formation and minimisation during steam reforming reactions, Catalysis Today, 37 (**1997**) 233-238.

[73] V. Palma, C. Ruocco, E. Meloni, F. Gallucci, A. Ricca, Enhancing Pt-Ni/CeO_2 performances for ethanol reforming by catalyst supporting on high surface silica, Catalysis Today, 307 (**2018**) 175-188.

[74] C. Montero, A. Remiro, B. Valle, L. Oar-Arteta, J. Bilbao, A.G. Gayubo, Origin and Nature of Coke in Ethanol Steam Reforming and Its Role in Deactivation of Ni/La_2O_3–αAl_2O_3 Catalyst, Industrial & Engineering Chemistry Research, 58 (**2019**) 14736-14751.

[75] H.D. Setiabudi, M.A.A. Aziz, S. Abdullah, L.P. Teh, R. Jusoh, Hydrogen production from catalytic steam reforming of biomass pyrolysis oil or bio-oil derivatives: A review, International Journal of Hydrogen Energy, 45 (**2020**) 18376-18397.

[76] S. Wang, Q. Cai, F. Zhang, X. Li, L. Zhang, Z. Luo, Hydrogen production via catalytic reforming of the bio-oil model compounds: Acetic acid, phenol and hydroxyacetone, International Journal of Hydrogen Energy, 39 (**2014**) 18675-18687.

[77] S. Sayas, A. Chica, Furfural steam reforming over Ni-based catalysts. Influence of Ni incorporation method, International Journal of Hydrogen Energy, 39 (**2014**) 5234-5241.

[78] G. Chen, J. Tao, C. Liu, B. Yan, W. Li, X. Li, Hydrogen production via acetic acid steam reforming: A critical review on catalysts, Renewable and Sustainable Energy Reviews, 79 (**2017**) 1091-1098.

[79] J.L. Contreras, J. Salmones, J.A. Colín-Luna, L. Nuño, B. Quintana, I. Córdova, B. Zeifert, C. Tapia, G.A. Fuentes, Catalysts for H_2 production using the ethanol steam reforming (a review), International Journal of Hydrogen Energy, 39 (**2014**) 18835-18853.

[80] S. Ogo, Y. Sekine, Recent progress in ethanol steam reforming using non-noble transition metal catalysts: A review, Fuel Processing Technology, 199 (**2020**) 106238.
[81] M. Greluk, M. Rotko, G. Słowik, S. Turczyniak-Surdacka, Hydrogen production by steam reforming of ethanol over Co/CeO_2 catalysts: Effect of cobalt content, Journal of the Energy Institute, 92 (**2019**) 222-238.
[82] D. Chen, W. Wang, C. Liu, Hydrogen production through glycerol steam reforming over beehive-biomimetic graphene-encapsulated nickel catalysts, Renewable Energy, 145 (**2020**) 2647-2657.
[83] C. Rioche, S. Kulkarni, F.C. Meunier, J.P. Breen, R. Burch, Steam reforming of model compounds and fast pyrolysis bio-oil on supported noble metal catalysts, Applied Catalysis B: Environmental, 61 (**2005**) 130-139.
[84] K. Tomishige, M. Asadullah, K. Kunimori, Syngas production by biomass gasification using $Rh/CeO_2/SiO_2$ catalysts and fluidized bed reactor, Catalysis Today, 89 (**2004**) 389-403.
[85] A.C. Basagiannis, P. Panagiotopoulou, X.E. Verykios, Low Temperature Steam Reforming of Ethanol Over Supported Noble Metal Catalysts, Topics in Catalysis, 51 (**2008**) 2-12.
[86] A. Zarei Senseni, M. Rezaei, F. Meshkani, Glycerol steam reforming over noble metal nanocatalysts, Chemical Engineering Research and Design, 123 (**2017**) 360-366.
[87] Y. Im, J.H. Lee, B.S. Kwak, J.Y. Do, M. Kang, Effective hydrogen production from propane steam reforming using M/NiO/YSZ catalysts (M=Ru, Rh, Pd, and Ag), Catalysis Today, 303 (**2018**) 168-176.
[88] A.K. Yadav, P.D. Vaidya, A study on the efficacy of noble metal catalysts for butanol steam reforming, International Journal of Hydrogen Energy, 44 (**2019**) 25575-25588.
[89] G. Guan, M. Kaewpanha, X. Hao, A. Abudula, Catalytic steam reforming of biomass tar: Prospects and challenges, Renewable and Sustainable Energy Reviews, 58 (**2016**) 450-461.

[90] T. Hou, S. Zhang, Y. Chen, D. Wang, W. Cai, Hydrogen production from ethanol reforming: Catalysts and reaction mechanism, Renewable and Sustainable Energy Reviews, 44 (**2015**) 132-148.

[91] X. Hu, G. Lu, Comparative study of alumina-supported transition metal catalysts for hydrogen generation by steam reforming of acetic acid, Applied Catalysis B: Environmental, 99 (**2010**) 289-297.

[92] M. Konsolakis, Z. Ioakimidis, T. Kraia, G.E. Marnellos, Hydrogen Production by Ethanol Steam Reforming (ESR) over CeO_2 Supported Transition Metal (Fe, Co, Ni, Cu) Catalysts: Insight into the Structure-Activity Relationship, Catalysts, 6 (**2016**) 39.

[93] M. Chen, Z. Zhou, Y. Wang, T. Liang, X. Li, Z. Yang, M. Chen, J. Wang, Effects of attapulgite-supported transition metals catalysts on glycerol steam reforming for hydrogen production, International Journal of Hydrogen Energy, 43 (**2018**) 20451-20464.

[94] B. Banach, A. Machocki, P. Rybak, A. Denis, W. Grzegorczyk, W. Gac, Selective production of hydrogen by steam reforming of bio-ethanol, Catalysis Today, 176 (**2011**) 28-35.

[95] A. Ishihara, A. Andou, T. Hashimoto, H. Nasu, Steam reforming of ethanol using novel carbon-oxide composite-supported Ni, Co and Fe catalysts, Fuel Processing Technology, 197 (**2020**) 106203.

[96] K.N. Papageridis, G. Siakavelas, N.D. Charisiou, D.G. Avraam, L. Tzounis, K. Kousi, M.A. Goula, Comparative study of Ni, Co, Cu supported on γ-alumina catalysts for hydrogen production via the glycerol steam reforming reaction, Fuel Processing Technology, 152 (**2016**) 156-175.

[97] G. Chen, J. Tao, C. Liu, B. Yan, W. Li, X. Li, Hydrogen production via acetic acid steam reforming: A critical review on catalysts, Renewable and Sustainable Energy Reviews, 79 (**2017**) 1091-1098.

[98] M.-S. Fan, A.Z. Abdullah, S. Bhatia, Catalytic Technology for Carbon Dioxide Reforming of Methane to Synthesis Gas, ChemCatChem, 1 (**2009**) 192-208.

[99] W.-J. Jang, J.-O. Shim, H.-M. Kim, S.-Y. Yoo, H.-S. Roh, A review on dry reforming of methane in aspect of catalytic properties, Catalysis Today, 324 (**2019**) 15-26.

[100] Z. He, Y. Jiao, J. Wang, Y. Chen, Bi-functional composite oxides M(Na, K)-Ni/La-Al_2O_3 catalysts for steam reforming of n-decane, Fuel, 212 (**2018**) 193-201.

[101] B. Banach, A. Machocki, Effect of potassium addition on a long term performance of Co–ZnO–Al_2O_3 catalysts in the low-temperature steam reforming of ethanol: Co-precipitation vs citrate method of catalysts synthesis, Applied Catalysis A: General, 505 (**2015**) 173-182.

[102] A. Casanovas, M. Roig, C. de Leitenburg, A. Trovarelli, J. Llorca, Ethanol steam reforming and water gas shift over Co/ZnO catalytic honeycombs doped with Fe, Ni, Cu, Cr and Na, International Journal of Hydrogen Energy, 35 (**2010**) 7690-7698.

[103] S. Ogo, T. Shimizu, Y. Nakazawa, K. Mukawa, D. Mukai, Y. Sekine, Steam reforming of ethanol over K promoted Co catalyst, Applied Catalysis A: General, 495 (**2015**) 30-38.

[104] A.J. Vizcaíno, A. Carrero, J.A. Calles, Comparison of ethanol steam reforming using Co and Ni catalysts supported on SBA-15 modified by Ca and Mg, Fuel Processing Technology, 146 (**2016**) 99-109.

[105] L. Xu, F. Wang, M. Chen, X. Fan, H. Yang, D. Nie, L. Qi, Alkaline-promoted Co-Ni bimetal ordered mesoporous catalysts with enhanced coke-resistant performance toward CO_2 reforming of CH_4, Journal of CO_2 Utilization, 18 (**2017**) 1-14.

[106] M.L. Dieuzeide, M. Laborde, N. Amadeo, C. Cannilla, G. Bonura, F. Frusteri, Hydrogen production by glycerol steam reforming: How Mg doping affects the catalytic behaviour of Ni/Al_2O_3 catalysts, International Journal of Hydrogen Energy, 41 (**2016**) 157-166.

[107] Y.-L. Lee, K.-J. Kim, W.-J. Jang, J.-O. Shim, K.-W. Jeon, H.-S. Na, H.-M. Kim, J.W. Bae, S.C. Nam, B.-H. Jeon, H.-S. Roh, Increase in stability of BaCo/CeO_2 catalyst by optimizing the loading amount of Ba promoter for high-temperature water-gas shift reaction using waste-derived synthesis gas, Renewable Energy, 145 (**2020**) 2715-2722.

[108] K. Seung-hoon, J. Jae-sun, Y. Eun-hyeok, L. Kwan-Young, M. Dong Ju, Hydrogen production by steam reforming of biomass-derived glycerol over Ni-based catalysts, Catalysis Today, 228 (**2014**) 145-151.

[109] N.D. Charisiou, K.N. Papageridis, L. Tzounis, V. Sebastian, S.J. Hinder, M.A. Baker, M. AlKetbi, K. Polychronopoulou, M.A. Goula, Ni supported on CaO-MgO-Al_2O_3 as a highly selective and stable catalyst for H_2 production via the glycerol steam reforming reaction, International Journal of Hydrogen Energy, 44 (**2019**) 256-273.

[110] S. Isarapakdeetham, P. Kim-Lohsoontorn, S. Wongsakulphasatch, W. Kiatkittipong, N. Laosiripojana, J. Gong, S. Assabumrungrat, Hydrogen production via chemical looping steam reforming of ethanol by Ni-based oxygen carriers supported on CeO_2 and La_2O_3 promoted Al_2O_3, International Journal of Hydrogen Energy, 45 (**2020**) 1477-1491.

[111] S. Natesakhawat, R.B. Watson, X. Wang, U.S. Ozkan, Deactivation characteristics of lanthanide-promoted sol–gel Ni/Al_2O_3 catalysts in propane steam reforming, Journal of Catalysis, 234 (**2005**) 496-508.

[112] A. Carrero, A.J. Vizcaíno, J.A. Calles, L. García-Moreno, Hydrogen production through glycerol steam reforming using Co catalysts supported on SBA-15 doped with Zr, Ce and La, Journal of Energy Chemistry, 26 (**2017**) 42-48.

[113] F. Bimbela, J. Ábrego, R. Puerta, L. García, J. Arauzo, Catalytic steam reforming of the aqueous fraction of bio-oil using Ni-Ce/Mg-Al catalysts, Applied Catalysis B: Environmental, 209 (**2017**) 346-357.

[114] L. Xu, W. Mi, Q. Su, Hydrogen production through diesel steam reforming over rare-earth promoted Ni/γ-Al_2O_3 catalysts, Journal of Natural Gas Chemistry, 20 (**2011**) 287-293.

[115] P. Osorio-Vargas, N.A. Flores-González, R.M. Navarro, J.L.G. Fierro, C.H. Campos, P. Reyes, Improved stability of Ni/Al_2O_3 catalysts by effect of promoters (La_2O_3, CeO_2) for ethanol steam-reforming reaction, Catalysis Today, 259 (**2016**) 27-38.

[116] J.A. Calles, A. Carrero, A.J. Vizcaíno, L. García-Moreno, P.J. Megía, Steam Reforming of Model Bio-Oil Aqueous Fraction Using Ni-(Cu, Co, Cr)/SBA-15 Catalysts, International Journal of Molecular Sciences, 20 (**2019**) 512.

[117] Y. Li, Z. Zhang, P. Jia, D. Dong, Y. Wang, S. Hu, J. Xiang, Q. Liu, X. Hu, Ethanol steam reforming over cobalt catalysts: Effect of a range of additives on the catalytic behaviors, Journal of the Energy Institute, 93 (**2020**) 165-184.

[118] D. Wang, J. Zhang, J. Sun, W. Gao, Y. Cui, Effect of metal additives on the catalytic performance of Ni/Al_2O_3 catalyst in thermocatalytic decomposition of methane, International Journal of Hydrogen Energy, 44 (**2019**) 7205-7215.

[119] L.P.R. Profeti, E.A. Ticianelli, E.M. Assaf, Production of hydrogen via steam reforming of biofuels on $Ni/CeO_2–Al_2O_3$ catalysts promoted by noble metals, International Journal of Hydrogen Energy, 34 (**2009**) 5049-5060.

[120] P. Frontera, A. Macario, A. Aloise, P.L. Antonucci, G. Giordano, J.B. Nagy, Effect of support surface on methane dry-reforming catalyst preparation, Catalysis Today, 218-219 (**2013**) 18-29.

[121] N.A.K. Aramouni, J.G. Touma, B.A. Tarboush, J. Zeaiter, M.N. Ahmad, Catalyst design for dry reforming of methane: Analysis review, Renewable and Sustainable Energy Reviews, 82 (**2018**) 2570-2585.

[122] R.Y. Abrokwah, W. Dade, V. Deshmane, M. Rahman, D. Kuila, Effects of Mesoporous Supports and Metals on Steam Reforming of Alcohols, Fuel Processing and Energy Utilization, Chapman and Hall/CRC, New York, **2019**, 93-108.

[123] L. Santamaria, G. Lopez, A. Arregi, M. Amutio, M. Artetxe, J. Bilbao, M. Olazar, Stability of different Ni supported catalysts in the in-line steam reforming of biomass fast pyrolysis volatiles, Applied Catalysis B: Environmental, 242 (**2019**) 109-120.

[124] N.D. Charisiou, G. Siakavelas, K.N. Papageridis, A. Baklavaridis, L. Tzounis, K. Polychronopoulou, M.A. Goula, Hydrogen production via the glycerol steam reforming reaction over nickel supported on alumina and lanthana-alumina catalysts, International Journal of Hydrogen Energy, 42 (**2017**) 13039-13060.

[125] T. Suteewong, H. Sai, R. Hovden, D. Muller, M.S. Bradbury, S.M. Gruner, U. Wiesner, Multicompartment Mesoporous Silica Nanoparticles with Branched Shapes: An Epitaxial Growth Mechanism, Science, 340 (**2013**) 337-341.

[126] S. Singh, R. Kumar, H.D. Setiabudi, S. Nanda, D.-V.N. Vo, Advanced synthesis strategies of mesoporous SBA-15 supported catalysts for catalytic reforming applications: A state-of-the-art review, Applied Catalysis A: General, 559 (**2018**) 57-74.

[127] Q. Zhang, T. Zhang, Y. Shi, B. Zhao, M. Wang, Q. Liu, J. Wang, K. Long, Y. Duan, P. Ning, A sintering and carbon-resistant Ni-SBA-15 catalyst prepared by solid-state grinding method for dry reforming of methane, Journal of CO_2 Utilization, 17 (**2017**) 10-19.

[128] T.-W. Kim, F. Kleitz, B. Paul, R. Ryoo, MCM-48-like Large Mesoporous Silicas with Tailored Pore Structure: Facile Synthesis Domain in a Ternary Triblock Copolymer−Butanol−Water System, Journal of the American Chemical Society, 127 (**2005**) 7601-7610.

[129] K. Wang, B. Dou, B. Jiang, Q. Zhang, M. Li, H. Chen, Y. Xu, Effect of support on hydrogen production from chemical looping steam reforming of ethanol over Ni-based oxygen carriers, International Journal of Hydrogen Energy, 41 (**2016**) 17334-17347.

[130] A.J. Vizcaíno, A. Carrero, J.A. Calles, Hydrogen production by ethanol steam reforming over Cu–Ni supported catalysts, International Journal of Hydrogen Energy, 32 (**2007**) 1450-1461.

[131] D. Liu, X.-Y. Quek, H.H.A. Wah, G. Zeng, Y. Li, Y. Yang, Carbon dioxide reforming of methane over nickel-grafted SBA-15 and MCM-41 catalysts, Catalysis Today, 148 (**2009**) 243-250.

[132] D. Zhao, J. Feng, Q. Huo, N. Melosh, G.H. Fredrickson, B.F. Chmelka, G.D. Stucky, Triblock copolymer syntheses of mesoporous silica with periodic 50 to 300 angstrom pores, Science, 279 (**1998**) 548-552.

[133] A. Zeleňáková, P. Hrubovčák, O. Kapusta, N. Kučerka, A. Kuklin, O. Ivankov, V. Zeleňák, Size and distribution of the iron oxide nanoparticles in SBA-15 nanoporous silica via SANS study, Scientific Reports, 9 (**2019**) 15852.

[134] N. Brodie-Linder, G. Dosseh, C. Alba-Simonesco, F. Audonnet, M. Impéror-Clerc, SBA-15 synthesis: Are there lasting effects of temperature change within the first 10min of TEOS polymerization?, Materials Chemistry and Physics, 108 (**2008**) 73-81.

[135] V. Chaudhary, S. Sharma, An overview of ordered mesoporous material SBA-15: synthesis, functionalization and application in oxidation reactions, Journal of Porous Materials, 24 (**2017**) 741-749.

[136] M.D. Argyle, C.H. Bartholomew, Heterogeneous Catalyst Deactivation and Regeneration: A Review, Catalysts, 5 (**2015**) 145-269.

[137] J. Sehested, Four challenges for nickel steam-reforming catalysts, Catalysis Today, 111 (**2006**) 103-110.

[138] J.A. Calles, A. Carrero, A.J. Vizcaíno, L. García-Moreno, Hydrogen production by glycerol steam reforming over SBA-15-supported nickel catalysts: Effect of alkaline earth promoters on activity and stability, Catalysis Today, 227 (**2014**) 198-206.

[139] A.M. Amin, E. Croiset, W. Epling, Review of methane catalytic cracking for hydrogen production, International Journal of Hydrogen Energy, 36 (**2011**) 2904-2935.

[140] F. Wang, Y. Li, W. Cai, E. Zhan, X. Mu, W. Shen, Ethanol steam reforming over Ni and Ni–Cu catalysts, Catalysis Today, 146 (**2009**) 31-36.

[141] P. Djinović, I.G. Osojnik Črnivec, B. Erjavec, A. Pintar, Influence of active metal loading and oxygen mobility on coke-free dry reforming of Ni–Co bimetallic catalysts, Applied Catalysis B: Environmental, 125 (**2012**) 259-270.

[142] N.D. Charisiou, K.N. Papageridis, G. Siakavelas, V. Sebastian, S.J. Hinder, M.A. Baker, K. Polychronopoulou, M.A. Goula, The influence of SiO_2 doping on the Ni/ZrO_2 supported catalyst for hydrogen production through the glycerol steam reforming reaction, Catalysis Today, 319 (**2019**) 206-219.

[143] A.J. Reynoso, J.L. Ayastuy, U. Iriarte-Velasco, M.A. Gutiérrez-Ortiz, Cobalt aluminate spinel-derived catalysts for glycerol aqueous phase reforming, Applied Catalysis B: Environmental, 239 (**2018**) 86-101.

[144] X. Hu, D. Dong, X. Shao, L. Zhang, G. Lu, Steam reforming of acetic acid over cobalt catalysts: Effects of Zr, Mg and K addition, International Journal of Hydrogen Energy, 42 (**2017**) 4793-4803.

[145] D. Moodley, M. Claeys, E. van Steen, P. van Helden, D. Kistamurthy, K.-J. Weststrate, H. Niemantsverdriet, A. Saib, W. Erasmus, J. van de Loosdrecht, Sintering of cobalt during FTS: Insights from industrial and model systems, Catalysis Today, 342 (**2020**) 59-70.

[146] A.K. Datye, Q. Xu, K.C. Kharas, J.M. McCarty, Particle size distributions in heterogeneous catalysts: What do they tell us about the sintering mechanism?, Catalysis Today, 111 (**2006**) 59-67.

[147] A. Ochoa, J. Bilbao, A.G. Gayubo, P. Castaño, Coke formation and deactivation during catalytic reforming of biomass and waste pyrolysis products: A review, Renewable and Sustainable Energy Reviews, 119 (**2020**) 109600.

[148] J. Sehested, Sintering of nickel steam-reforming catalysts, Journal of Catalysis, 217 (**2003**) 417-426.

[149] C.H. Bartholomew, Mechanisms of catalyst deactivation, Applied Catalysis A: General, 212 (**2001**) 17-60.

[150] D. Zubenko, S. Singh, B.A. Rosen, Exsolution of Re-alloy catalysts with enhanced stability for methane dry reforming, Applied Catalysis B: Environmental, 209 (**2017**) 711-719.

[151] E.B. Pereira, N. Homs, S. Martí, J.L.G. Fierro, P. Ramírez de la Piscina, Oxidative steam-reforming of ethanol over Co/SiO_2, $Co–Rh/SiO_2$ and $Co–Ru/SiO_2$ catalysts: Catalytic behavior and deactivation/regeneration processes, Journal of Catalysis, 257 (**2008**) 206-214.

[152] R. Huirache-Acuña, R. Nava, C.L. Peza-Ledesma, J. Lara-Romero, G. Alonso-Núez, B. Pawelec, E.M. Rivera-Muñoz, SBA-15 Mesoporous Silica as Catalytic Support for Hydrodesulfurization Catalysts—Review, Materials, 6 (**2013**) 4139-4167.

[153] M. Thommes, K. Kaneko, A.V. Neimark, J.P. Olivier, F. Rodriguez-Reinoso, J. Rouquerol, K.S. Sing, Physisorption of gases, with special reference to the evaluation of surface area and pore size distribution (IUPAC Technical Report), Pure and Applied Chemistry, 87 (**2015**) 1051-1069.

[154] S. Brunauer, P.H. Emmett, E. Teller, Adsorption of Gases in Multimolecular Layers, Journal of the American Chemical Society, 60 (**1938**) 309-319.

[155] E.P. Barrett, L.G. Joyner, P.P. Halenda, The Determination of Pore Volume and Area Distributions in Porous Substances. I. Computations from Nitrogen Isotherms, Journal of the American Chemical Society, 73 (**1951**) 373-380.

[156] A. Montaser, Inductively coupled plasma mass spectrometry, John Wiley & Sons, New York, **1998**, 1012.

[157] H.P. Klug, L.E. Alexander, X-ray diffraction procedures: for polycrystalline and amorphous materials, X-Ray Diffraction Procedures: For Polycrystalline and Amorphous Materials, John Wiley & Sons, New York, **1974**, 992.

[158] A.L. Patterson, The Scherrer Formula for X-Ray Particle Size Determination, Physical Review, 56 (**1939**) 978-982.

[159] H. Seiler, Secondary electron emission in the scanning electron microscope, Journal of Applied Physics, 54 (**1983**) R1-R18.

[160] Y. Lin, J.A. McCarthy, K.R. Poeppelmeier, L.D. Marks, Applications of Electron Microscopy in Heterogeneous Catalysis, Catalysis by Materials with Well-Defined Structures, Elsevier, Amsterdam, **2015**, 193-238.

[161] J. Goetze, B.M. Weckhuysen, Spatiotemporal coke formation over zeolite ZSM-5 during the methanol-to-olefins process as studied with operando UV-vis spectroscopy: a comparison between H-ZSM-5 and Mg-ZSM-5, Catalysis Science & Technology, 8 (**2018**) 1632-1644.

[162] G. Atthipalli, H. Wang, J.L. Gray, Catalyst-assisted vertical growth of carbon nanotubes on Inconel coated commercial copper foil substrates versus sputtered copper films, Applied Surface Science, 273 (**2013**) 515-519.

[163] A.E. Galetti, M.F. Gomez, L.A. Arrúa, M.C. Abello, Hydrogen production by ethanol reforming over NiZnAl catalysts: Influence of Ce addition on carbon deposition, Applied Catalysis A: General, 348 (**2008**) 94-102.

[164] G. Sierra Gallego, F. Mondragón, J.-M. Tatibouët, J. Barrault, C. Batiot-Dupeyrat, Carbon dioxide reforming of methane over La_2NiO_4 as catalyst precursor—Characterization of carbon deposition, Catalysis Today, 133-135 (**2008**) 200-209.

[165] J.D. Jimenez, C. Wen, M.M. Royko, A.J. Kropf, C. Segre, J. Lauterbach, Influence of Coordination Environment of Anchored Single-Site Cobalt Catalyst on CO_2 Hydrogenation, ChemCatChem, 12 (**2020**) 846-854.

[166] T. Sakamoto, K. Asazawa, K. Yamada, H. Tanaka, Study of Pt-free anode catalysts for anion exchange membrane fuel cells, Catalysis Today, 164 (**2011**) 181-185.

[167] N. Cakiryilmaz, H. Arbag, N. Oktar, G. Dogu, T. Dogu, Catalytic performances of Ni and Cu impregnated MCM-41 and Zr-MCM-41 for hydrogen production through steam reforming of acetic acid, Catalysis Today, 323 (**2019**) 191-199.

[168] H. Song, U.S. Ozkan, Changing the Oxygen Mobility in Co/Ceria Catalysts by Ca Incorporation: Implications for Ethanol Steam Reforming, The Journal of Physical Chemistry A, 114 (**2010**) 3796-3801.

[169] Z. Li, M. Si, X. Li, J. Lv, Effects of titanium silicalite and TiO_2 nanocomposites on supported Co-based catalysts for Fischer–Tropsch synthesis, Applied Organometallic Chemistry, 33 (**2019**) 4640.

[170] J. Chen, X. Zhang, H. Arandiyan, Y. Peng, H. Chang, J. Li, Low temperature complete combustion of methane over cobalt chromium oxides catalysts, Catalysis Today, 201 (**2013**) 12-18.

[171] A.L.M. da Silva, J.P. den Breejen, L.V. Mattos, J.H. Bitter, K.P. de Jong, F.B. Noronha, Cobalt particle size effects on catalytic performance for ethanol steam reforming – Smaller is better, Journal of Catalysis, 318 (**2014**) 67-74.

[172] H. Ma, L. Zeng, H. Tian, D. Li, X. Wang, X. Li, J. Gong, Efficient hydrogen production from ethanol steam reforming over La-modified ordered mesoporous Ni-based catalysts, Applied Catalysis B: Environmental, 181 (**2016**) 321-331.

[173] D.I. Wilson, S.L. Rough, Extrusion-spheronisation, Handbook of Powder Technology, Elsevier, Amsterdam, **2007**, 189-217.

[174] A.V. Zhensa, E.M. Kol'tsova, I.A. Petropavlovskii, V.V. Kostyuchenko, V.A. Filippin, Mathematical Modeling of Extrusion of Water–Oxide Pastes in the Production of α-Fe_2O_3 Catalysts, Theoretical Foundations of Chemical Engineering, 37 (**2003**) 197-203.

[175] H.C. Yoon, J. Otero, P.A. Erickson, Reactor design limitations for the steam reforming of methanol, Applied Catalysis B: Environmental, 75 (**2007**) 264-271.

7. Appendix

Article 1

"Effect of the incorporation of reducibility promoters (Cu, Ce, Ag) in Co/CaSBA-15 catalysts for acetic acid steam reforming"

International Journal of Energy Research, 2020

https://doi.org/10.1002/er.5832

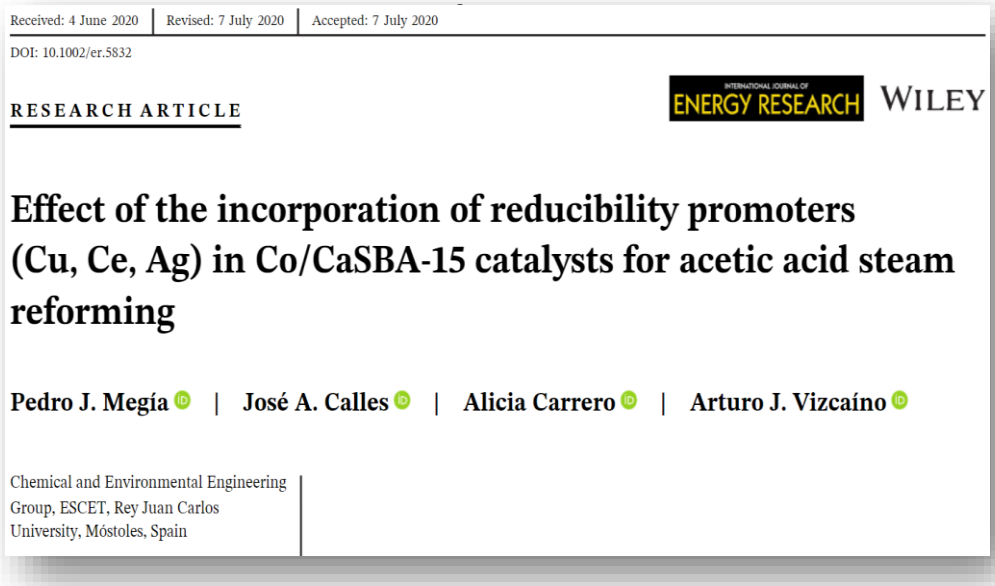

Received: 4 June 2020 | Revised: 7 July 2020 | Accepted: 7 July 2020

DOI: 10.1002/er.5832

RESEARCH ARTICLE

INTERNATIONAL JOURNAL OF ENERGY RESEARCH WILEY

Effect of the incorporation of reducibility promoters (Cu, Ce, Ag) in Co/CaSBA-15 catalysts for acetic acid steam reforming

Pedro J. Megía | José A. Calles | Alicia Carrero | Arturo J. Vizcaíno

Chemical and Environmental Engineering Group, ESCET, Rey Juan Carlos University, Móstoles, Spain

Impact JCR factor, JCR 2019: 3.741

Category: Energy & Fuels. 46 of 112 (Q2)

Abstract

In this work, we have faced the problem associated with the addition of Ca to Co/SBA-15, which gave rise to an increase in the dispersion of the particles at the expense of increasing its reduction temperature and thus, limiting its reducibility as demonstrated by XPS. This detrimental effect has been solved by the inclusion of reducibility promoters such as Cu, Ag and Ce. All these promoters led to an increase in the acetic acid conversion attributed to their beneficial effect in the catalyst reducibility. With the inclusion of Ce to Co/CaSBA-15, the high dispersion was maintained while the percentage of reduced Co species increased by ~90% compared to Co/CaSBA-15, leading to the best catalytic performance after 5 h TOS in the acetic acid steam reforming (S/C=2) at 600ºC (X ~ 99%, Y H_2 = 71.8 %) using a WHSV=30.1 h^{-1}. Furthermore, Co-Ce/CaSBA-15 showed a good stability with hydrogen yields close to thermodynamic value, despite we were working at low WHSV values. These results highlight the necessity of combining both dispersing additives and promoters of reducibility to enhance the catalytic performance.

Keywords: bio-oil; steam reforming; hydrogen production; calcium; cobalt

Introduction

Hydrogen is considered the energy carrier of the future since it can be converted into energy in an efficient way with the emission of only heat and water vapor [1]. Since hydrogen is not free form in nature, it is necessary to obtain it from raw materials using transformation processes. Nowadays most hydrogen is produced from fossil fuels, thus contributing to their future depletion and greenhouse gases emissions. This makes renewable hydrogen a promising alternative since different biomass feedstocks can be used for its production [2, 3]. In this line, the combination of biomass thermochemical conversion followed by steam reforming of the produced bio-oil is a promising alternative [4-6]. Bio-oil is a liquid product which has larger energy density than biomass, it is composed of different kind of oxygenated compounds such as acids, ketones, aldehydes and phenols among others [7]. This complex composition depends on the biomass used as feedstock together with its conversion route [8] which are responsible of many adverse properties of bio-oil, such as low heating value, corrosivity or immiscibility with other fuels that make it considered as a low-quality fuel [9-11]. By hydrogen production trough catalytic steam reforming, this bio-oil can increase its economical possibilities [12, 13]. Steam reforming technology is the most feasible method in producing hydrogen in large scale [14]. Besides, steam reforming of oxygenated compounds is an eco-friendly process since it is a carbon neutral process because the CO_2 produced will be consumed by next biomass generations [15].

Steam reforming process is endothermic and, thus, it is normally conduced at high temperatures in order to favor the global reaction [16]. According to literature, many papers can be found using bio-oil model compounds because of its complex composition [1, 5, 17-20]. In this context, carboxylic acids are the main component of bio-oil, such as acetic acid which is usually in high concentration, thus being frequently used as representative compound [18, 21-23]. In steam reforming reactions, other non desired reactions can also take place. The most important might be carbon deposition, which can deactivate the catalyst decreasing its activity towards hydrogen production [4, 17]. As a result, catalyst plays an important role in steam reforming reactions and

it will determine the hydrogen production efficiency from the feedstock selected [24-28]. Noble metal based-catalysts had demonstrated high activity and hydrogen selectivity. Transition metals, being cheaper than noble metals, have also shown good performance in terms of activity and hydrogen selectivity [5, 29]. Among transition metals used for reforming purpose, Co has been less reported than Ni [30]. However, it also provides high activity at moderate temperatures increasing hydrogen production because the water-gas shift (WGS) reaction is favored at these temperatures [31]. Both metals tend to form coke deposits and sinter throughout the steam reforming process. This explains why the selection of the support material is a key factor in this kind of processes [32, 33]. SBA-15 silica has been reported as an adequate support to improve the dispersion of the metallic phase, since metal particles can diffuse through the channels of its mesoporous structure allowing greater interaction between the support and the active phase, hindering metal sintering [34-36].

The presence of Ca in the catalyst structure may lead to better catalytic performance, since this material is considered an efficient solid sorbent because of its promising chemical and thermodynamic properties. In this sense, Quan et al. [29] have recently reported the use of CaO as support but given its low surface area, the dispersion of transitional metals on active spots could be reduced. In the recent literature, very few number of reports have been found with the inclusion of Ca to the SBA-15 structure. In previous works, it was verified that Ca-loading to SBA-15 for Ni or Co-based catalysts improved the metal dispersion, added basicity to the catalyst and increased the metal-support interaction [37]. This effect was quite significant with Co/CaSBA-15 sample in ethanol steam reforming but H_2 production was clearly limited probably due to the high reduction temperatures needed for the activation of this catalyst. On the other hand, it was verified that addition of certain promoters to SBA-15 based catalysts considerably dropped the reduction temperature [17, 38]. Other authors had also reported a decrease in the reduction temperature by the addition of different promoters to the initial catalyst [39, 40]. Thus, the aim of this work is to deeply analyse the effect of Ca addition to Co/SBA-15 to be used in acetic acid steam

reforming. Moreover, the enhancement of the activity of this catalyst by improving its reducibility was studied by adding Cu, Ag and Ce as catalyst promoters leading to Co-M/CaSBA-15 (M: Cu, Ag or Ce) never synthetized and neither used in reforming reactions before. This work proves the necessity of combining not only dispersing additives such as Ca, but also promoters of reducibility (Cu, Ag or Ce) to maintain the high dispersion of the active phase in Co/CaSBA-15, while improving the catalyst reducibility which may limit the catalytic performance in the acetic acid steam reforming.

Experimental

SBA-15 used as the support was prepared according to the hydrothermal method described by Zhao et al. [41]. It was subsequently modified by Ca incorporation (10 wt. %) following the wetness impregnation method using $Ca(NO_3)_2 \cdot 4H_2O$ according to the procedure outlined in previous publications [35]. Co/SBA-15 and Co-M/CaSBA-15 catalysts (Co: 7 wt. %; M: 2 wt. % of Cu, Ag or Ce) were prepared by wetness co-impregnation using the corresponding nitrates over the SBA-15 or modified CaSBA-15, respectively, and subsequently calcined at 550 ºC for 5 h according to those results obtained by TGA. TGA also was used in order to determine the amount of coke formed at the end of the reaction experiment. These results were obtained over airflow on a TA instruments SDT 2960 thermobalance using a 5 ºC heating ramp up to 1000 ºC. Metallic content was determined by ICP-AES employing a Varian VISTA-PRO AX CCD-Simultaneous ICP-AES spectrophotometer. XRD technique was used in order to ensure the presence of the corresponding metallic oxides in the calcined samples and the presence of metallic phase in the reduced ones. Mean crystallites size was calculated using the Scherrer equation which raise a relationship between the measured width at half intensity over the main diffraction peak of the corresponding metal phase [42]. H_2-TPR measurements were performed on a Micromeritics AUTOCHEM 2910 equipment. Samples were pretreated in Ar flow at 110 ºC for 30 minutes and then a reducing gas mixture (10 % H_2/Ar) was added at 35 N mL/min with a 5 ºC heating ramp until 980 ºC. The chemical states of cobalt element (reduced at 700ºC following the same procedure as the activation process) were recorded on an XPS Physical Electronics PHI 5700 spectrometer using non-monochromatic Al-Kα radiation (300 W, 15 kV and 1486.6 eV). Binding energy values were referenced to carbon C1s peak (284.8 eV). TEM micrographs were obtained on a JEOL JEM 2100 microscope (200 kV) with a resolution of 0.25 nm at National Centre for Electron Microscopy (CNME, Complutense University of Madrid). This equipment has also the possibility to acquire microanalysis results by energy dispersive X-ray spectroscopy (EDX). Samples need to be prepared in advance

being acetone suspended using an ultrasonic bath and then deposited on a carbon-coated copper or nickel grid. N_2 adsorption-desorption isotherms were measured on a Micromeritics Tristar 3000 analyser at 77 K. Surface areas were determined using the Brunauer-Emmett-Teller method (BET). Pore volume was derived from the desorption isotherm applying the Barret-Joyner-Halenda method (BJH). Prior to the analysis, samples were degasified under vacuum at 200 ºC during 4 h. Prepared catalysts were named as Co/SBA-15 and Co-M/CaSBA-15, where M correspond to each reducibility promoter (M: Cu, Ag or Ce).

Steam reforming reactions were performed in a fixed bed reactor on a Microactivity-Pro (PID Eng&Tech) unit at atmospheric pressure and isothermally at 600 ºC. Previously, samples were reduced at 700 ºC under pure H_2 flow according to H_2-TPR results. An acetic acid mixture (H_2O/acetic acid molar ratio of 4, double than stoichiometric value as shown in Eq. 1) was pumped at a WHSV = 30.1 h^{-1}, using N_2 as carrier and internal standard.

$$C_2H_4O_2 + 2\ H_2O \rightarrow 2\ CO_2 + 4\ H_2 \qquad \text{(Eq. 1)}$$

The outlet gas composition was measured by means of an Agilent 490 Micro-GC equipped with a thermal conductivity detector (TCD), a PoraPlot U column (10 m) and a Molecular Sieve 5A column (20 m) using He and Ar as carrier gas, respectively. Liquid outlet stream was recovered in a condenser trap at 4 ºC and subsequently analysed in a Varian CP-3900 chromatograph equipped with a CP WAX 52 CB (30 m × 0.25 mm, DF = 0.25) column and flame ionization detector (FID). Carbon deposition after each test was evaluated by TGA and Raman. TGA analysis were performed on the TA instruments SDT 2960 thermobalance as previously described, whereas, Raman spectra were acquired using a JASCO NRS-5000/7000 series Raman spectrometer.

Catalytic results were evaluated by means of conversion, hydrogen yield, carbon co-products selectivities and the amount of coke formed. Conversion, hydrogen yield and carbon co-products selectivities were estimated following equations:

$$X(\%)=\frac{F_{HAc_{inlet}}-F_{HAc_{outlet}}}{F_{HAc_{Inlet}}}\cdot 100 \qquad \text{(Eq. 2)}$$

$$Y_{H_2}(\%)=\frac{F_{H2}}{4\cdot F_{HAc_{Inlet}}}\cdot 100 \qquad \text{(Eq. 3)}$$

$$S_i\ (\%)=\frac{F_i}{2\cdot F_{HAc_{inlet}}-F_{HAc_{outlet}}}\cdot 100 \qquad \text{(Eq. 4)}$$

F_{HAc} is the molar flow rates of acetic acid at the inlet and the outlet streams, F_{H2} corresponds to the H_2 molar flowrate formed during the steam reforming reaction and F_i is related to the molar flowrate of carbon co-products in the gas stream.

On the other hand, coke deposition during the reaction was evaluated following the Eq. 5:

$$\text{Coke}\left(g_{coke}\cdot g_{cat}\cdot h^{-1}\right)=\frac{m_{coke}\ (g)\ TGA}{m_{cat}(g)\cdot TOS\ (h)} \qquad \text{(Eq. 5)}$$

Whereas m_{coke} is the amount of coke formed during the reaction determined by TGA, m_{cat} is the amount of catalyst introduced into the fixed bed reactor. TOS is the acronym of time-on-stream (5 h in all the experiments performed in the present work).

Results and discussion

Effect of Ca addition to Co/SBA-15

Catalysts characterization

The N_2 adsorption–desorption isotherms of Co/SBA-15 and Co/CaSBA-15 are displayed in Figure 1A. The conservation of the ordered mesoporous structure with hexagonal array typical of SBA-15 can be assumed after Co and Ca incorporation since both samples described a type IV isotherm with a H1-type hysteresis loop according to IUPAC classification. However, since the shape of Co/CaSBA-15 isotherm is slightly different to that of Co/SBA-15, some distortion of the porous structure may have already taken place although the overall ordered mesoporous structure was retained. This assumption is in agreement with the pore size distribution shown in Figure 1B.

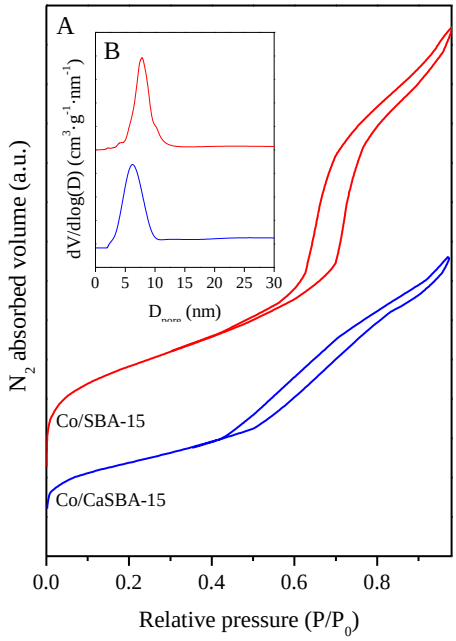

Figure 1. N_2 physisorption analysis at 77K of Co/SBA-15 and Co/CaSBA-15 catalysts: (A) isotherms; (B) pore size distribution.

As it can be discerned, while Co/SBA-15 present a narrow pore size distribution around 8 nm, this distribution is wider for Co/CaSBA-15 at lower values. In addition, the position of the inflection of Co/CaSBA-15 isotherm is slightly shifted toward smaller P/P_0 values when compared to Co/SBA-15 and the adsorbed N_2 decreased since a narrower hysteresis loop was achieved. Other authors have reported the same behavior. Whereas Sun et al. [43] observed this feature with the addition of Ca to SBA-15, Tantirungrotechai et al. [44] reported similar results when Ca was loaded to MCM-41. Both research works ascribed this phenomenon to the incorporation of calcium to the mesoporous structure. Based on BET surface area and pore volume results, summarized in Table 1, both samples showed high values for these parameters, but they are lower than those of SBA-15, mainly in the sample Co/CaSBA-15 [37, 44].

Table 1. Physicochemical properties of Co/SBA-15 and Co/CaSBA-15 catalysts.

	Ca [a] (wt. %)	**Co [a] (wt. %)**	**S_{BET} ($m^2 \cdot g^{-1}$)**	**D_{pore} [b] (nm)**	**V_{pore} [c] ($cm^3 \cdot g^{-1}$)**	**D_{Co^0} [d] (nm)**
SBA-15	-	-	550	7.5	1.0	-
CaSBA-15	8.3	-	338	7.3	0.8	-
Co/SBA-15	-	6.4	503	7.2	0.8	9.5
Co/CaSBA-15	7.8	6.6	285	6.8	0.5	7.3

[a] Determined by ICP-AES in reduced samples

[b] Measured at $P/P_0 = 0.97$

[c] BJH desorption average pore diameter

[d] Determined from XRD of reduced catalysts by Scherrer equation from the (111) diffraction plane of Co^0

Figure 2 shows the TEM micrographs and XRD of calcined Co/SBA-15 and modified Co/CaSBA 15 catalysts. The well-ordered hexagonal array, characteristic of SBA-15, can be clearly observed, corroborating the N_2-physisorption results. In Co/SBA-15 micrograph, dark zones can be distinguished over the support, ascribed to irregular metal oxides particles formed over the support and inside the SBA-15 channels, as reported elsewhere [28]. The presence of cobalt oxides, specifically Co_3O_4 (JCPDS 01-071-4921), was verified by XRD analysis. Cubic phase of Co_3O_4 showed the diffraction lines at $2\theta = 31.4^o$, 37^o, 45^o, 55.9^o, 59.7^o, 65.6^o, 77.8^o corresponding to the

planes (220), (311), (400), (422), (511), (440), and (533), respectively. On the contrary, these peaks cannot be observed in the modified Co/CaSBA-15, thus particles beyond the XRD detection limit (< 3nm) may have formed [37, 45]. The formation of a layer of a mixed Ca-Co-O phase, such as $CaCo_2O_4$ [46], cannot be discarded given the high dispersion of Co particles over the modified support. Moreover, in the TEM micrograph of calcined Co/CaSBA-15, Co oxide agglomerates cannot be appreciated. The absence of both XRD diffraction peaks and Co particles in TEM, indicates that the cobalt species are highly dispersed on the modified CaSBA 15 support. However, the presence of both Co and Ca was verified by EDX as well as by ICP-AES (see Table 1).

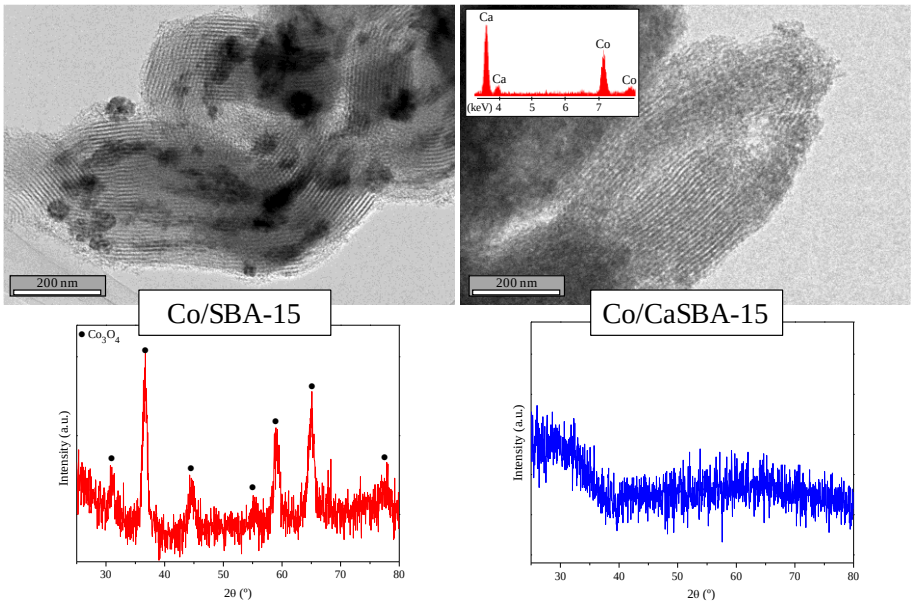

Figure 2. TEM micrographs and XRD patterns of calcined Co/SBA-15 and Co/CaSBA-15.

As the metal particle size and the catalyst reducibility are known to be closely related to catalytic activity, the reducibility of the catalysts was investigated through H_2-TPR experiment. The obtained profiles for Co/SBA-15 and modified Co/CaSBA-15 are displayed in Figure 3, and as it can be clearly seen, the reducibility of these samples is quite different. Regarding Co/SBA-15 profile, two main reduction stages can be

clearly differentiated. The first reduction stage presents a maximum around 248 ºC and a shoulder at 332 ºC. These peaks are attributed to the reduction of the larger supported Co_3O_4 particles in two steps: first, the reduction of Co_3O_4 to CoO and, subsequently, the reduction towards Co^0. Conversely, the reduction stage at higher temperature, with maxima located at 494 °C, is ascribed to the presence of smaller Co-oxide particles strongly interacting with the support [47, 48].

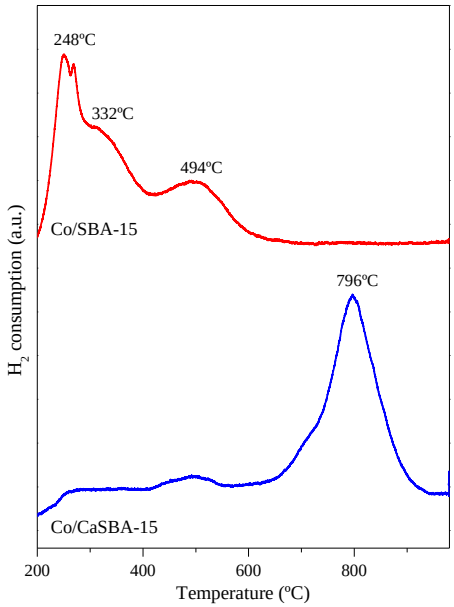

Figure 3. H_2-TPR profiles of Co/SBA-15 and Co/CaSBA-15

On the other hand, in the Co/CaSBA-15 profile, the presence of Ca shifted the reduction temperature towards higher values. This behavior is assigned to greater interaction of the active phase with the support [47, 48]. In fact, it has been described in literature that metal oxides with lower crystallite size tend to reduce at higher temperatures than bulk ones [49-52], thus, proving the XRD and TEM results of the calcined samples explained above. This effect was also reported in literature by other authors [53, 54], where a shift in the reduction temperatures towards higher values has been proposed as a consequence of smaller crystallite size. Co/CaSBA-15 profile displayed a broad peak between 610-950ºC with a clear maximum at 796ºC and a

shoulder around 710ºC. This reduction zone can be de convoluted in two different peaks corresponding to the two steps reduction of Co_3O_4 to CoO and subsequently reduced to Co^0 [55]. In addition to decreasing Co particle size, Ca addition might form mixed oxides despite they could not be detected by XRD, such as $CaCo_2O_4$, making harder the catalyst reducibility contributing to the increase in the reduction temperature.

After the activation process, to reduce the Co oxides, samples were again characterized by TEM and XRD analysis (Figure 4). Attending to Co/SBA-15, no diffraction peaks ascribed to the Co_3O_4 pattern could be distinguished in XRD profiles. Conversely, peaks corresponding to cubic Co^0 (JCPDS 00-001-1259) arise showing the diffraction at 2θ = 44.4º, 51.3° and 75.4°, ascribed to (111), (200) and (220) planes, respectively. Co^0 particles can be discerned over the support as round dark particles in TEM micrographs. Thus, it can be stated that Co oxides particles were reduced during the activation process.

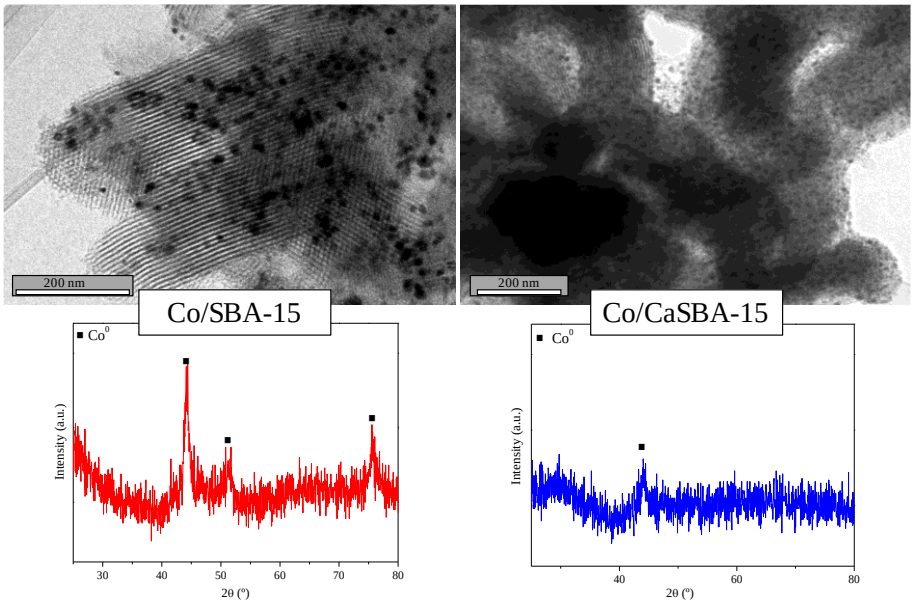

Figure 4. TEM micrographs and XRD patterns of reduced Co/SBA-15 and Co/CaSBA-15 at 700ºC.

TEM micrograph of Co/CaSBA-15 reveals the presence of metallic cobalt, unlike in the calcined sample. However, smaller particle size and greater homogeneity over the support is evident when compared to Co/SBA-15. Furthermore, as corroborating evidence, from the XRD pattern less wide diffraction peak of cubic Co^0 at $2\theta = 44.4°$ is achieved with Co/CaSBA15 leading to smaller particle size (see Table 1). Moreover, concerning this diffractogram, a change in the baseline can be appreciated at 46.6 ºC which may be attributed to the presence of monoclinic $CaCo_2O_4$ (JCPDS 00-051-1760), that would contribute to the decrease in the catalyst reducibility.

In summary, after the addition of calcium to the SBA-15 support, the overall ordered mesoporous structure of the initial material was maintained. When comparing the catalyst properties of Co/SBA-15 and Co/CaSBA-15, although the addition of Ca decreased the BET surface area, it leads to a decrease in the crystallite size of Co species over the support at the expense of the reduction temperature, which was shifted towards higher temperatures due to higher interaction between the active phase and the support or to the development of new Ca-Co compound.

Catalytic tests

The catalytic performance in terms of acetic acid conversion and hydrogen yield for Co/SBA-15 and Co/CaSBA-15 are displayed in Figure 5A and Figure 5B, respectively. Concerning conversion (Figure 5A), Co/SBA-15 reached total conversion after 5 h TOS while deactivation was observed for Co/CaSBA-15 since conversion becomes smaller with TOS. This phenomenon was also observed with the hydrogen yield obtained. Co/SBA-15 achieved a broadly constant hydrogen yield of 67 %, while for Co/CaSBA 15, this value is around 54 % at 1 h TOS and decays until 44 % at 5h TOS. Contrary to what might be expected given the smaller crystallite size in Co/CaSBA-15 [56-58], its poor Co reducibility as consequence of an increase of the reduction temperature led to worse catalytic results. Coking rate (calculated from TGA) increased from 34.8 mgcoke·gcat-1·h 1 for Co/SBA-15 until 95.2 $mg_{coke} \cdot g_{cat}^{-1} \cdot h^{-1}$ for Co/CaSBA-15.

Therefore, even though catalyst properties of Co/CaSBA-15 were promising, the catalytic performance through acetic acid steam reforming at 600ºC is worse when compared with Co/SBA-15: lower conversion and hydrogen selectivity and higher coke deposition were reached. These results may be attributed to the high interaction of Co particles with the support, thus hindering the Co species reducibility.

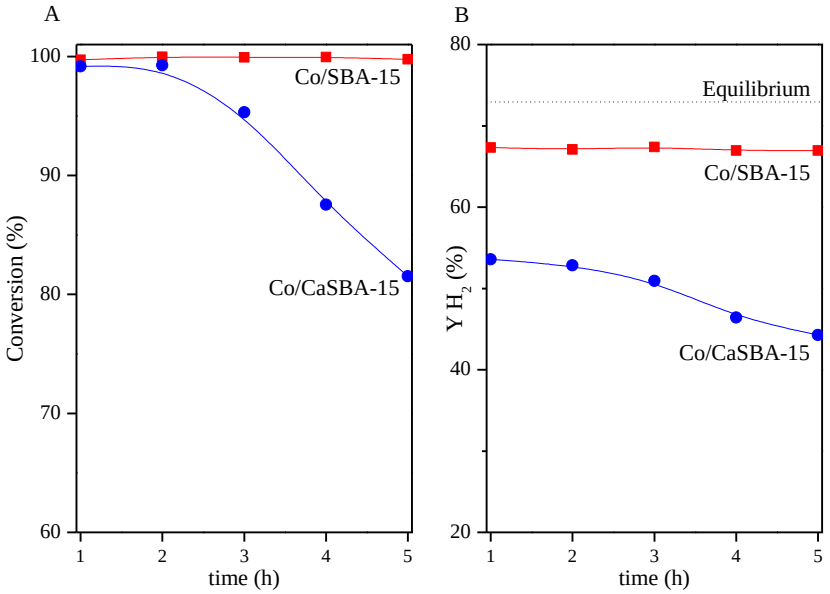

Figure 5. Catalytic performance of Co/SBA-15 and Co/CaSBA-15 trough acetic acid steam reforming (T= 600 ºC, WHSV=30.1 h^{-1}).

To shed light on the chemical state of the Co species within the catalysts after activation, XPS analyses were performed. Figure 6 shows the narrow scan spectra of the Co 2p region, in which two major binding energy features can be distinguished around 778-781 and 794 eV, assigned to Co $2p_{3/2}$ and Co $2p_{1/2}$, respectively. According to literature, peaks centred at 778 eV reveal the presence of Co^0, while peaks centred at 781 eV are characteristic of Co^{2+} [59, 60]. The remaining peak in region 784-787 eV present in all samples corresponds to a shake-up satellite attributed to Co^{2+} [61]. Concerning Co $2p_{1/2}$, two features ascribed to Co^{2+} and its shake-up satellite could be distinguished. The shift in Co $2p_{1/2}$ region towards higher binding energies in Co/CaSBA-15 compared to Co/SBA-15 sample, suggests that some surface Co^{2+}

particles are strongly interacting with the support [62]. The deconvolution of the Co $2p_{3/2}$ region confirmed the presence of Co^0 and Co^{2+} species in both samples. As it can be observed, the band at 778 eV ascribed to Co^0 species is predominant in Co/SBA-15 sample, while the feature at 781 eV predominates in the Co/CaSBA-15 sample. The $Co^0/(Co^0 + Co^{2+})$ ratio for the Co/SBA-15 sample reduced at 700 °C is 0.84, demonstrating that the surface Co is predominantly in a reduced state. Conversely, this value drops to 0.39 for the Co/CaSBA-15 sample, indicating the lower presence of Co^0 species. This confirms that Co reducibility is hindered by the presence of Ca in the support, thus decreasing the number of active sites during the acetic acid steam reforming, which resulted in worse catalytic performance.

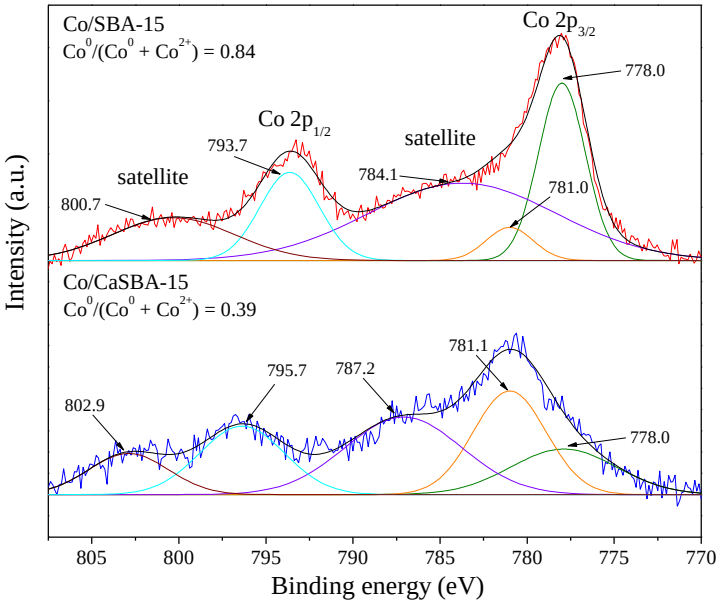

Figure 6. Co 2p XPS of reduced Co/SBA-15 and Co/CaSBA-15 catalysts.

The above results are the basis for the addition of reducibility promoters, such as Cu, Ag and Ce to Co/CaSBA-15 in order to keep its better metallic dispersion and metal-support interaction but increasing its reducibility to address the worse catalytic results achieved in acetic acid steam reforming.

Effect of the incorporation of reducibility promoters to Co/CaSBA-15

Catalysts characterization

N_2 adsorption-desorption isotherms performed at 77 K of Co-M/CaSBA-15 (Cu, Ag or Ce) catalyst are shown in Figure 7. As it can be appreciated, all the samples showed a type IV isotherm according to IUPAC classification, with a H1-type hysteresis loop, which reveals that the ordered mesoporous structure from initial CaSBA-15 material is preserved after the incorporation of all the promoters. Textural properties along with other physicochemical properties are summarized in Table 2, where Ca and Co and promoters loading measured by ICP-AES are displayed as well. From them, it is possible to check that the metal content was next to the theoretical value for Co (7%) and promoters (2%). On the other hand, Ca content was around 8 wt.% since we fixed 10 wt.% in the modified support and it was reduced by the active phase and promoter incorporation following the wetness impregnation method.

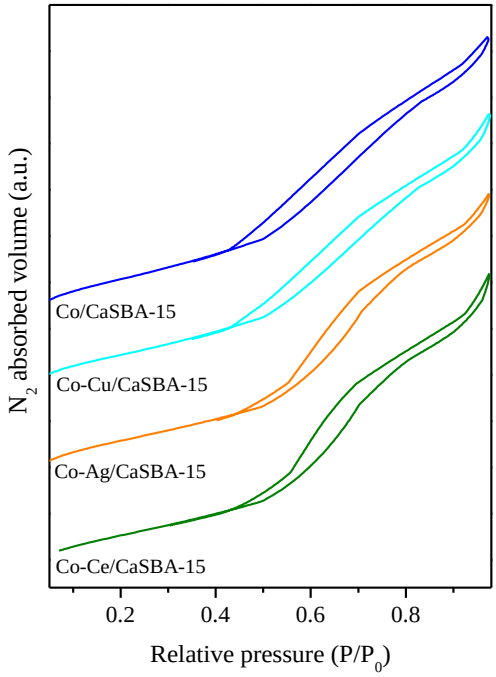

Figure 7. N_2 physisorption isotherms of Co-M/CaSBA-15 (M: Cu, Ag or Ce) catalysts at 77K.

Table 2. Physicochemical properties of Co-M/CaSBA-15 (M: Cu, Ag, Ce) catalysts.

	Ca [a] (wt. %)	Co [a] (wt. %)	M [a] (wt. %)	S_{BET} ($m^2 \cdot g^{-1}$)	D_{pore} [b] (nm)	V_{pore} [c] ($cm^3 \cdot g^{-1}$)	D_{Co^0} [d] (nm)
Co/CaSBA-15	7.8	6.6	-	285	6.8	0.5	7.3
Co-Cu/CaSBA-15	8.2	6.5	1.9	260	7.1	0.5	12.9
Co-Ag/CaSBA-15	7.8	7.0	1.9	281	7.0	0.5	9.0
Co-Ce/CaSBA-15	8.0	6.7	1.8	278	7.6	0.5	5.9

[a] Determined by ICP-AES (M: Cu, Ag or Ce) in reduced samples

[b] Measured at $P/P_0 = 0.97$

[c] BJH desorption average pore diameter

[d] Determined from XRD of reduced catalysts by Scherrer equation from the (111) diffraction plane of Co^0

Figure 8 presents the XRD patterns of calcined Co-M/CaSBA-15 catalysts in which the absence of diffraction peaks is observed for all samples except for Co-Cu/CaSBA-15. This fact is attributed to the presence of these species below the detection limit of crystallite size by XRD. Thereby, the high dispersion of Co over the support is remarkable in all prepared samples. Considering Co-Cu/CaSBA-15 sample, peaks at 2θ = 35 y 38º, assigned to (002) and (200) diffraction planes respectively of monoclinic CuO (JCPDS 07-089-2531) arise.

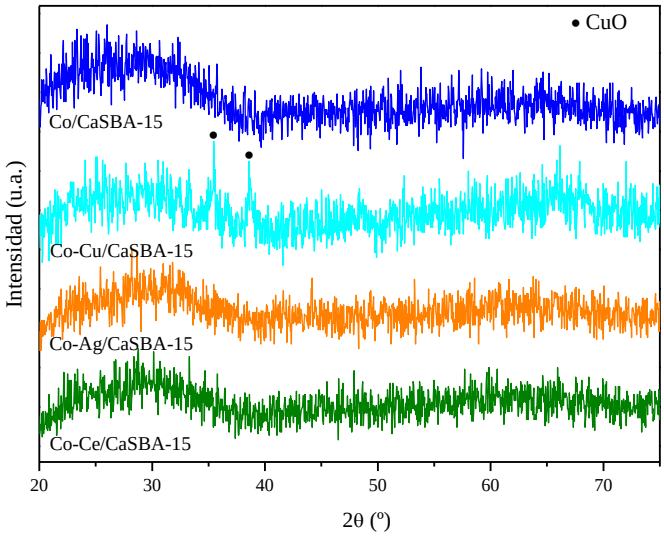

Figure 8. XRD of calcined Co-M/CaSBA-15 (M: Cu, Ag or Ce) catalysts.

Despite these peaks can be seen in the XRD diffractograms, as observed by TEM (Figure S1) there should be a high metal oxide dispersion over the support since no particles can be seen by this technique. The high dispersion of Co can be attributed to the presence of Ca as demonstrated in the previous section. The presence of Co and Cu in this sample was proved by EDX. It is important to outline that the hexagonal structure of cylindrical pores typical from SBA-15 material was maintained, supporting in this way the results obtained in the N_2 adsorption-desorption isotherms.

H_2-TPR analyses were performed and all the profiles are displayed in Figure 9. As explained before, the presence of Ca leads to an increase in the reduction temperature and thus most TPR profiles shifts to temperatures above 400ºC (high-temperature region, HT), assigned to a greater interaction of the active phase with the support [47, 48]. As a reminder, Co/CaSBA-15 profile showed a clear maximum at 796ºC and a shoulder around 710ºC, corresponding to the two reduction steps of Co_3O_4 to CoO and subsequently reduced to Co^0 [55]. These two peaks can be appreciated in all profiles, except for Co-Ag/CaSBA-15, which showed only one peak with maximum at 645ºC, related to the reduction of the Co oxides having strong interaction with Ag [63]. In the case of Co-Ce/CaSBA-15, while the HT zone is still present but slightly shifted towards lower temperatures, another peak arises at 305ºC, ascribed to the formation of Co_3O_4-CeO_2 interface thus having intimate contact between both metal oxides [64]. Similarly, apart from the HT zone, Co-Cu/CaSBA-15 sample showed a reduction zone at lower temperatures (167-191 ºC) attributed to the simultaneous reduction of Cu-oxides and Co-oxides with less interaction with the support into metallic Cu and Co, respectively [65]. In summary, attending to TPR profiles, it is possible to see how all the used promoters improved, in terms of reduction temperature, the reducibility of Co/CaSBA-15 which showed the highest reduction temperature at 796ºC. By Cu and Ce addition, HT zones are significantly shifted to lower reduction temperatures by promoter addition, thereby increasing the LT zones area (low-temperature region, below 400 ºC). This effect is more pronounced for Co-Ce/CaSBA-15 as it can be observed in the H_2-TPR results summarized in Table 3. Conversely, Co-Ag/SBA-15

showed most its area in the HT region but decreased the reduction temperature in 250ºC. On the other hand, attending to the degree of reduction (calculated from the experimental H_2 uptake related to the theoretical value) taking into account the theoretical and experimental consumption of H_2 along the TPR analysis, Co-Ce/CaSBA 15 demonstrated the highest level of reduction, achieving an experimental uptake in terms of μmol $H_2 \cdot g_{cat}^{-1}$ very similar to the estimated theoretical value.

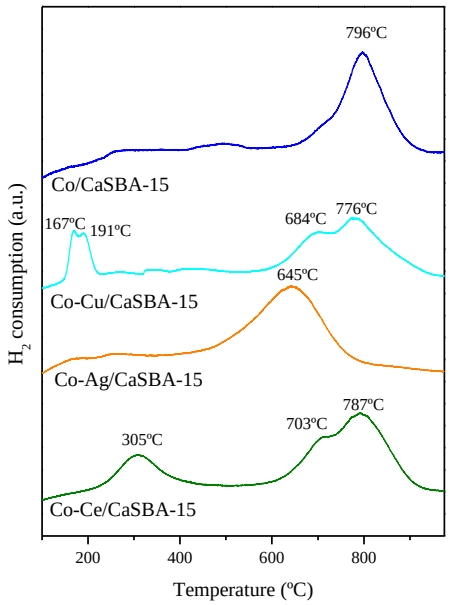

Figure 9. H_2-TPR profiles for Co-(Cu, Ag or Ce)/CaSBA-15 samples.

Table 3. Summary of reduction features in LT and HT region contribution of TPR profiles, theoretical and experimental H_2 consumption and degree of reduction for calcined Co-M/CaSBA-15 catalyst.

	Area contribution		Theoretical uptake	Experimental uptake	Degree of
	LT (%)	HT (%)	μmol $H_2 \cdot g_{cat}^{-1}$	μmol $H_2 \cdot g_{cat}^{-1}$	reduction (%)
Co/CaSBA-15	6.15	93.85	1425	1270	87
Co-Cu/CaSBA-15	18.89	81.11	1663	1528	92
Co-Ag/CaSBA-15	2.85	97.15	1660	1574	95
Co-Ce/CaSBA-15	21.41	78.59	1448	1459	~100

On the basis of the reduction degree estimated by TPR analysis, Figure 10 compares the XPS narrow scan spectra of the Co 2p region for Co/CaSBA-15 and Co-Ce/CaSBA-15 catalysts after being subjected to the activation process described in the Experimental Section. These catalysts were selected as the samples with the lowest and the highest reducibility, respectively. Two major features centred at binding energies around 780 and 796 eV can be observed, ascribed to Co $2p_{3/2}$ and Co $2p_{1/2}$ regions, respectively. As mentioned before, the presence of metallic Co is attributed to the peak centred at 778 eV, while peaks centred at 781 eV are characteristic of Co^{2+} [52, 53]. When compared to Co/CaSBA-15 sample, the $Co^0/(Co^0 + Co^{2+})$ ratio obtained for the activated Co-Ce/CaSBA-15 increases from 0.39 up to 0.76, value close to that obtained with Co/SBA-15 (see Figure 6). This result reveals that the Co present in the Co-Ce/CaSBA-15 catalyst surface is predominantly into a reduced state.

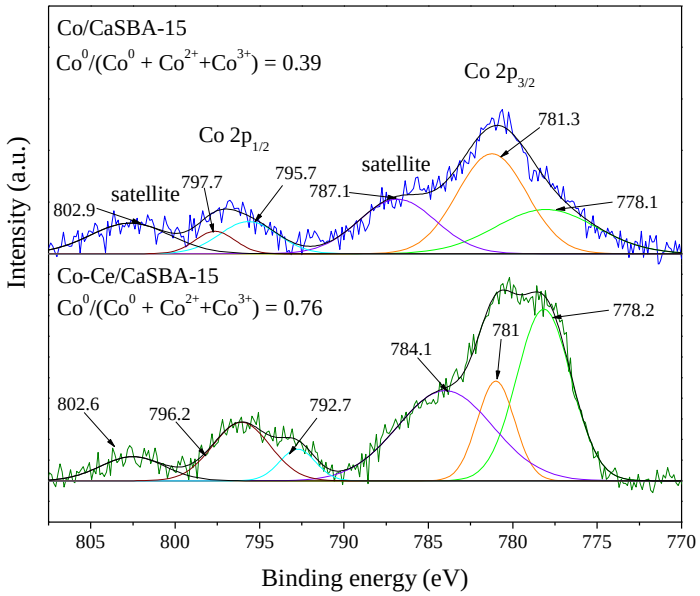

Figure 1. Co 2p XPS of Co/CaSBA-15 and Co-Ce/CaSBA-15 samples reduced at 700 ºC.

After the activation procedure, all the catalysts were also characterized by XRD. The obtained diffractograms are displayed in Figure 11. In addition to cubic Co^0 (JCPDS 00-001-1259), other peaks corresponding to cubic Cu^0 (JCPDS 00-001-1241) at 2θ =

43.5º, 50.4º and 74º and cubic Ag^0 (JCPDS 01-071-6549) at 2θ = 38.1º and 64.5º can be observed in the corresponding samples. In the case of the Co-Ce/CaSBA-15 sample, no diffraction peak corresponding to metallic Ce could be observed since Ce oxides need higher reduction temperatures, near to 1500ºC [66]. Additionally, no diffraction peak of CeO_2 appears, maybe due to the formation of non-stoichiometric $CeO_{2-\delta}$, not possible to be observed by XRD, or to the detection limit of the XRD equipment. Mean crystallites size of each sample was calculated using the Scherrer equation and the obtained results are summarized in Table 2. In the case of the Co-Ce/CaSBA-15 catalyst, the Co dispersion was even further improved when compared to Co/CaSBA-15. This evidences that the inclusion of Ce to Co/CaSBA-15 as a reducibility promoter can keep the high metal dispersion over the support but increases the presence of Co species in a reduced state.

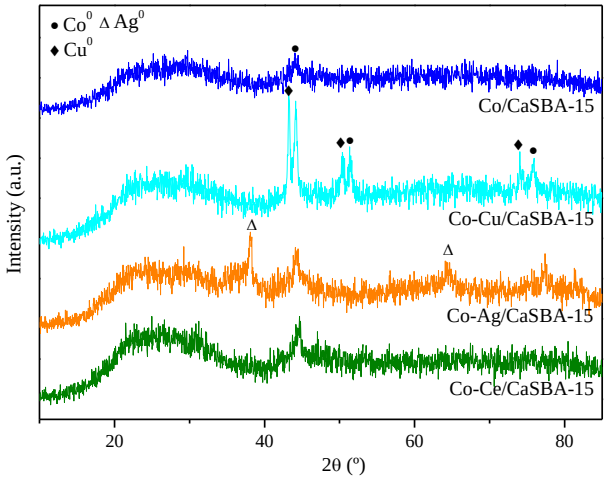

Figure 11. XRD of reduced at 700 ºC Co-M/CaSBA-15 (M: Cu, Ag or Ce) catalysts.

Catalytic tests

The catalytic results for Co-M/CaSBA-15 samples after 5h TOS in acetic acid steam reforming are shown in Figure 12. In this sense, the conversion is represented in Figure 12A. As it can be observed, all promoters lead to higher acetic acid conversion than Co/CaSBA-15 ascribed to the decrease in the reduction temperature leading to higher

number of Co metallic species. Therefore, catalyst reducibility is a good indicator of the activity in the steam reforming process. However, some deactivation was observed since the conversion becomes smaller with TOS. The highest conversion value was achieved with Co-Ce/CaSBA-15 sample, which shows the highest reducibility. Moreover, the stability of Co-Ce/CaSBA-15 catalyst was higher compared to the other promoted samples, which are supposed to be in an intermediate reduction state according to H_2-TPR results. The presence of CeO_2 in the catalyst formulation has been reported to have beneficial effects in catalyst stability since it promotes the coke gasification ant it is also active in WGS reaction due to its capacity to store, release and transport oxygen [67].

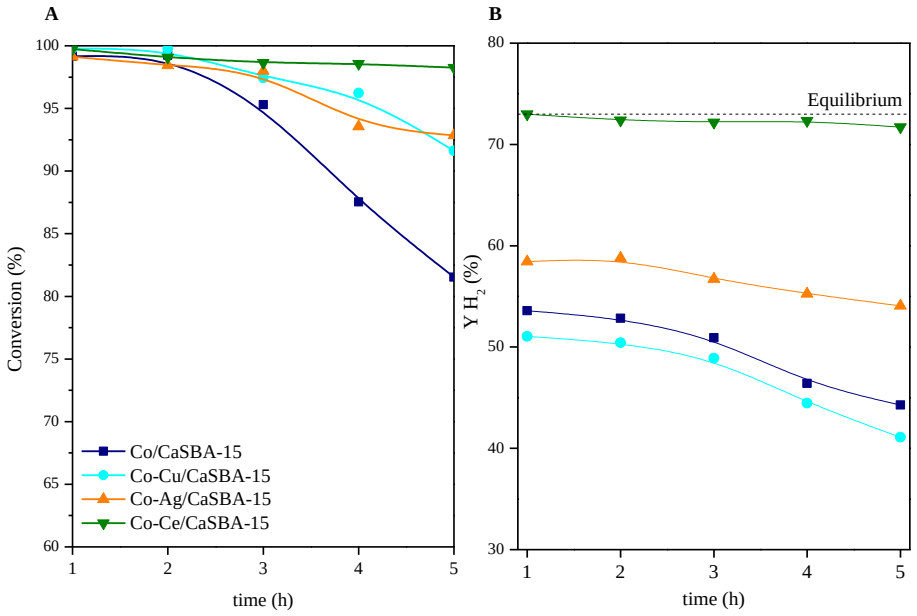

Figure 12. Catalytic results for Co-M/CaSBA-15 (M: Cu, Ag or Ce) with TOS at 600ºC, WHSV=30.1h^{-1}.

On the other hand, Figure 12B summarizes the H_2 yield with TOS, along with the value expected at equilibrium at the experimental conditions determined by Gibbs energy minimization. As observed when comparing the unpromoted sample with the other catalysts, Ag and Ce addition led to higher hydrogen yield, which is the main products of this reaction. The exception is the Cu promoted sample which reached slightly lower

hydrogen yield than the unpromoted sample. Despite the conversion increases when promoting Co/CaSBA-15 with Cu, the decrease in hydrogen yield could be ascribed to the participation of Cu in the decarboxylation reaction of acetic acid rather than the reforming reaction [68]. On the other hand, the most noticeable increase in H_2 yield was found by using Ce as promoter, being even higher than that of the Co/SBA-15 catalyst (Figure 5B). These results were in line with the lowest Co^0 size as determined by XRD (see Table 2). Thus, there is a relationship between the particle size and the catalytic activity as reported before [17, 56, 69, 70] since smaller crystallite size helps to enhance the catalytic activity since more active sites are accessible. Moreover, Co-Cu/CaSBA-15 sample present the highest crystallite size as mentioned before. Therefore, the catalytic behavior is affected not only by crystallite size but also by the reducibility. It must be highlighted that Co-Ce/CaSBA-15 reached the highest H_2 yield very close to the thermodynamic value estimated at the same reaction conditions. This effect is ascribed not only to the lowest Co particle size and the improvement in the reducibility achieved with this sample, but also due to the fact that the inclusion of Ce in the catalyst creates more oxygen vacancies, thus, facilitating the improvement of oxygen mobility [71] leading to the best catalytic performance.

This result is promising when compared to other catalysts for acetic acid steam reforming described in literature. Hu et al. [18], studied the effect of Zr, Mg and K addition to Co/Al_2O_3 (Co = 30 wt.%), they led to the conclusion that $Co\text{-}K/Al_2O_3$ promoted the hydrogen production by suppressing the formation of methane, reaching conversion values of acetic acid around 90 % at 400ºC using a S/C ratio of 1.2. Nabgan et al. [72] reported the use of Co/La_2O_3, in the acetic acid steam reforming with S/C=7.5 at different temperatures. They reached an acetic acid conversion values of 84.2 % at 600 ºC with a hydrogen molar fraction around 0.5. The conversion increased up to 99.8 % at 700 ºC, while the hydrogen molar fraction remains almost constant. Mizuno et al. [73] used $Co\text{-}Ni/MgAl_2O_4$ catalysts with S/C=4 at 500 ºC achieving complete conversion but hydrogen selectivities around 62 %. Luo et al. [74] evaluate the influence of Co concentration (2-6 wt. %) over Ni_xMg_yO catalyst, they led to the

conclusion that in the acetic acid steam reforming at 600ºC, S/C=3, the best catalytic performance was achieved with 4 wt.% of Co obtaining 79.4 % of conversion with a hydrogen yield of 71 %. Concerning Ni-based catalysts, Hu et al. [75] reported that 30Ni/Al_2O3 in the steam reforming of acetic acid with S/C=3 at 400 ºC resulted in 70.9 % of conversion with a hydrogen yield of 61.6 %. On the other hand, Nogueira et al. [76] published the catalytic performance of Ni-supported over MgO-modified Al_2O_3 reaching 93% of conversion and 48 % of hydrogen selectivity at 600 ºC with a S/C ratio of 2. For their part, Davidson et al. [77] prepared Ni-based catalysts over CeO_2 for being tested in acetic acid steam reforming with S/C=3.5 at 500 ºC, resulting in 96% of conversion and 34% of hydrogen yield. These values reported before, are lower than those achieved with Co-Ce/CaSBA-15 catalysts even though in several works higher S/C ratio was used leading to more favorable conditions for the acetic acid reforming reaction. Additionally, our group achieved similar results at the same operating conditions with Co-Cr/SBA-15 [38] when compared to Co-Ce/CaSBA-15 performance. While it is true that with Co-Ce/CaSBA-15 gives similar results in terms of conversion and hydrogen yield (next to the thermodynamic equilibrium), with this sample, we avoid the presence of Cr in the catalyst formulation given its toxicity.

Selectivities of carbon co-products in the gas stream at 5 h TOS are shown in Figure 13. Regarding the obtained results, significant differences may be observed. CH_4 selectivity in promoted samples, compared to Co/CaSBA-15, is lower in all cases with the exception of Cu-promoted sample. This is an indicator of higher activity in the methane steam reforming [35]. Consequently, higher selectivities towards the other products (H_2 and CO) were obtained according to Eq. 6.

$$CH_4 + H_2O \leftrightarrow CO + 3H_2 \qquad \text{(Eq. 6)}$$

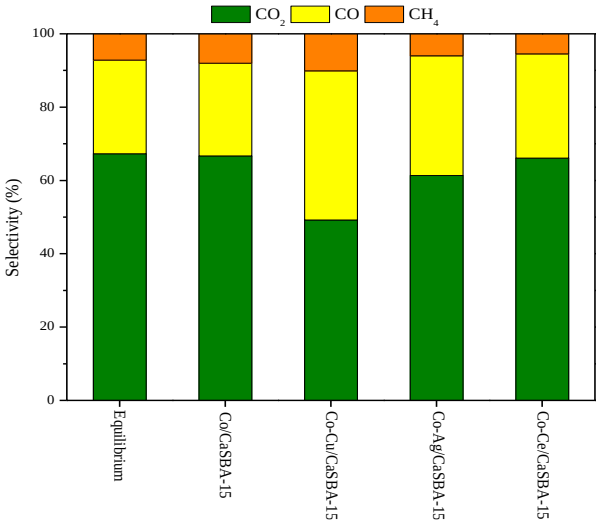

Figure 13. Carbon co-products selectivities in the gas stream for Co-M/CaSBA-15 (M: Cu, Ag or Ce) at 5h TOS, 600ºC, WHSV=30.1h^{-1}.

The increase of CO selectivity in the gas product distribution states that the CO, which is being formed during the methane steam reforming cannot be totally consumed by WGS reaction. The increase in CH_4 selectivity with Co-Cu/CaSBA-15 could be ascribed to the participation of Cu in the decarboxylation reaction of acetic acid [68]. This reaction is based on the adsorption of acetic acid to form acetate (CH_3COO^*) and/or acyl species (CH_3CO^*) which decompose to methyl species releasing CO_2 and CO, respectively [17]. Given that in this case the CO selectivity increases considerably with the Cu-promoted sample, the most likely option is the formation of acyl species, leading to an increase in CO selectivity through their decomposition.

Characterization of used catalysts

Carbon deposition is usually produced by secondary reactions along the acetic acid steam reforming, either from intermediates or from the main products, leading to catalysts deactivation limiting their industrial utilization [23]. The formation of large amount of coke deposits does not imply catalyst deactivation, since it also depends on its nature, the morphology and the location [76]. It should be noted that catalysts deactivation is not only related to carbon deposition, but also to active phase sintering

and/or oxidation. Accordingly, XRD patterns of used catalyst are illustrated in Figure 14. In all the used samples, Co^0 remains unaltered and no peaks attributed to Co-oxides can be distinguished enabling to conclude that metallic Co is the main state after 5 h TOS. Thus, reflection planes (111), (200) and (220) at $2\theta = 44.4°$, 51.3° and 75.4°, respectively attributed to cubic Co^0 (JCPDS 00-001-1259) can be clearly discerned. Again, for Co-Cu/CaSBA-15 and Co-Ag/CaSBA-15, peaks corresponding to cubic Cu^0 (JCPDS 00-001-1241) at $2\theta = 43.5º$ and 50.4º and cubic Ag^0 (JCPDS 01-071-6549) at $2\theta = 38.1º$ and 64.5º can be observed, respectively. The reflection peaks of graphitic carbon (JCPDS 00-041-1487) at $2\theta = 26.5°$ and 42.6° is detected in all the samples, associated with (002) and (100) diffraction planes, respectively. This corroborates the formation of carbon deposits throughout the steam reforming reaction. Sintering was evaluated by means of crystallite sizes calculated using the Scherrer equation from the line broadening of the Co^0 (111) diffraction. The results are shown in brackets below the corresponding XRD pattern in Figure 14. The calculated crystallite sizes after the steam reforming reaction where slightly higher in all the samples when compared to reduced catalysts. However, the order of Co crystallites size is maintained as: Cu > Ag > Co > Ce, as in the case of the activated samples (see Table 2). These results along with carbon deposition led to a decrease in the catalytic activity due to catalyst deactivation as mentioned above.

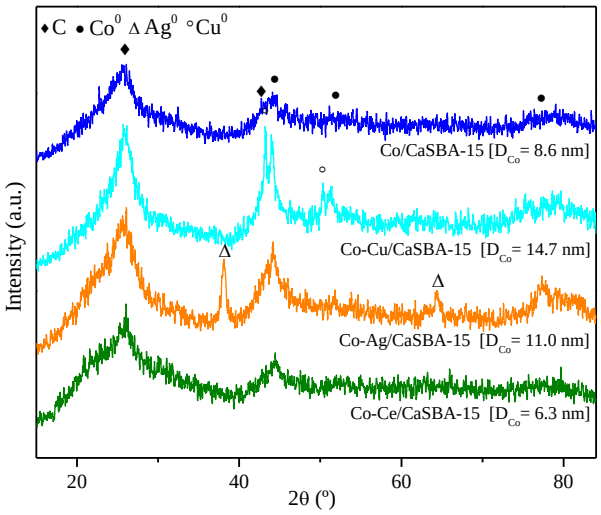

Figure 14. XRD patterns of used Co-M/CaSBA-15 (M: Cu, Ag or Ce) catalysts after 5 h TOS at 600ºC, 1 atm (crystallites sizes calculated from the line broadening of the Co^0 (111) diffraction, using the Scherrer equation are shown in brackets).

In addition to sintering, as mentioned before, coke deposition has been described as one of the major causes of deactivation in reforming catalysts [78, 79], not only referred to the amount but also to its nature. Consequently, TGA measurements of used catalysts under air flowing atmosphere were performed in order to characterize the gasification/combustion of formed coke. In this sense, the derivative thermogravimetric curves of each catalyst are represented in Figure 15. Generally, all the curves present a maximum at temperatures above 400 ºC. Depends on the oxidation temperatures, the formation of carbon nanofilaments with different ordering degree take place [80] since amorphous coke oxidizes at temperatures below 400 ºC [81-83]. As the combustion temperature increases, more ordered carbon deposits have been formed, and thus, more difficult will be their removal [80, 84]. Overall, all curves showed one maximum between 445-489 ºC and in the case of Co-Ce/CaSBA-15 another one arises around 548 ºC, suggesting the formation of carbon nanofilaments with different ordering degree. Only Co-Ag/CaSBA-15 showed a maximum at the lowest temperature, 445 ºC, which could be ascribed to the formation of some defective carbon deposits. Regarding coke rating displayed in Figure 15 in terms of

$mg_{coke} \cdot g_{cat}^{-1} \cdot h^{-1}$, Cu and Ag addition to Co/CaSBA-15 increase the amount of coke formed, suggesting that their addition promotes the formation of carbonaceous species over the catalyst surface. Instead, Ce the lowest carbon deposition was achieved for Co-Ce/CaSBA 15 catalyst, in line with the smaller Co^0 crystallite size measured by the Scherrer equation (see Table 2 and Figure 14), since smaller Co crystallites will prevent the formation of carbonaceous deposits [70, 85, 86].

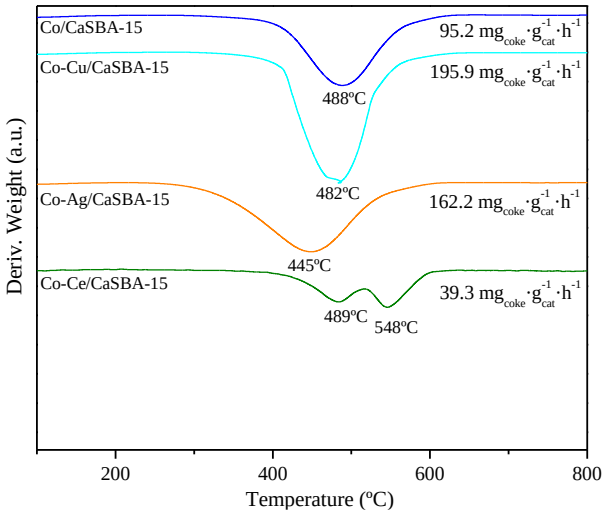

Figure 15. Derivative thermogravimetric analyses (airflow) of the used Co-M/CaSBA-15 catalysts.

The spent catalysts after 5 h TOS were also characterized by TEM as shown in Figure 16. As it can be observed, the initial structure of the SBA-15 support has been preserved even under reaction conditions. Besides, carbon nanofibers with different ordering degree can be distinguished in all samples, verifying the results obtained with DTG.

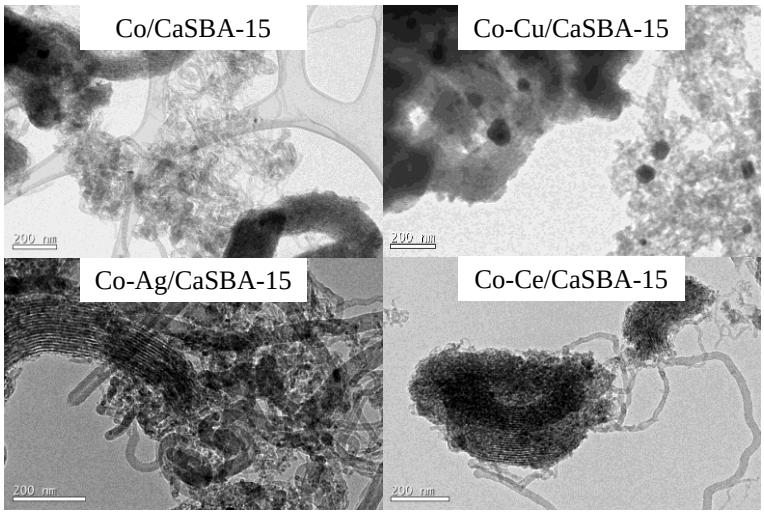

Figure 16. TEM micrographs of used Co-M/Ca-SBA-15 at 5 h TOS, 600 ºC.

Raman spectroscopy analysis was used to evaluate the nature of coke deposited during the steam reforming reaction, the spectra of spent catalysts are shown in Figure 17. The presence of two bands is noticeable in the range between 1100-1800 cm^{-1}, ascribed to the G band (~ 1590 cm^{-1}), characteristic of condensed, ordered or graphitic structures, and D band (~ 1340 cm^{-1}) attributed to disordered aromatic structures associated with aliphatic bonds of carbon materials [87, 88]. In all the samples is possible to observe both bands exhibiting the heterogeneity of the carbon species, which are present in the formed coke. The ratio of peaks area between D and G band (ID/IG) can give information about the graphitization degree of the carbon structures [67, 88, 89]. The higher I_D/I_G ratio, the lower graphitization degree [90, 91]. Thus, the calculated results are displayed in Figure 17. From the results, the I_D/I_G ratio increases in the following order: Co-Cu/CaSBA-15 < Co/CaSBA-15 < Co-Ag/CaSBA-15 < Co-Ce/CaSBA-15. These results imply that in Co-Ce/CaSBA-15 prevail formation of a large number of disordered carbon when compared to Co-Cu/CaSBA-15 in which the carbon deposition (more ordered carbon species) occurs in larger extent over the Co^0 surface [89]. The obtained results follow the same trend as H_2 selectivity (see Figure 12B) suggesting the relation between both parameters.

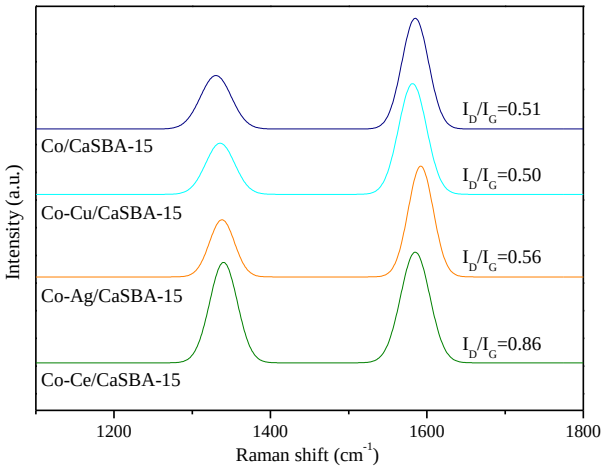

Figure 17. Raman spectra of used Co-M/CaSBA-15 samples.

Finally, in order to evaluate the stability of Co-Ce/CaSBA-15, a longer time-on-stream test was performed. The obtained results in terms of conversion and hydrogen selectivity are displayed in Figure 18. As it can be observed, conversion and hydrogen selectivity remain at acceptable values after 50 h, remaining the hydrogen selectivity next to the equilibrium value. These results evidence the high stability of this sample being thus, a promising catalysts for acetic acid steam reforming purposes.

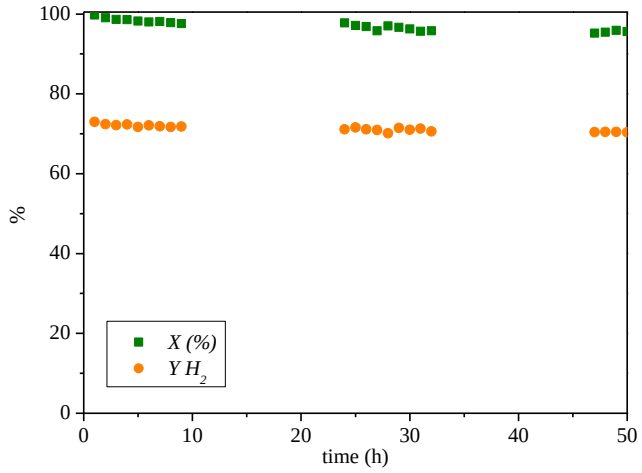

Figure 18. Catalytic results for Co-Ce/CaSBA-15 during the stability test with TOS at 600ºC, WHSV=30.1h^{-1}.

Conclusions

The influence of Ca incorporation to Co/SBA-15 was for first time evaluated in acetic acid steam reforming. The results showed how Ca addition results in the reduction of Co crystal size joined to a decrease in Co reducibility, as confirmed by H_2-TPR and XPS analysis. Therefore, the influence of reducibility promoter addition (Cu, Ag and Ce) to Co/CaSBA-15 has been studied in the same reaction. The addition of any of these promoters resulted in the enhancement of the catalytic performance since reducibility was improved in terms of reduction temperature, increasing the acetic acid conversion and the hydrogen yield. Only Cu could not improve the hydrogen yield, which might be due to the role of Cu in the decarboxylation reaction of acetic acid rather than the reforming reaction. Despite Ag addition improved the catalytic performance, it promotes the formation of carbonaceous species. On the other hand, Ce addition improved even further the high Co dispersion achieved in the Co/CaSBA-15 sample. As a consequence of the high dispersion (crystallite size ~40 % lower than Co/SBA-15) and good reducibility (comparable to that obtained for Co/SBA-15), Co-Ce/CaSBA-15 sample reached the best catalytic performance (X ~ 99%, Y H_2 = 71.8 %) after 5 h TOS in the acetic acid steam reforming increasing the hydrogen yield in a 62% compared to Co/CaSBA-15. Furthermore, Co-Ce/CaSBA-15 showed a good stability with hydrogen yields close to thermodynamic value, despite we were working at low WHSV values. Thus, these results prove the need for equilibrium between metal dispersion and reducibility to enhance the catalytic performance.

Acknowledgements

The authors acknowledge the financial support from the Regional Government of Comunidad de Madrid (project S2018/EMT-4344) and from the Spanish Ministry of Economy and Competitiveness (project ENE2017-83696-R).

References

[1] Z. Ma, R. Xiao, H. Zhang, Catalytic steam reforming of bio-oil model compounds for hydrogen-rich gas production using bio-char as catalyst, International Journal of Hydrogen Energy, 42 (**2017**) 3579-3585.

[2] K. Kang, R. Azargohar, A.K. Dalai, H. Wang, Hydrogen production from lignin, cellulose and waste biomass via supercritical water gasification: Catalyst activity and process optimization study, Energy Conversion and Management, 117 (**2016**) 528-537.

[3] A. Arregi, M. Amutio, G. Lopez, J. Bilbao, M. Olazar, Evaluation of thermochemical routes for hydrogen production from biomass: A review, Energy Conversion and Management, 165 (**2018**) 696-719.

[4] C. Quan, S. Xu, C. Zhou, Steam reforming of bio-oil from coconut shell pyrolysis over Fe/olivine catalyst, Energy Conversion and Management, 141 (**2017**) 40-47.

[5] W. Nabgan, T.A. Tuan Abdullah, R. Mat, B. Nabgan, Y. Gambo, M. Ibrahim, A. Ahmad, A.A. Jalil, S. Triwahyono, I. Saeh, Renewable hydrogen production from bio-oil derivative via catalytic steam reforming: An overview, Renewable and Sustainable Energy Reviews, 79 (**2017**) 347-357.

[6] A.G. Adeniyi, K.S. Otoikhian, J.O. Ighalo, Steam Reforming of Biomass Pyrolysis Oil: A Review, 17 (**2019**) 20180328.

[7] K.G. Kalogiannis, S.D. Stefanidis, A.A. Lappas, Catalyst deactivation, ash accumulation and bio-oil deoxygenation during ex situ catalytic fast pyrolysis of

biomass in a cascade thermal-catalytic reactor system, Fuel Processing Technology, 186 (**2019**) 99-109.

[8] G. Esteban-Díez, M.V. Gil, C. Pevida, D. Chen, F. Rubiera, Effect of operating conditions on the sorption enhanced steam reforming of blends of acetic acid and acetone as bio-oil model compounds, Applied Energy, 177 (**2016**) 579-590.

[9] A.V. Bridgwater, Review of fast pyrolysis of biomass and product upgrading, Biomass Bioenergy, 38 (**2012**) 68-94.

[10] S. Xiu, A. Shahbazi, Bio-oil production and upgrading research: A review, Renewable and Sustainable Energy Reviews, 16 (**2012**) 4406-4414.

[11] D. Vamvuka, Bio-oil, solid and gaseous biofuels from biomass pyrolysis processes—An overview, International Journal of Energy Research, 35 (**2011**) 835-862.

[12] K. Jacobson, K.C. Maheria, A. Kumar Dalai, Bio-oil valorization: A review, Renewable and Sustainable Energy Reviews, 23 (**2013**) 91-106.

[13] K.A. Resende, C.N. Ávila-Neto, R.C. Rabelo-Neto, F.B. Noronha, C.E. Hori, Thermodynamic analysis and reaction routes of steam reforming of bio-oil aqueous fraction, Renewable Energy, 80 (**2015**) 166-176.

[14] S.E. Hosseini, M. Abdul Wahid, M.M. Jamil, A.A.M. Azli, M.F. Misbah, A review on biomass-based hydrogen production for renewable energy supply, International Journal of Energy Research, 39 (**2015**) 1597-1615.

[15] A. Tanksale, J.N. Beltramini, G.M. Lu, A review of catalytic hydrogen production processes from biomass, Renewable and Sustainable Energy Reviews, 14 (**2010**) 166-182.

[16] C. Montero, A. Remiro, P.L. Benito, J. Bilbao, A.G. Gayubo, Optimum operating conditions in ethanol steam reforming over a Ni/La_2O_3-αAl_2O_3 catalyst in a fluidized bed reactor, Fuel Processing Technology, 169 (**2018**) 207-216.

[17] J.A. Calles, A. Carrero, A.J. Vizcaíno, L. García-Moreno, P.J. Megía, Steam Reforming of Model Bio-Oil Aqueous Fraction Using Ni-(Cu, Co, Cr)/SBA-15 Catalysts, International Journal of Molecular Sciences, 20 (**2019**) 512.

[18] X. Hu, D. Dong, X. Shao, L. Zhang, G. Lu, Steam reforming of acetic acid over cobalt catalysts: Effects of Zr, Mg and K addition, International Journal of Hydrogen Energy, 42 (**2017**) 4793-4803.

[19] D. Li, X. Li, J. Gong, Catalytic Reforming of Oxygenates: State of the Art and Future Prospects, Chemical Reviews, 116 (**2016**) 11529-11653.

[20] Y. Mei, C. Wu, R. Liu, Hydrogen production from steam reforming of bio-oil model compound and byproducts elimination, International Journal of Hydrogen Energy, 41 (**2016**) 9145-9152.

[21] W. Maqbool, P. Hobson, K. Dunn, W. Doherty, Supercritical Carbon Dioxide Separation of Carboxylic Acids and Phenolics from Bio-Oil of Lignocellulosic Origin: Understanding Bio-Oil Compositions, Compound Solubilities, and Their Fractionation, Industrial & Engineering Chemistry Research, 56 (**2017**) 3129-3144.

[22] X. Hu, Y. Wang, D. Mourant, R. Gunawan, C. Lievens, W. Chaiwat, M. Gholizadeh, L. Wu, X. Li, C.-Z. Li, Polymerization on heating up of bio-oil: A model compound study, AIChE Journal, 59 (**2013**) 888-900.

[23] G. Chen, J. Tao, C. Liu, B. Yan, W. Li, X. Li, Hydrogen production via acetic acid steam reforming: A critical review on catalysts, Renewable and Sustainable Energy Reviews, 79 (**2017**) 1091-1098.

[24] H. Ma, L. Zeng, H. Tian, D. Li, X. Wang, X. Li, J. Gong, Efficient hydrogen production from ethanol steam reforming over La-modified ordered mesoporous Ni-based catalysts, Applied Catalysis B: Environmental, 181 (**2016**) 321-331.

[25] Z. Zhang, X. Hu, G. Gao, T. Wei, D. Dong, Y. Wang, S. Hu, J. Xiang, Q. Liu, D. Geng, Steam reforming of acetic acid over NiKOH/Al_2O_3 catalyst with low nickel

loading: The remarkable promotional effects of KOH on activity, International Journal of Hydrogen Energy, 44 (**2019**) 729-747.

[26] D. Li, L. Zeng, X. Li, X. Wang, H. Ma, S. Assabumrungrat, J. Gong, Ceria-promoted Ni/SBA-15 catalysts for ethanol steam reforming with enhanced activity and resistance to deactivation, Applied Catalysis B: Environmental, 176-177 (**2015**) 532-541.

[27] S.D. Angeli, L. Turchetti, G. Monteleone, A.A. Lemonidou, Catalyst development for steam reforming of methane and model biogas at low temperature, Applied Catalysis B: Environmental, 181 (**2016**) 34-46.

[28] A. Carrero, J.A. Calles, L. García-Moreno, A.J. Vizcaíno, Production of Renewable Hydrogen from Glycerol Steam Reforming over Bimetallic Ni-(Cu,Co,Cr) Catalysts Supported on SBA-15 Silica, Catalysts, 7 (**2017**) 55.

[29] C. Quan, N. Gao, H. Wang, H. Sun, C. Wu, X. Wang, Z. Ma, Ethanol steam reforming on Ni/CaO catalysts for coproduction of hydrogen and carbon nanotubes, International Journal of Energy Research, 43 (**2019**) 1255-1271.

[30] X. Lian, Y. Xue, Z. Zhao, G. Xu, S. Han, H. Yu, Progress on upgrading methods of bio-oil: A review, International Journal of Energy Research, 41 (**2017**) 1798-1816.

[31] B. Banach, A. Machocki, P. Rybak, A. Denis, W. Grzegorczyk, W. Gac, Selective production of hydrogen by steam reforming of bio-ethanol, Catalysis Today, 176 (**2011**) 28-35.

[32] K. Bizkarra, V.L. Barrio, L. Gartzia-Rivero, J. Bañuelos, I. López-Arbeloa, J.F. Cambra, Hydrogen production from a model bio-oil/bio-glycerol mixture through steam reforming using Zeolite L supported catalysts, International Journal of Hydrogen Energy, 44 (**2019**) 1492-1504.

[33] T.K. Phung, T.L.M. Pham, A.-N.T. Nguyen, K.B. Vu, H.N. Giang, T.-A. Nguyen, T.C. Huynh, H.D. Pham, Effect of Supports and Promoters on the Performance of

Ni-based Catalysts in Ethanol Steam Reforming, Chemical Engineering & Technology, 43 (**2020**) 672-688.

[34] J.A. Calles, A. Carrero, A.J. Vizcaíno, L. García-Moreno, Hydrogen production by glycerol steam reforming over SBA-15-supported nickel catalysts: Effect of alkaline earth promoters on activity and stability, Catalysis Today, 227 (**2014**) 198-206.

[35] A.J. Vizcaíno, A. Carrero, J.A. Calles, Ethanol steam reforming on Mg- and Ca-modified Cu–Ni/SBA-15 catalysts, Catalysis Today, 146 (**2009**) 63-70.

[36] S. He, Z. Mei, N. Liu, L. Zhang, J. Lu, X. Li, J. Wang, D. He, Y. Luo, Ni/SBA-15 catalysts for hydrogen production by ethanol steam reforming: Effect of nickel precursor, International Journal of Hydrogen Energy, 42 (**2017**) 14429-14438.

[37] A.J. Vizcaíno, A. Carrero, J.A. Calles, Comparison of ethanol steam reforming using Co and Ni catalysts supported on SBA-15 modified by Ca and Mg, Fuel Processing Technology, 146 (**2016**) 99-109.

[38] P.J. Megía, A. Carrero, J.A. Calles, A.J. Vizcaíno, Hydrogen Production from Steam Reforming of Acetic Acid as a Model Compound of the Aqueous Fraction of Microalgae HTL Using Co-M/SBA-15 (M: Cu, Ag, Ce, Cr) Catalysts, Catalysts, 9 (**2019**) 1013.

[39] Y. Li, Z. Zhang, P. Jia, D. Dong, Y. Wang, S. Hu, J. Xiang, Q. Liu, X. Hu, Ethanol steam reforming over cobalt catalysts: Effect of a range of additives on the catalytic behaviors, Journal of the Energy Institute, 93 (**2020**) 165-184.

[40] V.G. Deshmane, S.L. Owen, R.Y. Abrokwah, D. Kuila, Mesoporous nanocrystalline TiO_2 supported metal (Cu, Co, Ni, Pd, Zn, and Sn) catalysts: Effect of metal-support interactions on steam reforming of methanol, Journal of Molecular Catalysis A: Chemical, 408 (**2015**) 202-213.

[41] D. Zhao, J. Feng, Q. Huo, N. Melosh, G.H. Fredrickson, B.F. Chmelka, G.D. Stucky, Triblock copolymer syntheses of mesoporous silica with periodic 50 to 300 angstrom pores, Science, 279 (**1998**) 548-552.

[42] A.T. D'Agostino, Determination of thin metal film thickness by x-ray diffractometry using the Scherrer equation, atomic absorption analysis and transmission/reflection visible spectroscopy, Analytica Chimica Acta, 262 (**1992**) 269-275.

[43] H. Sun, J. Han, Y. Ding, W. Li, J. Duan, P. Chen, H. Lou, X. Zheng, One-pot synthesized mesoporous Ca/SBA-15 solid base for transesterification of sunflower oil with methanol, Applied Catalysis A: General, 390 (**2010**) 26-34.

[44] J. Tantirungrotechai, P. Thananupappaisal, B. Yoosuk, N. Viriya-empikul, K. Faungnawakij, One-pot synthesis of calcium-incorporated MCM-41 as a solid base catalyst for transesterification of palm olein, Catalysis Communications, 16 (**2011**) 25-29.

[45] H.-S. Roh, I.-H. Eum, D.-W. Jeong, Low temperature steam reforming of methane over Ni–$Ce_{(1-x)}Zr_{(x)}O_2$ catalysts under severe conditions, Renewable Energy, 42 (**2012**) 212-216.

[46] H. Tran, T. Mehta, M. Zeller, R.H. Jarman, Synthesis and characterization of mixed phases in the Ca–Co–O system using the Pechini method, Materials Research Bulletin, 48 (**2013**) 2450-2456.

[47] T. Tsoncheva, L. Ivanova, J. Rosenholm, M. Linden, Cobalt oxide species supported on SBA-15, KIT-5 and KIT-6 mesoporous silicas for ethyl acetate total oxidation, Applied Catalysis B: Environmental, 89 (**2009**) 365-374.

[48] G. Prieto, A. Martínez, R. Murciano, M.A. Arribas, Cobalt supported on morphologically tailored SBA-15 mesostructures: The impact of pore length on metal dispersion and catalytic activity in the Fischer–Tropsch synthesis, Applied Catalysis A: General, 367 (**2009**) 146-156.

[49] R. Dębek, M.E. Galvez, F. Launay, M. Motak, T. Grzybek, P. Da Costa, Low temperature dry methane reforming over Ce, Zr and CeZr promoted Ni–Mg–Al hydrotalcite-derived catalysts, International Journal of Hydrogen Energy, 41 (**2016**) 11616-11623.

[50] J. Zheng, J. Cai, F. Jiang, Y. Xu, X. Liu, Investigation of the highly tunable selectivity to linear α-olefins in Fischer–Tropsch synthesis over silica-supported Co and CoMn catalysts by carburization–reduction pretreatment, Catalysis Science & Technology, 7 (**2017**) 4736-4755.

[51] D.G. Barton, S.L. Soled, G.D. Meitzner, G.A. Fuentes, E. Iglesia, Structural and Catalytic Characterization of Solid Acids Based on Zirconia Modified by Tungsten Oxide, Journal of Catalysis, 181 (**1999**) 57-72.

[52] R. Obeso-Estrella, J.L.G. Fierro, J.N.D. de León, S. Fuentes, G. Alonso-Nuñez, E. Lugo-Medina, B. Pawelec, T.A. Zepeda, Effect of partial Mo substitution by W on HDS activity using sulfide CoMoW/Al_2O_3–TiO_2 catalysts, Fuel, 233 (**2018**) 644-657.

[53] H.-P. Ren, Q.-Q. Hao, W. Wang, Y.-H. Song, J. Cheng, Z.-W. Liu, Z.-T. Liu, J. Lu, Z. Hao, High-performance Ni–SiO_2 for pressurized carbon dioxide reforming of methane, International Journal of Hydrogen Energy, 39 (**2014**) 11592-11605.

[54] G. Prieto, A. Martínez, P. Concepción, R. Moreno-Tost, Cobalt particle size effects in Fischer–Tropsch synthesis: structural and in situ spectroscopic characterisation on reverse micelle-synthesised Co/ITQ-2 model catalysts, Journal of Catalysis, 266 (**2009**) 129-144.

[55] A. Martínez, C. López, F. Márquez, I. Díaz, Fischer–Tropsch synthesis of hydrocarbons over mesoporous Co/SBA-15 catalysts: the influence of metal loading, cobalt precursor, and promoters, Journal of Catalysis, 220 (**2003**) 486-499.

[56] A.L.M. da Silva, J.P. den Breejen, L.V. Mattos, J.H. Bitter, K.P. de Jong, F.B. Noronha, Cobalt particle size effects on catalytic performance for ethanol steam reforming – Smaller is better, Journal of Catalysis, 318 (**2014**) 67-74.

[57] C. Cerdá-Moreno, J.F. Da Costa-Serra, A. Chica, Co and La supported on Zn-Hydrotalcite-derived material as efficient catalyst for ethanol steam reforming, International Journal of Hydrogen Energy, 44 (**2019**) 12685-12692.

[58] G. Słowik, M. Greluk, M. Rotko, A. Machocki, Evolution of the structure of unpromoted and potassium-promoted ceria-supported nickel catalysts in the steam reforming of ethanol, Applied Catalysis B: Environmental, 221 (**2018**) 490-509.

[59] J.D. Jimenez, C. Wen, M.M. Royko, A.J. Kropf, C. Segre, J. Lauterbach, Influence of Coordination Environment of Anchored Single-Site Cobalt Catalyst on CO2 Hydrogenation, ChemCatChem, 12 (**2020**) 846-854.

[60] T. Sakamoto, K. Asazawa, K. Yamada, H. Tanaka, Study of Pt-free anode catalysts for anion exchange membrane fuel cells, Catalysis Today, 164 (**2011**) 181-185.

[61] L.F. Liotta, G. Di Carlo, G. Pantaleo, A.M. Venezia, G. Deganello, Co_3O_4/CeO_2 composite oxides for methane emissions abatement: Relationship between Co_3O_4-CeO_2 interaction and catalytic activity, Applied Catalysis B: Environmental, 66 (**2006**) 217-227.

[62] C.A.H. Price, W. Arnold, L. Pastor-Pérez, B. Amini-Horri, T.R. Reina, Catalytic Upgrading of a Biogas Model Mixture via Low Temperature DRM Using Multicomponent Catalysts, Topics in Catalysis, (**2019**).

[63] S.G. Aspromonte, E.E. Miró, A.V. Boix, FTIR studies of butane, toluene and nitric oxide adsorption on Ag exchanged NaMordenite, Adsorption, 18 (**2012**) 1-12.

[64] B. Jin, X. Wu, D. Weng, S. Liu, T. Yu, Z. Zhao, Y. Wei, Roles of cobalt and cerium species in three-dimensionally ordered macroporous $Co_xCe_{1-x}O_\delta$ catalysts for the catalytic oxidation of diesel soot, Journal of Colloid and Interface Science, 532 (**2018**) 579-587.

[65] G. Fierro, M. Lo Jacono, M. Inversi, R. Dragone, P. Porta, TPR and XPS study of cobalt–copper mixed oxide catalysts: evidence of a strong Co–Cu interaction, Topics in Catalysis, 10 (**2000**) 39-48.

[66] J.R. Scheffe, A. Steinfeld, Thermodynamic Analysis of Cerium-Based Oxides for Solar Thermochemical Fuel Production, Energy & Fuels, 26 (**2012**) 1928-1936.

[67] P. Osorio-Vargas, N.A. Flores-González, R.M. Navarro, J.L.G. Fierro, C.H. Campos, P. Reyes, Improved stability of Ni/Al_2O_3 catalysts by effect of promoters (La_2O_3, CeO_2) for ethanol steam-reforming reaction, Catalysis Today, 259 (**2016**) 27-38.

[68] N. Cakiryilmaz, H. Arbag, N. Oktar, G. Dogu, T. Dogu, Catalytic performances of Ni and Cu impregnated MCM-41 and Zr-MCM-41 for hydrogen production through steam reforming of acetic acid, Catalysis Today, 323 (**2019**) 191-199.

[69] J. Pu, K. Nishikado, N. Wang, T.T. Nguyen, T. Maki, E.W. Qian, Core-shell nickel catalysts for the steam reforming of acetic acid, Applied Catalysis B: Environmental, 224 (**2018**) 69-79.

[70] A. Carrero, J.A. Calles, A.J. Vizcaíno, Effect of Mg and Ca addition on coke deposition over $Cu–Ni/SiO_2$ catalysts for ethanol steam reforming, Chemical Engineering Journal, 163 (**2010**) 395-402.

[71] H. Song, U.S. Ozkan, Changing the Oxygen Mobility in Co/Ceria Catalysts by Ca Incorporation: Implications for Ethanol Steam Reforming, The Journal of Physical Chemistry A, 114 (**2010**) 3796-3801.

[72] W. Nabgan, T.A.T. Abdullah, R. Mat, B. Nabgan, A.A. Jalil, L. Firmansyah, S. Triwahyono, Production of hydrogen via steam reforming of acetic acid over Ni and Co supported on La_2O_3 catalyst, International Journal of Hydrogen Energy, 42 (**2017**) 8975-8985.

[73] S.C.M. Mizuno, A.H. Braga, C.E. Hori, J.B.O. Santos, J.M.C. Bueno, Steam reforming of acetic acid over $MgAl_2O_4$-supported Co and Ni catalysts: Effect of the composition of Ni/Co and reactants on reaction pathways, Catalysis Today, 296 (**2017**) 144-153.

[74] X. Luo, Y. Hong, K. Shi, G. Yang, C. Pang, E. Lester, L. Jiang, T. Wu, Investigation on Co–Modified Ni_xMg_yO Solid Solutions for Hydrogen Production from Steam Reforming of Acetic Acid and a Model Blend, ChemistrySelect, 4 (**2019**) 9829-9835.

[75] X. Hu, G. Lu, Investigation of the steam reforming of a series of model compounds derived from bio-oil for hydrogen production, Applied Catalysis B: Environmental, 88 (**2009**) 376-385.

[76] F.G.E. Nogueira, P.G.M. Assaf, H.W.P. Carvalho, E.M. Assaf, Catalytic steam reforming of acetic acid as a model compound of bio-oil, Applied Catalysis B: Environmental, 160-161 (**2014**) 188-199.

[77] S.D. Davidson, K.A. Spies, D. Mei, L. Kovarik, I. Kutnyakov, X.S. Li, V. Lebarbier Dagle, K.O. Albrecht, R.A. Dagle, Steam Reforming of Acetic Acid over Co-Supported Catalysts: Coupling Ketonization for Greater Stability, ACS Sustainable Chemistry & Engineering, 5 (**2017**) 9136-9149.

[78] D.L. Trimm, Coke formation and minimisation during steam reforming reactions, Catalysis Today, 37 (**1997**) 233-238.

[79] A. Ochoa, J. Bilbao, A.G. Gayubo, P. Castaño, Coke formation and deactivation during catalytic reforming of biomass and waste pyrolysis products: A review, Renewable and Sustainable Energy Reviews, 119 (**2020**) 109600.

[80] A.E. Galetti, M.F. Gomez, L.A. Arrúa, M.C. Abello, Hydrogen production by ethanol reforming over NiZnAl catalysts: Influence of Ce addition on carbon deposition, Applied Catalysis A: General, 348 (**2008**) 94-102.

[81] D.S. Lima, C.O. Calgaro, O.W. Perez-Lopez, Hydrogen production by glycerol steam reforming over Ni based catalysts prepared by different methods, Biomass Bioenergy, 130 (**2019**) 105358.

[82] N.D. Charisiou, K.N. Papageridis, G. Siakavelas, V. Sebastian, S.J. Hinder, M.A. Baker, K. Polychronopoulou, M.A. Goula, The influence of SiO_2 doping on the Ni/ZrO_2 supported catalyst for hydrogen production through the glycerol steam reforming reaction, Catalysis Today, 319 (**2019**) 206-219.

[83] A. Moral, I. Reyero, C. Alfaro, F. Bimbela, L.M. Gandía, Syngas production by means of biogas catalytic partial oxidation and dry reforming using Rh-based catalysts, Catalysis Today, 299 (**2018**) 280-288.

[84] C.K.S. Choong, Z. Zhong, L. Huang, Z. Wang, T.P. Ang, A. Borgna, J. Lin, L. Hong, L. Chen, Effect of calcium addition on catalytic ethanol steam reforming of Ni/Al_2O_3: I. Catalytic stability, electronic properties and coking mechanism, Applied Catalysis A: General, 407 (**2011**) 145-154.

[85] Z. Taherian, M. Yousefpour, M. Tajally, B. Khoshandam, Catalytic performance of Samaria-promoted Ni and Co/SBA-15 catalysts for dry reforming of methane, International Journal of Hydrogen Energy, 42 (**2017**) 24811-24822.

[86] S. Helveg, J. Sehested, J.R. Rostrup-Nielsen, Whisker carbon in perspective, Catalysis Today, 178 (**2011**) 42-46.

[87] B. Guichard, M. Roy-Auberger, E. Devers, B. Rebours, A.A. Quoineaud, M. Digne, Characterization of aged hydrotreating catalysts. Part I: Coke depositions, study on the chemical nature and environment, Applied Catalysis A: General, 367 (**2009**) 1-8.

[88] C. Montero, A. Ochoa, P. Castaño, J. Bilbao, A.G. Gayubo, Monitoring Ni^0 and coke evolution during the deactivation of a $Ni/La_2O_3–\alpha Al_2O_3$ catalyst in ethanol steam reforming in a fluidized bed, Journal of Catalysis, 331 (**2015**) 181-192.

[89] N.D. Charisiou, G. Siakavelas, K.N. Papageridis, A. Baklavaridis, L. Tzounis, K. Polychronopoulou, M.A. Goula, Hydrogen production via the glycerol steam reforming reaction over nickel supported on alumina and lanthana-alumina catalysts, International Journal of Hydrogen Energy, 42 (**2017**) 13039-13060.

[90] K.C. Silva, P. Corio, J.J. Santos, Characterization of the chemical interaction between single-walled carbon nanotubes and titanium dioxide nanoparticles by thermogravimetric analyses and resonance Raman spectroscopy, Vib. Spectrosc, 86 (**2016**) 103-108.

[91] L. Tzounis, M. Kirsten, F. Simon, E. Mäder, M. Stamm, The interphase microstructure and electrical properties of glass fibers covalently and non-covalently bonded with multiwall carbon nanotubes, Carbon, 73 (**2014**) 310-324.

Article 2

"Hydrogen production from steam reforming of acetic acid as a model compound of the aqueous fraction of microalgae HTL using Co-M/SBA-15 (M: Cu, Ag, Ce, Cr) catalysts"

Catalysts 2019, 9, 1013

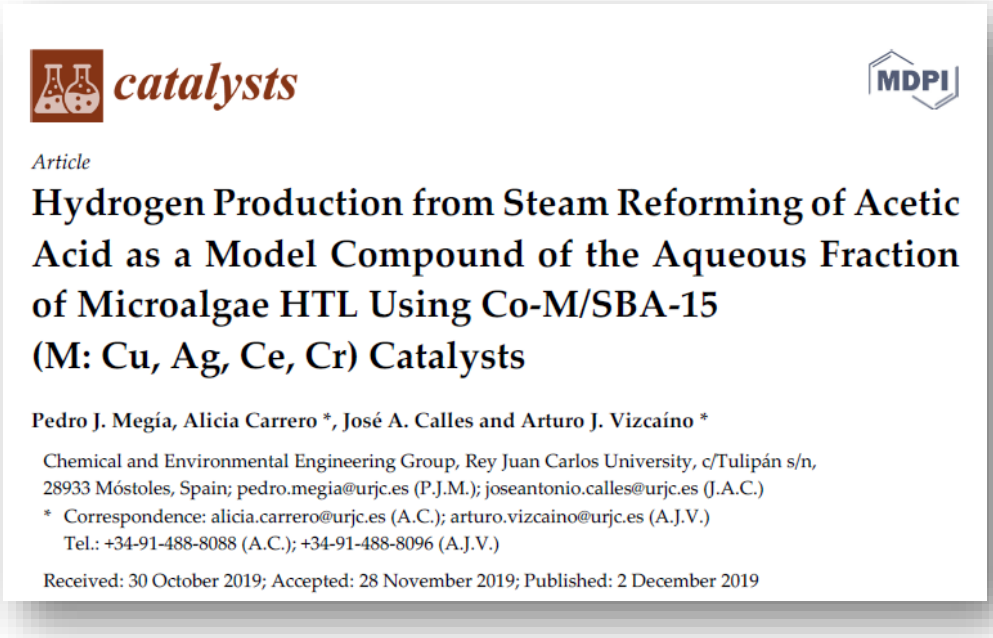

catalysts

MDPI

Article

Hydrogen Production from Steam Reforming of Acetic Acid as a Model Compound of the Aqueous Fraction of Microalgae HTL Using Co-M/SBA-15 (M: Cu, Ag, Ce, Cr) Catalysts

Pedro J. Megía, Alicia Carrero *, José A. Calles and Arturo J. Vizcaíno *

Chemical and Environmental Engineering Group, Rey Juan Carlos University, c/Tulipán s/n, 28933 Móstoles, Spain; pedro.megia@urjc.es (P.J.M.); joseantonio.calles@urjc.es (J.A.C.)

* Correspondence: alicia.carrero@urjc.es (A.C.); arturo.vizcaino@urjc.es (A.J.V.)
Tel.: +34-91-488-8088 (A.C.); +34-91-488-8096 (A.J.V.)

Received: 30 October 2019; Accepted: 28 November 2019; Published: 2 December 2019

Impact JCR factor, JCR 2019: 3.520

Category: Chemistry Physical. 65 of 159 (Q2)

Abstract

Hydrogen production derived from thermochemical processes of biomass is becoming an interesting alternative to conventional routes using fossil fuels. In this sense, steam reforming of the aqueous fraction of microalgae hydrothermal liquefaction (HTL) is a promising option to face renewable hydrogen production. Since HTL aqueous fraction is a complex mixture, acetic acid has been chosen as model compound. This work studies the modification of Co/SBA-15 catalyst incorporating a second metal leading to Co-M/SBA-15 (M: Cu, Ag, Ce and Cr). All catalysts were characterized by N_2 physisorption, ICP-AES, XRD, TEM, H_2-TPR, H_2-TPD and Raman spectroscopy. The characterization results evidenced that Cu and Ag incorporation decreased the cobalt oxides reduction temperatures, while Cr addition led to smaller Co^0 crystallites better dispersed on the support. Catalytic tests done at 600 °C, showed that Co-Cr/SBA-15 sample gave hydrogen selectivity values above 70 mol % with a significant reduction in coke deposition.

Keywords: microalgae; acetic acid; steam reforming; hydrogen; cobalt; mesostructured materials

Introduction

An increase in global pollution has resulted in a search for alternative energy resources that can be substituted in place of widely used fossil fuels [1]. It is known that energy provided from hydrogen does not result in pollutants emissions when it is used in fuel cell applications [2-4]. In addition, hydrogen is extensively used in chemical and petroleum industries [5,6]. Nowadays, a hydrogen based energy system must use renewable energy sources to be sustainable. In this sense, hydrogen production processes such as biomass gasification, and steam reforming (SR) of pyrolysis bio-oil have been widely described in the literature [7-10]. However, the use of microalgae hydrothermal liquefaction integrated with the steam reforming of the aqueous fraction is less known. Microalgae HTL requires temperatures between 250-350 °C and high pressures that can maintain the water coming from the microalgae crops in liquid state (40-250 bar). This process provides a great advantage when compared to the traditional biomass pyrolysis process, as it does not require a previous stage for biomass drying associated with high energy consumption [11-13]. Microalgae HTL products are a complex mixture of different compounds where carboxylic acid, ketones, phenols, aldehydes, fatty acids and nitrogen compounds [14] can be easily found with a high water content. Therefore, because of this they are not suitable to be use as fuel. However, this worthless aqueous fraction can be revalorized by hydrogen production through catalytic steam reforming [15,16] but the complex composition mentioned above usually force the use of model compounds [17-20]. Among them, acetic acid is a major component, which can account even for the 56 % of the water-soluble products [17]. The overall equation of the acetic acid steam reforming is:

$$C_2H_4O_2 + 2\ H_2O \rightarrow 2\ CO_2 + 4\ H_2$$

Nowadays, SR catalysts are a critical point of study where activity, hydrogen selectivity and deactivation are the main concerns of the scientific community. Many papers can be found using different active phases such as Ni, Co, Pt or Ru, with Ni being the most studied [21]. Hu et al. [22] studied the performance of different

transition metals supported over Al_2O_3 in acetic acid steam reforming. Their study led to the conclusion that Ni and Co were more active than the other metals tested (Fe and Cu). They attributed this behavior to the ability for cracking not only C-C bonds, but also C-H bonds. However, Co-based catalysts have been less reported despite the fact they also provide high activity at moderate temperatures and also increases hydrogen yield [23,24].

Catalysts support selection is also an important point. For example, when Co was supported on Al_2O_3 or TiO_2 high metal dispersion was reported but cobalt aluminates or titanates were formed avoiding the reduction of some Co species [25]. On the other hand, the interaction of Co with silica has been studied leading to the conclusion that this support does not affect to its reducibility but instead promote the sintering of cobalt particles in the calcination and reduction steps [26,27]. Apart from that, there are other advanced supports such as SBA-15, which is a mesostructured material with high surface area that may allow higher metal dispersion when compared with the amorphous silica. Furthermore, SBA-15 presents a uniform distribution of mesopores that hinders the formation of Co agglomerates preventing also catalysts deactivation due to metal sintering [28].

Co-based catalysts have shown deactivation through sintering and surface cobalt oxidation [21]. Pereira et al. [29] proposed the preparation of bimetallic catalysts to stabilize Co/SiO_2 catalyst to safeguard the Co particles in a reduced state during the reforming. Combining diverse metals in the same carrier has been reported as an effective way to improve the catalyst performance by facilitating the metal reducibility [30]. As reducibility promoters noble metals, transition metals or CeO_2 among others can be used. Wang et al. [31] reported that Cu addition to Ni/attapulgite catalyst decreased the temperature for the reduction of nickel species. In line with this, Eschemann et al. [32] proved the efficiency of silver as a reduction promoter in Co/TiO_2 catalyst since Co-Ag bonds improve the reducibility of cobalt oxides [32,33]. Besides, Harun et al. [34] achieved better Ni^0 dispersion over Al_2O_3 surface when Ag was included in the catalyst formulation. Similarly, it was described that CeO_2,

presents a synergistic effect with cobalt oxides since more oxygen vacancies are formed leading to higher reducibility [35]. In addition to promoting the cobalt reducibility to avoid possible crystallites oxidation, it is necessary to obtain a small crystallite size in order to increase activity and reduce the coke formation according to its growth mechanism [36]. Accordingly, Cerdá Moreno et al. [37] found that lower Co particle size for ethanol steam reforming led to better catalytic activity. Recently, we have found that Ni-Cr/SBA-15 showed better catalytic behavior than Ni/SBA-15 in the steam reforming of pyrolysis bio-oil aqueous fraction by decreasing Ni^0 particles size [38]. Furthermore, Casanovas et al. [39,40] reported that the incorporation of Cr to Co/ZnO samples results in better catalytic performance when these catalysts were tested in ethanol steam reforming.

So far, we have not been able to find any references using the promoters described above in Co/SBA-15 catalysts to be tested in acetic acid steam reforming. Therefore, the main goal of this study is the preparation of novel cobalt catalysts incorporating a second metal leading to Co M/SBA-15 (M: Cu, Ag, Ce and Cr) to achieve high hydrogen production rate through acetic acid steam reforming as model compound of microalgae HTL aqueous fraction.

Experimental

Catalysts synthesis

Mesostructured SBA-15 material, synthesized using the hydrothermal method described elsewhere [84], was used as catalysts support. Pluronic 123 and TEOS were used as surfactant and silica precursor (Aldrich) respectively.

Synthesis of Co-M/SBA-15 (M: Cu, Ag, Ce or Cr) catalysts was accomplished by the incipient wetness impregnation method described in previous work [85]. Metal loading was selected as 7 wt.% of Co and 2 wt.% of promoter [86]. In this way, mixed aqueous solutions of the corresponding nitrates were used for the co-impregnation: $Co(NO_3)_2 \cdot 6H_2O$ (Acros Organics) and $Cu(NO_3)_2 \cdot 3H_2O$, $Cr(NO_3)_3 \cdot 9H_2O$, $Ce(NO_3)_3 \cdot 6H_2O$, $AgNO_3$ (Aldrich). Subsequently, the prepared samples were calcined under air at 550 °C.

Catalysts characterization

N_2 adsorption/desorption at 77 K on a Micromeritics TRISTAR 3000 sorptometer was used for the measurement of textural properties. Prior to the analysis samples were outgassed under vacuum at 200 ℃ for 4h. To determine the chemical composition of the catalysts, ICP-AES technique was used. The equipment was a Varian VISTA-PRO AX CCD-Simultaneous ICP AES spectrophotometer. Samples were previously treated by acidic digestion. XRD measurements were recorded using a Philips X'pert PRO diffractometer using Cu Kα radiation. The Scherrer equation was used to estimate the metal crystallites mean diameter. Reducibility of the samples was studied by TPR analyses. A Micromeritics AUTOCHEM 2910 equipment was used. The experiment is carried out flowing 35 NmL/min of gas (10% H_2/Ar) through the sample and increasing temperature up to 980 ℃ with a 5 ℃/min heating ramp. Samples were previously outgassed under Ar flow at 110 °C for 30 min. Co dispersion of the catalysts was determined by hydrogen TPD in the same apparatus. For that, the samples were first reduced under 35 N mL/min of gas (10% H_2/Ar), then cooled to 50 ℃, and saturated with H_2. After that, the physically absorbed H_2 is removed by flushing Ar

and finally heated up to 700 °C at 5 °C/min in Ar flow (30 N mL/min). TEM micrographs were obtained on a JEOL JEM 2100 microscope (200 kV) with a resolution of 0.25 nm at National Centre for Electron Microscopy (CNME, Complutense University of Madrid). It also has the possibility to achieve microanalysis results by energy dispersive X-ray spectroscopy (EDX). Samples preparation involve their suspension in acetone and subsequently deposition on a carbon-coated copper or nickel grid.

Carbon deposited during catalytic tests was measured by thermogravimetric analysis (TGA), TEM and Raman spectroscopy. TGA analysis were performed in airflow with a heating rate of 5 °C/min up to 1000 °C on a TA instruments SDT 2960 thermobalance. Raman spectra were recorded using a JASCO NRS-5000/7000 series Raman spectrometer.

Catalytic tests

Acetic acid steam reforming reactions were performed at 600 °C on a MICROACTIVITY-PRO unit (PID Eng. & Tech. S.L.) as described in previous works [7,38,85,87]. The reactor consists in a fixed-bed tubular reactor in stainless steel 316 (i.d. = 9.2 mm, L = 300 mm). The reactor is located inside an electric oven of low thermal, where temperature in the catalytic bed was measured by means of a K-thermocouple. All the components inside the hot box were maintained at 200 °C to prevent condensation in the pipes and to preheat the reactants. A schematic diagram is displayed in Figure 1.

The reactions were carried out isothermally at atmospheric pressure. Before tests, all catalysts were reduced under pure hydrogen (30 mL/min) up to 700 °C with a heating rate of 2 °C/min. Temperature was maintained for 30 minutes. Reaction feed was a mixture of acetic acid and water using a steam to carbon molar ratio of 2, using N_2 as carrier and internal standard (GHSV = 11000 h 1). The composition of the outlet gas was measured online with an Agilent 490 Micro-GC equipped with a thermal conductivity detector (TCD), a PoraPlot U column (10 m) and a Molecular Sieve 5A

column (20 m) using He and Ar as carrier gas, respectively. Condensable vapors were trapped in the condenser at 4 °C and analysed in a Varian CP-3900 chromatograph equipped with a CP-WAX 52 CB (30 m × 0.25 mm, DF = 0.25) column and flame ionization detector (FID).

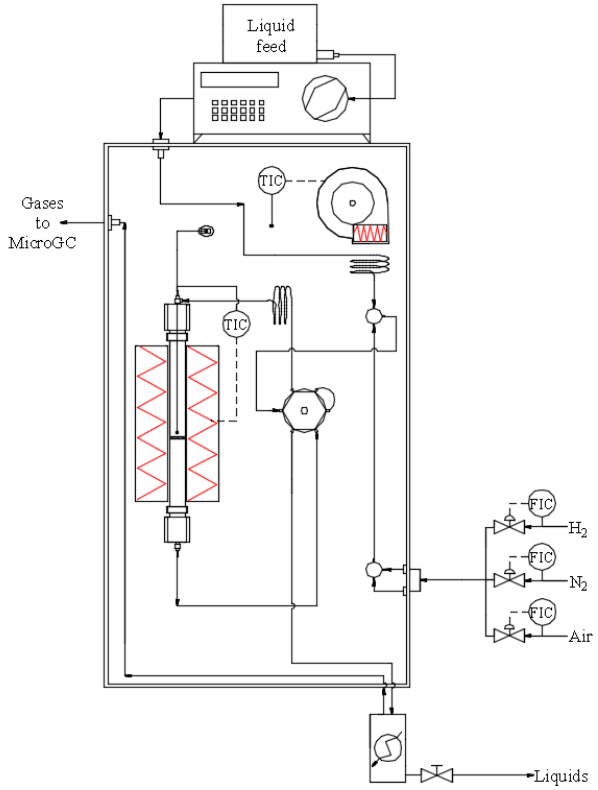

Figure 1. Schematic diagram of the catalytic testing setup [38].

Results and Discussion

Catalysts characterization

Nitrogen physisorption profiles displayed in Figure 2 show type IV isotherms with a H1-type hysteresis loop according to the IUPAC classification, indicating the preservation of the initial mesostructure of SBA-15 used as the support of these samples. Textural properties calculated from these analyses are summarized in Table 1 along with other physicochemical properties.

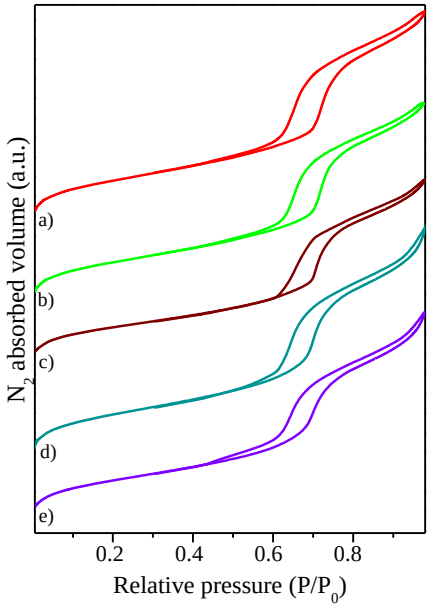

Figure 2. N_2 physisorption isotherms of calcined a) Co/SBA-15; b) Co-Cu/SBA-15; c) Co-Ag/SBA-15; d) Co-Ce/SBA 15; e) Co-Cr/SBA 15 catalysts at 77K.

The metals loading is close to the nominal value used during the catalysts preparation. Metal addition to bare SBA-15 leads to a decrease in BET surface area with Co-Ag/SBA-15 being the sample with the smallest pore size, pore volume and surface area. This phenomenon has been described previously [42] and was ascribed to Ag structures growing in the mesopores of SBA-15. Similar textural properties were found in Co-(Cu, Ce or Cr)/SBA-15 samples.

Table 1. Physicochemical properties of Co-M/SBA-15 (M: Cu, Ag, Ce, Cr) catalysts.

Catalyst	**Co[a] (wt.%)**	**M[a] (wt.%)**	**S_{BET} ($m^2 \cdot g^{-1}$)**	**D_{pore}[b] (nm)**	**V_{pore}[c] ($cm^3 \cdot g^{-1}$)**	**D_{Co^0}[d] (nm)**	**Dispersion (%)[e]**
SBA-15	-	-	550 ± 3	7.5 ± 0.1	0.97 ± 0.02	-	-
Co/SBA-15	6.4 ± 0.1	-	503 ± 4	7.2 ± 0.1	0.83 ± 0.01	9.5 ± 0.5	7.5 ± 0.2
Co-Cu/SBA-15	6.5 ± 0.1	2.0 ± 0.1	476 ± 4	7.2 ± 0.1	0.79 ± 0.03	9.7 ± 0.3	6.3 ± 0.1
Co-Ag/SBA-15	6.4 ± 0.1	1.6 ± 0.1	419 ± 4	6.9 ± 0.1	0.71 ± 0.01	12.3 ± 0.4	3.9 ± 0.6
Co-Ce/SBA-15	6.6 ± 0.1	1.7 ± 0.1	494 ± 1	7.4 ± 0.1	0.84 ± 0.01	9.6 ± 0.2	6.5 ± 0.1
Co-Cr/SBA-15	6.8 ± 0.1	1.8 ± 0.1	469 ± 1	7.1 ± 0.1	0.81 ± 0.02	7.2 ± 0.1	9.9 ± 0.3

[a] Determined by ICP-AES (M: Cu, Ag, Ce or Cr) in reduced samples

[b] BJH desorption average pore diameter

[c] Measured at $P/P_0 = 0.97$

[d] Determined from XRD of reduced catalysts by Scherrer equation from the (111) diffraction plane of Co^0

[e] Determined from H_2-TPD results using formula from Li et al. [41] assuming H/Co = 1.

Figure 3 shows the XRD patterns of the calcined samples. Peaks corresponding to cubic Co_3O_4 appear in all samples (JCPDS 01-071-4921). Attending to Co-Cu/SBA-15 sample, a small peak at 38.3° can be observed due to the formation of monoclinic CuO (JCPDS 01-089-2531). In case of Co-Ce/SBA 15, two small peaks over 28.5° and 47.5° can be seen due to the presence of cubic CeO_2 (JCPDS 01-089-8436). Ag and Cr oxides were not detected by XRD due to the overlap of the main diffraction peaks of cubic Ag_2O (JCPDS 00-012-0793), rhombohedral Cr_2O_3 (JCPDS 00-002-1362) and cubic $CoCr_2O_4$ spinel (JCPDS 00-022-1084), with the Co_3O_4 pattern. The higher Co content compared to Ag and Cr also contributes to the non detection of Ag and Cr oxides by XRD as were observed in previous works [43,44]. XRD patterns corresponding to Co-(Cu, Ag or Ce)/SBA-15 present narrower Co_3O_4 peaks and slightly larger Co_3O_4 crystallites were obtained comparing when compared to Co/SBA-15 sample.

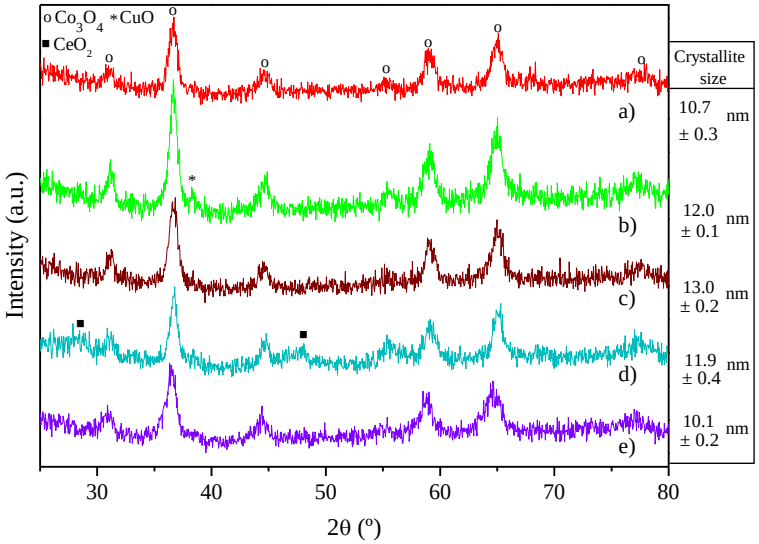

Figure 3. XRD of calcined a) Co/SBA-15; b) Co-Cu/SBA-15; c) Co-Ag/SBA-15; d) Co-Ce/SBA 15; e) Co-Cr/SBA 15 catalysts. Co_3O_4 crystallites sizes calculated from the (311) diffraction plane using Scherrer equation are displayed on the right.

Figure 4 shows the TEM micrographs of calcined samples. Irregular metal oxides particles can be observed, some of them formed in the channels of SBA-15, while other particles were formed over the external surface as previously reported [43]. The presence of Co and promoters (Cu, Ag, Ce or Cr) were evaluated in the corresponding sample by EDX indicating an intimate contact between Co oxide and promoters. Co-Ag/SBA-15 catalyst has large metallic nanostructures through the SBA-15 channels and Ag_2O particles can be also observed over the support [45]. The incorporation of high Ag loadings (> 1wt. %) affects support structure and distribution of Ag_2O particles over the catalyst because the probability of Ag-Ag bond formation increases [32,33]. On the other side, it is noticeable how Co Cr/SBA-15 sample clearly shows the highest dispersion over the support with very small metal oxide particles, which is in agreement with the lower metal diameter calculated from XRD (Table 1).

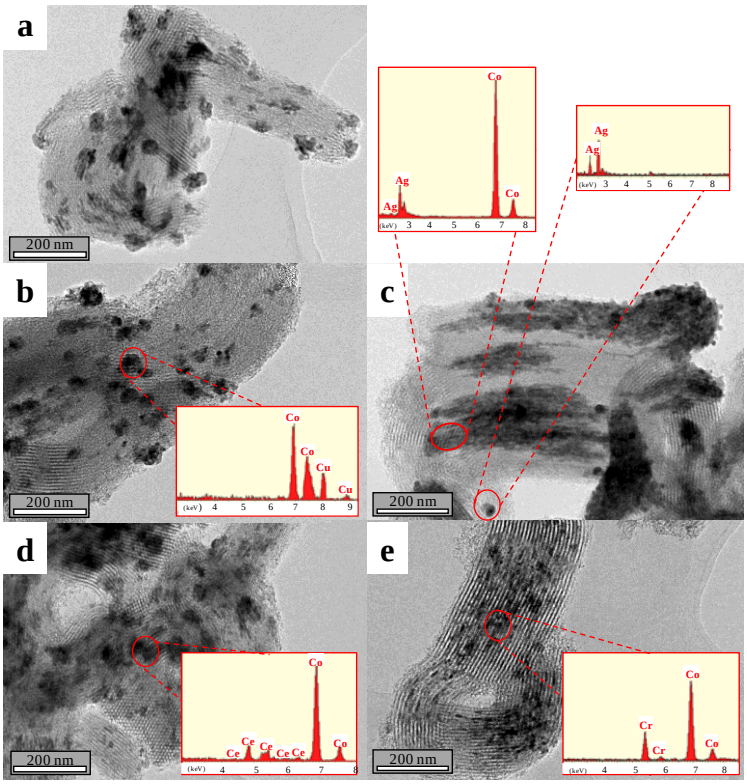

Figure 4. TEM micrographs of calcined samples (a: Co/SBA-15; b: Co-Cu/SBA-15; c: Co-Ag/SBA-15; d: Co-Ce/SBA 15; e: Co-Cr/SBA-15).

Figure 5 displays the H_2-TPR profiles of the calcined catalysts. In the case of Co/SBA-15 sample, the reduction profile shows two main reduction stages. The first one with maxima found at 248-267 °C and a shoulder around 332 °C. These peaks are attributed to the reduction of Co_3O_4 to CoO and subsequently to Co^0. The reduction stage at high temperature, with a maximum placed at 494 °C, can be attributed to the presence of Co-oxide species with stronger interaction with the support [46]. Cu addition led to a clear decrease of the reduction temperature as observed in Co-Cu/SBA-15 profile. The reduction zone is located at temperatures between 140-260 °C with two maxima at 150 and 194 °C. Whereas the lower temperature peak is ascribed to the simultaneous reduction of CuO and Co_3O_4 to Cu^0 and CoO respectively, the other one is related to the reduction of CoO to Co^0 [47]. This effect of Cu in lowering reduction temperature of metal oxides was observed in previous

works for Ni-based catalysts [43]. Co-Ag/SBA-15 catalyst showed two clearly different reduction areas, also at low temperature. While the zone over 267 °C is related to the Co oxides next to Ag, the other one around 166 °C is attributed to the reduction of segregated Ag_2O particles to Ag^0 [48]. On the other hand, Co Ce/SBA-15 sample showed a reduction profile similar to Co/SBA-15 with the peak at 494 °C shifted to higher reduction temperature due to an emerging peak assigned to superficial cerium oxide [49]. Finally, in the reduction profile of Co-Cr/SBA-15 had a new peak around 182 °C, probably due to the reduction of Cr-oxides to Cr^{3+} which can be affected by the presence of Co_3O_4 [50] although it could not be detected by XRD. The peak attributed to Co_3O_4 reduction at 271 °C remained unaltered whereas the peak of CoO reduction shifts to higher temperatures due to the presence of Cr species [51] or to the confinement of Co oxides into SBA-15 channels because of their smaller size. Based on the literature, the most likely option is the formation of a cobalt chromate mixed oxide [52], although it could not be detected by XRD due to the overlap of the main diffraction lines of $CoCr_2O_4$ with those of Co_3O_4.

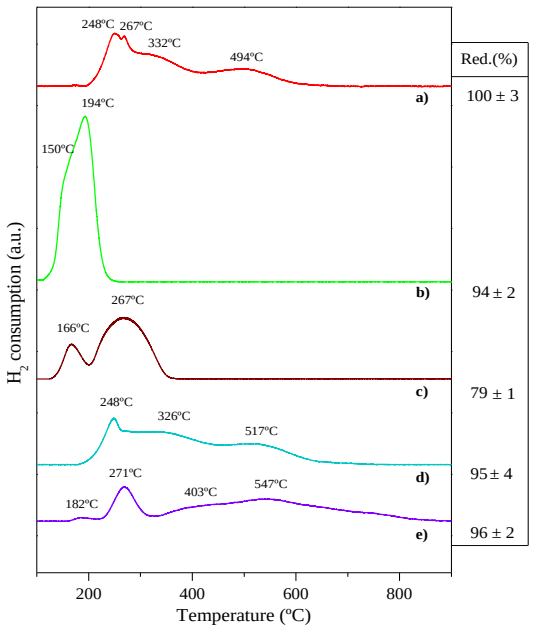

Figure 5. H_2-TPR profiles for a) Co/SBA-15; b) Co-Cu/SBA-15; c) Co-Ag/SBA-15; d) Co-Ce/SBA 15; e) Co-Cr/SBA 15 samples. Red. (%) data displayed on the right correspond to reducibility.

The XRD patterns of the samples after reduction at 700 °C under pure H_2 flow are displayed in Figure 6. No peaks ascribed to Co_3O_4 pattern can be detected whereas cubic Co^0 (JCPDS 00 001 1259) peaks corresponding to (111), (200) and (220) planes showing the reflection at 2θ = 44.4°, 51.3° and 75.4° can be observed in all samples after the reduction process.

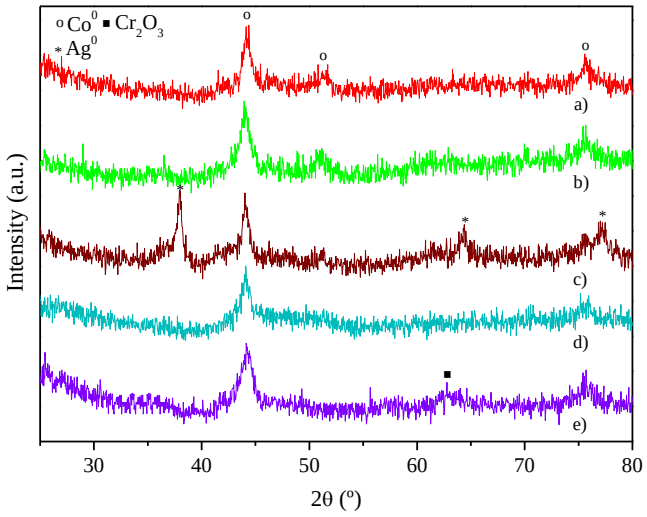

Figure 6. XRD of reduced a) Co/SBA-15; b) Co-Cu/SBA-15; c) Co-Ag/SBA-15; d) Co Ce/SBA 15; e) Co Cr/SBA 15 catalysts at 700 °C.

Cubic Ag^0 (JCPDS 00-043-1038) diffraction peaks arose in the Co-Ag/SBA-15 sample at 2θ = 38.1°, 64.5° and 77°, ascribed to (111), (200) and (220) reflection planes, respectively. In this case, some Co-oxides could remain in this sample explaining its low reducibility (see Figure 5) but they were not detected because there is an overlapping between Ag^0 and Co_3O_4 patterns at 38.1 and 64.5°. In Co-Cr/SBA-15 catalyst a peak placed at 2θ = 63.7° was assigned to rhombohedral Cr_2O_3 (JCPDS 00-002-1362) probably coming from the release of CoO from the spinel $CoCr_2O_4$. No diffraction peaks of cubic Cu^0 (JCPDS 00-001-1241) were distinguished in Co-Cu/SBA-15 sample due to the overlapping between Cu^0 and Co^0 diffraction peaks. Co-Ce/SBA-15 reduced sample showed only the diffraction peak of metallic Co. The

absence of CeO_2 diffraction peaks prompted us to think about the formation of a non-stoichiometric $CeO_{2-\delta}$ that cannot be detected by XRD [53].

Co^0 crystallite sizes were calculated by the Scherrer equation from the diffraction plane (111). In general, whereas Co-Cu/SBA-15 and Co-Ce/SBA-15 samples present a crystallite size similar to Co/SBA-15, Co-Ag/SBA-15 had the largest crystallites (see Table 1) which differs from the literature as silver loading in Co-Ag/SBA-15 is higher than in references [31, 32]. In contrast, Co-Cr/SBA-15 presented the lowest Co crystallite size because making a parallelism with the paper of Amin et al. [54] Cr-oxides can suppress the extension growth of Cu oxides in that case, Co-oxides in our case.

H_2-TPD analysis was carried out in order to measure the dispersion of the metallic phase over the support. The results, summarized in Table 1, follow the opposite trend as Co^0 crystallite sizes calculated from the Scherrer equation. Co-Cr/SBA-15 sample reached the highest active phase dispersion over the support. This effect can be clearly observed in Figure 7, where Co^0 crystallite sizes are displayed against dispersion and it is clear that the only promoter that improves the base Co/SBA-15 catalyst is Cr. In addition, other authors have reported smaller crystallite size when Cr was incorporated to the catalyst formulation suggesting the capacity of Cr_2O_3 to act as a textural promoter preventing metallic sintering [55-57]. It should be noted that in a previous work we reported the same behavior with Ni-Cr/SBA-15 sample [38,43], in line with the results obtained by Xu et al. during the co-impregnation of Cr and Ni over char as support [58].

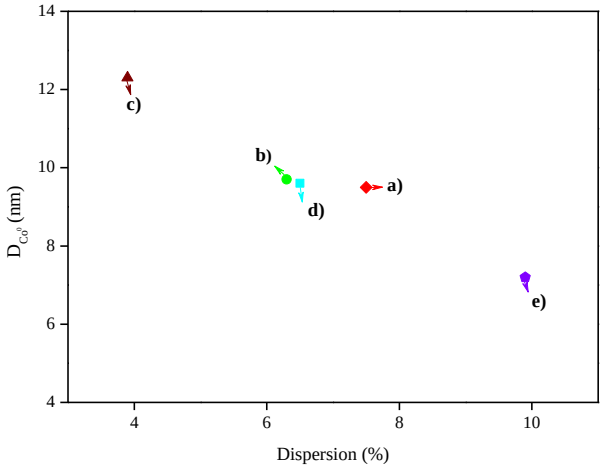

Figure 7. Comparison between Co0 crystallites size and Dispersion over the SBA-15 material used as support for a) Co/SBA-15; b) Co-Cu/SBA-15; c) Co-Ag/SBA-15; d) Co Ce/SBA 15; e) Co Cr/SBA 15.

Catalytic tests

AASR (acetic acid steam reforming) reactions were carried out after the reduction of the catalysts. All experiments were performed using an aqueous solution of acetic acid with a S/C molar ratio = 2 and a WHSV = 30.1 h^{-1} at atmospheric pressure and 600 °C using N_2 as carrier gas. Conversion data are not shown because all catalysts reached complete conversion along 5 h of time-on-stream, which implies high activity for all the samples in acetic acid conversion at these reaction conditions. However, different product distributions were achieved indicating different activities in acetic acid steam reforming reaction, ascribed to the role of a second metal in secondary reactions. In this sense, hydrogen and carbon co-products distribution (dry basis) are displayed in Figure 8. The H_2 content expected at equilibrium at the experimental conditions, predicted by means of the software GasEQ, based on the method of free Gibbs energy minimization, is also shown.

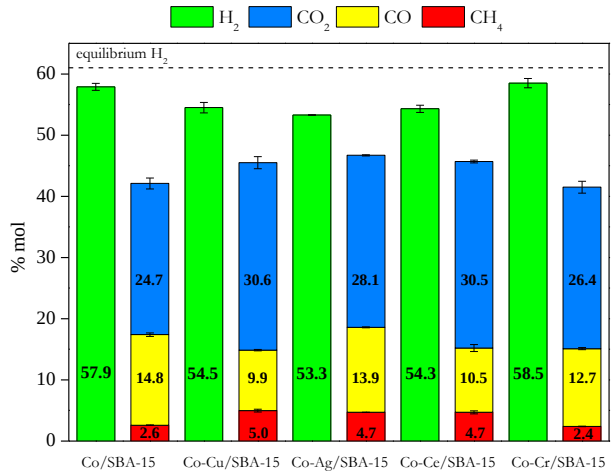

Figure 8. Products distribution in outlet gas stream produced in the acetic acid steam reforming over Co M/SBA-15 (M: Cu, Ag, Ce, Cr) catalysts at T=600 °C, P=1atm, time-on-stream=5 h.

Regarding products distribution, all catalysts reached high hydrogen concentration, above 53%. As known, Co-based catalysts allow the breaking of C-C bonds (only methane is produced as hydrogen-containing product) but also of C-H bonds [22]. Moreover, an effective catalyst must also be active in WGS reaction in order to eliminate CO from the metal surface during steam reforming. Over Co, methane reforming and WGS activity was presented and this clearly shown by products formation. Among them, CO_2 formation is highest and followed by CO, CH_4, thus WGS is more pronounced compared to other disproportionation and decomposition reactions. Cu, Ag and Ce addition to Co/SBA-15 decreases the hydrogen content in the gas outlet stream in line with higher co-carbon products percentages. In contrast, Co-Cr/SBA-15 reached the highest hydrogen concentration in the product stream. This behavior is related to the small Co crystallite size (see Table 1) leading to higher active sites surface area [59,60]. Therefore, Cr addition improved the catalytic performance by preventing Co agglomeration. In fact, Casanovas et al. [40] have published similar behavior adding Cr to Co/ZnO being more active and selective for ethanol steam reforming. On the other side, Co-Ag/SBA-15 achieved the lowest hydrogen concentration and therefore carbon containing products composition was higher, probably due to the pore blocking effect and the highest Co crystallite size.

Co-Cu/SBA-15 and Co-Ce/SBA-15 showed higher CO_2/CO molar ratio compared to the other samples (3/2) suggesting that the activity for WGS reaction was increased [60]. If WGS reaction is favored, an increase in the hydrogen production is expected but the hydrogen content reached with these two catalysts was lower than with Co/SBA-15 (CO_2/CO ratio = 1.7) thus, it is possible to assume that the presence of a second metal hinders reactants access to Co active centers, thereby avoiding their catalytic role breaking C-H bonds. Finally, Co-Cu/SBA-15, Co Ag/SBA-15 and Co-Ce/SBA-15 showed an increase of CH_4 from 2% to almost 5% in comparison to the Co/SBA-15 sample. CH_4 formation can be due to the decomposition of acetic acid or methanation [61]. Particularly, Co-Cu/SBA-15 and Co-Ce/SBA 15 produce more CH_4 in line with the reduction of H_2 and CO content which indicates that Cu and Ce promote the methanation reaction ($3H_2 + CO \rightarrow CH_4 + H_2O$) [62]. Instead, the increase of produced methane with Co-Ag/SBA-15 could be due to the decomposition of acetic acid since the CO content was kept constant while both CO_2 and CH_4 concentrations increase, which would be in accordance with the stoichiometry of the reaction $CH_3COOH \rightarrow CH_4 + CO_2$. However, other parallel and consecutive reactions varying the CO, CO_2 and CH_4 content can be taking place.

Regarding the evolution of H_2 selectivity, calculated as the ratio between hydrogen produced and 4 times the reacted acetic acid (stoichiometry), with reaction time showed in Figure 9, Co-Cu/SBA-15 and Co-Ag/SBA-15 samples exhibited a decrease at 2 h but after that, it remains almost constant. Regardless, the H_2 selectivity of the rest of catalysts remains almost unaltered with time on stream. Therefore, no deactivation was detected for Co/SBA-15, Co-Ce/SBA-15 and Co-Cr/SBA-15 samples. In addition, it can be assessed that Co-Cr/SBA-15 sample also achieved the highest H_2 selectivity close to the thermodynamic value at the present reaction conditions. This result is promising compared to those obtained by Ni-based catalysts widely referenced in literature for acetic acid steam reforming reactions. In this sense, Thaicharoensutcharittham et al. [63] reported that $Ni/Ce_{0.75}Zr_{0.25}O_2$ catalyst with a Ni loading of 5 wt.% reached hydrogen selectivity of 33.54 mol% with a S/C=1, and 64.39

mol% using a S/C=3. On the other hand, Wang et al. [64] achieved hydrogen selectivity between 54.5 and 70.9 mol% for reaction tests carried out at 550 °C and 650 °C respectively, with S/C=3 using Ni/Attapulgite catalysts. In another work, Nogueira et al. [65] published the catalytic performance of Ni catalysts supported on (MgO)-modified γ-Al_2O_3 reaching, a H_2 selectivity of 67.5 mol% at higher S/C ratio (S/C = 4). Additionally, our group tested at similar operation conditions (600 °C, GHSV: 11000 h-1) Ni-based catalysts in AASR with a S/C=4 [38]. In that work, we achieved up to 60 mol% of hydrogen content for both Ni/SBA-15 and Ni-Cr/SBA-15, which implied H_2 selectivities between 56.6-59.9 mol%. These values are lower than those achieved with Co-M/SBA-15 catalysts in the present work, even though lower S/C ratio has been used that should lead to worse catalytic results. Despite differences in reaction conditions, mainly S/C molar ratio, these H_2 selectivities values are lower than that achieved by Co-Cr/SBA-15 sample. Furthermore, we also observed the beneficial effect of adding Cr to catalysts in our recently published works [38,43], where we reached using Cr as promoter added to Ni/SBA-15 catalysts, better catalytic performance using different feedstock in steam reforming reaction.

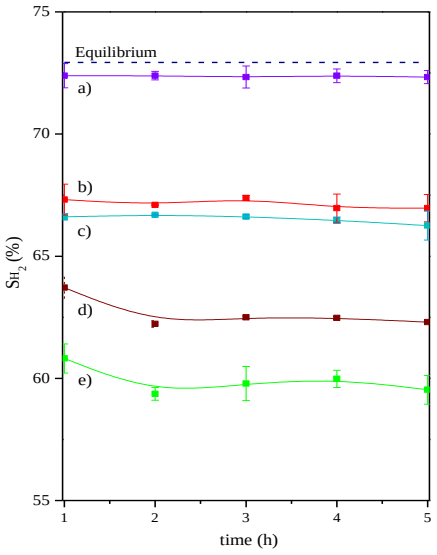

Figure 9. Hydrogen selectivity of gas stream produced in the acetic acid steam reforming over a) Co-Cr/SBA-15; b) Co/SBA-15; c) Co-Ce/SBA-15; d) Co-Ag/SBA-15; e) Co-Cu/SBA-15 catalysts at T=600 °C, P=1atm.

Coke formation during steam reforming has been reported as the main cause of SR catalysts deactivation [36]. It must be emphasized that catalyst deactivation is not only related to the amount of coke, but also to the nature of the coke formed, the morphology and the location over the catalyst structure [66]. In this sense, XRD patterns of used catalysts after 5 h (TOS) are shown in Figure 10. Peaks corresponding to cubic Co^0 (JCPDS 00-001-1259) at 2θ = 44.4°, 51.3° and 75.4° can be still distinguished. In contrast to reduced samples (Figure 5), reflection peaks corresponding to graphitic carbon (JCPDS 00-041-1487) at 2θ = 26.5°, 42.6°, 53.9° and 78.8° ascribed to (002), (100), (004) and (006) reflection planes, respectively, appear as a consequence of the coke deposition along the acetic acid steam reforming being more pronounced in Co-Ag/SBA-15 sample. Cobalt crystallites sizes of used catalysts (calculated from Scherrer equation) are shown on the right side of Figure 10. Comparing these results with those found in reduced samples (Table 1), it can be concluded that cobalt crystallites sizes were very similar, which indicates no significant sintering throughout the reforming reaction.

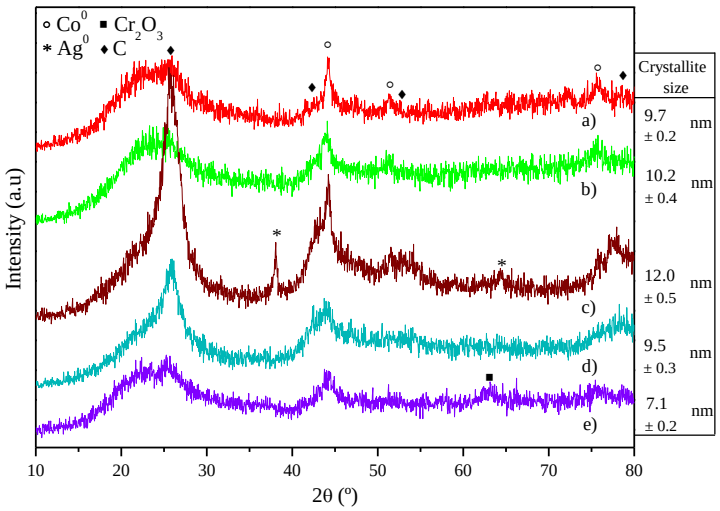

Figure 10. XRD patterns of used a) Co/SBA-15; b) Co-Cu/SBA-15; c) Co-Ag/SBA-15; d) Co-Ce/SBA-15; e) Co-Cr/SBA-15 catalysts. Co^0 crystallites sizes calculated from the (111) diffraction plane using Scherrer equation are displayed on the right.

TGA can be used for the identification of the type of coke formed during the reaction since more ordered coke will need higher temperature to be oxidized [67]. It is normally reported that amorphous carbon is more reactive than graphitic in reactions with O_2 [68] because it oxidizes at low temperatures whereas filamentous or graphitic carbon does at higher temperatures [69-71]. Figure 11 displays the derivative thermogravimetric (DTG) curves of the used catalysts along with the amount of coke formed during the reaction in terms of $mg_{coke} \cdot g_{cat}^{-1} \cdot h^{-1}$. There are significant differences in the total coke content, in the order Co-Ag/SBA-15 (282,6 mg) > Co-Ce/SBA-15 (90 mg) > Co-Cu/SBA-15 (51,6 mg) > Co/SBA-15 (34,8 mg) > Co-Cr/SBA-15 (15,4 mg) which follows the reverse order of the hydrogen content in the outlet stream during AASR (see Figure 6).

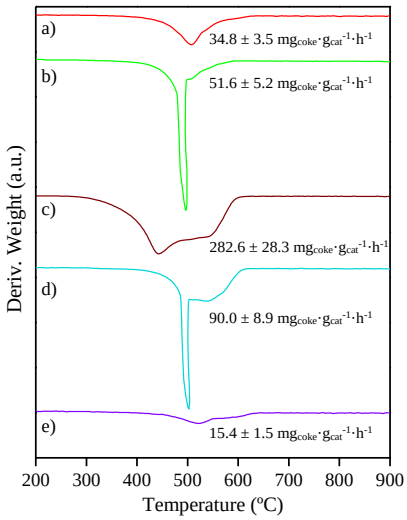

Figure 11. DTG curves of used a) Co/SBA-15; b) Co-Cu/SBA-15; c) Co-Ag/SBA-15; d) Co-Ce/SBA-15; e) Co-Cr/SBA-15 samples after 5 h time-on-stream.

In general, all DTG profiles show a maximum around 500 °C and a shoulder around 550 °C, indicating the formation of some kind of carbon nanofibers with different ordering degree [69,70]. Co-Ag/SBA-15 showed a maximum around 441 °C which can be related to the formation of some defective carbon deposits. Co-Ag/SBA-15 obtained the worst catalytic results (high CH_4 concentration and the lowest H_2

concentration), in line with the highest carbon deposition. Besides, it is noteworthy that Co-Cr/SBA-15 reduced the coke production two times compared to Co/SBA-15. It is known that Cr_2O_3 has been used as an oxide catalyst with outstanding carbon deposition resistance properties [72,73]. In our case, the reduction in carbon deposition can be also ascribed to the role of chromium avoiding the formation of large Co crystallites as it could be observed by TEM and measured by the Scherrer equation, because smaller Co crystallites will prevent the initiation of carbon nucleation leading to coke formation [74]. On the other hand, Cr_2O_3 has catalytic activity in the WGS reaction, lowering the CO concentration into the gas phase surrounding the catalytic bed, thus favoring the formation of H_2 and CO_2 [75]. In this sense, the extent Boudouard reaction ($2\ CO(g) \rightarrow CO_2\ (g) + C(s)$), which is one of the main routes for coking, will be reduced.

Used catalysts were also analysed by TEM as shown in Figure 12. In all cases, carbon nanofibers with different ordering degree can be observed. Besides, Co-Ag/SBA-15 micrograph shows some zones of defective coke deposits, in concordance with DTG results.

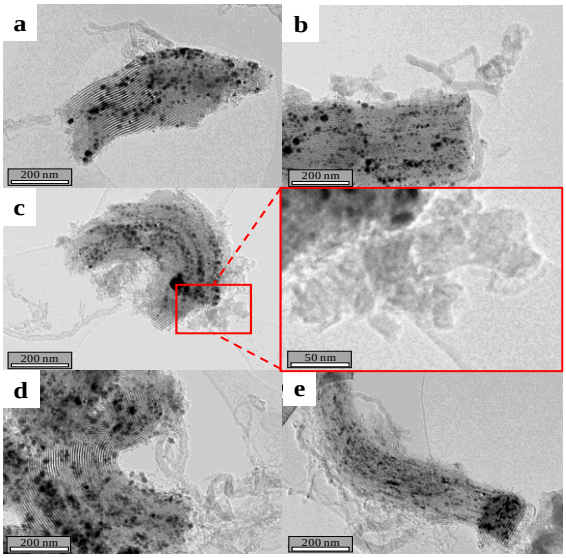

Figure 12. TEM micrographs of used a: Co/SBA-15; b: Co-Cu/SBA-15; c: Co-Ag/SBA-15; d: Co-Ce/SBA-15; e: Co-Cr/SBA-15 (5 h time-on-stream at 600 °C).

Finally, the Raman spectra of used catalysts in the range 1200-1700 cm^{-1} are presented in Figure 13. As it can be observed, two main bands appear in all cases, at 1330-1340 (D-band) and 1586-1591 cm^{-1} (G-band). G-band is ascribed to the stretching mode of carbon sp^2 bonds of condensed graphitic aromatic structures such as graphite layer [76], whereas D-band is related to the carbon atoms vibration of disordered aromatic structures such as amorphous or defective filamentous carbon [70,77-79].

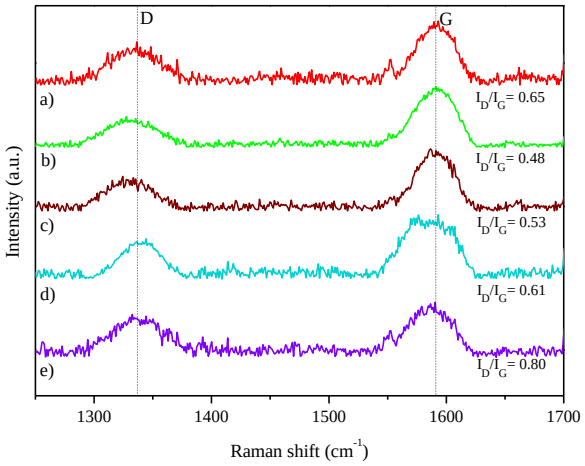

Figure 13. Raman spectra of used a) Co/SBA-15; b) Co-Cu/SBA-15; c) Co-Ag/SBA-15; d) Co-Ce/SBA-15; e) Co-Cr/SBA-15 catalysts.

The presence of both bands exhibits the heterogeneity of carbon species constituting the coke formed during the AASR reaction. It has been reported that the intensity of the D band relative to the G band can be used as a qualitative measure of the formation of different kinds of carbon with different degree of graphitization or disorder in the carbon structure [78-80]. Smaller I_D/I_G values indicate higher crystallinity due to higher contribution of the graphitic carbon structures formed [81,82] but it also implies more layers constituting the deposited carbon [83]. In these sense, the estimated values are summarized also in Figure 13. As can be seen, the ID/IG ratio decreases in the following order: Co-Cr/SBA-15 (I_D/I_G = 0.80) > Co/SBA-15 (I_D/I_G = 0.65) > Co-Ce/SBA-15 (I_D/I_G = 0.61) > Co-Ag/SBA-15 (I_D/I_G = 0.53) > Co-Cu/SBA-15 (I_D/I_G = 0.48). These results indicate that carbon deposition over the Co-Cu/SBA-15

sample occurs in larger extent on the Co surface when compared with the other samples, leading to the growth of well-ordered carbon, which may be responsible of catalyst deactivation since it acts as a shell covering the active Co sites layer by layer [80]. It must be highlighted that the H_2 selectivity represented in Figure 9, decreases in the same order as I_D/I_G ratio. Therefore, the H_2 selectivity is directly related to the kind of carbon deposited on the catalyst.

AASR test done at long time-on-stream displayed in Figure 14 showed that Co-Cr/SBA-15 achieved good stability after 50 h time-on-stream. Conversion values were near 95% at the end of the reaction, while almost constant hydrogen selectivity (~72 mol%) was obtained. These results evidence that Co-Cr/SBA-15 sample is a promising option for acetic acid steam reforming, since hydrogen selectivity remains close to the equilibrium value for a long period and, in addition, this value is greater than those obtained with the Ni-based catalysts described in literature.

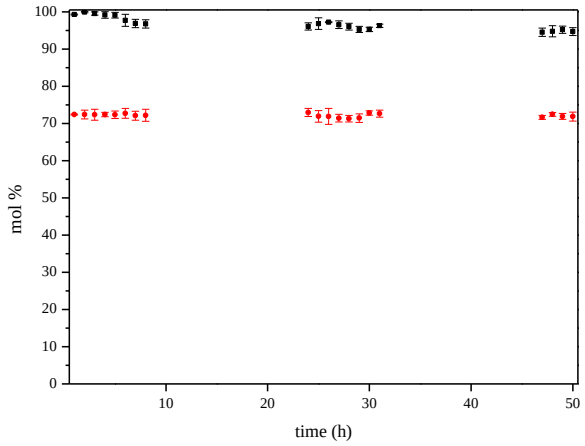

Figure 14. Acetic acid conversion (■) and hydrogen selectivity (●) during stability test of Co-Cr/SBA-15 catalyst at T=600 °C, P=1atm.

Conclusions

The incorporation of a second metal like Cu, Ag, Ce or Cr to Co/SBA-15 sample catalyst resulted in bimetallic catalysts with very different properties and catalytic behavior in acetic acid steam reforming. Co-Ag/SBA-15 presented some pore blocking of SBA-15 structure due to the presence of isolated silver oxide particles. Cu and Ag addition to Co/SBA-15 led to a significantly decrease in the reduction temperature as shown in H_2-TPR profiles. Cu addition to Co/SBA-15 favors Co oxides reducibility keeping almost unaltered Co^0 crystallites size. In contrast, Co-Ag/SBA-15 showed also lower reduction temperatures but larger Co^0 crystallites than Co/SBA-15. However, Ce addition does not affect significantly neither reducibility nor Co^0 crystallite size. Finally, Cr addition to Co/SBA-15 strongly decreases Co crystallites size, induced by the presence of chromium oxides, improving metal dispersion with a slight decrease in the reduction temperature.

Regarding acetic acid steam reforming, Co-Cu/SBA-15 and Co-Ag/SBA-15 gave lower hydrogen selectivity than unmodified Co/SBA-15 catalyst. However, Cr addition improved the catalytic behavior reaching the highest hydrogen selectivity next to the thermodynamic equilibrium. After the steam reforming tests, cobalt crystallites sizes in the used catalysts were very similar to those in fresh samples, indicating that coke deposition and not sintering is the cause of catalysts deactivation. Besides, the amount of coke formed on Co-Cr/SBA-15 was much lower than on the rest of the catalysts after 5 h of time on stream. Another difference resided in the nature of coke deposited because disordered aromatic structures such as amorphous or defective filamentous carbon were formed in a higher extent on Co-Cr/SBA-15 (I_D/I_G = 0.80) while the contribution of condensed graphitic aromatic structures increased in Co Cu/SBA-15 (I_D/I_G = 0.48).

Thus, Cr addition to Co/SBA-15 resulted in the best catalytic performance on acetic acid steam reforming, but Cr toxicity opens the way to the search for other metals providing similar catalytic properties.

Acknowledgments

The authors acknowledge the financial support from the Spanish Ministry of Economy and Competitiveness (project ENE2017-83696-R) and from the Regional Government of Madrid (project S2018/EMT-4344).

References

[1] J. Dobosz, M. Małecka, M. Zawadzki, Hydrogen generation via ethanol steam reforming over Co/HAp catalysts, Journal of the Energy Institute, 91 (**2018**) 411-423.

[2] A.J. Vizcaíno, A. Carrero, J.A. Calles, Hydrogen production from bioethanol, Nova Science Publishers, New York, **2012**, 247-294.

[3] I.E. Agency, Hydrogen Production and Storage: R&D Priorities and Gaps, IEA Publications, Paris, France, **2006**.

[4] C. Ruocco, V. Palma, A. Ricca, Kinetics of Oxidative Steam Reforming of Ethanol Over Bimetallic Catalysts Supported on CeO_2–SiO_2: A Comparative Study, Topics in Catalysis, 62 (**2019**) 467-478.

[5] L. He, J.M.S. Parra, E.A. Blekkan, D. Chen, Towards efficient hydrogen production from glycerol by sorption enhanced steam reforming, Energy & Environmental Science, 3 (**2010**) 1046-1056.

[6] Y. Wang, C. Wang, M. Chen, Z. Tang, Z. Yang, J. Hu, H. Zhang, Hydrogen production from steam reforming ethanol over Ni/attapulgite catalysts - Part I: Effect of nickel content, Fuel Processing Technology, 192 (**2019**) 227-238.

[7] A. Carrero, A.J. Vizcaíno, J.A. Calles, L. García-Moreno, Hydrogen production through glycerol steam reforming using Co catalysts supported on SBA-15 doped with Zr, Ce and La, Journal of Energy Chemistry, 26 (**2017**) 42-48.

[8] E. Shayan, V. Zare, I. Mirzaee, Hydrogen production from biomass gasification; a theoretical comparison of using different gasification agents, Energy Conversion and Management, 159 (**2018**) 30-41.

[9] T. John, S. George, M.M. K., M. Pin-Ching, K. Ben, G. Maria, E.R. J., B. Dan, Renewable hydrogen production, International Journal of Energy Research, 32 (**2008**) 379-407.

[10] J.-L. Zheng, Y.-H. Zhu, M.-Q. Zhu, K. Kang, R.-C. Sun, A review of gasification of bio-oil for gas production, Sustainable Energy & Fuels, 3 (**2019**) 1600-1622.

[11] D. López Barreiro, W. Prins, F. Ronsse, W. Brilman, Hydrothermal liquefaction (HTL) of microalgae for biofuel production: State of the art review and future prospects, Biomass Bioenergy, 53 (**2013**) 113-127.

[12] W.-H. Chen, B.-J. Lin, M.-Y. Huang, J.-S. Chang, Thermochemical conversion of microalgal biomass into biofuels: A review, Bioresource Technology, 184 (**2015**) 314-327.

[13] D. Chiaramonti, M. Prussi, M. Buffi, A.M. Rizzo, L. Pari, Review and experimental study on pyrolysis and hydrothermal liquefaction of microalgae for biofuel production, Applied Energy, 185 (**2017**) 963-972.

[14] Y. Guo, T. Yeh, W. Song, D. Xu, S. Wang, A review of bio-oil production from hydrothermal liquefaction of algae, Renewable and Sustainable Energy Reviews, 48 (**2015**) 776-790.

[15] K. Jacobson, K.C. Maheria, A. Kumar Dalai, Bio-oil valorization: A review, Renewable and Sustainable Energy Reviews, 23 (**2013**) 91-106.

[16] J. Remón, F. Broust, G. Volle, L. García, J. Arauzo, Hydrogen production from pine and poplar bio-oils by catalytic steam reforming. Influence of the bio-oil composition on the process, International Journal of Hydrogen Energy, 40 (**2015**) 5593-5608.

[17] D. Zhou, L. Zhang, S. Zhang, H. Fu, J. Chen, Hydrothermal Liquefaction of Macroalgae Enteromorpha prolifera to Bio-oil, Energy & Fuels, 24 (**2010**) 4054-4061.

[18] C. Yang, L. Jia, C. Chen, G. Liu, W. Fang, Bio-oil from hydro-liquefaction of Dunaliella salina over Ni/REHY catalyst, Bioresource Technology, 102 (**2011**) 4580-4584.

[19] U. Jena, K.C. Das, Comparative Evaluation of Thermochemical Liquefaction and Pyrolysis for Bio-Oil Production from Microalgae, Energy & Fuels, 25 (**2011**) 5472-5482.

[20] B. Maddi, E. Panisko, T. Wietsma, T. Lemmon, M. Swita, K. Albrecht, D. Howe, Quantitative characterization of the aqueous fraction from hydrothermal liquefaction of algae, Biomass Bioenergy, 93 (**2016**) 122-130.

[21] J.M. Silva, M.A. Soria, L.M. Madeira, Challenges and strategies for optimization of glycerol steam reforming process, Renewable and Sustainable Energy Reviews, 42 (**2015**) 1187-1213.

[22] X. Hu, G. Lu, Comparative study of alumina-supported transition metal catalysts for hydrogen generation by steam reforming of acetic acid, Applied Catalysis B: Environmental, 99 (**2010**) 289-297.

[23] B. Banach, A. Machocki, P. Rybak, A. Denis, W. Grzegorczyk, W. Gac, Selective production of hydrogen by steam reforming of bio-ethanol, Catalysis Today, 176 (**2011**) 28-35.

[24] A. Ishihara, A. Andou, T. Hashimoto, H. Nasu, Steam reforming of ethanol using novel carbon-oxide composite-supported Ni, Co and Fe catalysts, Fuel Processing Technology, 197 (**2020**) 106203.

[25] A.Y. Khodakov, W. Chu, P. Fongarland, Advances in the Development of Novel Cobalt Fischer−Tropsch Catalysts for Synthesis of Long-Chain Hydrocarbons and Clean Fuels, Chemical Reviews, 107 (**2007**) 1692-1744.

[26] J. Llorca, J.-A. Dalmon, P. Ramírez de la Piscina, N.s. Homs, In situ magnetic characterisation of supported cobalt catalysts under steam-reforming of ethanol, Applied Catalysis A: General, 243 (**2003**) 261-269.

[27] T. Tsoncheva, L. Ivanova, C. Minchev, M. Fröba, Cobalt-modified mesoporous MgO, ZrO_2, and CeO_2 oxides as catalysts for methanol decomposition, Journal of Colloid and Interface Science, 333 (**2009**) 277-284.

[28] J.A. Calles, A. Carrero, A.J. Vizcaíno, Ce and La modification of mesoporous Cu–Ni/SBA-15 catalysts for hydrogen production through ethanol steam reforming, Microporous and Mesoporous Materials, 119 (**2009**) 200-207.

[29] E.B. Pereira, N. Homs, S. Martí, J.L.G. Fierro, P. Ramírez de la Piscina, Oxidative steam-reforming of ethanol over Co/SiO_2, $Co–Rh/SiO_2$ and $Co–Ru/SiO_2$ catalysts: Catalytic behavior and deactivation/regeneration processes, Journal of Catalysis, 257 (**2008**) 206-214.

[30] G. Chen, J. Tao, C. Liu, B. Yan, W. Li, X. Li, Hydrogen production via acetic acid steam reforming: A critical review on catalysts, Renewable and Sustainable Energy Reviews, 79 (**2017**) 1091-1098.

[31] Y. Wang, M. Chen, Z. Yang, T. Liang, S. Liu, Z. Zhou, X. Li, Bimetallic Ni-M (M = Co, Cu and Zn) supported on attapulgite as catalysts for hydrogen production from glycerol steam reforming, Applied Catalysis A: General, 550 (**2018**) 214-227.

[32] T.O. Eschemann, J. Oenema, K.P. de Jong, Effects of noble metal promotion for Co/TiO_2 Fischer-Tropsch catalysts, Catalysis Today, 261 (**2016**) 60-66.

[33] T. Jermwongratanachai, G. Jacobs, W. Ma, W.D. Shafer, M.K. Gnanamani, P. Gao, B. Kitiyanan, B.H. Davis, J.L.S. Klettlinger, C.H. Yen, D.C. Cronauer, A.J. Kropf, C.L. Marshall, Fischer–Tropsch synthesis: Comparisons between Pt and Ag promoted Co/Al_2O_3 catalysts for reducibility, local atomic structure, catalytic activity, and oxidation–reduction (OR) cycles, Applied Catalysis A: General, 464-465 (**2013**) 165-180.

[34] N. Harun, S.Z. Abidin, O.U. Osazuwa, Y.H. Taufiq-Yap, M.T. Azizan, Hydrogen production from glycerol dry reforming over Ag-promoted Ni/Al_2O_3, International Journal of Hydrogen Energy, (**2018**).

[35] M. Konsolakis, M. Sgourakis, S.A.C. Carabineiro, Surface and redox properties of cobalt–ceria binary oxides: On the effect of Co content and pretreatment conditions, Applied Surface Science, 341 (**2015**) 48-54.

[36] D.L. Trimm, Coke formation and minimisation during steam reforming reactions, Catalysis Today, 37 (**1997**) 233-238.

[37] C. Cerdá-Moreno, J.F. Da Costa-Serra, A. Chica, Co and La supported on Zn-Hydrotalcite-derived material as efficient catalyst for ethanol steam reforming, International Journal of Hydrogen Energy, 44 (**2019**) 12685-12692.

[38] J.A. Calles, A. Carrero, A.J. Vizcaíno, L. García-Moreno, P.J. Megía, Steam Reforming of Model Bio-Oil Aqueous Fraction Using Ni-(Cu, Co, Cr)/SBA-15 Catalysts, International Journal of Molecular Sciences, 20 (**2019**) 512.

[39] A. Casanovas, M. Roig, C. de Leitenburg, A. Trovarelli, J. Llorca, Ethanol steam reforming and water gas shift over Co/ZnO catalytic honeycombs doped with Fe, Ni, Cu, Cr and Na, International Journal of Hydrogen Energy, 35 (**2010**) 7690-7698.

[40] A. Casanovas, C. de Leitenburg, A. Trovarelli, J. Llorca, Catalytic monoliths for ethanol steam reforming, Catalysis Today, 138 (**2008**) 187-192.

[41] Z. Li, M. Si, X. Li, J. Lv, Effects of titanium silicalite and TiO2 nanocomposites on supported Co-based catalysts for Fischer–Tropsch synthesis, Applied Organometallic Chemistry, 33 (**2019**) 4640.

[42] Y. Tang, M. Yang, W. Dong, L. Tan, X. Zhang, P. Zhao, C. Peng, G. Wang, Temperature difference effect induced self-assembly method for Ag/SBA-15 nanostructures and their catalytic properties for epoxidation of styrene, Microporous and Mesoporous Materials, 215 (**2015**) 199-205.

[43] A. Carrero, J.A. Calles, L. García-Moreno, A.J. Vizcaíno, Production of Renewable Hydrogen from Glycerol Steam Reforming over Bimetallic Ni-(Cu,Co,Cr) Catalysts Supported on SBA-15 Silica, Catalysts, 7 (**2017**) 55.

[44] A.J. Vizcaíno, A. Carrero, J.A. Calles, Hydrogen production by ethanol steam reforming over Cu–Ni supported catalysts, International Journal of Hydrogen Energy, 32 (**2007**) 1450-1461.

[45] X. Sun, L. Sun, J. Wang, Y. Yan, M. Wang, R. Xu, Confination of Ag nanostructures within SBA-15 by a "two solvents" reduction technique, Journal of the Taiwan Institute of Chemical Engineers, 57 (**2015**) 139-142.

[46] A. Martínez, C. López, F. Márquez, I. Díaz, Fischer–Tropsch synthesis of hydrocarbons over mesoporous Co/SBA-15 catalysts: the influence of metal loading, cobalt precursor, and promoters, Journal of Catalysis, 220 (**2003**) 486-499.

[47] G. Fierro, M. Lo Jacono, M. Inversi, R. Dragone, P. Porta, TPR and XPS study of cobalt–copper mixed oxide catalysts: evidence of a strong Co–Cu interaction, Topics in Catalysis, 10 (**2000**) 39-48.

[48] S.G. Aspromonte, E.E. Miró, A.V. Boix, FTIR studies of butane, toluene and nitric oxide adsorption on Ag exchanged NaMordenite, Adsorption, 18 (**2012**) 1-12.

[49] S.S.Y. Lin, D.H. Kim, S.Y. Ha, Metallic phases of cobalt-based catalysts in ethanol steam reforming: The effect of cerium oxide, Applied Catalysis A: General, 355 (**2009**) 69-77.

[50] D. Yun, J. Baek, Y. Choi, W. Kim, H. Jong Lee, J. Yi, Promotional Effect of Ni on a CrO_x Catalyst Supported on Silica in the Oxidative Dehydrogenation of Propane with CO_2, ChemCatChem, 4 (**2012**).

[51] J. Chen, X. Zhang, H. Arandiyan, Y. Peng, H. Chang, J. Li, Low temperature complete combustion of methane over cobalt chromium oxides catalysts, Catalysis Today, 201 (**2013**) 12-18.

[52] C. Zoican Loebick, S. Lee, S. Derrouiche, M. Schwab, Y. Chen, G.L. Haller, L. Pfefferle, A novel synthesis route for bimetallic CoCr–MCM-41 catalysts with higher metal loadings. Their application in the high yield, selective synthesis of Single-Wall Carbon Nanotubes, Journal of Catalysis, 271 (**2010**) 358-369.

[53] J.R. Scheffe, A. Steinfeld, Thermodynamic Analysis of Cerium-Based Oxides for Solar Thermochemical Fuel Production, Energy & Fuels, 26 (**2012**) 1928-1936.

[54] N.A.S. Amin, E.F. Tan, Z.A. Manan, SCR of NOx by C3H6: comparison between $Cu/Cr/CeO_2$ and $Cu/Ag/CeO_2$ catalysts, Journal of Catalysis, 222 (**2004**) 100-106.

[55] W.-H. Cheng, I. Chen, J.-s. Liou, S.-S. Lin, Supported Cu Catalysts with Yttria-Doped Ceria for Steam Reforming of Methanol, Topics in Catalysis, 22 (**2003**) 225-233.

[56] X. Huang, L. Ma, M.S. Wainwright, The influence of Cr, Zn and Co additives on the performance of skeletal copper catalysts for methanol synthesis and related reactions, Applied Catalysis A: General, 257 (**2004**) 235-243.

[57] Z. Wang, J. Xi, W. Wang, G. Lu, Selective production of hydrogen by partial oxidation of methanol over Cu/Cr catalysts, Journal of Molecular Catalysis A: Chemical, 191 (**2003**) 123-134.

[58] L. Xu, l.e. Duan, M. Tang, P. Liu, X. Ma, Y. Zhang, H.G. Harris, M. Fan, Catalytic CO_2 reforming of CH_4 over Cr-promoted Ni/char for H_2 production, International Journal of Hydrogen Energy, 39 (**2014**) 10141-10153.

[59] A.L.M. da Silva, J.P. den Breejen, L.V. Mattos, J.H. Bitter, K.P. de Jong, F.B. Noronha, Cobalt particle size effects on catalytic performance for ethanol steam reforming – Smaller is better, Journal of Catalysis, 318 (**2014**) 67-74.

[60] H. Ma, L. Zeng, H. Tian, D. Li, X. Wang, X. Li, J. Gong, Efficient hydrogen production from ethanol steam reforming over La-modified ordered mesoporous Ni-based catalysts, Applied Catalysis B: Environmental, 181 (**2016**) 321-331.

[61] X. Hu, D. Dong, X. Shao, L. Zhang, G. Lu, Steam reforming of acetic acid over cobalt catalysts: Effects of Zr, Mg and K addition, International Journal of Hydrogen Energy, 42 (**2017**) 4793-4803.

[62] P. Biswas, D. Kunzru, Steam reforming of ethanol on Ni–CeO_2–ZrO_2 catalysts: Effect of doping with copper, cobalt and calcium, Catalysis Letters, 118 (**2007**) 36-49.

[63] S. Thaicharoensutcharittham, V. Meeyoo, B. Kitiyanan, P. Rangsunvigit, T. Rirksomboon, Hydrogen production by steam reforming of acetic acid over Ni-based catalysts, Catalysis Today, 164 (**2011**) 257-261.

[64] Y. Wang, M. Chen, T. Liang, Z. Yang, J. Yang, S. Liu, Hydrogen Generation from Catalytic Steam Reforming of Acetic Acid by Ni/Attapulgite Catalysts, Catalysts, 6 (**2016**) 172.

[65] F.G.E. Nogueira, P.G.M. Assaf, H.W.P. Carvalho, E.M. Assaf, Catalytic steam reforming of acetic acid as a model compound of bio-oil, Applied Catalysis B: Environmental, 160-161 (**2014**) 188-199.

[66] B. Valle, B. Aramburu, P.L. Benito, J. Bilbao, A.G. Gayubo, Biomass to hydrogen-rich gas via steam reforming of raw bio-oil over Ni/La_2O_3-αAl_2O_3 catalyst: Effect of space-time and steam-to-carbon ratio, Fuel, 216 (**2018**) 445-455.

[67] J. Chen, X. Yang, Y. Li, Investigation on the structure and the oxidation activity of the solid carbon produced from catalytic decomposition of methane, Fuel, 89 (**2010**) 943-948.

[68] S. Nagasawa, M. Yudasaka, K. Hirahara, T. Ichihashi, S. Iijima, Effect of oxidation on single-wall carbon nanotubes, Chemical Physics Letters, 328 (**2000**) 374-380.

[69] C.K.S. Choong, Z. Zhong, L. Huang, Z. Wang, T.P. Ang, A. Borgna, J. Lin, L. Hong, L. Chen, Effect of calcium addition on catalytic ethanol steam reforming of

Ni/Al_2O_3: I. Catalytic stability, electronic properties and coking mechanism, Applied Catalysis A: General, 407 (**2011**) 145-154.

[70] A.E. Galetti, M.F. Gomez, L.A. Arrúa, M.C. Abello, Hydrogen production by ethanol reforming over NiZnAl catalysts: Influence of Ce addition on carbon deposition, Applied Catalysis A: General, 348 (**2008**) 94-102.

[71] S. Natesakhawat, R.B. Watson, X. Wang, U.S. Ozkan, Deactivation characteristics of lanthanide-promoted sol–gel Ni/Al_2O_3 catalysts in propane steam reforming, Journal of Catalysis, 234 (**2005**) 496-508.

[72] W. Qi, S. Chen, Y. Wu, K. Xie, A chromium oxide coated nickel/yttria stabilized zirconia electrode with a heterojunction interface for use in electrochemical methane reforming, RSC Advances, 5 (**2015**) 47599-47608.

[73] L.a. Garcia, R. French, S. Czernik, E. Chornet, Catalytic steam reforming of bio-oils for the production of hydrogen: effects of catalyst composition, Applied Catalysis A: General, 201 (**2000**) 225-239.

[74] S. Helveg, J. Sehested, J.R. Rostrup-Nielsen, Whisker carbon in perspective, Catalysis Today, 178 (**2011**) 42-46.

[75] S. Natesakhawat, X. Wang, L. Zhang, U.S. Ozkan, Development of chromium-free iron-based catalysts for high-temperature water-gas shift reaction, Journal of Molecular Catalysis A: Chemical, 260 (**2006**) 82-94.

[76] G. Sierra Gallego, F. Mondragón, J.-M. Tatibouët, J. Barrault, C. Batiot-Dupeyrat, Carbon dioxide reforming of methane over La_2NiO_4 as catalyst precursor—Characterization of carbon deposition, Catalysis Today, 133-135 (**2008**) 200-209.

[77] A. Carrero, J.A. Calles, A.J. Vizcaíno, Effect of Mg and Ca addition on coke deposition over $Cu–Ni/SiO_2$ catalysts for ethanol steam reforming, Chemical Engineering Journal, 163 (**2010**) 395-402.

[78] C. Montero, A. Ochoa, P. Castaño, J. Bilbao, A.G. Gayubo, Monitoring Ni0 and coke evolution during the deactivation of a Ni/La_2O_3–αAl_2O_3 catalyst in ethanol steam reforming in a fluidized bed, Journal of Catalysis, 331 (**2015**) 181-192.

[79] P. Osorio-Vargas, N.A. Flores-González, R.M. Navarro, J.L.G. Fierro, C.H. Campos, P. Reyes, Improved stability of Ni/Al_2O_3 catalysts by effect of promoters (La2O3, CeO2) for ethanol steam-reforming reaction, Catalysis Today, 259 (**2016**) 27-38.

[80] N.D. Charisiou, G. Siakavelas, K.N. Papageridis, A. Baklavaridis, L. Tzounis, K. Polychronopoulou, M.A. Goula, Hydrogen production via the glycerol steam reforming reaction over nickel supported on alumina and lanthana-alumina catalysts, International Journal of Hydrogen Energy, 42 (**2017**) 13039-13060.

[81] K.C. Silva, P. Corio, J.J. Santos, Characterization of the chemical interaction between single-walled carbon nanotubes and titanium dioxide nanoparticles by thermogravimetric analyses and resonance Raman spectroscopy, Vibrational Spectroscopy, 86 (**2016**) 103-108.

[82] L. Tzounis, M. Kirsten, F. Simon, E. Mäder, M. Stamm, The interphase microstructure and electrical properties of glass fibers covalently and non-covalently bonded with multiwall carbon nanotubes, Carbon, 73 (**2014**) 310-324.

[83] Z. Ferencz, E. Varga, R. Puskás, Z. Kónya, K. Baán, A. Oszkó, A. Erdőhelyi, Reforming of ethanol on Co/Al_2O_3 catalysts reduced at different temperatures, Journal of Catalysis, 358 (**2018**) 118-130.

[84] D. Zhao, J. Feng, Q. Huo, N. Melosh, G.H. Fredrickson, B.F. Chmelka, G.D. Stucky, Triblock copolymer syntheses of mesoporous silica with periodic 50 to 300 angstrom pores, Science, 279 (**1998**) 548-552.

[85] A.J. Vizcaíno, A. Carrero, J.A. Calles, Ethanol steam reforming on Mg- and Ca-modified Cu–Ni/SBA-15 catalysts, Catalysis Today, 146 (**2009**) 63-70.

[86] A. Carrero, J.A. Calles, A.J. Vizcaíno, Hydrogen production by ethanol steam reforming over Cu-Ni/SBA-15 supported catalysts prepared by direct synthesis and impregnation, Applied Catalysis A: General, 327 (**2007**) 82-94.

[87] A.J. Vizcaíno, A. Carrero, J.A. Calles, Comparison of ethanol steam reforming using Co and Ni catalysts supported on SBA-15 modified by Ca and Mg, Fuel Processing Technology, 146 (**2016**) 99-109.

Article 3

"Agglomerated Co-Cr/SBA-15 catalysts for hydrogen production through acetic acid steam reforming"

International Journal of Hydrogen Energy, 45 (2020), 15941-50

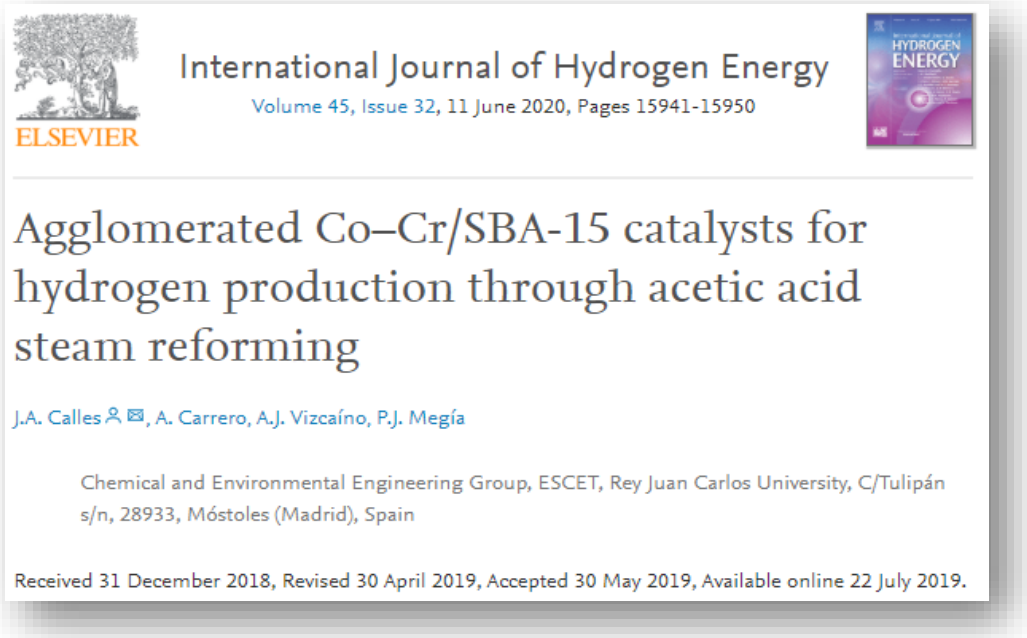

ELSEVIER

International Journal of Hydrogen Energy

Volume 45, Issue 32, 11 June 2020, Pages 15941-15950

Agglomerated Co–Cr/SBA-15 catalysts for hydrogen production through acetic acid steam reforming

J.A. Calles, A. Carrero, A.J. Vizcaíno, P.J. Megía

Chemical and Environmental Engineering Group, ESCET, Rey Juan Carlos University, C/Tulipán s/n, 28933, Móstoles (Madrid), Spain

Received 31 December 2018, Revised 30 April 2019, Accepted 30 May 2019, Available online 22 July 2019.

Impact JCR factor, JCR 2019: 4.939

Category: Energy & Fuels. 30 of 112 (Q2)

Abstract

Hydrogen produced from renewable resources is becoming interesting as an alternative to conventional fossil fuels. Co-based catalysts have been reported for their active role in steam reforming of acetic acid as the main model compound of bio-oil aqueous fraction. In the present work, a series of Co-Cr/SBA-15 extrudates were prepared by varying the binder (bentonite) content and particle size in order to get catalyst particles suitable to be used in a steam reformer at industrial scale. Catalysts were characterized by N_2-physisorption, ICP-AES, TEM, SEM, XRD and H_2-TPR. The physicochemical characterization results showed that no remarkable changes occur after the extruding process of the powdered sample, except for the particle size and mechanical strength. Acetic acid steam reforming tests were done at 600 ºC and WHSV = 30.1 h^{-1} varying the feed flow rate and the catalysts particle size in order to study the influence of internal and external diffusion limitations. Extruded particles with an effective diameter of 1.5 mm and 30 wt.% of bentonite get similar conversion and hydrogen selectivity than powder sample. Besides, the agglomerated catalysts are also stable up to 12 h of TOS.

Keywords: extrudates, binder, acetic acid, renewable hydrogen, chromium, cobalt catalysts

Introduction

High emission rate of greenhouse gases as well as solid particles and NO_x derived from the use of fossil fuels, contribute to global pollution. Additionally, they are a limited resource. Between many alternatives, hydrogen nowadays is becoming an interesting energy carrier because only water is produced when it is used in energy applications [1, 2]. At industrial scale, it is actually produced from hydrocarbons, which are neither sustainable nor renewable. However, hydrogen can be obtained from fossil fuels, water and biomass using different methods [3-8]. Hydrogen production from biomass-derived products, such as bio-oils, oxygenated hydrocarbons (bio-oil aqueous fraction, bioalcohols, etc.), alkanes and bio-alcohols, is a remarkable alternative.

Fast biomass pyrolysis is becoming a quite interesting chance because the bio oil produced is considered a potential source of hydrogen [9]. This bio-oil can be segregated into two different fractions: an organic one to be used for biofuels production and a low value aqueous fraction. Bio-oil aqueous fraction can increase its value by hydrogen production through catalytic steam reforming. The overall equation of this process is as follows:

$$C_nH_mO_k + (2n-k)\ H_2O \rightarrow n\ CO_2 + (2n+m/2-k)\ H_2 \quad \text{Eq. 1}$$

Bio-oil aqueous fraction usually present different and complex compositions, depending on the raw material used as biomass source for the bio-oil production (lignocellulosic waste or microalgae biomass) [10-14]. Regardless the raw material, in general terms, it is easy to find carboxylic acids, furans, ketones, phenols, etc. Due to the complex composition of bio-oil aqueous fraction, many research groups focus their studies on the steam reforming of bio-oil model compounds [10, 11, 15-17]. Among the main compounds found in bio-oil aqueous fraction, acetic acid used to be in high concentration (around 20 wt. %) when bio-oil is produced from biomass fast pyrolysis [10, 11]. Moreover, compared with other hydrogen sources such as methanol and ethanol, acetic acid is non-flammable and much safer to store and transport [18].

In steam reforming processes, the catalyst plays a crucial role where deactivation due to coke deposition or sintering, together with maximizing hydrogen selectivity are the main aspects to be investigated. Noble metal-based catalysts are usually reported as active [1, 18] but they involve high cost. In addition, transition metals such as Ni or Co show good performance for use in catalytic steam reforming and they are cheaper than noble metals [1]. While Ni has been widely reported as active phase for steam reforming, Co has caused less attention despite it provides high catalytic activity at lower temperatures where water-gas shift reaction is favored, increasing hydrogen production [19].

In our previous work [20], Co-based catalysts were synthetized in order to use them for catalytic glycerol steam reforming. Results showed how Co/SBA-15 catalysts suffer a severe conversion drop along the time. The catalyst stability can be improved using promoters such as Ce, La or Zr. In these cases, we obtained higher stability and glycerol conversion comparing to Co/SBA-15. Casanovas et al. [21], achieved better catalytic performance towards ethanol steam reforming using Cr as promoter in Co-based catalysts. Zhang et al. [22] achieved lower acetic acid conversion values and worse hydrogen yields using Co/La_2O_3 and Co/Al_2O_3 catalysts diluted with quartz than those obtained with Ni-based catalysts in a temperature range between 500-700 ºC. In the same way, Hu et al. [23] studied different transition metal catalysts over Al_2O_3 reaching better activity and stability with Ni and Co catalysts in comparison to Fe and Cu-based ones for acetic acid steam reforming being the Ni catalysts the sample with the lowest coke deposition and metal sintering ensuring its stability. We have recently carried out a screening of promoters in Co-based catalysts [24], and the addition of Cr leaded to the highest enhancement of catalytic activity in terms of hydrogen production (around 59% v/v), total conversion and it also achieved the lowest concentration of gaseous carbon products and coke deposition. In other work, Nabgan et al. [25] obtained through acetic acid steam reforming using Co supported on La_2O_3 catalysts a conversion of 84.2% at 600 ºC even having a higher value of space velocity. Therefore, we can conclude that comparing our previous results using Co-Cr/SBA-15 [24], with

those described in the literature at similar experimental conditions for acetic acid steam reforming [26] are promising.

The inconvenience in the vast majority of the catalysts used in steam reforming is that they are usually prepared as fine powders which are inadequate to be used in fixed bed reactors at industrial scale because of the high pressure drop caused by the catalyst. In general, this is solved by using pelletized materials such as granules, spheres and extrudates in order to avoid pressure drop and to acquire high mechanical strength [27-29], which are manufactured with the inclusion of binders [30, 31]. Extrusion is the most important shaping technique applied in the manufacturing of fixed-bed catalysts [32]. Compared with other techniques such as coating or impregnation methods, extrusion easy produced agglomerated samples with high loading of active components since the use of solid core materials is avoided [33, 34]. Extrudates are commonly manufactured with the addition of an inorganic binder such as bentonite, attapulgite, kaolin or sepiolite to enhance the strength, and an organic additive like methylcellulose or hydroxyethyl cellulose to enhance the viscosity of the paste during the extrusion [27, 31]. Nevertheless, no reports about the preparation of agglomerated Co-based catalysts for acetic acid steam reforming have been reported. Therefore, the aim of this work is the synthesis of new extruded Cr-doped Co based catalyst for its use in acetic acid steam reforming (AcASR). Bentonite and methylcellulose have been used as the binder and the organic additive respectively. This allow us to select a catalyst with suitable mechanical and catalytic properties to be used in a pilot plant steam reformer.

Experimental

Catalysts preparation

Synthesis of SBA-15 was done following the hydrothermal method described elsewhere [35]. The incorporation of active phase and promoter was done following the incipient wetness impregnation using the corresponding nitrates solution to achieve 7 wt.% of active phase and 2 wt.% of promoter in the final catalyst. Afterwards samples were calcined at 550 ºC in air static conditions for 5 h (1.8 °C/min heating rate).

Extruded materials were prepared following the methodology reported by Pariente et al. [31]. Briefly, the procedure is as follows: powder catalyst (70-80 wt.%) was blended with sodium bentonite (30-20 wt.%) as inorganic binder and synthetic methylcellulose polymer (10 wt.% over the mixture) to improve the viscosity of the paste during the extrusion [30]. All components were mixed up with deionized water to get a homogeneous paste. Afterwards, the paste was placed in a damp atmosphere, which provides plasticity and cohesive properties to be easily extrudable [31]. After that, the paste was extruded through a circular die using homemade extruders. Pellets were obtained by cutting the extruded material in cylinders with different lengths and diameters. Particle size has been defined with an effective diameter, determined using Eq. 2.

$$D_{eff} = \frac{V_p}{S_p} \qquad \text{Eq. 2}$$

where, V_P is volume, and S_P is the surface of the extruded materials.

Finally, these pellets were dried at 110 °C for 3 h with a heating rate of 0.1 °C/min and then calcined at 650 ºC (0.5 °C/min) for 2 h to guarantee the removal of the organic additive. Samples were named as CoCrS-X-Y, where X corresponds to the amount of bentonite in terms of wt.% while Y refers to the effective diameter in mm.

Catalytic tests

Acetic acid steam reforming reactions were performed on a MICROACTIVITY-PRO unit (PID Eng & Tech. S.L.) as described in previous works [20, 36]. The equipment lodges a tubular fixed bed reactor made of stainless steel (i.d. = 9.2 mm, L = 300mm) placed in an electric oven [37]. Catalyst powder has a bulk density of 0.45 g/cm3, while extruded pellets have density values between 0.19 and 0.22 g/cm^3. These pellets are placed inside the reactor leading to a bed density of 0.14 and 0.20 g/cm^3 (2.1 and 1.3 mm respectively). Reactions were carried out isothermally at 600 ºC and atmospheric pressure. All catalysts were previously reduced under pure hydrogen stream (30 mL/min) at 600 °C for 6.5 h with a heating rate of 2 °C/min. A mixture of acetic acid and water was fed to the reactor at WHSV = 30.1 h^{-1} defined as the ratio between the inlet flowrate and the mass of the catalyst, with N_2 as carrier gas and internal standard in the micro-GC (60-100 mL·min^{-1}). Condensable vapors were trapped in a condenser at 4 °C and analysed in a Varian CP-3900 chromatograph equipped with a CP-WAX 52 CB (30 m × 0.25 mm, DF = 0.25) column and flame ionization detector (FID). The composition of the gas effluent was measured online with an Agilent 490 Micro-GC equipped with a PoraPlot U column (10 m), a molecular sieve 5A column (20 m) and a thermal conductivity detector (TCD). Carbon deposited during catalytic tests was evaluated by thermogravimetric analyses (TGA), Raman spectroscopy and elemental analysis. TGA measurements were performed in air flow (100 Ncm^3/min) on a TA Instruments SDT 2960 thermobalance, with a heating rate of 5 °C/min up to 900 °C. Raman spectra were recorded using a JASCO NRS-5000/7000 series Raman spectrometer. The elemental C and H analysis was performed with an elemental analyser type Flash 2000 (Thermo Fisher Scientific), equipped with a thermal conductivity detector (TCD), using sulphanilic acid as standard.

Catalysts characterization

The textural properties of prepared materials were measured by N_2 adsorption/desorption at 77 K on a Micromeritics TRISTAR 3000 sorptometer. Samples were previously outgassed under vacuum at 200 °C for 4 h.

ICP-AES technique was used to determine the chemical composition of the catalysts, using a Varian VISTA-PRO AX CCD-Simultaneous ICP-AES spectrophotometer. Previously, solid samples were dissolved by acidic digestion.

XRD measurements were recorded using a Philips X'pert Pro diffractometer using Cu Kα radiation to determine the crystalline phase.

Reducibility of the samples was studied by means of TPR experiments. These analyses were performed on a Micromeritics AUTOCHEM 2910 equipment by passing a 10% H_2/Ar flow (35 N mL/min) through the sample (100 mg) and increasing temperature up to 980 °C at a heating rate of 5 °C/min. Samples were previously outgassed under Ar flow at 110 °C for 30 min.

TEM micrographs were obtained on a Philips TECNAI 20 microscope (200 kV) with a resolution of 0.28 nm. The apparatus has also the possibility to perform elemental microanalysis by EDX. Samples were prepared by suspending the material in acetone by ultrasonication and subsequent deposition on a carbon-coated copper grid.

In order to analyse the surface morphology of extruded samples, scanning electron microscopy (SEM) was performed on a Phillips XL30 Environmental Scanning Electron Microscope equipped with a tungsten filament and an accelerating voltage of 15 kV.

Mechanical strength of extruded pellets was determined on a Chatillon DFS II (compression mechanical test stand series). The crushing pressure was defined as the maximum force measured prior to fracture divided by the cross-sectional area of the pellet [38].

Results and discussion

Catalysts characterization

ICP-AES results are summarized in Table 1 along with other physicochemical properties of the prepared catalysts. As it can be seen, cobalt and chromium content in powder Co-Cr/SBA-15 catalyst is near to the nominal values. Attending to the extruded catalysts, metal content is lower due to the bentonite dilution, so, that the higher the bentonite loading, the lower Co and Cr content, according to the dilution degree.

Table 1. Physicochemical properties of powder Co-Cr/SBA-15 and extruded CoCr-X-Y catalysts.

Sample	Co (wt.%)[a]	Cr (wt.%)[a]	S_{BET} (m^2/g)	V_p[b] (cm^3/g)	D_p[c] (nm)	$D_{Co_3O_4}$[c] (nm)
CoCrS	6.4	1.7	490	0.7	5.5	7.1
CoCrS-20-2.1	5.3	1.4	355	0.5	5.8	8.1
CoCrS-25-2.1	4.9	1.3	335	0.5	5.8	8.0
CoCrS-30-2.1	4.5	1.2	322	0.5	5.5	8.1

[a] Determined by ICP-AES in calcined samples
[b] Pore Volume measured at $P/P_0 = 0.97$
[c] BJH desorption average pore diameter
[d] Determined from XRD of calcined catalysts by Scherrer equation from the (311) diffraction plane of Co_3O_4

Figure 1 shows the nitrogen adsorption-desorption at 77K of all samples. Powder catalyst draws a type IV isotherm (according to the I.U.P.A.C. classification) with a H1-type hysteresis loop typical for SBA-15 material. The hysteresis loop is due to the process of mesopores filling and it is governed by the capillary condensation phenomenon and by the percolative properties of the solid. Regarding the extruded materials, all of them also show a type IV isotherm, which indicates the preservation of the initial mesostructure of SBA-15 support. Textural properties summarized in Table 1 indicate that BET surface area values decrease with the bentonite loading. On the other side, average pore diameter of extruded catalysts, are similar to the powder CoCrS sample. Besides, the pore size distribution (not shown) remain narrow and centered around 5.5-5.8 nm indicating again that SBA-15 structure is preserved after agglomeration.

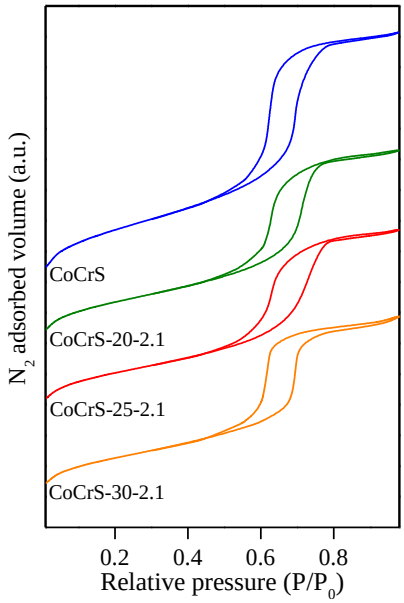

Figure 1. Nitrogen adsorption-desorption at 77K of calcined powder CoCrS and extruded materials.

In Figure 2, the SEM images of the surface of two agglomerated catalysts are shown. As it can be appreciated, as the bentonite content is higher, the particle surface seems to be more uniform without surface defects in case of 30 wt. % of bentonite used, since when the bentonite content increases, the catalyst paste acquires more plasticity [31, 39]. Bentonite is known to have high content of lamellar montmorillonite [40] flowing better than SBA-15 particles, thus, the extrusion is more uniform at higher bentonite content. This fact is in agreement with other authors [41], who observed that the higher the content of binder with zeolites, the smaller were the surface defects on the agglomerated catalyst.

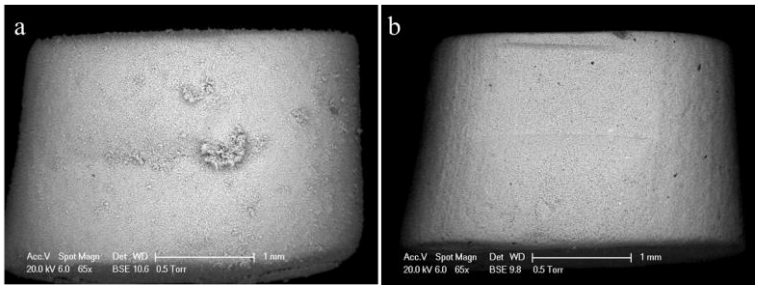

Figure 2. SEM images of calcined a: CoCrS-20-2.1; b: CoCrS-30-2.1.

Figure 3 shows the X-ray patterns of calcined samples. Powder CoCrS shows a wide peak between 20-30º attributed to the amorphous silica forming the walls of the support pores. Attending to cobalt presence, peaks of Co_3O_4 phase (JCPDS 43-1003) can be observed at different positions: 31.2, 36.5, 44.5, 55.3, 58.9, 64.6, 71.6 and 77.2º, which can be assigned to the (220), (311), (400), (422), (511), (440), (442) and (533) diffraction planes respectively, according to the XRD pattern of Co_3O_4 cubic crystalline. No peaks corresponding to chromium species were detected due to the low concentration of this metal in the samples. In extruded materials, the Co_3O_4 diffraction can be observed as in the powder catalyst, but new peaks appear at 2θ = 26.6, 28.0, 34.6 and 60.7º. Theses peaks are attributed to the presence of bentonite in the agglomerated samples [42].

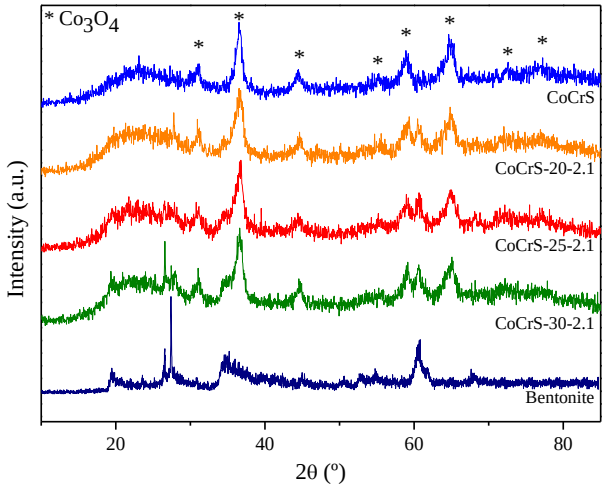

Figure 3. Comparison of XRD patterns of CoCrS samples and bentonite.

Metal distribution in calcined CoCrS can be observed in Figure 4. The well-ordered hexagonal array of cylindrical channels is in accordance with the N_2-physisorption isotherm. Dark zones observed on the mesoporous structure of SBA-15 correspond to cobalt and chromium oxides nanoparticles as could be proved in EDX analysis. Large particles seem to be placed over the external surface while other smaller particles with an irregular shape that seems to be adapted to the support pores shape.

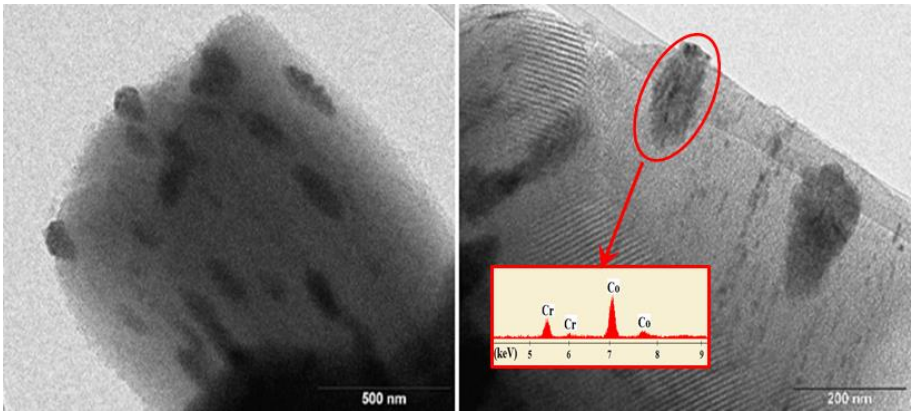

Figure 4. TEM images of the calcined powder CoCrS.

The H_2-TPR profile obtained for Co-Cr/SBA15 (see Figure 5) displays two main zones, one at low temperatures (< 350ºC) and the other at higher temperatures (> 350ºC).

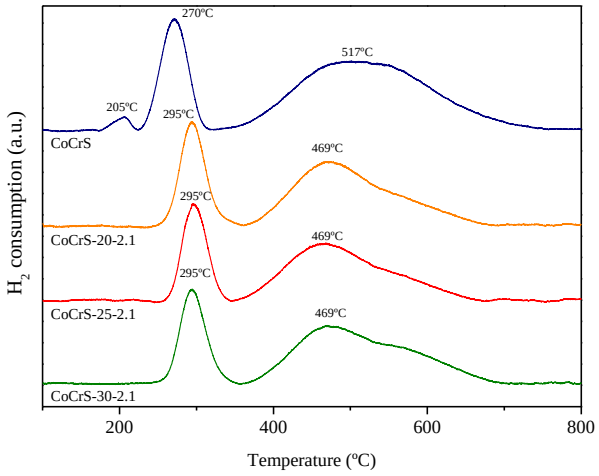

Figure 5. H_2-TPR profiles of the calcined powder CoCrS and extruded materials.

In the first zone, two peaks with maximum located at 205 and 270 ºC can be observed. Since Cr-oxides have lower reduction temperatures than Co-oxides [43], the contribution of Cr-oxides to the first reduction zone should be higher. In this sense, the maximum at 205 ºC is ascribed to the reduction of Cr-oxides species whose reduction can be affected by the presence of Co_3O_4 in the sample [43]. On the other hand, the

peak at 270 ºC is attributed to the reduction of Co_3O_4 to CoO. Finally, the peak at high temperature, with maxima at 517 ºC, corresponds to the reduction of CoO to Co^0 affected to the presence of Cr species [44].

Attending to the extruded materials, the peak around 205 ºC disappears and the peak at 270 ºC slightly shifts to higher temperature probably due to the higher calcination temperatures used for the extruded materials during the agglomeration process (100 ºC above CoCrS). On the other side, the high temperature peak moves to lower values indicating less interaction with the support [45] since higher calcination temperatures lead to a slightly sinterization of the Co particles (see Table 1) making the surface interaction between metal phase and the support smaller. Therefore, the agglomeration process did not exhibit remarkable changes in the H_2-TPR profiles with the exception of the maxima at higher temperatures.

Catalytic tests

AcASR reactions were carried out at atmospheric pressure and isothermally at 600 ºC after activation of the samples by H_2 reduction. Experiments were performed using an acetic acid solution at WHSV = 30.1 h^{-1}. N_2 was used as carrier gas and as internal standard in the micro-GC in order to determine all the gas products concentration. It is noteworthy that with higher particle diameter, the porosity of the catalyst bed will be higher as determined in Section 3.2, therefore the flow velocity will be smaller [46, 47].

Thus, firstly, experiments were performed in order to avoid external diffusion effects by varying the feed flowrate while keeping WHSV constant according to Akpan et al. [48]. In this mean, catalytic results using catalyst particles with 2.1 mm of effective diameter and 20 wt.% of bentonite as binder in terms of hydrogen content in the outlet gas stream and acetic acid conversion are displayed in Figure 6. Experiments were done modifying the mass of catalysts, the N_2 flow and the feed flow rate from 0.3-0.5 g, 60-100 mL/min and 0.075-0.125 mL/min, respectively (see Table 2). As it can be seen, the faster the flow, the higher the conversion value is obtained up to a feed flowrate of

0.1125 mL/min. If the flow rate is increased, no changes are observed in either the hydrogen content or the conversion indicating the absence of external mass transfer effect at these conditions [48]. The acetic acid conversion becomes higher because the increase of the feed flow rate, increases the turbulence and Reynolds number inside the reactor and therefore the mass transfer coefficient is improved. As a result, the AcA concentration external gradient disappears by increasing feed flow rate [49]. In conclusion, the reaction conditions selected were those corresponding to the experiment number 3: 0.45 g_{cat}; 0.1125 mL/min of acetic acid solution and 90 mL/min of N_2. At that point, the concentration of reactants over the catalyst surface should be the same as that of the gas phase and therefore there are no diffusional limitations.

Table 2. Experimental conditions for external diffusion effects tests.

Conditions	$m_{catalyst}$ (g)	Q_{feed} (mL/min)	N_2 flow (mL/min)
1	0.300	0.0750	60
2	0.375	0.0935	75
3	0.450	0.1125	90
4	0.500	0.1250	100

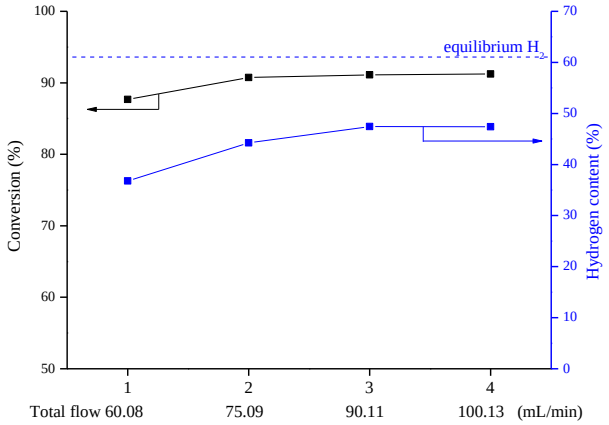

Figure 6. Hydrogen content in the outlet gas stream and acetic acid conversion at different reaction conditions as named in Table 2 (atmospheric pressure, 600 ºC, S/C = 2, WHSV = 30.1 h^{-1}).

Since some particles were broken and some fines appeared during the experiments described above, two new extruded catalysts with different bentonite content (25 and

30 wt.%) but the same geometry were prepared and tested under the selected conditions. In Figure 7, the conversion is represented on the right axis and the mechanical strength is referred to the left axis. As it can be observed, the mechanical strength becomes higher (with a linear behavior) when the bentonite content was increased, although the conversion follows an opposite behavior. However, despite the conversion drop, the hydrogen content was maintained between 57-59 mol % in all samples.

After the SR reactions, it could be observed that the amount of fines was rather reduced when the bentonite content was higher. Bentonite content was not increased since Pariente et al. [31] increased it up to 35 wt.% and they did not observe any improvement in the mechanical strength of the extruded materials. Since the acetic acid conversion drop was only 4 mol % in the sample with 30 wt.% of bentonite and the mechanical strength was the highest one (in line with almost no fines formed during the AcASR reaction), this value of the bentonite content was selected to evaluate the internal diffusion resistance.

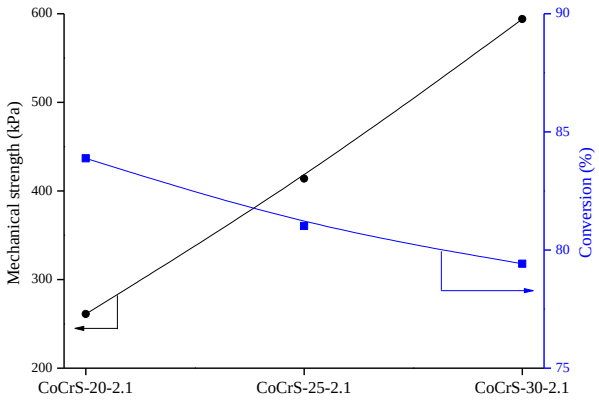

Figure 7. Mechanical properties and conversions for extruded material varying the bentonite content (atmospheric pressure, 600 ºC, S/C = 2, WHSV = 30.1 h^{-1}).

To determine the resistance to the mass transfer inside the pores of the catalyst particles, several AcASR reactions were done using extruded catalysts with different sizes ranging from D_{eff} =1.3 to 2.1 mm. The catalytic results of these tests are shown

in Figure 8a. Coke measured by TGA formation in terms of $g_{coke} \cdot gcat^{-1} \cdot h^{-1}$ are shown in Figure 8b. Results show that larger pellet sizes leas to lower acetic acid conversion. By decreasing the particle size to an effective diameter of 1.5 mm, the conversion increased up to 96 % from a conversion close to 79 % reached by the sample with an effective diameter of 2.1 mm (CoCrS-30-2.1). Hydrogen, on the other side, did not exhibit remarkable changes but CoCrS-30-1.5 sample reached the highest value (59.1%). This effect can be explained since a decrease in effective particle diameter minimize the influence of internal mass transfer related to the resistance found by reactant molecules to reach active sites placed inside the catalyst particle pores [49].

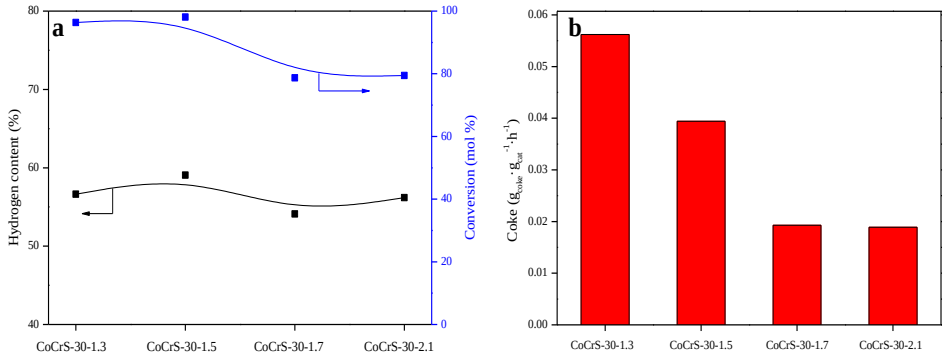

Figure 8. Catalytic results in terms of hydrogen content and conversion (a) and coke deposition (b) for extruded materials with different effective diameters (atmospheric pressure, 600 ºC, S/C = 2, WHSV = 30.1 h^{-1}).

It can also be observed that as the effective diameter decreases, the amount of deposited coke also increases. This fact is attributed to higher conversion and to a non-uniform coke distribution over the pellet because coke presents preferential deposition in the external surface of the particle as reported Forzatti et al. [50].

Once selected the conditions in which diffusional limitations do not affect to AcASR reactions (90.11 mL/min of total flow and 1.5 mm of effective diameter), and thus the kinetic control has been achieved, a new sample was prepared with the selected effective diameter using less amount of bentonite (25 wt.%) to be tested under conditions number 3 (see Table 2). As shown in Figure 9, the final product distribution

in addition to acetic acid conversion did not exhibited remarkable changes compared to the sample with CoCrS-30-1.5. Coke formation rate was comparable in both cases 0.0394 and 0.0391 gcoke·gcat^{-1}·h^{-1}, because the surface area was similar and as said before, in agglomerated samples coke tend to be deposited over the exterior part of the pellet [50]. Furthermore, in Figure 9, the catalytic results with powder sample obtained in a previous work [24] are also displayed. Comparing the results obtained with the extruded catalysts with those obtained with the powdered sample, it is noteworthy that whereas the hydrogen content in the outlet stream was similar (the same behavior is observed with the co-carbon product distribution), lower conversion was observed ascribed to the dilution with bentonite done in the agglomerated catalysts. Furthermore, the mechanical strength of the agglomerated catalysts was measured. The obtained results were 928 kPa and 636 kPa for CoCrS-30-1.5 and CoCrS-25-1.5 catalysts respectively. Based on these results, the main conclusion is that increasing the bentonite content enhances the mechanical strength without reduction in the catalytic activity.

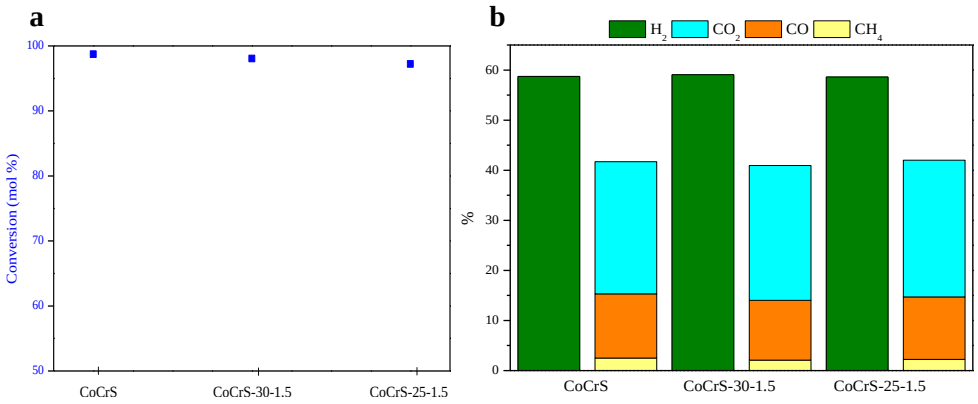

Figure 9. Comparison of extruded materials (D_{eff}=1.5 mm) with the powder sample: (a) conversion; (b) gas product distribution (atmospheric pressure, 600 ºC, S/C = 2, WHSV = 30.1 h^{-1}).

Finally, the selected extruded material was tested under the same conditions up to 12 h TOS. The conversion results for this experiment are displayed in Figure 10a. As can be observed, at least during the first 6 hours of the reaction, a decrease in the

conversion takes place up to a value close to 95%, from which it remains almost constant throughout the experiment. In order to explain the conversion drop, the formed coke was characterized using different techniques.

Taking into account the derivative thermogram (DTG) shown in Figure 10 b of the spent catalyst, a maximum around 508ºC can be observed. This maximum is attributed to some kind of defective carbon nanofibers because it is oxidized below 550 ºC while filamentous or graphitic carbon does at higher temperature [51, 52]. The formation of this type of carbon deposits results in the decrease of the catalytic activity by the deactivation of the catalyst.

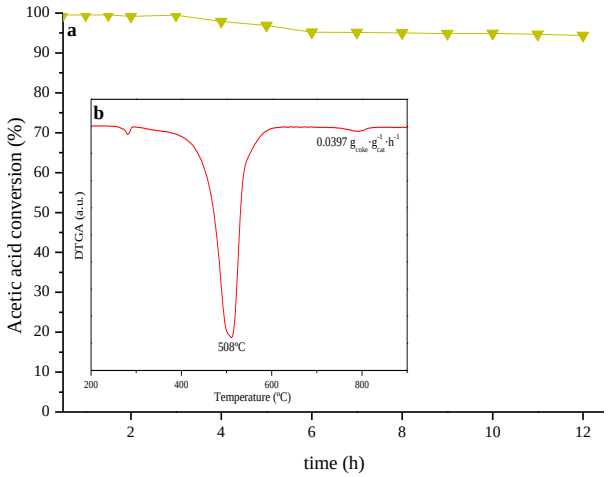

Figure 10. (a) Evolution of conversion with time-on-stream during the acetic acid steam reforming using the CoCrS-30-1.5 catalyst (atmospheric pressure, 600 ºC, S/C = 2, WHSV = 30.1 h^{-1}). (b) DTG profile of used catalysts.

Raman spectroscopy is known to be a suitable technique for characterizing the structure of carbonaceous materials. In this sense, the Raman spectra obtained after 12 h TOS is represented in Figure 11. Regarding the spectra in the range 1100-1800 cm^{-1}, two bands centered at 1350 and 1590 cm^{-1} can be distinguished ascribed to D-band and G-band, respectively. While G-band is attributed to the stretching mode of carbon sp^2 bonds of condensed graphitic aromatic structures, D-band is related to the carbon atoms vibration of disordered aromatic structures such

as amorphous or defective filamentous [52-54]. In the current spectra, G-band is more intense than D-band indicating the predomination of more ordered aromatic structures. This assumption is in agreement with elemental analysis results, since lower C/H molar ratio indicates that the coke is more aliphatic while the higher C/H indicates that the coke is more aromatic. After 12h TOS, the C and H content was 24.75% and 0.32% respectively, which implies a C/H ratio of 6.5 stating that the coke formed is more aromatic than aliphatic. These results together with those obtained by DTG, allow us to confirm that a part of the formed coke presents a disordered structure. This defective carbon has a deactivating effect that has led to a slightly decrease in conversion at short times on stream, since tip-growth of filaments ceases when carbon is formed at a rate higher than bulk diffusion and surface migration, causing an excess of carbon to deposit as encapsulating carbon, which ultimately deactivates the catalyst [15, 55].

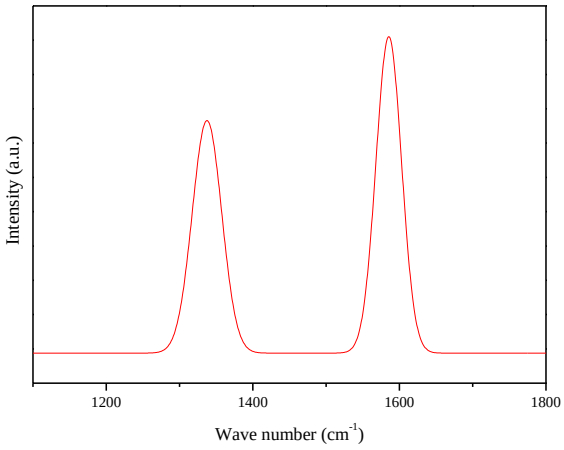

Figure 11. Raman spectra of used CoCrS-30-1.5 sample after 12 h TOS.

All these results allow as to conclude that the agglomeration procedure was successful using 30 wt.% of bentonite with an effective diameter of 1.5 mm since promising results were achieved.

Conclusions

The performance of extruded Co-Cr/SBA-15 catalysts has been studied through acetic acid steam reforming. The influence of internal and external diffusion effects has been tested over different bentonite/catalyst ratio and particle sizes. The results showed that the agglomeration procedure has no remarkable influence over the textural properties or the reducibility of metallic active species, being these results close to those obtained for the powder sample. The external and internal diffusion tests allowed to select flow rate and catalysts particle size needed to avoid concentration gradients. Under these experimental conditions, CoCrS-30-1.5 (30 wt.% bentonite and 1.5 mm effective diameter) showed a good performance for hydrogen production, reaching similar results in terms of hydrogen content and conversion compared to the powder form. Therefore, a successful agglomeration process has been developed, opening a door towards the preparation of new catalysts for steam reforming suitable for their use at industrial scale.

Acknowledgements

The authors acknowledge the financial support from the Regional Government of Madrid (project S2013/MAE-2882) and from the Spanish Ministry of Economy and Competitiveness (project ENE2017-83696-R). In addition, the authors gratefully acknowledge IMDEA Energy for the permission to use the equipment to carry out the mechanical strength analysis.

References

[1] A.J. Vizcaíno, A. Carrero, J.A. Calles, Hydrogen production from bioethanol, Nova Science Publishers, New York, **2012**, 247-294.

[2] I.E. Agency, Hydrogen Production and Storage: R&D Priorities and Gaps, IEA Publications, Paris, France, **2006**.

[3] S. Ayalur Chattanathan, S. Adhikari, N. Abdoulmoumine, A review on current status of hydrogen production from bio-oil, Renewable and Sustainable Energy Reviews, 16 (**2012**) 2366-2372.

[4] C. Barca, A. Soric, D. Ranava, M.-T. Giudici-Orticoni, J.-H. Ferrasse, Anaerobic biofilm reactors for dark fermentative hydrogen production from wastewater: A review, Bioresource Technology, 185 (**2015**) 386-398.

[5] R. Chaubey, S. Sahu, O.O. James, S. Maity, A review on development of industrial processes and emerging techniques for production of hydrogen from renewable and sustainable sources, Renewable and Sustainable Energy Reviews, 23 (**2013**) 443-462.

[6] I. Dincer, C. Acar, Review and evaluation of hydrogen production methods for better sustainability, International Journal of Hydrogen Energy, 40 (**2015**) 11094-11111.

[7] L. Gradisher, B. Dutcher, M. Fan, Catalytic hydrogen production from fossil fuels via the water gas shift reaction, Applied Energy, 139 (**2015**) 335-349.

[8] M. Ni, M.K.H. Leung, D.Y.C. Leung, K. Sumathy, A review and recent developments in photocatalytic water-splitting using TiO_2 for hydrogen production, Renewable and Sustainable Energy Reviews, 11 (**2007**) 401-425.

[9] K. Jacobson, K.C. Maheria, A. Kumar Dalai, Bio-oil valorization: A review, Renewable and Sustainable Energy Reviews, 23 (**2013**) 91-106.

[10] J. Remón, F. Broust, G. Volle, L. García, J. Arauzo, Hydrogen production from pine and poplar bio-oils by catalytic steam reforming. Influence of the bio-oil composition on the process, International Journal of Hydrogen Energy, 40 (**2015**) 5593-5608.

[11] A. Remiro, B. Valle, L. Oar-Arteta, A.T. Aguayo, J. Bilbao, A.G. Gayubo, Hydrogen production by steam reforming of bio-oil/bio-ethanol mixtures in a continuous thermal-catalytic process, International Journal of Hydrogen Energy, 39 (**2014**) 6889-6898.

[12] V. Paasikallio, J. Kihlman, C.A.S. Sánchez, P. Simell, Y. Solantausta, J. Lehtonen, Steam reforming of pyrolysis oil aqueous fraction obtained by one-step fractional condensation, International Journal of Hydrogen Energy, 40 (**2015**) 3149-3157.

[13] C. Ji, Z. He, Q. Wang, G. Xu, S. Wang, Z. Xu, H. Ji, Effect of operating conditions on direct liquefaction of low-lipid microalgae in ethanol-water co-solvent for bio-oil production, Energy Conversion and Management, 141 (**2017**) 155-162.

[14] Z. Du, M. Mohr, X. Ma, Y. Cheng, X. Lin, Y. Liu, W. Zhou, P. Chen, R. Ruan, Hydrothermal pretreatment of microalgae for production of pyrolytic bio-oil with a low nitrogen content, Bioresource Technology, 120 (**2012**) 13-18.

[15] J.A. Calles, A. Carrero, A.J. Vizcaíno, L. García-Moreno, Hydrogen production by glycerol steam reforming over SBA-15-supported nickel catalysts: Effect of alkaline earth promoters on activity and stability, Catalysis Today, 227 (**2014**) 198-206.

[16] X. Han, Y. Wang, Y. zhang, Y. Yu, H. He, Hydrogen production from oxidative steam reforming of ethanol over Ir catalysts supported on Ce–La solid solution, International Journal of Hydrogen Energy, 42 (**2017**) 11177-11186.

[17] Y. Mei, C. Wu, R. Liu, Hydrogen production from steam reforming of bio-oil model compound and byproducts elimination, International Journal of Hydrogen Energy, 41 (**2016**) 9145-9152.

[18] G. Chen, J. Tao, C. Liu, B. Yan, W. Li, X. Li, Hydrogen production via acetic acid steam reforming: A critical review on catalysts, Renewable and Sustainable Energy Reviews, 79 (**2017**) 1091-1098.

[19] B. Banach, A. Machocki, P. Rybak, A. Denis, W. Grzegorczyk, W. Gac, Selective production of hydrogen by steam reforming of bio-ethanol, Catalysis Today, 176 (**2011**) 28-35.

[20] A. Carrero, A.J. Vizcaíno, J.A. Calles, L. García-Moreno, Hydrogen production through glycerol steam reforming using Co catalysts supported on SBA-15 doped with Zr, Ce and La, Journal of Energy Chemistry, 26 (**2017**) 42-48.

[21] A. Casanovas, M. Roig, C. de Leitenburg, A. Trovarelli, J. Llorca, Ethanol steam reforming and water gas shift over Co/ZnO catalytic honeycombs doped with Fe, Ni, Cu, Cr and Na, International Journal of Hydrogen Energy, 35 (**2010**) 7690-7698.

[22] F. Zhang, M. Wang, L. Zhu, S. Wang, J. Zhou, Z. Luo, A comparative research on the catalytic activity of La_2O_3 and γ-Al_2O_3 supported catalysts for acetic acid steam reforming, International Journal of Hydrogen Energy, 42 (**2017**) 3667-3675.

[23] X. Hu, G. Lu, Comparative study of alumina-supported transition metal catalysts for hydrogen generation by steam reforming of acetic acid, Applied Catalysis B: Environmental, 99 (**2010**) 289-297.

[24] P.J. Megía, A. Carrero, J.A. Calles, A.J. Vizcaíno, Influence of promoters addition to Co-based catalysts on acetic acid steam reforming, European Hydrogen Energy Conference. EHEC 2018: Proceedings, Malaga, **2018**, 125.

[25] W. Nabgan, T.A.T. Abdullah, R. Mat, B. Nabgan, A.A. Jalil, L. Firmansyah, S. Triwahyono, Production of hydrogen via steam reforming of acetic acid over Ni and Co supported on La_2O_3 catalyst, International Journal of Hydrogen Energy, 42 (**2017**) 8975-8985.

[26] A.G. Adeniyi, K.S. Otoikhian, J.O. Ighalo, Steam Reforming of Biomass Pyrolysis Oil: A Review, 17 (**2019**) 20180328.

[27] G. Chandrasekar, M. Hartmann, M. Palanichamy, V. Murugesan, Extrusion of AlSBA-15 molecular sieves: An industrial point of view, Catalysis Communications, 8 (**2007**) 457-461.

[28] R.V. Jasra, N.V. Choudary, S.G.T. Bhat, Separation of Gases by Pressure Swin, Separation Science and Technology, 26 (**1991**) 885-930.

[29] D.W. Breck, Zeolite molecular sieves: structure, chemistry, and use, John Wiley & Sons, New York, **1973**.

[30] J.A. Melero, J. Iglesias, J. Sainz-Pardo, P. de Frutos, S. Blázquez, Agglomeration of Ti-SBA-15 with clays for liquid phase olefin epoxidation in a continuous fixed bed reactor, Chemical Engineering Journal, 139 (**2008**) 631-641.

[31] M.I. Pariente, F. Martínez, J.Á. Botas, J.A. Melero, Extrusion of Fe_2O_3/SBA-15 mesoporous material for application as heterogeneous Fenton-like catalyst, AIMS Environmental Science, 2 (**2015**) 154-168.

[32] L. Zhao, Y. Zhao, S. Wang, H. Yue, B. Wang, J. Lv, X. Ma, Hydrogenation of Dimethyl Oxalate Using Extruded Cu/SiO_2 Catalysts: Mechanical Strength and Catalytic Performance, Industrial & Engineering Chemistry Research, 51 (**2012**) 13935-13943.

[33] D.I. Wilson, S.L. Rough, Extrusion-spheronisation, Handbook of Powder Technology, Elsevier, Amsterdam, **2007**, 189-217.

[34] A.V. Zhensa, E.M. Kol'tsova, I.A. Petropavlovskii, V.V. Kostyuchenko, V.A. Filippin, Mathematical Modeling of Extrusion of Water–Oxide Pastes in the Production of α-Fe_2O_3 Catalysts, Theoretical Foundations of Chemical Engineering, 37 (**2003**) 197-203.

[35] D. Zhao, J. Feng, Q. Huo, N. Melosh, G.H. Fredrickson, B.F. Chmelka, G.D. Stucky, Triblock copolymer syntheses of mesoporous silica with periodic 50 to 300 angstrom pores, Science, 279 (**1998**) 548-552.

[36] A. Carrero, J.A. Calles, L. García-Moreno, A.J. Vizcaíno, Production of Renewable Hydrogen from Glycerol Steam Reforming over Bimetallic Ni-(Cu,Co,Cr) Catalysts Supported on SBA-15 Silica, Catalysts, 7 (**2017**) 55.

[37] J.A. Calles, A. Carrero, A.J. Vizcaíno, L. García-Moreno, P.J. Megía, Steam Reforming of Model Bio-Oil Aqueous Fraction Using Ni-(Cu, Co, Cr)/SBA-15 Catalysts, International Journal of Molecular Sciences, 20 (**2019**) 512.

[38] M. Zakeri, A. Samimi, M.S. Afarani, A. Salehirad, Interaction between Weibull parameters and mechanical strength reliability of industrial-scale water gas shift catalysts, Particuology, 32 (**2017**) 160-166.

[39] T.V. Bharat, Y. Gapak, Hydration kinetics of bentonite buffer material: Influence of vapor pressure, bentonite plasticity, and compaction density, Applied Clay Science, 157 (**2018**) 41-50.

[40] V.A. Arus, S. Nousir, R. Sennour, T.C. Shiao, I.D. Nistor, R. Roy, A. Azzouz, Intrinsic affinity of acid-activated bentonite towards hydrogen and carbon dioxide, International Journal of Hydrogen Energy, 43 (**2018**) 7964-7972.

[41] G. Liu, J. Guo, F. Meng, X. Zhang, L. Wang, Effects of Colloidal Silica Binder on Catalytic Activity and Adhesion of HZSM-5 Coatings for Structured Reactors, Chinese Journal of Chemical Engineering, 22 (**2014**) 875-881.

[42] L. Zhirong, M. Azhar Uddin, S. Zhanxue, FT-IR and XRD analysis of natural Na-bentonite and Cu(II)-loaded Na-bentonite, Spectrochimica Acta Part A: Molecular and Biomolecular Spectroscopy, 79 (**2011**) 1013-1016.

[43] D. Yun, J. Baek, Y. Choi, W. Kim, H. Jong Lee, J. Yi, Promotional Effect of Ni on a CrO_x Catalyst Supported on Silica in the Oxidative Dehydrogenation of Propane with CO_2, ChemCatChem, 4 (**2012**).

[44] J. Chen, X. Zhang, H. Arandiyan, Y. Peng, H. Chang, J. Li, Low temperature complete combustion of methane over cobalt chromium oxides catalysts, Catalysis Today, 201 (**2013**) 12-18.

[45] G. Prieto, A. Martínez, R. Murciano, M.A. Arribas, Cobalt supported on morphologically tailored SBA-15 mesostructures: The impact of pore length on metal dispersion and catalytic activity in the Fischer–Tropsch synthesis, Applied Catalysis A: General, 367 (**2009**) 146-156.

[46] J. Yang, J. Wu, L. Zhou, Q. Wang, Computational study of fluid flow and heat transfer in composite packed beds of spheres with low tube to particle diameter ratio, Nuclear Engineering and Design, 300 (**2016**) 85-96.

[47] M. Zhang, H. Dong, Z. Geng, Computational study of flow and heat transfer in fixed beds with cylindrical particles for low tube to particle diameter ratios, Chemical Engineering Research and Design, 132 (**2018**) 149-161.

[48] E. Akpan, Y. Sun, P. Kumar, H. Ibrahim, A. Aboudheir, R. Idem, Kinetics, experimental and reactor modeling studies of the carbon dioxide reforming of methane (CDRM) over a new $Ni/CeO_2–ZrO_2$ catalyst in a packed bed tubular reactor, Chemical Engineering Science, 62 (**2007**) 4012-4024.

[49] H.C. Yoon, J. Otero, P.A. Erickson, Reactor design limitations for the steam reforming of methanol, Applied Catalysis B: Environmental, 75 (**2007**) 264-271.

[50] P. Forzatti, L. Lietti, Catalyst deactivation, Catalysis Today, 52 (**1999**) 165-181.

[51] C.K.S. Choong, Z. Zhong, L. Huang, Z. Wang, T.P. Ang, A. Borgna, J. Lin, L. Hong, L. Chen, Effect of calcium addition on catalytic ethanol steam reforming of Ni/Al_2O_3: I. Catalytic stability, electronic properties and coking mechanism, Applied Catalysis A: General, 407 (**2011**) 145-154.

[52] A.E. Galetti, M.F. Gomez, L.A. Arrúa, M.C. Abello, Hydrogen production by ethanol reforming over NiZnAl catalysts: Influence of Ce addition on carbon deposition, Applied Catalysis A: General, 348 (**2008**) 94-102.

[53] A. Carrero, J.A. Calles, A.J. Vizcaíno, Effect of Mg and Ca addition on coke deposition over $Cu–Ni/SiO_2$ catalysts for ethanol steam reforming, Chemical Engineering Journal, 163 (**2010**) 395-402.

[54] C. Montero, A. Ochoa, P. Castaño, J. Bilbao, A.G. Gayubo, Monitoring Ni^0 and coke evolution during the deactivation of a $Ni/La_2O_3–\alpha Al_2O_3$ catalyst in ethanol steam reforming in a fluidized bed, Journal of Catalysis, 331 (**2015**) 181-192.

[55] A.M. Amin, E. Croiset, W. Epling, Review of methane catalytic cracking for hydrogen production, International Journal of Hydrogen Energy, 36 (**2011**) 2904-2935.

Article 4

"Coke evolution in simulated bio-oil aqueous fraction steam reforming using Co/SBA 15"

Catalysis Today, 2020

https://doi.org/10.1016/j.cattod.2020.04.069

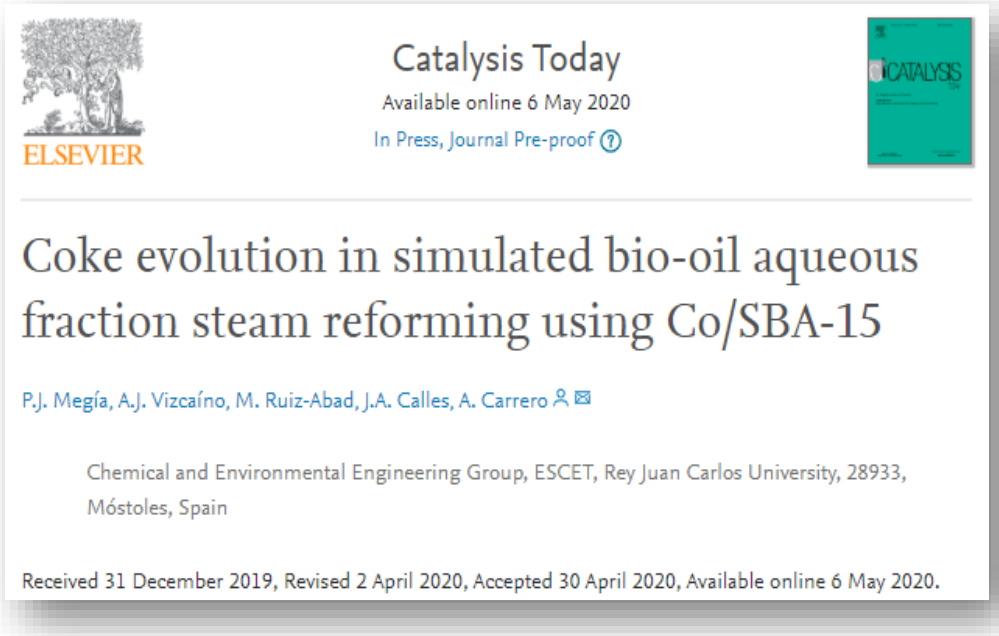

ELSEVIER

Catalysis Today

Available online 6 May 2020

In Press, Journal Pre-proof

Coke evolution in simulated bio-oil aqueous fraction steam reforming using Co/SBA-15

P.J. Megía, A.J. Vizcaíno, M. Ruiz-Abad, J.A. Calles, A. Carrero

Chemical and Environmental Engineering Group, ESCET, Rey Juan Carlos University, 28933, Móstoles, Spain

Received 31 December 2019, Revised 2 April 2020, Accepted 30 April 2020, Available online 6 May 2020.

Impact JCR factor, JCR 2019: 5.825

Category: Chemistry Applied. 8 of 71 (Q1)

Abstract

This paper studies Co/SBA-15 catalyst deactivation during the steam reforming of model compounds from the aqueous fraction of bio-oil coming from biomass HTL. We observed how deactivation took place in two clearly differentiated stages. In the first one (TOS <20 h), where conversion decreased strongly, Co sintering deduced from XRD and, pore blockage by coke deposition were observed. At this first stage, coke seemed to be filamentous and some encapsulated Co particles could be appreciated by TEM. The encapsulating coke reduced the number of accessible centers to catalyze the reforming reaction. In the second stage (TOS >20 h), filamentous coke was also observed but more condensed and therefore more aromatic, as verified by higher C/H ratio determined by elemental analysis. In this stage, despite the amount of coke deposited was growing, no drop on specific surface area was observed. Besides, since no peaks corresponding to cobalt oxides were detected in the XRD patterns, catalyst deactivation cannot be attributed to metallic active sites oxidation. The t-Student statistical analysis showed that Co/SBA-15 catalyst deactivation is mainly affected by the amount of coke deposited and its C/H ratio.

Keywords: deactivation, coke deposition, cobalt, SBA-15, steam reforming, aqueous fraction, biomass HTL.

Introduction

Biomass-to-energy conversion processes could be good candidates to produce renewable energy [1] as an alternative to conventional fossil fuels, which have a great contribution in global climate change. In these sense, biomass hydrothermal liquefaction (HTL) [2-5], can be used to produce clean fuels. Due to its composition, biomass stores energy through chemical bonds mainly between hydrogen, oxygen and carbon molecules [6]. By breaking down these chemical bonds through thermochemical processes, such as HTL, it is possible to release vast amount of energy in order to produce bio-fuels [7]. HTL is very suitable in the thermochemical conversion of wet biomass like municipal solid waste, microalgae or animal by-products where bio-oil along with synthesis gas and a solid residue are obtained [2, 7]. This process provides a great advantage when compared to the traditional biomass pyrolysis process, since it does not require a previous step for biomass drying associated with high energy consumption [8-10]. The solid residue and gas phase produced during HTL process, can be also reused reducing the overall cost and contributing to the reduction of NO_x and SO_2 emissions [11]. The bio-oil can be segregated into two different phases: an organic phase and an aqueous phase [12]. The organic phase composed of non-polar compounds can be upgraded by hydro-treating to obtain fuels. The aqueous phase has low value and it contains mainly water but also several oxygenated organic compounds such as acetic acid, phenol and hydroxyacetone [1, 13]. This worthless aqueous phase, can be revalorized by producing hydrogen by a catalytic reforming process [14]. Given that the aqueous fraction is a mixture of oxygenated compounds, the overall reaction that takes place can be summarized as:

$$C_nH_mO_k+(2n-k)\ H_2 \leftrightarrow n\ CO_2 + (2n+m/2-k)\ H_2$$

The viability of this process is related to the development of active and stable catalysts, with high selectivity towards hydrogen production. One problem associated with the reforming catalysts is the deactivation, which may be caused by sintering or oxidation

of the active phase, although coke formation is typically the main cause. Steam reforming catalysts are usually based on noble or transition metals. While noble metals are active but involve high cost [15], cheaper transition metals such as Co, has demonstrated good results in steam reforming processes [14, 16-19]. This behavior has been ascribed to Co ability for cracking not only C-C bonds, but also C-H bonds in comparison with other transition metals [20]. Moreover, Co is also active in water-gas-shift reaction, which may increase hydrogen production rate and lower CO concentration among the products ($CO + H_2O \leftrightarrow CO_2 + H_2$) [21].

In addition, metal dispersion over the support has been described in literature to have an important role in enhancing the reforming reaction in terms of conversion, hydrogen selectivity and resistance to coke formation [22, 23]. In this regard, ordered mesoporous silica SBA-15 materials as supports have raised considerable interest among other supports since the distribution of mesopores is uniform preventing the formation of metal agglomerates leading to catalyst sintering [24, 25]. This structure provides high dispersion of the active phase and facilitates the mass transport through the pores comparing to other non-ordered supports [26].

As mentioned before, the reforming of oxygenated compounds provides high hydrogen yield, but consecutive competitive reactions can take place leading to the formation of undesirable by-products such as coke deposits [27, 28]. The attenuation of these reactions depends on the composition and physicochemical properties of the catalysts as well as the reaction conditions [29]. Coke formation can take place through the Boudouard reaction ($2CO\ (g) \leftrightarrow CO_2\ (g) + C$), methane decomposition ($CH_4 \leftrightarrow C + 2H_2$) or polymerization (hydrocarbons → polymers → coke) [30, 31]. Sehested [32] reported for hydrocarbon reforming reactions the formation of different kinds of carbon deposits, amorphous or filamentous, with disparate roles in catalyst deactivation. The main cause reported of deactivation due to coke formation is the formation of encapsulating coke, which blocks metal active sites [33-35]. The condensation of oxygenated reaction intermediates, after being adsorbed on metal sites, plays an important role in the formation of encapsulating coke, while more

ordered coke structures are mainly formed by methane decomposition and Boudouard reaction [36]. Further, according to Barbarias et al. [37] aromatic compounds have high capability for condensing and forming a coke structures on the catalyst surface, which is responsible for fast catalyst deactivation. When filamentous coke is formed, it covers the catalyst but the access of reactants to metal active sites may not be hindered [33]. Apart from that, deactivation can be also due to active phase sintering and/or its oxidation, decreasing in such a way the number of active centers [38-41]. Valle et al. [42], notice that during the steam reforming of raw bio-oil obtained from pine sawdust using Ni/La_2O_3-αAl_2O_3, the increase in temperature in the 550–700 °C range attenuates the formation of encapsulating coke, whereas in the 550–650 °C range the formation of filamentous coke was favored, which does not block the metal sites. Similarly, Ochoa et al. [43] found out that the presence of phenols and alcohols in the raw bio-oil plays an important role in coke formation, while the influence of the content of acids, ketones and aldehydes within coke deposition is lower. For their part, Remiro et al. [44] reported three different deactivation reasons in the steam reforming of bio-oil using a Rh/ZDC catalyst: structural changes, coke deposition and Rh sintering. These causes, according to their characterization results were a consequence in the physicochemical and morphological properties of the catalysts.

Thus, this work contributes to understand the relationship between Co/SBA-15 deactivation, coke deposition and Co sintering during the steam reforming of simulated bio-oil aqueous fraction got from biomass HTL and mainly composed by acetic acid, phenol and hydroxyacetone. Although this catalyst was used before in acetic acid steam reforming, the evolution of carbon deposits over the support and/or metal particles in the simulated bio-oil aqueous fraction, has never been described. For this purpose, N_2-physisorption, thermogravimetric analysis, X-ray diffraction, elemental analysis and transmission electron microscopy techniques were used to characterize the catalysts used under reforming conditions at different time-on-stream.

Experimental

Catalysts synthesis and properties

Co-based catalyst (nominal content: 7 wt.% Co) supported over SBA-15, was prepared by the incipient wetness impregnation method described elsewhere [14, 45]. The support was synthetized following the hydrothermal method described by Zhao et al. [46] obtaining a BET surface area of 550 m^2/g and total pore volume of 0.97 cm^3/g. After the impregnation and calcination processes, these values were 503 m^2/g and 0.83 cm^3/g, respectively [14]. Prior to reforming reactions, the catalyst was in situ reduced at 700ºC by flowing pure hydrogen (30 mL/min) with a heating ramp of 2 °C/min. Once the desired temperature was reached, it was kept for 30 minutes. Under these conditions, cobalt oxide species are expected to be completely reduced according to the temperature-programmed reduction (TPR) analysis (Figure S1), measured in a Micromeritics AUTOCHEM 2910. This apparatus was also used to determine the metal dispersion over the support (7.5 % [14]) by H_2 temperature-programmed desorption (H_2 TPD) assuming H/Co = 1 in accordance with Li et al. [47]. Cobalt content in the reduced catalyst (6.4 wt.% [14]) was determined by ICP-AES technique, treating previously the sample by acidic digestion. The equipment was a Varian VISTA-PRO AX CCD-Simultaneous ICP-AES spectrophotometer.

Catalytic experiments

The activity of the catalyst at different time-on-stream was evaluated in a fixed-bed reactor using a Microactivity PRO unit (PID Eng. and Tech. S.L.) following the same procedure reported in a previous work [48]. The reactor is made in stainless steel 316 (i.d. = 9.2 mm, L = 300 mm) and it is placed into an electric oven. The temperature is measured in the catalytic bed by means of a K-type thermocouple. In order to prevent condensation of reactants in the pipes and to act as a preheater of the mixture, all the components inside the equipment are maintained at 200 °C during the test. The experiments were performed under operation conditions where diffusion limitations were absent, in which deactivation by coke was observed: 300 mg of catalyst, 600 °C;

atmospheric pressure; WHSV 30.2 h^{-1}; eight different time-on-streams (TOS) between 1-50h.

The model compounds mixture similar to biomass HTL aqueous fraction was composed by 1.57, 8.25 and 17.5 mol% of phenol, hydroxyacetone and acetic acid, respectively, in water, which gives a steam-to-carbon ratio of 1.1. The mixture was fed to the reactor at WHSV = 30.2 h^{-1}, defined as the ratio between the inlet flowrate and the mass of catalyst. N_2 was used as carrier gas and internal standard in a Micro-GC which is online connected to the reactor system to measure the gas product composition. The Agilent 490 Micro-GC is equipped with a TCD, a Molecular Sieve 5A column (20 m) and a PoraPlot U column (10 m) using Ar and He as carrier gas, respectively. Condensable products flowing from the reactor were collected in a condenser at 4 °C and periodically analysed in a Varian CP-3900 chromatograph equipped with a CP-WAX 52 CB (30 m × 0.25 mm, DF = 0.25) column and flame ionization detector (FID).

The catalytic behavior was expressed by means of total conversion and gaseous products distribution. Total conversion (X) is calculated as

$$X = \sum(F_{i,0} - F_i)/ \sum F_{i,0} \quad \text{(eq. 1)}$$

where $F_{i,0}$ and F_i are the molar flowrates of the reactant i (acetic acid, hydroxyacetone and phenol) at the inlet and outlet of the reactor, respectively.

Gaseous products distribution (C_i) is calculated as the ratio between the molar flowrate of each product (F_i) and the molar flowrate of all the reaction products (excluding water and reactants):

$$C_i = F_i/ (\sum F_i) \quad \text{(eq. 2)}$$

Characterization of used catalysts.

The catalysts porous structure was evaluated by means of N_2 adsorption-desorption at 77K on a Micromeritics TRISTAR 3000 sorptometer. Samples were previously outgassed under vacuum at 200 °C for 4 h.

The morphology of used samples, was evaluated by means of transmission electron microscopy (TEM) analysis. Samples were previously prepared via dispersion in acetone using an ultrasonic bath and subsequently deposited on a carbon-coated copper grid. The micrographs were acquired in a JEOL JEM 2100 microscope (200 kV) with a resolution of 0.25 nm at the National Centre for Electron Microscopy (CNME, Complutense University of Madrid). The apparatus is equipped with microanalysis system by energy dispersive spectroscopy (EDS). X-ray diffraction analysis (XRD) were performed on a Philips X'pert PRO diffractometer using Cu Kα radiation in order to estimate the crystalline state of the Co particles and coke crystallinity after reforming experiments. The Scherrer equation was used to estimate the metal crystallites mean diameter.

In order to evaluate the coke amount and nature, different analyses were performed by the following techniques: (i) Thermogravimetric analysis (TGA), with the aim of quantifying the amount of coke formed, under airflow with a heating rate of 5 °C/min up to 1000 °C on a TA instruments SDT 2960 thermobalance; (ii) Elemental C and H analysis, to determine the coke nature, using an elemental analyser type Flash 2000 provided by Thermo Fisher Scientific equipped with a thermal conductivity detector (TCD) using sulphanilic acid as standard; and (iii) Transmission electron microscopy in order to observe coke deposits after each catalytic run using same microscope described above at the CNME (Complutense University of Madrid).

Results

Synthetic bio-oil aqueous fraction steam reforming was performed using Co/SBA-15 catalysts. Figure 1 displays the catalytic behavior with time-on-stream. As observed, at low TOS conversion decay is more pronounced and it is smoothed until almost no loss of conversion is observed between 20 and 50 h. In the conversion profile, two main stages can be distinguished. In the first one before 20 h of time on stream, the deactivation effect is more severe decreasing the conversion value up to 80 mol%. In this period, CO decreases while CO_2 increases suggesting that Boudouard reaction is favored. However, the fact that H_2 content in the gas stream remains almost constant suggests that water-gas-shift reaction can be also taking place.

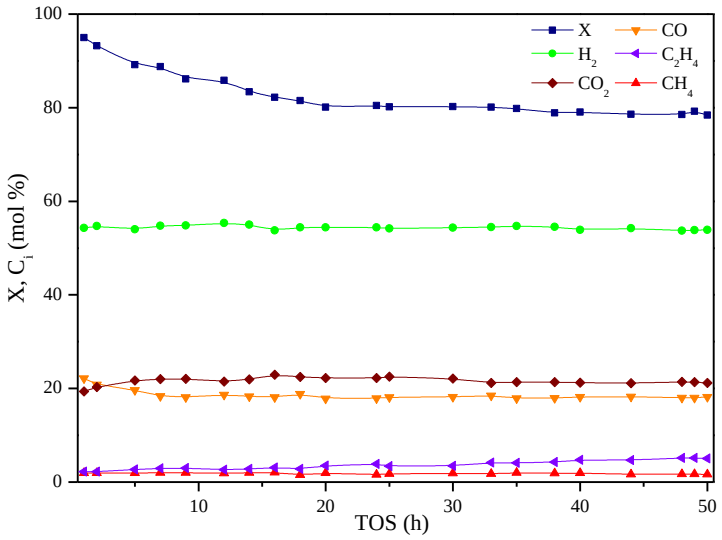

Figure 1. Conversion (X) and reaction products distribution (Ci) with TOS (T=600 ºC, P=1 atm, WHSV=30.2 h^{-1}).

In the next stage, at higher time-on-stream, the conversion remains almost constant. This behavior indicates that the main deactivation is produced during the first 20 h of reaction. On the other hand, the concentration of ethylene from 20 to 50 h TOS increases. As it is reported, ethylene promotes coke formation [49] for its capability of cracking and polymerization towards aromatics [29, 50]. Therefore, it is possible to

assume that in the first stage, most ethylene is being reformed according to $C_2H_4 + 2H_2O \rightarrow 2CO + 4H_2$ and/or leading to encapsulating coke, while in the second stage the ethylene conversion routes are unfavored. Conversely, from these results, methane cannot be correlated to possible catalyst deactivation since its concentration seems roughly constant with time-on-stream [51].

The XRD diffractograms of activated and spent Co/SBA-15 catalysts at different time-on-stream are displayed in Figure 2. In all samples, cubic phase of Co^0 (JCPDS 00-001-1259) can be observed, both in the activated and the used catalysts after the reforming reaction. Peaks show the reflection at $2\theta = 44.4°$ and 51.3°, ascribed to (111) and (200) planes respectively. No peaks attributed to CoO and Co_3O_4 can be observed, indicating that Co^0 has not been oxidized during the reaction, probably due to the reduction capacity of H_2 in the products stream. The presence of coke in the used samples has been proved according to the reflection peaks at $2\theta = 26.5°$, 42.6° and 53.9°, associated with the (002), (100) and (004) planes, features of graphitic carbon (JCPDS 00-041-1487). The main carbon diffraction peak, which increase with TOS is placed at $2\theta = 26.5°$. The Co^0 particle sizes have been calculated for the activated and the spent catalysts using the Scherrer equation [52] and these data are displayed on the right side of Figure 2. The results show the evolution of particle size with TOS towards slightly higher values, indicating some sintering of Co^0 crystallites at the reaction temperature (600 ºC), mainly between 0 and 20 h of TOS. However, sintering is a complex mechanism that depends not only on temperature, but also on the characteristics of the catalysts and reaction conditions [41]. Metal sintering also plays an important role in deactivation in terms of the generation of carbon deposits since large metal particles favor the growth of carbon nanofibers [53, 54]. Thus, sintering must be considered as one possible cause for deactivation of Co/SBA-15 during bio-oil aqueous fraction reforming, while Co oxidation can be discarded at least from XRD results.

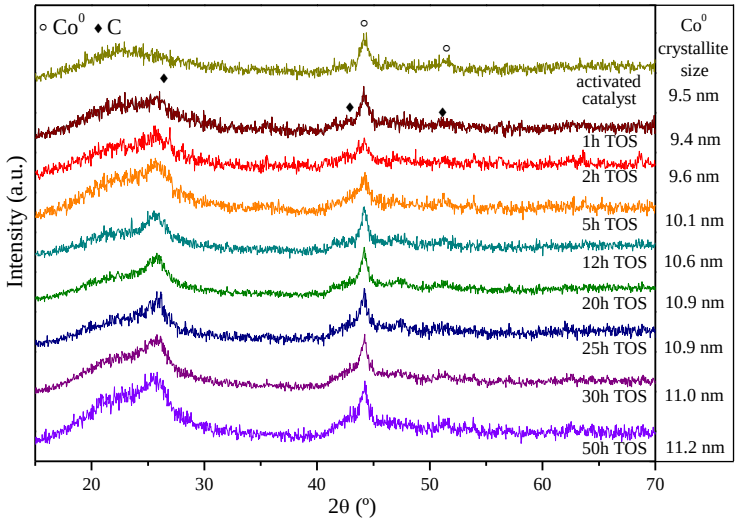

Figure 2. XRD diffraction spectra of activated and spent Co/SBA-15 for different TOS.

In order to determine the amount of coke deposited and its nature, TGA and elemental analysis techniques were performed over the used samples. The obtained results are shown in Table 1 and Figure S2. In reference to coke formation, an upward trend with TOS can be clearly observed, most coke being formed between 0-20 h. After this point, coke is gradually formed with an increase of 0.26 g_{coke}/g_{cat} between 20-50 h versus 0.73 g_{coke}/g_{cat} formed in the first stage (0-20 h). Since most coke is formed during the first stage, it is possible to assume that coke selectivity is higher compared to the second stage. This assumption is in line with the above described given that in this period Boudouard reaction is favored leading to coke formation while decreasing the CO content. Attending to DTG profiles (Figure S2), two zones can be distinguished in all the profiles. The maximum oxidation temperature in zone at higher temperatures, shifts from ~540 ºC at TOS = 1 h to ~570 ºC for TOS higher than 12 h. Based on the literature, the fact that the maximum combustion temperature of the formed carbon increases over time-on-stream is related to more condensed and ordered carbon deposits, and thus, more difficult to be oxidized [55, 56]. In the low temperature zone, the lowest oxidation temperature achieved was ~460 ºC for 1 h TOS indicating the formation of some kind of defective carbon nanofibers [14] since amorphous coke

oxidizes at much lower temperatures (around 300-400 ºC) [38, 57, 58]. As carbon deposits are formed they evolve towards more condensed coke, increasing the ordering degree leading to more graphitic structures [33]. In view of these results, elemental analysis of the used samples was performed, and the values are summarized in Table 1.

Table 1. Values of coke deposition, $T_{DTG,max}$ and C/H ratio on used catalysts

TOS (h)	coke (wt.%)	g_{coke}/g_{cat}	$T_{DTG,max}$ (ºC)	C/H
1	7.46	0.08	540-550	4.34
2	11.33	0.13	545-555	6.14
5	15.46	0.18	540-550	8.22
12	23.43	0.31	560-570	10.01
20	42.35	0.73	560-570	10.49
25	42.71	0.75	560-570	10.47
30	47.35	0.85	560-570	10.52
50	49.53	0.98	560-570	10.51

Higher carbon-to-hydrogen ratio (C/H) are associated to more aromatic or condensed structures [29, 59]. As the reaction time increases, the C/H ratio increases until an asymptotic value is reached at 12 h time-on-stream. This implies that the coke formed at short TOS is more aliphatic and/or defective than the coke found at long TOS. As the reaction time increases this defective coke may condense leading to more ordered structures. These results corroborate the TGA results explained above.

In order to analyze how this coke formation affects the textural properties of the Co/SBA-15 catalysts and elucidate its location, Table 2 summarizes the results of surface area (calculated according to Brunauer-Emmett-Teller, BET) and pore volume, obtained from the corresponding N_2-physisorption isotherms. Both, fresh and used catalysts presented a type IV isotherm according to the IUPAC classification with a H1 hysteresis loop, indicating the preservation of the mesostructure of SBA-15 material after active phase incorporation and the reforming reaction. Both total pore volume and BET surface area become smaller as time-on-stream increases. This could

be explained by increased deposition of coke which may lead to a decrease in the physical properties [29]. This behavior was also reported by Jampa et al. [60] using Cu-based catalysts supported over mesoporous materials in the autothermal steam reforming of methanol.

Table 2. Textural properties of used Co/SBA-15 catalysts at different TOS.

TOS (h)	BET (m^2/g)	V_{pore}^* (cm^3/g)
0	503	0.8
1	484	0.8
2	353	0.6
5	304	0.5
12	284	0.4
20	188	0.3
25	187	0.3
30	184	0.3
50	183	0.3

*Measured at $P/P_0 = 0.97$

Furthermore, the sorption capacity for nitrogen obtained by N_2-physisorption as a function of carbon content can give an idea of the location of coke deposits. In this sense, from the results of Tables 1 and 2, accessible void volume, S (cm^3 N_2/cm^3 catalyst) and coke volume, C (cm^3 coke/cm^3 catalyst) were calculated [61, 62]. As it will be shown later, these experimental data can be expressed as follows with a linear trend:

$$S = V_0 - k \cdot C \quad \text{(eq. 3)}$$

where V_0 is referred to initial void volume (0.38 cm^3 N_2/cm^3 catalyst). According to the k-coefficient value obtained, different possibilities of coke distribution can take place, depending on the location of the coke formed on the catalyst during the reaction [61]. These different possibilities are schematically shown in Figure 3, in agreement with Bibby et al. [62]. In the initial state (fresh SBA-15) no coke is shown and the sorption capacity is $S=V_0$.

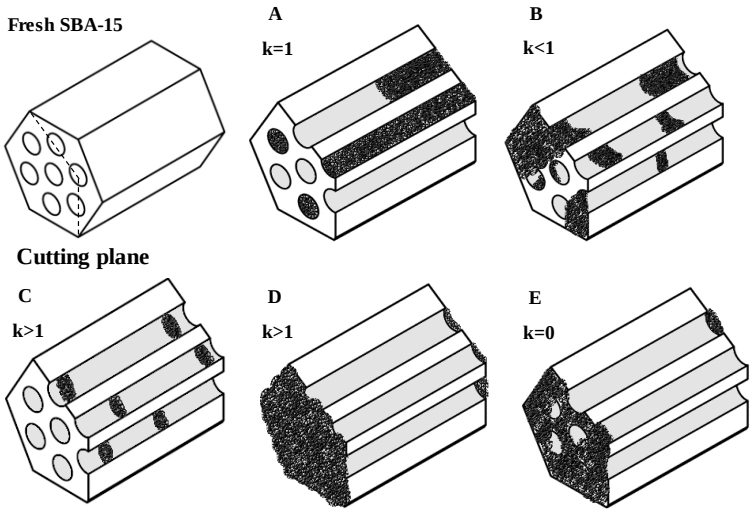

Figure 3. Possible coke distributions in Co/SBA-15 (based on [62])

Figure 3A shows how coke is filling the SBA 15 pores and the volume of coke corresponds exactly with the loss in sorption capacity (k=1). If some coke is formed also in the external surface (Figure 3B) the total volume of coke is higher than the loss in sorption capacity and, thus, k<1. When the internal coke is deposited isolating part of the SBA-15 pores, a small volume of coke can have a huge effect in the sorption capacity (Figure 3C, k>1). In the coke distribution shown in Figure 3D, the external coke blocks most the pores on both sides, thus, greatly reducing the sorption capacity with low coke volume (k>1). In the last case, represented in Figure 3E, coke formation predominates outside the structure of SBA-15. In this case, unlike the previous one, coke blocks some pores but allows access to them through the other end. Therefore, there is no effect on adsorption capacity and k = 0.

The calculated parameters for each reaction time (S and C) are represented in Figure 4. The calculated data, show two clearly differentiated zones: one for short reaction times, which lead to a k-value of 1.6, while in the other, for reaction times longer than 20 h the k-value is next to zero. These results evidence the presence of two different coke formation mechanisms. The first one, attributed to lower time-on-stream in which most sorption capacity is lost. Coke could be formed inside and/or outside the SBA-15

pores, being mostly formed over the external surface. Thus, that the most likely option is a combination of both cases, having a small volume of coke that isolates some pores and another volume that covers the external part of the support as it will be later shown by TEM. Moreover, external filamentous coke is less effective at blocking access to the active phase unless it completely covers the pore openings [62]. For TOS above 20 h (second stage), the final BET surface area did not change significantly despite the coke formation is increasing (see Tables 1 and 2). Therefore, according to E case, filamentous coke is being formed in the external part of the catalyst without inducing pore blocking.

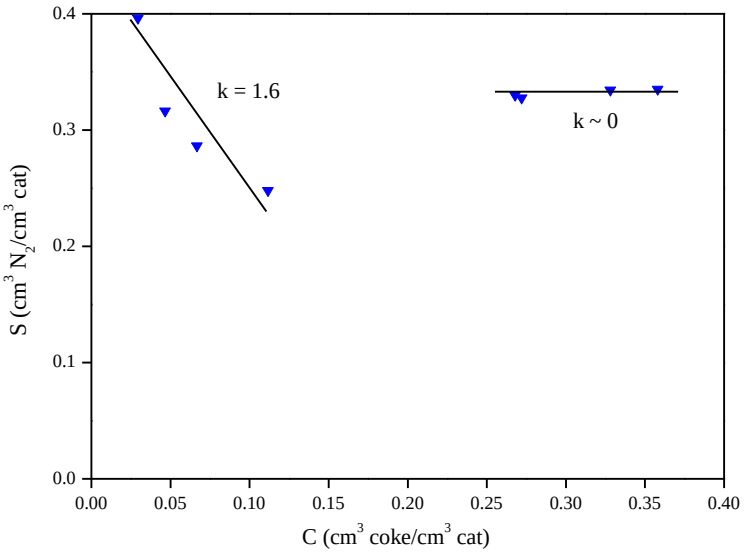

Figure 4. Sorption capacity for N_2 vs. coke content on Co/SBA-15 catalysts at different TOS.

Figure 5 shows TEM images of the catalysts after the reforming reaction at different TOS. In general, coke nanofilaments can be observed in all cases. As the reaction time increases, a growth in the thickness of the coke filaments walls is observed (averaged values from 30 measurements shown within Figure 5), which is associated to more condensed coke. This fact is corroborated by the results obtained from elemental analysis since higher C/H ratio were obtained with TOS. On the other hand, the presence of encapsulated cobalt particles (verified by EDS) is observed in the first

stage (between 0-20 h). This kind of coke has been described as the main cause of activity loss since metallic particles are blocked reducing its catalytic activity [63]. According to literature, whereas the formation of filamentous coke can be formed from CO by the Boudouard reaction and from the methane decomposition, the encapsulating coke can be mainly formed by the condensation of oxygenates present in the product distribution [30, 63-65]. Therefore, the conversion drop observed in this first stage could be ascribed to the loss of reactants access to some Co^0 particles covered by coke. In the second stage, it is still possible to observe the cobalt particles that were encapsulated during the first stage. Moreover, more condensed carbon nanofibers also can be distinguished compared to short reaction times, reaching wall thickness around 12 nm within 20 h TOS. In Figure 5, on the right side, histograms with Co particle size distribution from the count of the least 30 units are shown. Despite the trend in particle size is the same as from XRD, differences between the average size values obtained by both techniques may be due to some Co crystallites aggregated into the same particle.

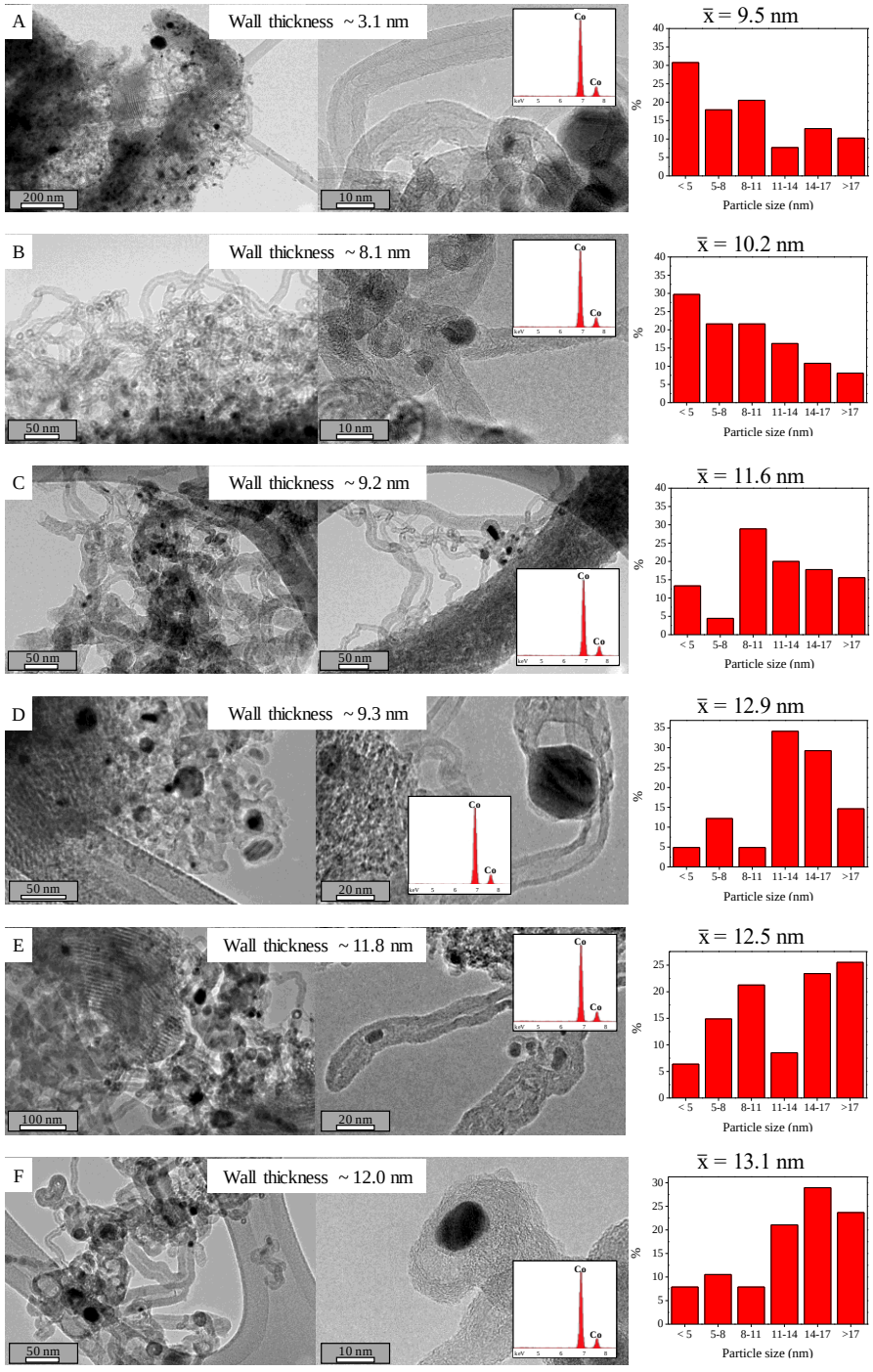

Figure 5. TEM images and Co particle size histograms of used Co/SBA-15 after: (A) 1 h; (B) 2 h; (C) 5 h; (D) 12 h; (E) 20 h; (F) 50h of time on stream.

As described above, there are several possible reasons for the loss of activity of the Co/SBA-15 catalyst in the reforming reaction of aqueous fraction. In this sense, the main parameters from the characterization results are represented in Figure 6 versus time-on-stream together with conversion.

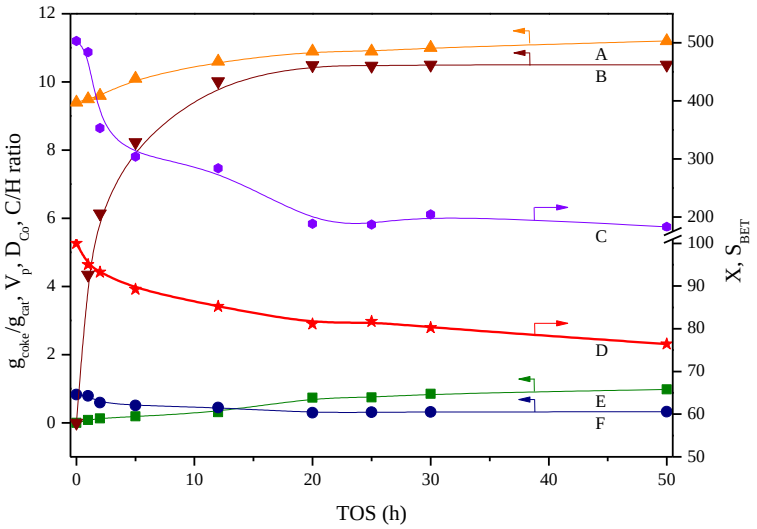

Figure 6. Changes in reaction parameters over TOS (A) D_{Co}; (B) C/H ratio; (C) S_{BET}; (D) Conversion, X; (E) g_{coke}/g_{cat}; (F) V_p.

In order to elucidate which parameter/s have the main influence on the activity loss, their influence over total conversion was evaluated by means of a t-Student statistical analysis. In this regard, the dependent variable (Y) was the total conversion while D_{Co} (mean crystallites size), C/H ratio, SB_{ET}, g_{coke}/g_{cat} and V_p were independent variables (X). The Student's t-value characterizes the relative significance of the parameter in a particular correlation [66]. The p-values were used as a tool to check the significance of each interaction among the variables with conversion. The smaller the p-value, the more significant is the corresponding coefficient term (if the p-value is lower than 0.05, it can be considered as statistically significant) [67]. The obtained results are listed with 95% confidence in Table 3.

Table 3. Multi-linear regression results at 95% confidence

	t Stat	p-value
g_{coke}/g_{cat}	-3.23	0.048
S_{BET} (m^2/g)	2.56	0.083
V_p (cm^3)	-3.05	0.056
D_{Co} (nm)	-3.86	0.031
C/H ratio	-5.75	0.010

As mentioned above, the parameters with p-value higher than 0.05 are not considered significant in the conversion drop and, thus, are discarded. Concerning this research, pore volume and BET surface area presented higher values and, therefore, they should have minor effect on the deactivation of the Co/SBA-15 catalyst. Hereafter, the t-Student statistical analysis was re-performed taking into account just the amount of coke produced (g_{coke}/g_{cat}), the diameter of Co crystallites (nm) and the C/H ratio. The corresponding calculations resulted in p-values of 0.045, 0.164 and 0.014 as well as t-stat values of -2.65, -1.63, -3.67 respectively. This suggests that the slight sintering effect of Co^0 particles neither has major significance in the conversion drop until 50 h TOS.

Figure 7 shows how conversion becomes smaller when the coke deposition increases up to 0.98 g_{coke}/g_{cat} and when C/H ratio tends to zero. In other words, when the amount of coke is high and it is more aliphatic and less ordered, resembling amorphous coke. In this way, we can conclude that deactivation of the Co/SBA-15 catalyst in the HTL aqueous fraction reforming is mainly a consequence of the amount of coke formed during the reaction, as well as its nature, although as it has been found, sintering could also have an effect on the conversion drop. Therefore, more ordered coke deposits will lead to less deactivation even though the formation rate could be high.

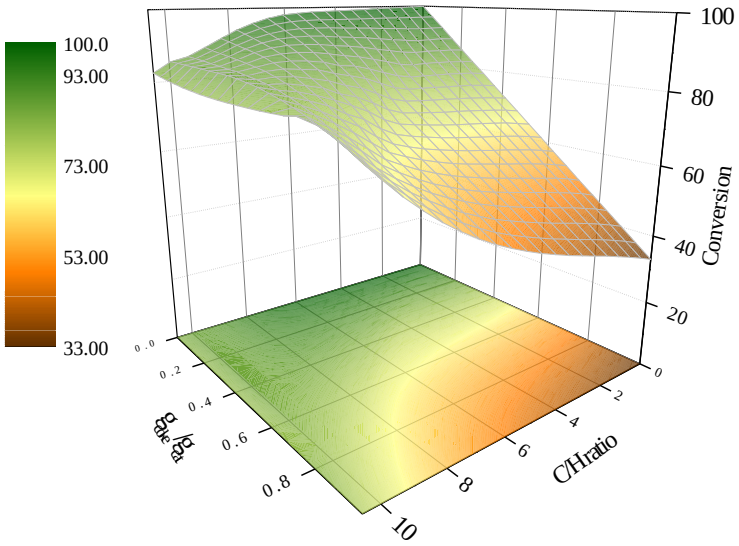

Figure 7. Effect of coke deposition and C/H ratio on bio-oil aqueous fraction reforming.

In overview, Figure 8 displays the catalyst evolution during the reforming of bio-oil aqueous fraction. As delimited above, two different stages take place with TOS. In stage 1 (TOS < 20 h) the formation of defective filamentous coke takes place over the catalysts (0.73 g_{coke}/g_{cat}) decreasing the BET surface area pore volume since carbon is formed not only in the external surface (blocking pores) but also inside the pores, leading to isolation of active centers. There are also encapsulating carbon deposits that hinder the catalytic role of some Co^0 particles, related to the condensation of oxygenated compounds present in the reaction medium as by-products. Slight sintering takes place but it seems to have minor effect on catalyst deactivation. Additionally, no oxidation could be detected of the active phase during the reaction. Stage 2 can be considered as a period in which conversion is in steady state. In that period, above 20 h TOS, the filamentous carbon structures tend to condensate leading to more aromatic carbon deposits but the coke filaments grow out of the support without blocking new pores. This results in no remarkable changes in conversion, BET surface area and C/H ratio, while the amount of coke increases in 0.25 g_{coke}/g_{cat}.

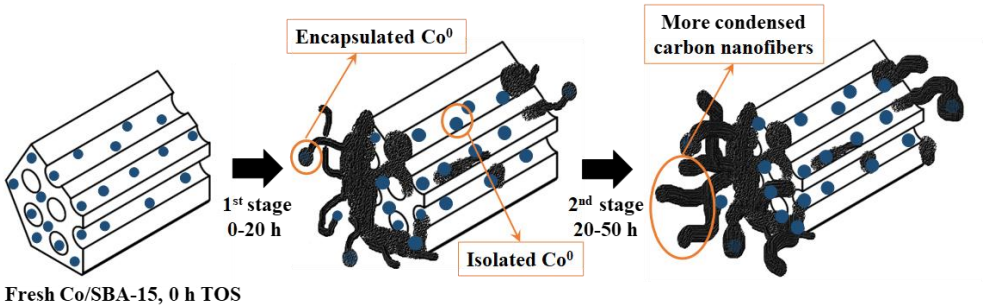

Figure 8. Evolution of coke and Co^0 particles during the deactivation of Co/SBA-15 in the reforming of bio-oil aqueous fraction.

Conclusions

The deactivation of Co/SBA-15 in the reforming of a mixture of model compounds representing the aqueous fraction from biomass HTL is a consequence of coke formation, its composition (C/H ratio) and Co sintering. The oxidation of Co was discarded as a cause of deactivation since no cobalt oxides were found by XRD within 50 h of reaction. Results evidenced two different stages to understand deactivation of Co/SBA-15. The first one, at short TOS (< 20 h), is ascribed to the formation of defective carbon nanofibers over the catalyst surface as well as inside the SBA-15 pores. This fact led to a significant drop in conversion and BET surface area since coke was covering not only the pore mouths but also was deposited inside them leading to isolated metallic Co particles. During this step, some Co particles were also encapsulated within coke nanofibers, hindering the catalytic role of these active centers. These facts are responsible of a conversion drop up to 81 mol % at 20 h time-on-stream. During the second stage of deactivation, between 20-50 h TOS, coke deposited became more ordered and aromatic as deduced by its higher C/H ratio. Coke deposits grow as filaments out of the support, as inferred from almost constant BET surface values and therefore not blocking the SBA-15 pores. In both stages, Co^0 crystallite size calculated form XRD of used samples indicated a slight sintering with minor influence on Co/SBA-15 deactivation.

The combination of different techniques for coke characterization with a t-Student analysis, let us to conclude that the progressive growth of carbon nanofibers and its nature (C/H ratio) have more influence than sintering on the conversion drop observed during the steam reforming of a mixture of acetic acid, hydroxyacetone and phenol as model compounds from the biomass HTL aqueous fraction.

Acknowledgements

This work has been carried out with financial support from the Regional Government of Madrid (project S2018/EMT-4344) and from the Spanish Ministry of Economy and Competitiveness (project ENE2017-83696-R).

References

[1] F.J. Gutiérrez Ortiz, A. Kruse, F. Ramos, P. Ollero, Integral energy valorization of municipal solid waste reject fraction to biofuels, Energy Conversion and Management, 180 (**2019**) 1167-1184.

[2] H.C. Ong, W.-H. Chen, A. Farooq, Y.Y. Gan, K.T. Lee, V. Ashokkumar, Catalytic thermochemical conversion of biomass for biofuel production: A comprehensive review, Renewable and Sustainable Energy Reviews, 113 (**2019**) 109266.

[3] A.T. Sipra, N. Gao, H. Sarwar, Municipal solid waste (MSW) pyrolysis for bio-fuel production: A review of effects of MSW components and catalysts, Fuel Processing Technology, 175 (**2018**) 131-147.

[4] S.S. Toor, L. Rosendahl, I. Sintamarean, Recipe-based co-HTL of biomass and organic waste, Direct Thermochemical Liquefaction for Energy Applications, Woodhead Publishing, Elsevier, Amsterdam, **2018**, 169-189.

[5] A. Sánchez-Bayo, R. Rodríguez, V. Morales, N. Nasirian, L.F. Bautista, G. Vicente, Hydrothermal Liquefaction of Microalga Using Metal Oxide Catalyst, Processes, 8 (**2019**) 15.

[6] I.M. Gandidi, M.D. Susila, N.A. Pambudi, Co-cracking of real MSW into bio-oil over natural kaolin, IOP Conference Series: Earth and Environmental Science, 60 (**2017**) 012019.

[7] P. McKendry, Energy production from biomass (Part 1): Overview of Biomass, Bioresource Technology, 83 (**2002**) 37-46.

[8] D. López Barreiro, W. Prins, F. Ronsse, W. Brilman, Hydrothermal liquefaction (HTL) of microalgae for biofuel production: State of the art review and future prospects, Biomass Bioenergy, 53 (**2013**) 113-127.

[9] W.-H. Chen, B.-J. Lin, M.-Y. Huang, J.-S. Chang, Thermochemical conversion of microalgal biomass into biofuels: A review, Bioresource Technology, 184 (**2015**) 314-327.

[10] D. Chiaramonti, M. Prussi, M. Buffi, A.M. Rizzo, L. Pari, Review and experimental study on pyrolysis and hydrothermal liquefaction of microalgae for biofuel production, Applied Energy, 185 (**2017**) 963-972.

[11] Y. Younan, M.W.M. van Goethem, G.D. Stefanidis, A particle scale model for municipal solid waste and refuse-derived fuels pyrolysis, Comput. Chem. Eng., 86 (**2016**) 148-159.

[12] R.V.S. Silva, V.B. Pereira, K.T. Stelzer, T.A. Almeida, G.A. Romeiro, D.A. Azevedo, Comprehensive study of the liquid products from slow pyrolysis of crambe seeds: Bio-oil and organic compounds of the aqueous phase, Biomass Bioenergy, 123 (**2019**) 78-88.

[13] S. Zhang, Y. Yan, T. Li, Z. Ren, Upgrading of liquid fuel from the pyrolysis of biomass, Bioresource Technology, 96 (**2005**) 545-550.

[14] P.J. Megía, A. Carrero, J.A. Calles, A.J. Vizcaíno, Hydrogen Production from Steam Reforming of Acetic Acid as a Model Compound of the Aqueous Fraction of Microalgae HTL Using Co-M/SBA-15 (M: Cu, Ag, Ce, Cr) Catalysts, Catalysts, 9 (**2019**) 1013.

[15] J.M. Silva, M.A. Soria, L.M. Madeira, Challenges and strategies for optimization of glycerol steam reforming process, Renewable and Sustainable Energy Reviews, 42 (**2015**) 1187-1213.

[16] J.A. Calles, A. Carrero, A.J. Vizcaíno, P.J. Megía, Agglomerated Co–Cr/SBA-15 catalysts for hydrogen production through acetic acid steam reforming, International Journal of Hydrogen Energy, 45 (**2020**) 15941-15950.

[17] B.L. Augusto, M.C. Ribeiro, F.J.C.S. Aires, V.T. da Silva, F.B. Noronha, Hydrogen production by the steam reforming of ethanol over cobalt catalysts supported on different carbon nanostructures, Catalysis Today, 344 (**2020**) 66-74.

[18] G. Chen, J. Tao, C. Liu, B. Yan, W. Li, X. Li, Hydrogen production via acetic acid steam reforming: A critical review on catalysts, Renewable and Sustainable Energy Reviews, 79 (**2017**) 1091-1098.

[19] S.S. Itkulova, Y.Y. Nurmakanov, S.K. Kussanova, Y.A. Boleubayev, Production of a hydrogen-enriched syngas by combined CO_2-steam reforming of methane over Co-based catalysts supported on alumina modified with zirconia, Catalysis Today, 299 (**2018**) 272-279.

[20] X. Hu, G. Lu, Comparative study of alumina-supported transition metal catalysts for hydrogen generation by steam reforming of acetic acid, Applied Catalysis B: Environmental, 99 (**2010**) 289-297.

[21] B. Banach, A. Machocki, P. Rybak, A. Denis, W. Grzegorczyk, W. Gac, Selective production of hydrogen by steam reforming of bio-ethanol, Catalysis Today, 176 (**2011**) 28-35.

[22] J.A. Calles, A. Carrero, A.J. Vizcaíno, L. García-Moreno, P.J. Megía, Steam Reforming of Model Bio-Oil Aqueous Fraction Using Ni-(Cu, Co, Cr)/SBA-15 Catalysts, International Journal of Molecular Sciences, 20 (**2019**) 512.

[23] W.-J. Jang, J.-O. Shim, H.-M. Kim, S.-Y. Yoo, H.-S. Roh, A review on dry reforming of methane in aspect of catalytic properties, Catalysis Today, 324 (**2019**) 15-26.

[24] J.A. Calles, A. Carrero, A.J. Vizcaíno, Ce and La modification of mesoporous Cu–Ni/SBA-15 catalysts for hydrogen production through ethanol steam reforming, Microporous and Mesoporous Materials, 119 (**2009**) 200-207.

[25] O. González, H. Pérez, P. Navarro, L.C. Almeida, J.G. Pacheco, M. Montes, Use of different mesostructured materials based on silica as cobalt supports for the Fischer–Tropsch synthesis, Catalysis Today, 148 (**2009**) 140-147.

[26] Y. Qiu, S. Chen, C. Wang, R. Lyu, D. Zhang, C. Liu, Y. Zhang, J. Li, Preparation of SBA-15 with penetrating pores and their performance in Fischer–Tropsch synthesis, New J. Chem., 41 (**2017**) 14109-14115.

[27] Y.C. Sharma, A. Kumar, R. Prasad, S.N. Upadhyay, Ethanol steam reforming for hydrogen production: Latest and effective catalyst modification strategies to minimize

carbonaceous deactivation, Renewable and Sustainable Energy Reviews, 74 (**2017**) 89-103.

[28] A.R. Passos, S.H. Pulcinelli, C.V. Santilli, V. Briois, Operando monitoring of metal sites and coke evolution during non-oxidative and oxidative ethanol steam reforming over Ni and NiCu ex-hydrotalcite catalysts, Catalysis Today, 336 (**2019**) 122-130.

[29] C. Montero, A. Remiro, B. Valle, L. Oar-Arteta, J. Bilbao, A.G. Gayubo, Origin and Nature of Coke in Ethanol Steam Reforming and Its Role in Deactivation of $Ni/La_2O_3–\alpha Al_2O_3$ Catalyst, Industrial & Engineering Chemistry Research, 58 (**2019**) 14736-14751.

[30] D.L. Trimm, Coke formation and minimisation during steam reforming reactions, Catalysis Today, 37 (**1997**) 233-238.

[31] V. Palma, C. Ruocco, E. Meloni, F. Gallucci, A. Ricca, Enhancing $Pt-Ni/CeO_2$ performances for ethanol reforming by catalyst supporting on high surface silica, Catalysis Today, 307 (**2018**) 175-188.

[32] J. Sehested, Four challenges for nickel steam-reforming catalysts, Catalysis Today, 111 (**2006**) 103-110.

[33] C. Montero, A. Ochoa, P. Castaño, J. Bilbao, A.G. Gayubo, Monitoring Ni^0 and coke evolution during the deactivation of a $Ni/La_2O_3–\alpha Al_2O_3$ catalyst in ethanol steam reforming in a fluidized bed, Journal of Catalysis, 331 (**2015**) 181-192.

[34] J.A. Calles, A. Carrero, A.J. Vizcaíno, L. García-Moreno, Hydrogen production by glycerol steam reforming over SBA-15-supported nickel catalysts: Effect of alkaline earth promoters on activity and stability, Catalysis Today, 227 (**2014**) 198-206.

[35] A.M. Amin, E. Croiset, W. Epling, Review of methane catalytic cracking for hydrogen production, International Journal of Hydrogen Energy, 36 (**2011**) 2904-2935.

[36] A. Ochoa, I. Barbarias, M. Artetxe, A.G. Gayubo, M. Olazar, J. Bilbao, P. Castaño, Deactivation dynamics of a Ni supported catalyst during the steam reforming

of volatiles from waste polyethylene pyrolysis, Applied Catalysis B: Environmental, 209 (**2017**) 554-565.

[37] I. Barbarias, G. Lopez, M. Amutio, M. Artetxe, J. Alvarez, A. Arregi, J. Bilbao, M. Olazar, Steam reforming of plastic pyrolysis model hydrocarbons and catalyst deactivation, Applied Catalysis A: General, 527 (**2016**) 152-160.

[38] N.D. Charisiou, K.N. Papageridis, G. Siakavelas, V. Sebastian, S.J. Hinder, M.A. Baker, K. Polychronopoulou, M.A. Goula, The influence of SiO_2 doping on the Ni/ZrO2 supported catalyst for hydrogen production through the glycerol steam reforming reaction, Catalysis Today, 319 (**2019**) 206-219.

[39] A.J. Reynoso, J.L. Ayastuy, U. Iriarte-Velasco, M.A. Gutiérrez-Ortiz, Cobalt aluminate spinel-derived catalysts for glycerol aqueous phase reforming, Applied Catalysis B: Environmental, 239 (**2018**) 86-101.

[40] X. Hu, D. Dong, X. Shao, L. Zhang, G. Lu, Steam reforming of acetic acid over cobalt catalysts: Effects of Zr, Mg and K addition, International Journal of Hydrogen Energy, 42 (**2017**) 4793-4803.

[41] D. Moodley, M. Claeys, E. van Steen, P. van Helden, D. Kistamurthy, K.-J. Weststrate, H. Niemantsverdriet, A. Saib, W. Erasmus, J. van de Loosdrecht, Sintering of cobalt during FTS: Insights from industrial and model systems, Catalysis Today, (**2019**).

[42] B. Valle, B. Aramburu, M. Olazar, J. Bilbao, A.G. Gayubo, Steam reforming of raw bio-oil over Ni/La_2O_3-αAl_2O_3: Influence of temperature on product yields and catalyst deactivation, Fuel, 216 (**2018**) 463-474.

[43] A. Ochoa, B. Aramburu, B. Valle, D.E. Resasco, J. Bilbao, A.G. Gayubo, P. Castaño, Role of oxygenates and effect of operating conditions in the deactivation of a Ni supported catalyst during the steam reforming of bio-oil, Green Chem., 19 (**2017**) 4315-4333.

[44] A. Remiro, A. Ochoa, A. Arandia, P. Castaño, J. Bilbao, A.G. Gayubo, On the dynamics and reversibility of the deactivation of a Rh/CeO_2ZrO_2 catalyst in raw bio-oil steam reforming, International Journal of Hydrogen Energy, 44 (**2019**) 2620-2632.

[45] A.J. Vizcaíno, A. Carrero, J.A. Calles, Ethanol steam reforming on Mg- and Ca-modified Cu–Ni/SBA-15 catalysts, Catalysis Today, 146 (**2009**) 63-70.

[46] D. Zhao, J. Feng, Q. Huo, N. Melosh, G.H. Fredrickson, B.F. Chmelka, G.D. Stucky, Triblock copolymer syntheses of mesoporous silica with periodic 50 to 300 angstrom pores, Science, 279 (**1998**) 548-552.

[47] Z. Li, M. Si, X. Li, J. Lv, Effects of titanium silicalite and TiO_2 nanocomposites on supported Co-based catalysts for Fischer–Tropsch synthesis, Applied Organometallic Chemistry, 33 (**2019**) 4640.

[48] A. Carrero, J.A. Calles, L. García-Moreno, A.J. Vizcaíno, Production of Renewable Hydrogen from Glycerol Steam Reforming over Bimetallic Ni-(Cu,Co,Cr) Catalysts Supported on SBA-15 Silica, Catalysts, 7 (**2017**) 55.

[49] S. Cavallaro, N. Mondello, S. Freni, Hydrogen produced from ethanol for internal reforming molten carbonate fuel cell, Journal of Power Sources, 102 (**2001**) 198-204.

[50] M. Chen, Y. Wang, Z. Yang, T. Liang, S. Liu, Z. Zhou, X. Li, Effect of Mg-modified mesoporous Ni/Attapulgite catalysts on catalytic performance and resistance to carbon deposition for ethanol steam reforming, Fuel, 220 (**2018**) 32-46.

[51] V. Nichele, M. Signoretto, F. Pinna, F. Menegazzo, I. Rossetti, G. Cruciani, G. Cerrato, A. Di Michele, Ni/ZrO_2 catalysts in ethanol steam reforming: Inhibition of coke formation by CaO-doping, Applied Catalysis B: Environmental, 150-151 (**2014**) 12-20.

[52] J. Bermúdez-Polonio, Métodos de difracción de rayos X: principios y aplicaciones, Pirámide, Madrid, **1981**, 354-361.

[53] Z. Taherian, M. Yousefpour, M. Tajally, B. Khoshandam, Catalytic performance of Samaria-promoted Ni and Co/SBA-15 catalysts for dry reforming of methane, International Journal of Hydrogen Energy, 42 (**2017**) 24811-24822.

[54] A. Carrero, J.A. Calles, A.J. Vizcaíno, Effect of Mg and Ca addition on coke deposition over $Cu–Ni/SiO_2$ catalysts for ethanol steam reforming, Chemical Engineering Journal, 163 (**2010**) 395-402.

[55] A.E. Galetti, M.F. Gomez, L.A. Arrúa, M.C. Abello, Hydrogen production by ethanol reforming over NiZnAl catalysts: Influence of Ce addition on carbon deposition, Applied Catalysis A: General, 348 (**2008**) 94-102.

[56] C.K.S. Choong, Z. Zhong, L. Huang, Z. Wang, T.P. Ang, A. Borgna, J. Lin, L. Hong, L. Chen, Effect of calcium addition on catalytic ethanol steam reforming of Ni/Al_2O_3: I. Catalytic stability, electronic properties and coking mechanism, Applied Catalysis A: General, 407 (**2011**) 145-154.

[57] D.S. Lima, C.O. Calgaro, O.W. Perez-Lopez, Hydrogen production by glycerol steam reforming over Ni based catalysts prepared by different methods, Biomass Bioenergy, 130 (**2019**) 105358.

[58] A. Moral, I. Reyero, C. Alfaro, F. Bimbela, L.M. Gandía, Syngas production by means of biogas catalytic partial oxidation and dry reforming using Rh-based catalysts, Catalysis Today, 299 (**2018**) 280-288.

[59] J. Goetze, B.M. Weckhuysen, Spatiotemporal coke formation over zeolite ZSM-5 during the methanol-to-olefins process as studied with operando UV-vis spectroscopy: a comparison between H-ZSM-5 and Mg-ZSM-5, Catalysis Science & Technology, 8 (**2018**) 1632-1644.

[60] S. Jampa, A.M. Jamieson, T. Chaisuwan, A. Luengnaruemitchai, S. Wongkasemjit, Achievement of hydrogen production from autothermal steam reforming of methanol over Cu-loaded mesoporous CeO_2 and Cu-loaded mesoporous CeO_2–ZrO_2 catalysts, International Journal of Hydrogen Energy, 42 (**2017**) 15073-15084.

[61] A. de Lucas, P. Canizares, A. Durán, A. Carrero, Coke formation, location, nature and regeneration on dealuminated HZSM-5 type zeolites, Applied Catalysis A: General, 156 (**1997**) 299-317.

[62] D.M. Bibby, N.B. Milestone, J.E. Patterson, L.P. Aldridge, Coke formation in zeolite ZSM-5, Journal of Catalysis, 97 (**1986**) 493-502.

[63] J. Vicente, C. Montero, J. Ereña, M.J. Azkoiti, J. Bilbao, A.G. Gayubo, Coke deactivation of Ni and Co catalysts in ethanol steam reforming at mild temperatures in

a fluidized bed reactor, International Journal of Hydrogen Energy, 39 (**2014**) 12586-12596.

[64] A.L. Alberton, M.M.V.M. Souza, M. Schmal, Carbon formation and its influence on ethanol steam reforming over Ni/Al_2O_3 catalysts, Catalysis Today, 123 (**2007**) 257-264.

[65] L.S. Lobo, J.L. Figueiredo, C.A. Bernardo, Carbon formation and gasification on metals. Bulk diffusion mechanism: A reassessment, Catalysis Today, 178 (**2011**) 110-116.

[66] H. Du, Z. Ring, Y. Briker, P. Arboleda, Prediction of gas chromatographic retention times and indices of sulfur compounds in light cycle oil, Catalysis Today, 98 (**2004**) 217-225.

[67] M. Shiva, H. Atashi, A.A. Mirzaei, M. Arsalanfar, A. Zare, Study of syngas conversion to light olefins by statistical models, Fuel, 123 (**2014**) 205-210.